Dynamic Analysis of Raising Sunken Vessels Using Buoyant Systems

Arun Kumar Devaki Bhavan Velayudhan

Submitted in fulfilment of the requirements for the degree of

Doctor of Philosophy

Department of Naval Architecture and Marine Engineering

Universities of Strathclyde and Glasgow

May 2014

Declaration of Authenticity and Author's Right

This thesis is the result of the author's original research. It has been composed by the author and has not been previously submitted for examination which has led to the award of a degree.

To my beloved mother

Mrs. M.R.Vanaja Kumari Amma

Acknowledgements

All glory and honour be to the **Almighty God** who showed his abundant grace on me and guided me with his blessings to make this research a success.

I express my heartfelt thanks and gratitude to my primary supervisor Prof. Nigel Barltrop for his invaluable guidance, patience and constant encouragement without which I would not have completed this research successfully. I would also like to thank my second supervisor Dr.Narakorn Srinil for his guidance and suggestions. I also express my gratitude to my first supervisor Late Dr. Kamlesh Varyani for his guidance and support.

I extend my wholehearted gratitude to Prof.Atilla Incecik, Head, Department of Naval Architecture & Marine Engineering for his guidance, support and help. I would like to express my sincere thanks to committee members Prof.Sandy Day and Mr.David Clelland for their valuable suggestions.

I owe my gratitude in no small measure to my parents for their patience, sacrifice and unfailing encouragement during the course of this work.

This work is part of SuSy (Surfacing System for Ship Recovery) project funded by the European Commission FP 7 framework (www.su-sy.eu). I am very grateful for this support.

Table of Contents

Abstract

In this research, mathematical formulations for the dynamics of raising sunken vessels using buoyant systems are developed in a form which is suitable for integrating control techniques to ensure both hydrodynamic and structural stability for a safe and stable salvaging operation based on both rigid body modeling and flexible body modeling concepts.

Due to the coupled nature of salvage dynamics and for integrating controller techniques, the mathematical modeling is carried out as two subsystems. In the primary model, the salvage dynamics is formulated in such a way that the variation in additional buoyancy due to flow rate of filling gas inside the lift bags is the controlling force with respect to hydrostatic force due to weight, buoyancy and suction break out, hydrodynamic forces and uncertainty arises due to any external disturbances. In the secondary model, the purging of gas through the valves is taken as the control parameter by accounting the excess buoyancy available after suction break out and to the variation in pressure difference between gas inside lift bag and surrounding sea water pressure for a stable ascent.

According to the simplified two-degree-of-freedom equations of rigid-body vessel motion, a state space model is developed for integrating the primary controller. Initially a proportional derivative (PD) controller is selected as the primary controller for regulating the flow rate of filling gas inside the lift bags according to the buoyancy requirement and extended to other classic controllers like proportional integral and derivative (PID) controller and sliding mode controller (SMC) for improving the performance. Numerical simulations are carried out in MATLAB & SIMULINK by solving the standard State Dependent Ricatti Equation in a body-fixed coordinate reference frame. Preliminary results in terms of coordinate positions or trajectories, linear and angular velocity components of the raising body are evaluated based on an experimental pontoon model. A number of case studies are carried out for different target depths with the developed linear state space model including sensitivity analysis such as

change in hydrodynamic coefficients, breakout lift force and the effect of external disturbances and uncertainty. SMC is found to be the optimum choice among these conventional controllers by satisfying the Lyapunov stability condition even for higher water depths with system robustness and capability to handle parameter variations, external disturbances and uncertainty. The tuning effort and chattering were found to be the two major draw backs of conventional sliding mode controller (CSMC), which is improved by integrating it with artificial intelligence such as fuzzy logic controller to bring together the advantages of both controllers to become fuzzy sliding mode controllers (FSMCs).

In FSMCs, the performance of the CSMC is improved by dynamically computing the sliding surface slope by a FLC and adaptively computing the controller gain by another FLC. FLCs are designed using MATLAB's fuzzy logic interface based on Mamdani's implification method the combined models will be developed in SIMULINK. A two input fuzzy sliding mode controller (TIFSMC) is designed first and later simplified to single input fuzzy sliding mode controller (SIFSMC), for reducing the tuning effort and computational time. With the development of SIFSMC, the tuning process becomes standardized and hassle free and hence the well known chattering problem associated with SMCs is avoided. The comparative performance of the fuzzy sliding mode controllers over CSMC has been investigated by performing numerical simulations on the pontoon model. It is found that both FSMCs show 30% of improvement in the tracking performance when compared to the CSMC, while maintaining its robustness. It is also noted that FSMCs are less sensitive to external disturbances and uncertainties in comparison with CSMC. The responses obtained by the SIFSMC are the same as those obtained by the TIFSMC, with the former involving a much less tuning effort and computational time. Simulation studies reveals the fact that for complicated non linear underwater operations like marine salvage involving uncertainty and external disturbances, a closed loop control system is mandatory and an adaptive controller like SIFSMC is the optimum choice as the primary controller for regulating the gas flow rate.

Purge valve modeling is carried out according to the excess buoyancy available after suction breakout and to the variation in pressure difference between gas inside the lift bags and surrounding sea water for a stable ascent. A PID controller is designed as the secondary controller for regulating the purging of gas through the valves and found to be effective in

maintaining the ascent velocity within the stable region. Then a supervisory fuzzy logic controller is designed to monitor or switch between the primary and secondary controllers based on the buoyancy requirement for a safe and stable salvaging operation. The Gaussian membership functions are used for representing input and output variables, and the *centroid* method is used for defuzzification. Using a trial and error approach, the best inference mechanism to use in this case seems to be the *prod-probor* method. Because of simplicity and availability of the graphical user interface (GUI) in MATLAB, Mamdani inference engine is employed for designing the FLC that uses *minimum* operator for a fuzzy implication and *max-min* operator for composition The defuzzification technique used is found using trial and error and *Centre of Gravity approach* is the one which provides least integral square error. From the simulation studies, it is found that FLC is capable to maintain hydrodynamic stability in diving plane by suitably defining the linguistic fuzzy rules, which are created based on the author's experience in conducting numerical simulation using primary and secondary controllers.

Finally, in order to find the optimum location of lift bags on the vessel and to determine the controlled response of individual lift bags or the real case of lifting a very flexible structure, such as a long pipe, using **multiple controlled lift bags**, the problem is extended to a detailed flexible body modeling and control. In this regard, a chemical tanker is taken and modeled as an elastic Euler-Bernoulli beam with free–free boundary conditions. Free vibration analysis is carried out on the model via an analytical as well as finite element method, and the obtained responses such as natural frequencies and mode shapes are evaluated and compared. From the mode shape plots, the lift bags are located suitably on the "nodes of a mode" of the beam, where the displacement is negligible. Then the eigenvectors are normalized with respect to mass, and the equation of motion is developed in principal coordinates after defining the nodal forces and moments. Then the modal contributions of individual modes are analyzed according to their dc gain/peak gain value to define, which ones have greatest contribution and later several modal reduction techniques such as '*modred-mdc*' and '*modred-del*' are used to obtain the smallest state space models for individual lift bags that represents the pertinent system dynamics. Highest dc gain is obtained for the first two rigid modes, which implies that rigid body modes are more significant compared to flexible modes for the control of lifting during marine salvage. However flexible modes relate to structural hull girder moments which should also be considered. Preliminary results in terms of coordinate positions or trajectories, linear

and angular velocity components of the raising body at various sections of the vessel or beam nodes can be estimated. Longitudinal distribution of shear force and bending moments across the tanker are also evaluated. The full and reduced order modal responses for lift bags are compared in both frequency and time domains. It is observed that '*unsorted modred-mdc*' is the preferred choice for modal order reduction compared to other modal reduction methods. Using a flexible body modeling approach the state space model is available for individual nodes on the beam. Thus controlled response of individual lift bags can be simulated. This is an advantage of flexible body modeling & control over rigid body modeling & control. Finally a supervisory fuzzy logic controller is integrated with the 4*4 flexible state space model obtained using '*unsorted modred-mdc*' to obtain the controlled stable responses of individual external lift bags.

1 Introduction

Marine salvage is an operation of rescuing a ship/vessel, its cargo or other properties from impending peril. The salvage comprises of towing and refloating a sunken or stranded vessel with the main purposes to prevent the marine environment from pollution and to clear a channel for the navigation. Ships sink or capsize because they lose their buoyancy or stability due to the collision, battle or weather damage, flooding and other means. The rescue of a damaged vessel is a very difficult task when compared to an intact ship in the same location. Salvaging of sunken ships requires both the recovery of sufficient buoyancy to bring the ship afloat and the suitable buoyancy distribution to regain the satisfactory condition of stability, trim and strength [113-116, 119, 125].

As far as marine salvage operation is concerned, literature sources reporting systematic data and information useful for system modeling are relatively few. Studies regarding the dynamics of salvage operation are of course complicated by the fact that, in addition to the influence of complicated hydrodynamic forces, moments and breakout forces, the external disturbances and uncertainty are always to be taken in to account. There are three methods commonly used in the marine salvage industry to extract the sunken objects from the sea bottom, i.e. by using the floating cranes (see Figure 1), the Remotely Operated Vehicles (ROVs) (see Figure 2) and the buoyancy systems (see Figure 3). Floating cranes can be used for water depths of 2000 m with a good controllability; however the weight of cables becomes more than that of the payload for deeper lifts and hence the process becomes awkward and costly. As the cranes are fitted onto a moving vessel, there will be operational constraints due to the limiting sea state affected by weather conditions. Excessive cost of hiring and the limited availability of cranes are the major problems facing the salvage industry. ROVs, on the other hand, can be used in higher water

depths and they are highly controllable. Nevertheless, they can be only used for lifting smaller objects as the lifting capacity is limited by the size and power of the thrusters used for the propulsion. Buoyancy systems have the advantage that they can be used for lifting any size of objects from any depth with comparatively less costs [86, 113-119].

Figure 1: Floating Cranes for marine salvage [61]

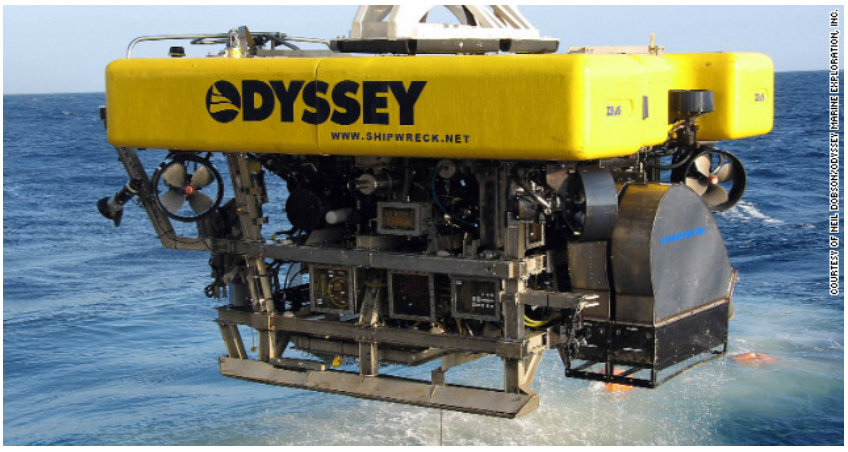

Figure 2: 8 Ton ROV used for marine salvage [87]

Figure 3: Scuba diver attaching inflated bags to the sunken vessel.
Photo - courtesy of J W Automarine [32, 61]

The concept of using buoyancy systems (e.g. the gas inflated bags) for salvaging sunken vessels from the deep ocean has been around for centuries. This operation is based on the well-known 'Archimedes' principle for which the force on the object can be determined by subtracting the weight of the object in air from the weight of the fluid displaced by that object [95]. In general, the bottoms of inflatable bags are attached to the payload to be lifted and inflated using pipes from the gas generating system. In salvage industry, there are mainly two types of lift bags are generally available for recovering sunken objects; one is parachute type and other is cylindrical type. Parachute type bags are generally preferred for lifting purpose, whereas cylindrical type lift bags are used for providing stability [33, 61, 98, 107, 111, 125].

Parachute type bags are fitted with a suitable attachment point at or near the crown to allow a load restraining harness of heavy duty polyester webbing, which is fabricated to the top of the bag as shown in Figure 4(a). The harness together with the airbag skin has a safe working load

ratio of 6:1. Due to the relatively small storage space required for these bags in comparison with the upward force they are capable of exerting, they become essential tools for underwater salvage operations [132]. Cylindrical type bags (Figure 4(b)) are normally fitted inside the compartments of the vessel (normally in ballast tanks) to provide additional buoyancy as well as to make sure that the centre of buoyancy is above the centre of gravity [61, 98, 107, 111].

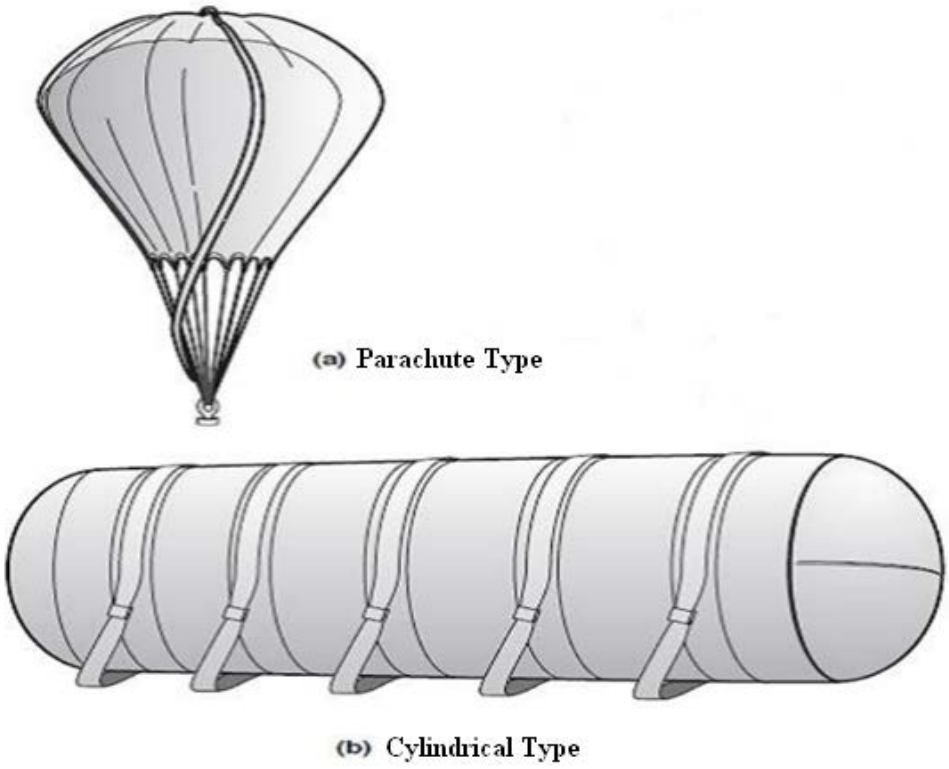

Figure 4 (a) & (b): Commercial Inflated Lift Bags [125]

The main drawback of using the inflating bags for marine salvage operation is due to the difficulty in controlling the vertical speed and pitch motion as the ship ascends. Due to the suction break out force, a large buoyancy force may be initially required to separate the ship from the seabed, resulting in an excessive vertical speed and pitch angle after break out. During the ascent, any trapped air inside the hull may also expand and further increase the buoyancy.

Also due to the pressure difference between gas inside the lift bag and surrounding sea water pressure in accordance with the decrease in water depth during the ascent, the gas inside the lift bag expands. All these factors lead to an increase in buoyancy force and hence result in an excessive vertical speed as well as pitch angle during the ascend. Excessive vertical speed results in a potentially-hazardous working environment to divers and salvaging crews and this may cause the lift bag to breach the surface of the water so fast that the air escapes from the bottom (see Figure 5). High values of pitch angle cause the lift slings to break loose from payload and hence results to a further buoyancy loss. These all factors make the payload to sink back to the bottom which, in turn, results in a loss of time, damage to the hull, high operating and maintenance costs, and the risk to divers and crew members. Open bottom bags dump excess gas from the bottom during the ascent whereas enclosed lift bags only have a limited capacity to dump excess gas through the pressure release valves [33, 61, 125].

Figure 5: A 25 ton capacity lift bag that broke free from USS Spiegel Grove during the salvage operation. The lift bag reached an altitude of approximately 30 meters. Photo - courtesy of Resolve Towing and Salvage, Inc [32, 98]

Hence, in order to ensure hydrodynamic and structural stability during the ascent, it is required to design the following two types of control subsystems and a supervisory controller to monitor these sub controllers.

a. **Primary Controller**

The function of the primary controller (Figure 6) is used to regulate the flow rate of filling gas inside the lift bags according to the buoyancy requirement with respect to hydrostatic, hydrodynamic, suction break out force components and uncertainty arises due to external disturbances for a stable ascent. It should be a closed loop control system (e.g. classic controllers like PD, PID or SMC) working on the output or feedback obtained from sensors.

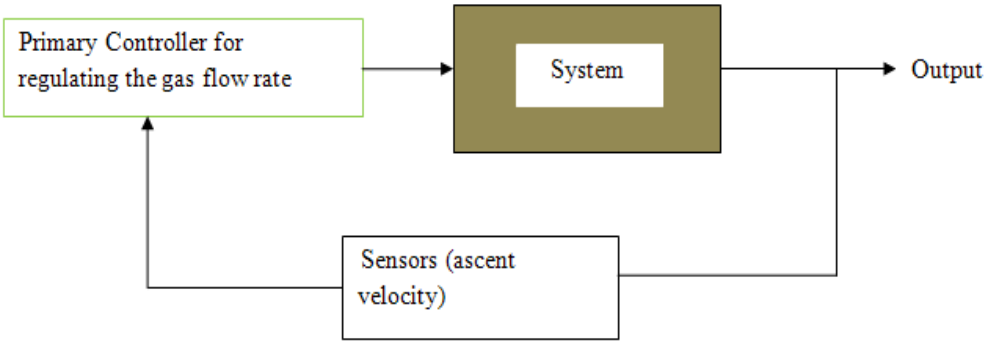

Figure 6: Design of a primary controller for regulating the gas flow rate

a. Secondary Controller

A secondary controller is proposed to regulate the opening of a purge valve fitted on the lift bags in accordance with the excess buoyancy available after suction breakout and to the variation in pressure difference b/w gas inside the lift bags and surrounding seawater pressure for a stable ascent. It can be controlled either mechanically (spring loaded) or electrically. But for adequate performance, it is better to control purge valves electrically. Therefore, in this thesis, a proportional integral and derivative (PID) algorithm is selected to regulate the purge valve opening based on the work of Farrell & Wood [32] as shown in Figure 7. In this case, the PID controller works according to the output from pressure sensor fitted on the lift bags, which can be used to estimate ascent velocity by converting pressure head into velocity head. Therefore purge valves with PID controller and sensor

(can be called an automatic purge valve) is considered as an integrated system fitted on the lift bags [33].

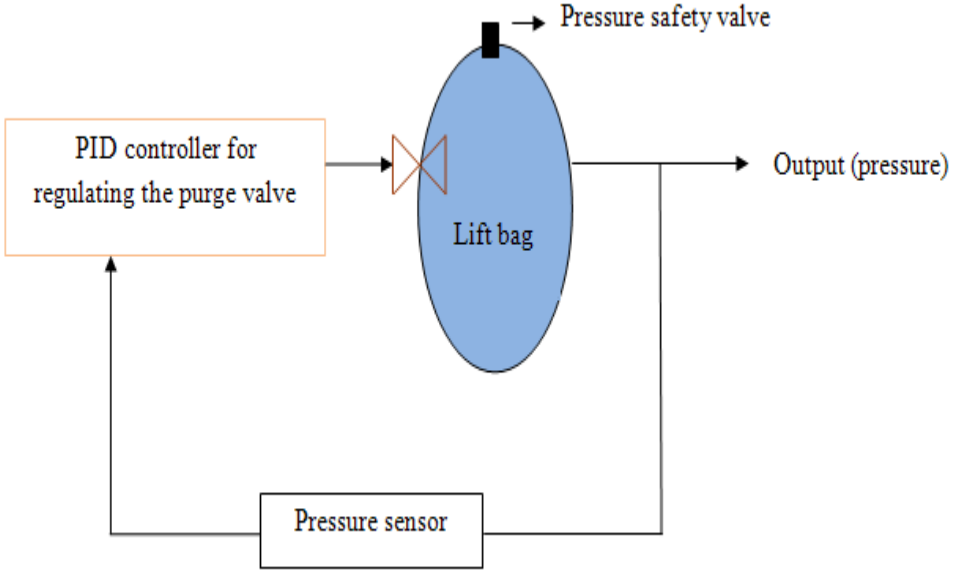

Figure 7: Design of a secondary controller for regulating the purge valve opening

c. <u>Supervisory Controller</u>

As we have two sub controllers; the primary controller for regulating the flow rate of filling gas inside the lift bags and secondary controller for regulating the purging of gas through valves, now it is necessary to design a supervisory controller that can be used to monitor or switch between the primary controller and secondary controller according to the buoyancy requirement or ascent rate as shown in Figure 8 for a safe and stable salvage operation.

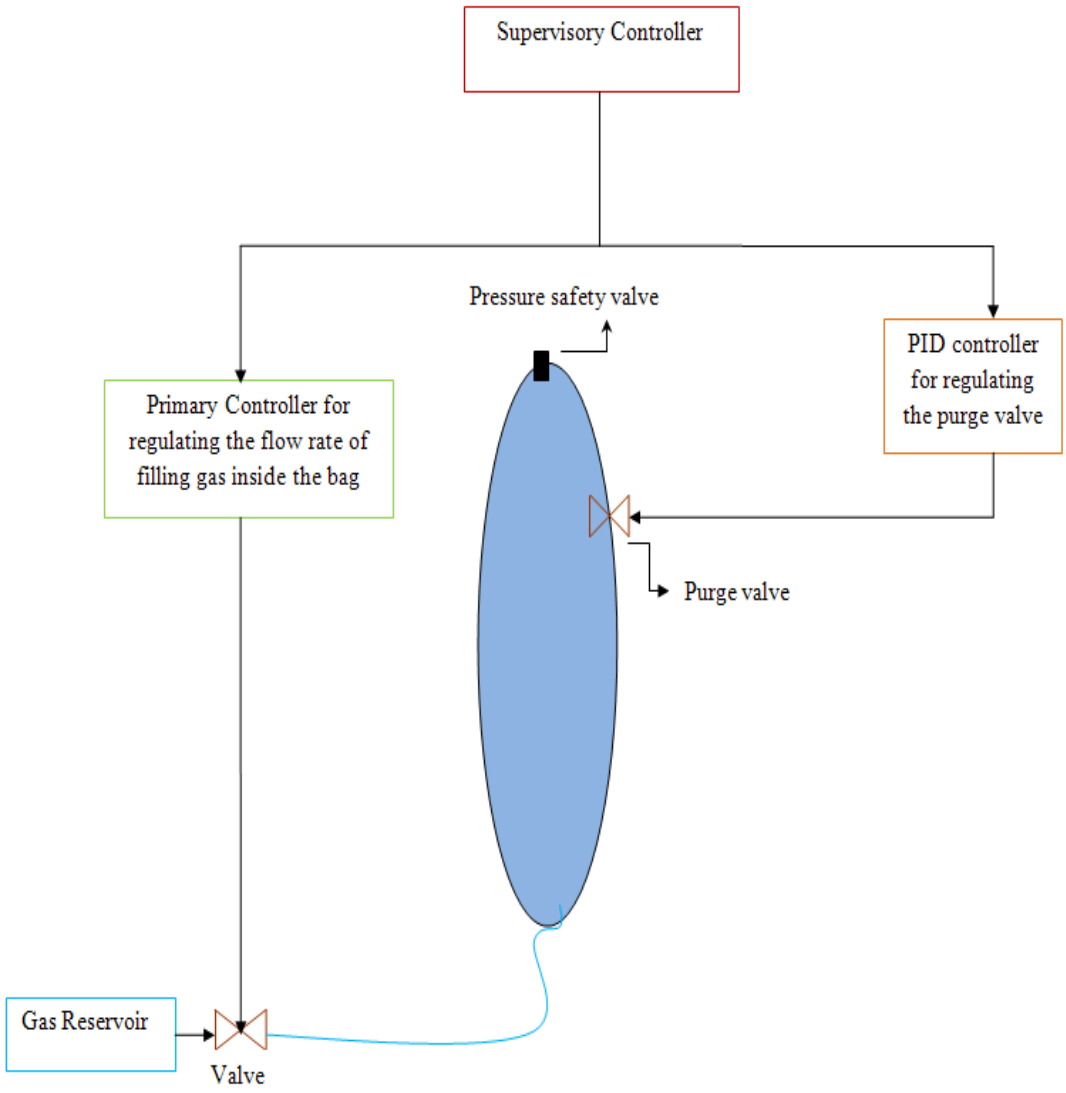

Figure 8:

Design of a supervisory controller for marine salvage

For example,

1. For suction break out, increase the buoyancy by increasing the flow rate of filling gas inside the lift bags; i.e. to operate the primary controller.

2. During the ascent, reduce the ascent rate by opening the purge valves fitted on the lift bags; i.e. to operate the secondary controller.
3. When the payload reaches near water surface, reduce the ascent rate by simultaneously operating the primary and secondary controller.
4. etc……..

Hence the supervisory controller may be based on linguistic commands or the information (rules) provided by the salvor, which leads to the design of an intelligent controller for monitoring this task.

Concluding Remarks

In order to ensure hydrodynamic and structural stability during a salvage operation using buoyant systems, it is required to design two types of control sub systems; a primary controller for regulating the flow rate of filling gas inside the lift bags and a secondary controller for regulating the purging of gas through the valves fitted on lift bags. Then a supervisory controller should be designed to monitor or switch between these sub controllers according to the buoyancy requirement for a stable ascent.

2 Aim and Approach of the Research

The primary aim of this research is to develop a numerical simulation tool for the dynamics of raising sunken vessel using buoyant systems by modeling the equation of motion in diving plane and regulating the motion variables by designing suitable control techniques to ensure a safe and steady ascent.

A rigid body state space model will be developed after formulating the equation of motion in the diving plane for integrating the controller techniques. At the beginning, a proportional derivative (PD) controller will be designed as the primary controller for regulating flow rate of filling gas inside the lift bags according to buoyancy requirement. Then the control strategy will be extended to other classic controls like proportional integral and derivative (PID) controller and sliding mode controller (SMC) for improving the performance. A sensitivity analysis will be performed on these controllers by taking account of considerable variation in hydrodynamic coefficients and suction breakout force. The performance of the controllers under the effect of external disturbances and uncertainties will also be investigated. Numerical simulations will be performed on a pontoon model in MATLAB & SIMULINK by solving the State Dependent Ricatti Equation (SDRE) in body-fixed coordinate system by using a numerical integration routine with variable time-step size.

The performance of the already designed conventional sliding mode controller (CSMC) will be improved by integrating it with fuzzy logic algorithm to bring together the advantages of both controllers. A two input fuzzy sliding mode controller (TIFSMC) will be designed first and simplified to single input fuzzy sliding mode controller (SIFSMC), for reducing the tuning effort and computational time. Fuzzy logic controllers will be designed using MATLAB's fuzzy logic interface and the combined models will be developed in SIMULINK. The comparative performance of the fussy sliding mode controllers over CSMC will be investigated by performing numerical simulations on the pontoon model.

A PID controller will be designed as the secondary controller to regulate the purge valve opening fitted on the lift bags according to the excess buoyancy available after suction breakout and to the variation in pressure difference between gas inside the lift bags and surrounding sea water pressure for a stable ascent. Then a supervisory fuzzy logic controller will be designed to monitor or switch between the primary and secondary controllers based on the depth error and depth rate.

Finally, in order to find the optimum location of lift bags on the vessel and to determine the controlled response of individual lift bags or the real case of lifting a sunken vessel using **multiple controlled lift bags**, the problem will be extended to a detailed flexible body modeling and control. For that a model analysis will be performed on a chemical tanker by approximating it as an Euler-Bernoulli beam with free-free boundary conditions and modal reduction techniques will be used to obtain the smallest state space model of individual lift bags. Supervisory fuzzy logic controller will be integrated with these state space models to obtain the controlled responses of individual lift bags.

3 Critical Review

An extensive review of literatures available from sources such as internet, journals, research papers and books related to marine salvage, buoyancy systems, dynamics of marine vehicles, marine control systems and soil-structure interaction problems is presented. Those contributed to the present study are described briefly in the current section. As far as marine salvage operation is concerned, literature sources reporting systematic data and information useful for system modeling are relatively few.

3.1 State-of-the-art of Marine Salvage

In more recent years, the most publicized salvage was performed by an American treasure hunter Mel Fisher in very shallow water say 60 feet. He spent 17 years of his life in marine salvage industry. At this time, numerous individuals and groups have spent millions for doing research in this field with some success though majority are unpublished. After World War I, a Royal Navy ship "Laurentic" which was sunk by a mine near Greenland, led to a salvage of 14 tons of gold worth $550,000,000 at current value in the form of 3211 ingots, leaving only 25 ingots behind. In the 30's, 5½ tons of gold and 42 tons of sliver were salvaged from a sunken ship, the "Egypt", by a private Italian company Sorina. During World War II, a remarkable salvor, Sir Williams retrieved a multimillion dollar cargo of gold from a sunken British ship "Niagara" by an observation bell, which was fired by Japanese during the voyage from Singapore to Australia. Most of these divers went free diving-using no equipment and staying submerged as long as their breath lasted (say 5 or 6 minutes) [43, 45, 86, 125]. It is observed that the divers can work and perform well in shallow water, though the practicality of divers decreases drastically with depth and the accompanying decompression. Divers have the advantages of human vision, judgement and manipulative skills. However, depth limitations, dive duration, risk, support requirements and cost often offset these advantages [121-125].

In late 19th century, Mr. Denerouz invented a self contained underwater breathing apparatus and later in 1933, Commandant Yves Le Prieur developed a SCUBA system with a full face mask and free flow system. With the invention of SCUBA, the diving became a recognized method for salvage as well as deploying and recovering subsea equipments. The current experimentation and research in advanced diving systems utilizing pressurized habitats, lock-out saturated diving techniques and the various combinations for deep diving [43, 121-122].

Another milestone in the history of marine salvage is the appearance of manned submersibles and ROVs. Manned submersibles and atmospheric diving systems take man deeper than ambient pressure diving and incur no decompression debt. Perry developed a relatively small exploratory submersible PC3B that was used to trace a sunken atomic bomb off Spain. Later highly sophisticated submarines capable of diving up to 20000 ft like Woods Hole "Alvin" and Ifremer's "Nautile" are appeared. These submarines are capable of exploring 97% of the bottom of the sea. The manned submersibles are generally limited to 1000 meters. Also they have short endurance due to human physical and psychological limitations and are costly to operate because of requirements to to ensure human safety. Owing to the dangers associated with deep-sea diving, Remotely Operated Vehicles (ROV) linked to the surface by umbilical started to replace human divers in the late 1970's, to carry out observation, inspection and recovery tasks. One of the most widely used ROV was the eyeball RCV 225 and later ROVs ahave progressed to some very sophisticated equipment like AT & T's "Scrab" capable of cutting and burying cable, digging trenches and making surveys. Then hybrid ROVs like "Mantis" having dual capability of being used with a pilot and/or having an autopilot have been developed. These ROVs can perform complicated tasks via tele-operation by human pilots on the surface vessels. However, the dragging force on the tether, time delay and operator fatigue make them difficult to operate and the daily operating cost is still expensive. Further developments in the field of sub-sea robotics led to the Autonomous Underwater Vehicles (AUV). Such AUVs benefit from an on-board autonomous control system and can be linked to the surface via an acoustic modem to allow for the monitoring of the vehicle during a mission. They are more mobile and could have much wider reachable scope than ROVs. On-board power and intelligence could help AUV self-react properly to changes in the system and its environment, thus avoiding many disastrous

situations. With the continuous advancements in navigation, control, artificial intelligence, material science, computer, sensor and communication systems, AUVs have become a very attractive platform in exploring the oceans, and numerous AUV prototypes have been developed, such as ODIN, REMUS, and ODYSSEY etc [43, 45, 86, 121-125].

The primary method of salvaging a sunken vessel is by means of providing self lift. The conventional method of obtaining self-lift is by introducing compressed air in to a compartment or tank. To do this, initially the space that is to be dewatered must be sufficiently sealed to hold air pressure of few pounds over that of ambient sea pressure. Main ballast tanks that are intact can be blown down if the vents are closed and water may have expelled through the opening at the bottom. Another recent development has been the application of generated in-place foams to displace water from within salvage objects that considerably reduce the external lift requirement. The depth range for the use of foam will be from 400 to 600 feet with water temperatures ranging from 29^0F to 70^0 F. A well known example was the use of two-component-urethane foam supplied in self-contained pressurized containers. When viewing the self lift aspects of past salvage operations, it is revealed that self-lift alone was never successful except when the vessel was near enough to the surface to be entered through hatches which were, or could be extended via cofferdams to a point above water. A well known example for this case is the unsuccessful salvage of submarine 'S-5' (875 tons) in 1920 as it discarded the use of any external lifting forces, while included only self-lift and required removal of water from all compartments and tanks. It is concluded that the external lift may be the deciding factor that makes the salvage success or failure [121-123].

Source of external lift includes surface vessels such as lift ships and barges, floating cranes and submersible pontoons. Salvage ships, lift craft and cranes use purchase lift systems to raise whole or parts of sunken ships. Navy salvage ships can bow lift up to 200 tons, lift craft 600 tons over the stern and commercial cranes over 7,500 tons. Some sheer leg cranes can lift over 3,600 tons. Combining crane and sheer leg purchases with deck purchases will increase the lift capacity. Lift ships have sheaves at the bow through which the lift cables are led to winches on deck. These lifting cables are hauled in by the winches or with a block and tackle purchase

arrangement. Lift barges have several lift stations in each side and are generally used in pairs. The wire cable slings are rigged between them and hoisting is accomplished by block and tackle power on deck. Lift ships and barge have floodable spaces permitting large changes in draft, in combination with tidal action to make lifts. U.S.Navy has raised sunken submarine 'USS F-4' having dead weight 400 tons off Honolulu harbor in 1915 from a depth of 306 feet by the method of sweeping wire cables and chain slings under the hull and lifting with the scows. By using a command lift ship USNS MIZAR, U.S. Navy has recovered a deep research vessel, ALVIN from a depth of 5051 feet of Cape Cod, Massachusetts with the aid of a manned deep diving submersible DRV ALUMINAUT by attaching lift lines with her two manipulators and lifted to the surface in 1969. British salvage operations recovered the wreck of HMS THETIS by using a specially designed lift ship that literally hauls the sunken vessel from bottom by cables at the surface in 1939. TRUCULENT was salvaged in 1950 by using two large lift ships each having 600 tons lift capacity and also blowing out the main ballast tanks. In 1966, a German sunken submarine 'HAI' was raised to the surface by a sea-going crane 'MAGNUS III' having improved sea keeping qualities. SMIT [107] has lifted a sunken Russian nuclear submarine 'Kursk' using a semi submersible barge 'Giant 4' and returning her safely to the port of Murmansk. With the assistance of floating sheerlegs, SMIT salvage [107] removed the wreck of a 17645 DWT chemical tanker 'Vicuna' that had undergone an explosion and sank in the port of Paranagua, Brazil, while the ship was discharging methanol at Cattalini pier. Floating cranes are generally found to be less seaworthy than other floating vessels because of the height of the crane boom, though they have the advantage in boom reach [121-125].

Submersible pontoons can provide a major external lift force of pre calculated amounts. Once the attachment is made, the pontoon become a valuable tool as it is not affected by sea state and can be left for long periods while other pontoons are being rigged. With the aid of salvage pontoons, U.S.Navy has recovered sunken submarines 'S-4' in 1924 and 'S-51' in 1925. Salvage pontoons are found to be a suitable choice for lifting sunken vessels and were used for the recovery of sunken submarine SQUALUS in 1939. In this case, control pontoons were used for limiting the distance the ship was lifted. With this invention, there had been a significant change in the techniques for raising sunken submarine within the limits of diving capability. But the problem

with the use of salvage pontoons is the lack of experienced personnel and realistic training. In order to gain experience, in 1969, U.S. Navy conducted an exercise of lifting a sunken submarine 'ex-HAKE' from a depth of 100 feet by using salvage pontoons in Chesapeake Bay. With this experience, U.S. Navy successfully righted and refloated a capsized destroyer escort hulk "REUBEN JAMES" with salvage pontoons in 1970. By the combined use of salvage pontoons and floating cranes, U.S. Navy successfully lifted a sunken harbor tug YTM-538. Collapsible pontoons of rubber and fabric have been used for test and evaluation basics only as in the salvage exercise involving ex-German submarines U-1105 and U-3008. Their advantage lies in the ease of transporting them to the salvage site and of handling them during placement, but they are vulnerable to damage and unreliable. It is noticed that collapsible pontoons of multi-ply construction have proved to be satisfactory after transporting them in commercial containers [121-123].

Lifting items with the ROV can be the simplest and most reliable type of recovery method (although the lift capacity is very small). ROVs may lift by gripping the target with its manipulator or through the application of a special recovery tool. The ship must recover the vehicle with the target attached or the target must be re-rigged for recovery when the ROV nears the surface. With the use of ROVs, SMIT Salvage team [107] succeeded in lifting the Japanese fishing vessel 'Ehime Maru', which sank after a collision with a submarine from a depth of 600 meters. SMIT [107] has developed a diverless pollutant recovery system 'POLREC' which is capable of recovering oils, chemicals and other pollutants from wrecks in very deep water. The POLREC system utilizes a remote operated offloading unit that is cost effective as well as enables a diverless solution for the recovery of pollutants. By using POLREC system, SMIT Salvage successfully recovered the 4000 tonnes of styrene cargo on board of the chemical tanker 'Ievoli Sun' that sank during a storm in the Channel near France at a depth of 95 meters. The POLREC system has also proved to be cost effective in the successful recovery of pollutants from tanker wrecks off the Korean and French coast. These kind of ROVs, can be used in higher water depths and they are highly controllable. Nevertheless, the major drawback is the lift capacity of the vehicle as it is limited by the size and power of the thrusters used for the propulsion.

Another threshold is the use of inflated bags for lifting sunken objects in an immersed fluid. These range from ballast baskets to pontoon bags, air bags and lift bags with a lifting capacity 25 kg to 600 metric tons and can be used as a means of lifting sunken objects without the use of heavy cranes and equipment [32, 61, 86, 98, 107, 113-119, 125]. These kinds of buoyant systems can be used for lifting any size of objects from any depth with comparatively less costs. But the problem with the use of lift bags is how to control the vertical acceleration during the ascent. In order to achieve some control over the ascent, some of the modern lift bags are fitted with manual dump valves that are attached to a lanyard for manually controlling the purging of gas by a diver. However, a problem arises when the lift bags being in the dynamic marine environment start to spin on their vertical axis due to the high current and seas, which causes the umbilical to become wrapped around the bag and cuts off the air vent and leads to an uncontrolled ascent. As a remedy for these cases, Farrell & Wood [32] designed an automatic purge valve to control a lift bag's ascent by limiting the expansion of gas through the valve installed on top of the lift bag. The automated purge valve monitors the changes in pressure to determine the ascent velocity of the lift bag and the resulting velocity is then evaluated by a proportional, integral and derivative (PID) control algorithm that outputs a signal to a purge valve installed on the top of the lift bag. The purge valve then opens or closes to control the purging of the expanded air volume and thereby allowing a smooth controlled ascent. The main drawback of this automatic purge valve system is that it never accounts the effect of suction breakout and hydrodynamic forces in the system modeling. Also the process of filling gas inside the lift bags is not controlled. Hence a safe and stable salving operation cannot be ensured. Nicholls-Lee et al. [86] investigated the concept design of a light weight cryogenic buoyancy system for the controlled removal of heavy objects from the sea bed. The system can be used to lift or lower large displacement objects under full remote control for a maximum depth of 350 m. But the limitation of this system is that in the modeling, they never include hydrodynamic forces in the system of equations and formulated only the equation of motion in vertical direction (heave), hence it is not suitable for controlling the pitch motions of the payload. Drobyshevski [26] presented stability aspects of up righting a capsized ship in the inverted mode and derived a mathematical formula for estimating

the maximum lift force supported by the lift bags.

From the literature review, out of the various salvage techniques, the buoyant systems or lift bags are found to be the most suitable choice for lifting any vessel from any depth with comparatatively less costs. But the main problem associated with the use of lift bags is how to control the ascent velocity and pitch angle during the ascent. It seems that there is no simulation system currently available for modeling and control of buoyant systems to salvage sunken vessels from sea bottom. Therefore a further literature survey is carried out about the modeling dynamics of raising sunken vessels using buoyant systems and how to maintain hydrodynamic stability by designing suitable control techniques to ensure a safe and stable ascent as explained in the next section.

3.2 Modelling Dynamics and Selection of Industrial Control Systems

The mathematical formulation for the salvage dynamics and relative performance of industrial control systems adaptable for a safe and viable salvage operation has been investigated by conducting a literature survey about dynamics of underwater vehicles, marine control systems, soil-structure interaction problems, buoyancy systems and robotics.

A critical review of literatures related to dynamics of marine vehicles, marine control systems such as Proportional Derivative controller (PD), Proportional Integral and Derivative controller (PID), Sliding Mode Controller (SMC), Fuzzy Logic Controller (FLC) and Neural Network (NN) has been carried out. Those which contributed to the present study are briefly described below.

Underwater vehicle dynamics is highly nonlinear, coupled and time-varying. In addition to these, the hydrodynamic parameters are often poorly known and the vehicle may be subjected to unknown forces due to ocean currents. These difficulties make the control problem challenging. A well established model for marine vehicles in the control communities at present time is

described in Fossen [36] and Fossen [37]. It is a nonlinear six degree of freedom (DOF) model, written as an Euler-Lagrange system where the main force contributors are divided into separated terms. This makes the system easy to follow and a popular tool for nonlinear control and observer design. Perez and Fossen [92] derived the kinematic models that are used for the transformation of motion variables and forces between different coordinate systems used in both sea keeping and maneuvering problems. An advantage of this formulation is the use of matrix notation and operations that can be easily carried out in MATLAB. Many solutions have been proposed to solve the nonlinear complex problem of three dimensional tracking of underwater vehicles. A common approach applied has been to linearize the nonlinear dynamics about certain operating points usually given by the forward speed. Fjellstad [34] investigated the automatic feedback control of unmanned underwater vehicles (UUV). Euler quaternions are used for representing the singularity free attitude representation. It is found that, Euler parameters provide less computational effort in the calculation of kinematic equations in comparison with Euler angles. Fossen & Johansen [38] presented a survey of control allocation methods for over actuated vessels by modeling them as optimization problems, in order to minimize the use of control effort subject to actuator rate and position constraints, power constraints as well as operational constraints. Fossen & Paulson [39] derived a direct adaptive autopilot based on feedback linearization for the steering of ships. It is observed that the optimal course-keeping autopilots are superior to conventional autopilots in terms of performance and fuel economy. Paulsen et al. [89] derived an output feedback control system with a wave filter for providing asymptotic stability for marine vehicles. Simulation results shows that the rudder action required for this kind of controller is significantly less compared to PD controllers without wave filter. Fossen and Perez [40] addressed the problem of positioning and heading control of ships and offshore rigs by using Kalman filter and thus avoids the oscillatory wave induced motion from velocity and position measuring instruments.

Stansbery & Cloutier [110] developed a State Dependent Riccati Equation (SDRE) control method to maneuver a space craft in to the close proximity of a tumbling target. To demonstrate the performance of the controller, a six degree of freedom model was formed. The resulting controller produced desirable response to a wide range of target attitude variations as well as

position offsets from the target. Caccia & Veruggio [13] designed a general purpose guidance and control system based on an outer control loop generating reference values for inner speed controllers to execute user-defined task functions for unmanned under water vehicle autopilot performing auto heading, auto depth and auto speed operations. This approach, which does not require any pre planning, proved its feasibility in controlling the vehicle's motion in the presence of a high uncertainty in position estimates, typical of underwater robotics, and, because of its Lyapunov-based nature, seems to be suitable for accomplishing reactive guidance tasks in unknown environments. Hong-jian et al. [51] developed a semi physical virtual simulation system, which acts as a capable tool for long range training and intelligent behavioral operation for an AUV.

Among various control techniques, the proportional-integral-derivative (PID) controller is found to be one of the dominant classical control techniques suitable for linear underwater vehicle control systems. But tuning the control coefficients K_P, K_I, and K_D for a desired performance is one of the difficult problems faced by control engineers. Ziegler & Nichols [150] has proposed a classical technique for determining the optimal combination of three control coefficients. Lee et al. [72] designed a 6 DOF PID controller for determining the attitude and position of AUVs. They proposed a Clonal Selection algorithm for tuning the control coefficients. It is observed that the proposed technique provides better responses than the existing Ziegler-Nichols technique with respect to the settling time, overshoot and an affinity in submerging under water and turning the yaw angle through simulation. Bakkeheim et al. [9] used a Lypunov function as a design tool on a Proportional- Integral (PI) controller for marine thruster speed control by integrator resetting in order to improve the transient performance of the system with dynamic controllers. Alfro-Cid et al. [3-4] developed two PID controllers for the navigation and propulsion systems of an oil platform supply ship- Cyber Ship II. The control parameters have been optimized using genetic algorithms. Moreira et al [83] developed a two – dimensional path following guidance and control system for an autonomous marine surface vehicle, using a way- point guidance system, which is formulated based on the line of sight projection algorithm. The speed controller is achieved through state feedback linearization and heading controller is obtained through a

PID. It is seen that the presented approach can be extended to higher dimensional control and guidance problems.

The sliding mode controller (SMC) due to its robustness against modeling imprecisions and external disturbances has been successfully applied to the dynamic control of underwater vehicles. The SMC is a variable structure controller that restricts the system states inside a certain subspace of the whole state space and makes them asymptotically converge to their equilibrium point. It became widespread after the publication of a book by Itkis [57] and a paper by Utkin [126]. Yoerger and Slotine [139] and Healey and Lienard [49] at the Naval Postgraduate School (NPS) were among the first to demonstrate the applications of SMC to an AUV. Yorger & Slotine [139] developed a sliding mode depth controller for trajectory control of underwater vehicles neglecting cross coupling terms. They have investigated the effects of uncertainty of the hydrodynamic coefficients and negligence of cross-coupling terms by conducting computer simulations. Healey and Lienard [49] proposed multi variable sliding mode autopilot for the combined steering, diving and speed control of Autonomous Underwater Vehicles (AUV) with decoupled design. The proposed controller provides stability in vertical plane. Cristi et al. [22] applied the adaptive sliding mode control on an Autonomous Underwater Vehicle (AUV) in the diving plane, in which they used the adaptive control for compensating linear parameter uncertainties and the sliding mode control for handling the nonlinear systems. Fossen [37] described the use of a multi variable sliding mode controller in dynamic positioning of remotely operated vehicles (ROV). Dougherty & Woolweaver [25] investigated the efficacies of sliding mode control on the MUST vehicle. From the analysis it is found that sliding mode control has proved its capability in handling an uncertainty of the order of 50% in the estimation of the vehicles hydrodynamic parameters in the case of the heading and depth control of underwater vehicles. Jomes-Rui et al. [60] described the modeling and control of a remotely operated vehicle (ROV) using sliding mode controller and PID controllers. From the analysis it is found that results obtained from sliding mode controllers are much better than PID controllers.

Even though SMC has been well known for its robustness to parameter variations, it has the inherent problem of chattering phenomenon. This high-frequency control activity causes high heat losses in electrical power circuits and premature wear in actuators. In addition, the high control activity may excite unmodelled high-frequency dynamics, which in turn causes degradation to the controller performance. To overcome the undesired effects of chattering, Slotine & Li [105] proposed the adoption of a thin boundary layer neighbouring the switching surface, by replacing the sign function by a saturation function. The boundary layer approach makes the control activity continuous within the boundary layer and discontinuous outside the boundary layer. The adoption of a properly designed thin boundary layer has proven effective in completely eliminating chattering, however, leading to an inferior tracking performance. McGookin [80] presented the simulation results of a guidance and control system for homing and docking operations of an autonomous under water vehicle (AUV) using an optimal higher order sliding mode controller based on the State Dependent Riccatic Equation (SDRE). It is seen that higher order sliding mode controllers provide a minimum of controller effort and avoid chattering. Lee et al. [72] presented a discrete - time quasi sliding mode controller for the depth and contouring control of an autonomous underwater vehicle VORAM in the presence of parameter uncertainties and a long sampling interval. It is observed that the controller makes the system stable without any observer even in the presence of system uncertainties and external disturbances. Salgado & Jouvencel [100] proposed a higher order sliding mode controller for the depth control of a torpedo shaped AUV "TAIPAN" to avoid the chattering effects as inherently seen with conventional sliding mode controller. The results are compared with a conventional sliding mode controller and a PD controller. It is found that higher order sliding mode controller is faster and precise than other control laws. Soylu et al. [108] designed a chattering free sliding mode controller for the trajectory control of remotely operated vehicles (ROVs). The controller uses an adaptive term instead of the conventional discontinuous switching term, which continuously compensates for the unknown system dynamics caused by poorly approximated non linear hydrodynamics or sudden environmental loads.

The process of obtaining optimal performance from a SMC involves tuning important design parameters associated with it. For an inexperienced designer, this parameter tuning process can

be extremely tedious and time consuming. Therefore parameter optimization techniques like Genetic Algorithm are used nowadays for an optimum performance. This method of parameter optimization provides solutions for a given problem by emulating the natural evolution process of species. McGookin & Murray-Smith [81] developed a genetic algorithm for the optimization of a sliding mode controller for the diving and heading maneuvers of a linear submarine model. From the analysis it is shown that for submarine applications, Genetic Algorithms provided a much faster method for obtaining an optimum design than conventional tuning based on trial and error methods.

Because of the possibility to express human experience in an algorithmic manner, fuzzy logic has been largely employed in dynamic control of underwater systems. Fuzzy logic control (FLC) has become a developing area of research after the introduction of fuzzy logic by Zadeh [147]. In Fuzzy logic controllers, the controlling action is through artificial intelligence i.e. linguistic expressions (fuzzy rules) based on the knowledge of operator. Therefore FLC is suitable for controlling the systems with complex, ill-defined, time varying and non linear dynamics. The theoretical basis of fuzzy logic control (FLC) is that any real continuous function over a compact set can be approximated to any degree of accuracy by the fuzzy inference system. A fuzzy system provides an effective approach to handle nonlinear systems even without knowing the proper system dynamics by the smooth approximation of a nonlinear mapping from system input space to system output space. DeBitetto [24] has investigated a 14-rule fuzzy logic controller for the depth control of a UUV. Ren & Yang [97] proposed a novel approach to meet the attitude control of a fully submerged hydrofoil catamaran through a Tagaki- Sugeno (T-S) fuzzy interpolation system. The effectiveness of the fuzzy controller is demonstrated by conducting simulation on the vessel “HB200BA1”. However, determining the linguistic rules and the membership functions requires experimental data and, therefore, very time-consuming and it is difficult to determine response time and stability.

Due to the similarity between the Fuzzy logic control & Sliding mode controller, there is a growing technique to integrate the advantages of FLC & SMC to acquire stability, optimum

performance and robustness is an acting area of research in control engineering, which leads to the design of fuzzy sliding mode controller (FSMC). The first approach taken by many researchers is to use FLC for the determination of the movement of the sliding surface of a classical SMC. Lee et al. [75] developed a SMC with a fuzzy variable boundary layer. In this controller, the absolute value of the switching function and the angle between the switching function and state vector were used as inputs and the thickness of the boundary layer was obtained as the output. Choi et al. [17] suggested an important study, where a translation and rotation scheme has been defined for second-order systems and the existence of sliding mode with the linear time-varying sliding surface has been proved. Fung et al. [41] proposed a FSMC for a slider-crank mechanism, where switching function and its derivative were taken as inputs and change of control gain as output. Yagiz and Hacioglu [135] developed a fuzzy sliding mode controller in which a fuzzy logic algorithm is used for dynamically computing the sliding surface slope with respect to the error states. Robustness of the proposed controller is investigated by implementing it on a planner robot and the results have been compared with a conventional SMC and a PID controller. It is found that FSMC has supreme trajectory tracking ability compared to the other two methods without losing its robust behavior. Eksin et al. [27-29] introduced a single input single output FSMC with a self tuning sliding regime, where the slope of the sliding surface is continuously updated by a new time-varying coefficient. The proposed method shows good transient response over classical controller techniques and reduces tuning effort. Zhang et al. [148] proposed a fuzzy time-varying sliding mode controller with global robustness for non linear systems having uncertainties. Yorgancioglu and Komurcugil [141] proposed a single input fuzzy logic controller for continuously computing the slope of the sliding surface, with the result that the sliding surface is rotated in such a direction that the tracking performance of the system under control is improved. They have concluded that the proposed fuzzy moving sliding surface approach with one dimensional rule base significantly reduce the large number of linguistic fuzzy rules and hence reduces tuning effort and computational time in comparison with conventional controllers. In order to enhance the tracking performance inside the boundary layer, some adaptive strategy should be used for uncertainty/disturbance compensation. The problem of compensating uncertainty or disturbance in the dynamic positioning of remotely operated underwater vehicles is considered by Bessa et al. [11] by implementing an adaptive

fuzzy sliding mode controller for handling the stabilization and trajectory tracking problems. The adopted approach is based on the sliding mode control strategy and enhanced by an adaptive fuzzy algorithm. The stability and convergence properties of the closed-loop system are analytically proved using Lyapunov stability theory and Barbalat's lemma. It is observed that the incorporation of an adaptive fuzzy algorithm within the boundary layer made a better trade-off between tracking performance and chattering. Xin and Zaojian [133] developed a fuzzy sliding mode controller with adaptive disturbance approximation to deal with the tracking regulation of an underwater robot, where the stability and convergence of the closed loop system is satisfied by Lyapunov stability condition. Second approach for improving the performance of SMC is to adaptively tune the controller gain with respect to error states by a FLC. Abdelhameed [1] has proposed a technique to adaptively tune the switching gain of the sliding mode controller by using a fuzzy logic system, where a chattering index and the absolute values of the sliding function and its first derivative are used as inputs. Ha et al. [47] presented a fuzzy tuning approach to SMC for tracking-performance enhancement in a class of nonlinear systems. The sliding surface can rotate or shift in the phase space in such a direction that that tracking behavior can be improved. Tokat et al. [120] proposed new approaches for on-line tuning of the linear sliding surface slope in sliding mode controllers. A new switching function definition was made in new coordinate axes for better transient response. They observed that by adaptively tuning the control gain by fuzzy logic, the performance of the conventional sliding mode controller can be considerable improved such as reducing chattering, better tracking performance and good transient response.

Almost independently from above nonlinear control researches, due to the approximation capacities of neural networks (NN) for nonlinear mappings and their learning characteristics, considerable interests have been taken on the applications of neural networks to the subsea control problems [23, 54-56, 69-70, 90, 128, 130, 143-146]. Using NN in constructing controllers has the advantage that the dynamics of the controlled system need not be completely known. There are two main approaches in NN, one is learning with a forward model and the other is by direct learning. In the former approach, generally, the forward model is trained by the output error or state error and then used for gain derivation, while in the latter approach, the state

or output error is used directly to map the desired control input. Yuh [144] developed a neural network controller using a recursive adaptation algorithm with a critic function. (reinforced learning approach). The particularity of this controller is that the system has the capability to adjust itself online and directly without an explicit model of vehicle dynamics. The common feature of these neural network control schemes was just to approximate the smooth uncertainties of the vehicles' dynamics using general multi-layer neural networks, and the networks' weights values were updated by back propagation algorithm. Li & Lee [76] presented a semi-globally stable neural network adaptive control scheme for diving control of an AUV, where the unstructured uncertainties in the pitch motion of the vehicle are assumed to be unbounded, whereas they still satisfy certain growth conditions characterized by 'bounding functions'. Adaptation laws for the unknown bounds of uncertainties are derived from Lypunov-based method as well as the update laws of the networks' weights values. Under a certain relaxed assumptions on the control gain functions, the presented control scheme can guarantee that all the signals in the closed-loop system are uniformly ultimately bounded (UUB). Ishii et al. [56] have proposed a neural network based control system called "Self-Organizing Neural-Net-Controller System" (SONCS) for the heading control of an AUV "Twin-Burger". They have used a quick adaptation method of the controller called "Imaginary Training" to improve the time-consuming adaptation process of SONCS. However, it is difficult to obtain analytical results concerning with the stability of networks [70]. In practice, while we construct a neural network to approximate a given unknown dynamics, we could not exactly determine the number of hidden neurons or the basis of given unknown function a priori. Therefore, there always remains certain mismatching, that is the network's reconstruction error. For this reason, robustness has become one of the most important issues in the neural network control problems. Also NN-based controllers have the disadvantage that no formal mathematical characterization exists for the closed-loop system behavior. The validation of the final design can only be demonstrated experimentally.

3.3 Summary of Literature Survey

The effectiveness of various methods for recovering sunken vessels from sea bottom is examined and relative performance of industrial control systems adaptable for under water dynamics has also been investigated and leads to the following conclusions:

- Buoyant systems can be used for lifting any vessel from any depth with comparatively less costs. But control is the biggest problem.

- PD & PID controller are the simple classic controller technique suitable for linear deterministic systems, but they are not suitable for non linear systems involving uncertainty and external disturbances.

- SMC is found to be a suitable choice for handling non linear underwater problems having uncertainty arises due to external disturbances such as wind, current etc. SMC shows robustness, insensitiveness to parameter variations and external disturbance and good transient performance, but chattering is the disadvantage.

- FLC is the intelligent control technique suitable for complex systems where the system dynamics is properly unknown. Human experience can be incorporated, where it is difficult to check the stability and robustness, also expert knowledge and cycles of trial & error is required for the desired performance.

- Neural Network is much a complex intelligent control technique. Not suitable for real time control and there is unpredictability in training time.

- Due to the adaptive nature, FSMC is found to be the optimum choice for handling non linear underwater problems involving uncertainty, external disturbances, system modeling errors etc and avoids chattering associated with SMCs.

3.4 Contributions of the Thesis

- A mathematical formulation for the dynamics of raising sunken vessels using buoyant systems is developed according to the principles of submarine dynamics, soil-structure interaction problems and thermodynamics and a linear mathematical state space model is formulated in Section 4.1 for integrating the primary controller based on the two degree of freedom equation of motion in diving plane.

- Purge valve Modelling is carried out according to the work of Farell & Wood [33] in Section 4.2.

- The relative efficacies of various controller techniques as a primary controller for regulating the gas flow rate are investigated in this thesis. Initially a PD controller is designed to regulate the flow rate of filling gas inside the bags in Section 5.1.1 and then extended to a PID controller in Section 5.1.2 for superior performance. Later a conventional sliding mode controller is designed for the same purpose with robustness and capability to handle external disturbance, uncertainty and modeling errors in Section 5.1.3. The performances of these three classic controllers are investigated by conducting numerical simulation case studies on a pontoon model.

- The performance of the conventional sliding mode controller is improved by integrating it with fuzzy logic algorithms for dynamically computing the sliding surface slope and to adaptively tuning the controller gain to make fuzzy sliding mode controllers. A two input fuzzy sliding mode controller and a single input fuzzy sliding mode controller are designed in Section 6.1.1 and Section 6.1.2. The effectiveness of the proposed controllers

over conventional SMC is investigated by performing simulation on the pontoon model in Section 6.2.

- A PID controller is designed as the secondary controller to regulate the purge valve opening according to the excess buoyancy available after suction breakout and to the variation in pressure difference between gas inside the lift bag and surrounding sea water pressure for a stable ascent in Section 7.1.

- A supervisory fuzzy logic controller is designed in Chapter 8 to monitor or switch between the primary and secondary controllers for a safe and stable salvage operation.

- In order to find the optimum location of lift bags on the vessel and to determine the individual response of lift bags or to use multiple controlled lift bags, the rigid body modeling & control is extended to flexible body modeling & control in Chapter 9. A chemical tanker is appropriately selected for this purpose.

- Simulation programs are written in MATLAB & SIMULINK.

3.5 Organisation of the Thesis

The thesis is organized in to 11 chapters. Their contents are outlined as follows:

Chapter 4 is the rigid body mathematical modeling. In this section, a mathematical model describing the rigid body dynamics of lifting a sunken vessel using gas inflating systems will be presented and analyzed with respect to hydrostatic force due to weight, buoyancy and suction breakout and hydrodynamic forces in vertical diving plane. Here modeling is carried out in such a way that the variation of additional buoyancy provided by lift bags due to change in *gas flow rate* is taken as the control parameter. Purge valve modeling is carried out separately by considering the excess buoyancy available after suction breakout and to the pressure difference between gas inside the lift bags and surrounding sea water pressure in accordance with the depth variations for a stable ascent. Here *purge valve area* is considered to be the control parameter.

Chapter 5 is the primary controller design by conventional approach. A PD controller is initially selected as the primary controller for regulating the flow rate of filling gas inside the lift bags and then extended to PID and SMC for improving the performance. The effectiveness of these classic controllers is investigated by conducting numerical simulations on a pontoon model.

Chapter 6 presents the modification of primary controller by artificial intelligence. In this section a new design approach is implemented by integrating fuzzy logic algorithm with the sliding mode controller to bring together the advantages of both controllers. The performance of the CSMC is improved by dynamically computing the sliding surface by a FLC and adaptively tuning the controller gain by another FLC. A TIFSMC is designed first and simplified to SIFSMC for reducing the tuning effort and computational time. Computational simulations are carried out on the pontoon model to show the comparative performance of fuzzy sliding mode controllers over conventional sliding mode controller.

Chapter 7 discusses the design of the secondary controller. A PID controller is selected as the secondary controller to regulate the area of purge valve opening in accordance with the excess buoyancy available after suction breakout and according to the variation in pressure difference between the gas inside the lift bags and surrounding sea water pressure for a stable ascent.

Chapter 8 covers the design of supervisory controller. A fuzzy logic controller is designed to monitor or switch between the primary and secondary controllers for a safe and stable salvage operation.

Chapter 9 presents the flexible body modeling and control approach for the marine salvage operation. In order to find the optimum location of lift bags on the vessel and to find the controlled responses of individual lift bags, the rigid body modeling & control is extended to a detailed flexible body modeling & control. In this section, the vessel or payload is considered as an Euler-Bernoulli beam with free-free boundary conditions and the supervisory fuzzy logic controller is integrated to the smallest state space models of individual lift bags to obtain the controlled responses.

Chapter 10 describes the analysis of all numerical simulation results and leads to a number of conclusions.

Chapter 11 covers the future recommendations in the area of this research.

Appendix A contains the estimation of additional buoyancy required for inflating

Appendix B presents the derivation of analytical Solution of Euler- Bernoulli Beam with Free-Free boundary conditions.

4 Rigid Body Mathematical Modelling

Ship calculations for the salvaging operation are typically less detailed than those in the preliminary design, which depends on the available information pertaining to a particular ship scenario. A number of assumptions are usually required to simplify the problem. Forces acting on a sunken vessel consist of hydrostatic (i.e. weight, buoyancy and suction breakout force) and hydrodynamic components. The variation of hydrodynamic forces with velocities, accelerations and control surface deflections are expressed in terms of hydrodynamic coefficients. These coefficients can be derived from physical model tests or theory, the number of coefficients used being subject to the amount of data available, past experience etc. The most significant task in this thesis is how to model the salvage dynamics in a form which is suitable for integrating control techniques to ensure hydrodynamic stability during the ascent. Due to the coupled nature of salvage dynamics and to integrate controller techniques, the mathematical modeling is carried out as two subsystems. In the primary model, the salvage dynamics is formulated in such a way that the variation in additional buoyancy due to flow rate of filling gas inside the lift bags is the controlling force with respect to hydrostatic force due to weight, buoyancy and suction break out and hydrodynamic forces. In the secondary model, the purging of gas through the valve is taken as the contol parameter by accounting the excess buoyancy available after suction break out and to the variation in pressure difference between gas inside lift bag and surrounding sea water pressure for a stable ascent. The purpose of the simulation system is to bring the vessel with the lift bags just below the surface by the supervisory controller and towed to the nearby port.

4.1 Primary Model of a Raising Vessel

To describe the motion of a raising vessel, two reference frames are considered as seen in Figure 9, including the earth - and body-fixed frames. The origin of the body-fixed frame coincides with the centre of gravity (C_g) of the vessel being in the principle plane of symmetry. The origin of the earth-fixed coordinate system is considered to be fixed at sea bottom. The positions and orientations of the vessel (kinematic variables) are described with respect to the earth-fixed coordinates whereas the linear and angular velocities of the vessel (dynamic variables) are defined in body-fixed coordinates. The transformation between the two coordinate systems is done by Euler angles (Φ, θ, ψ) or by using kinematic relations [6, 36-37].

To describe the dynamics of the sunken vessel ascending from the seafloor, it is preliminarily assumed that:

- the vessel behaves as a rigid body
- the acceleration of a point on the surface of the earth is neglected,
- the external loads comprise of the breakout, hydrostatic and hydrodynamic components, and the seabed is flat creating a total breakout lift force of 1.3 times the ship's wet weight [101, 129].

4.1.1 Equations of Vessel Motion

As the problem is concerned with the dynamics of raising sunken vessels (i.e. the control surfaces are inactive and the depth control is by regulating the additional buoyancy provided by the inflating system), it is further assumed to consider only the diving or vertical-plane (surge, heave and pitch) motions in the stability analysis. However, the surge equation couples with heave and pitch, through the meta-centric height. This dynamic coupling could be eliminated by redefining hydrodynamic coefficients with respect to the ship's C_g instead of its geometric centre

[12, 22, 34, 65]. For a sunken vessel, it is also known that the forward speed is zero. However, due to external forces such as currents, the surge motion may exist, which can be considered as an external disturabance to the system. As an adaptive non linear controller can effectively handle system modeling errors, external disturbances and uncertainty and thereby maintain hydrodynamic stability in diving plane, so that in this study, we discard the surge terms in the development of equation of motion. Thus, the system model variables include the heave velocity (w), pitch angle (θ), pitch rate (q) and global depth position from sea bottom (z) [49, 50, 96, 105, 139-140].

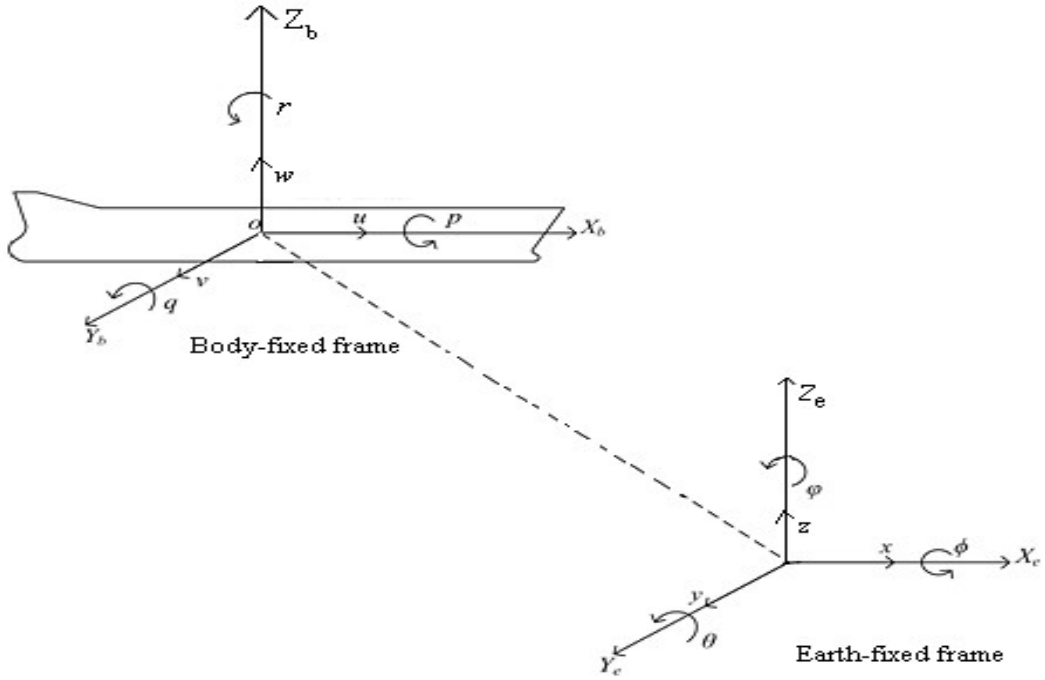

Figure 9: Vessel model and reference coordinates [36, 37]

The equations of motion presented here are the core of the simulation program in MATLAB & SIMULINK. These equations, using body axes variables are solved for the motions in diving plane. These variables are then transformed to the earth–fixed coordinates using the kinematic

relations (i.e. by Euler angles) [36-37]. The system is then placed in state space form so that state space model can be formed simply by assigning states to the associated variables.

According to Newton – Euler approach, the equations of motion for heave and pitch are [37]:

$$m\left(\dot{w} - x_G\dot{q} - z_G q^2\right) = Z \quad (1)$$

$$I_{yy}\dot{q} + m\left[z_G(wq) - x_G\dot{w}\right] = M \quad (2)$$

Where, m is the vessel mass, I_{yy} the mass moment of inertia, x_G, z_G the coordinates of the centre of gravity in X_b and Z_b directions respectively, Z the heave force and M the pitch moment.

The right hand side of the above equations consists of hydrostatic, hydrodynamic, break out and control force components.

4.1.1.1 Hydrostatic Force and Moments

Hydrostatic force and moments are due to the vessel weight W and buoyancy B. The buoyancy of the sunken vessel may be changed due to the sea density variation and to the compressibility of the hull, which can be accounted by considering a linear change in volume with depth.

Therefore, the buoyancy force provided by the sea water is given by [31]

$$B = \rho\nabla g + \mu z(\rho / \rho_o) \quad (3)$$

In which μ is the increase in buoyancy per unit increase in depth in sea water of standard density ρ_o, ρ the actual density of surrounding sea, ∇ the volumetric form displacement, g the gravitational acceleration and z the vertical coordinate position or depth from sea bottom.

The net hydrostatic force in the inertia coordinate system is (B-W) in the positive *Z* direction (upwards) (i.e. buoyancy is taken as positive and gravity is negative). Therefore, in the body-fixed coordinate system, the hydrostatic components of force and moments for heave/pitch motions are [36-37]:

$$Z_{hs} = (B - W)\cos\theta \tag{4}$$

$$M_{hs} = -(z_B B - z_G W)\sin\theta - (x_B B - x_G W)\cos\theta \tag{5}$$

Where θ is the pitch angle and $x_{B,}$ z_B are the coordinates of the centre of buoyancy in X_b and Z_b directions respectively.

4.1.1.2 Hydrodynamic Force and Moments

The hydrodynamic components of force and moments for heave/pitch motions are [12, 34, 36 - 37, 65, 96]:

$$Z_{hd} = Z_{\dot{w}}\dot{w} + Z_{\dot{q}}\dot{q} + Z_w w + Z_q q \tag{6}$$

$$M_{hd} = M_{\dot{w}}\dot{w} + M_{\dot{q}}\dot{q} + M_w w + M_q q \tag{7}$$

Where,

$$Z_{\dot{w}} = \frac{1}{2}\rho l^3 (Z_{\dot{w}}'), Z_{\dot{q}} = \frac{1}{2}\rho l^4 (Z_{\dot{q}}'), Z_w = \frac{1}{2}\rho l^2 (Z_w'), Z_q = \frac{1}{2}\rho l^3 (Z_q'),$$
$$M_{\dot{w}} = \frac{1}{2}\rho l^4 (M_{\dot{w}}'), M_{\dot{q}} = \frac{1}{2}\rho l^5 (M_{\dot{q}}'), M_w = \frac{1}{2}\rho l^3 (M_w'), M_q = \frac{1}{2}\rho l^4 (M_q') \tag{8}$$

in which $Z_{\dot{w}}'$ the non dimensional added mass coefficient in heave, $Z_{\dot{q}}'$ the non dimensional added mass coefficient in pitch, Z_w' & Z_q' are the non dimensional heave force coefficients induced by angle of attack, $M_{\dot{w}}'$ the non dimensional added mass moment of inertia coefficient in heave, $M_{\dot{q}}'$ the non dimensional added mass moment of inertia coefficient in pitch, M_w' & M_q' are the non

dimensional pitch moment coefficients from heave and pitch respectively and *l* is the length of the vessel. Forces and moments due to external disturbances such as wind, current etc that creates uncertainty during the marine salvage operation are also to be accounted during the controller design.

4.1.1.3 Breakout Force

The breakout or suction force (*R*) accounts for the difference between the total lift force required (*F*) and the object's wet weight (*G* = *W*-*B*). It is theoretically and empirically difficult to estimate this breakout force due to the involvement of several variables and unknowns. In general, the amount of breakout force & estimation of break out time depends on the seafloor soil characteristics (i.e. the compressibility of soil skeleton and pore water, permeability etc.), the embedment depth and time, the object shape parameters and the loading conditions. The total lift force (*F*) required for the complete extraction of the object from the sea bottom should be greater than their submerged weight (*G*) due to the ground reaction (*R*) exerted by the soil (see Figure 10) [35, 82, 101, 129].

Sawicki and Mierczynski [101] proposed a simple formula for the estimation of total lift force as:

$$F = G + R = (1 + k_p) * G \tag{9}$$

Where k_p is an empirical coefficient depending on the nature of subsoil and its values are given as [101]:

$$\mathrm{k_p} = \begin{cases} 0.05\text{-}0.1 & \text{coarse} & \text{sand} \\ 0.15\text{-}0.20 & \text{fine} & \text{sand} \\ 0.25\text{-}0.45 & \text{clayey} & \text{bottom} \end{cases} \tag{10}$$

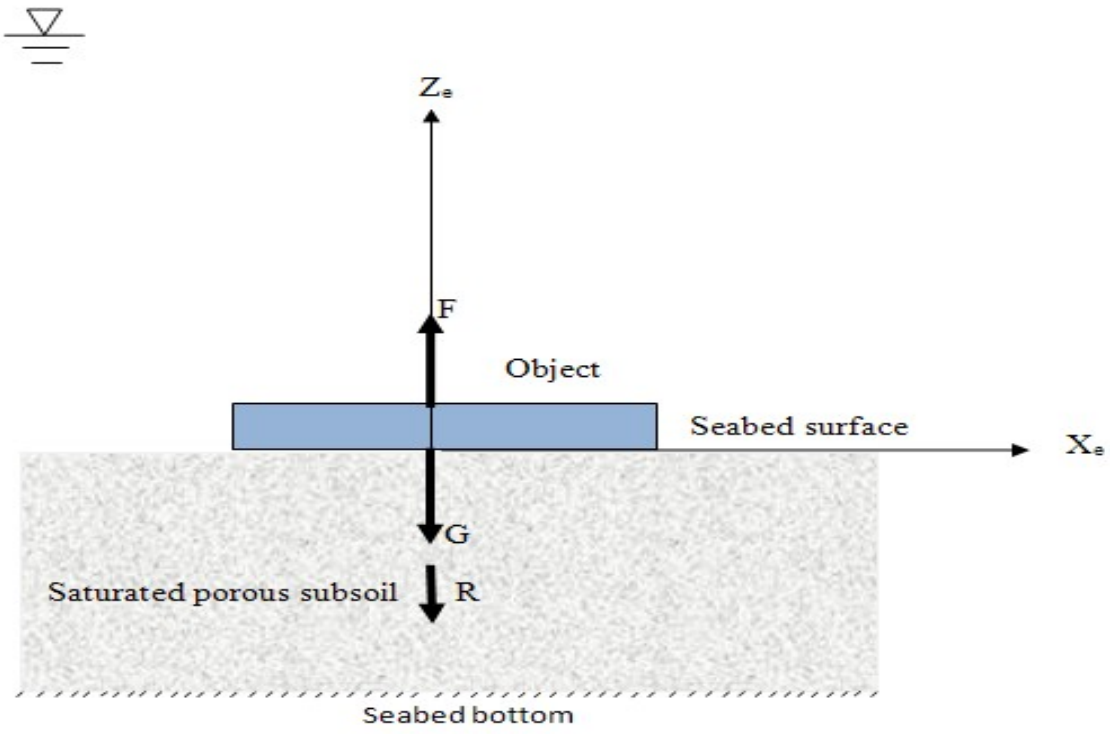

Figure 10: Lift force model to extract an object from the seabed [101]

Vaudrey [129] investigated the efficacy of 3 analytical methods (i.e. Muga, Liu and Lee methods) for the prediction of breakout forces with different object shapes such as a cylinder, sphere and block, with and without breakout force reduction techniques. From the analysis, it was observed that the use of breakout reduction methods such as the mud suction tubes, water flooding and air jetting would reduce the total lift force by approximately 15% and eliminate the snap loading condition. The selection of breakout reduction methods depends on the particular salvage operation, bottom soil conditions and the availability of equipments. From the above literature [101,129], the total lift force is assumed to be 1.3 times the wet weight of the vessel. Break out time can be calculated based on the work of Mei et al [82] & Foda [35]. Note that the

break out component of suction lift force is only 0.3 times the wet weight in the negative *Z* direction.

Therefore, heave component of break out suction force in body fixed coordinate system (i.e. in positive *Z* direction) can be written as:

$$Z_{suction} = 0.3\,(B - W)\cos\theta \tag{11}$$

Similarly, pitch component of break out suction force in body fixed frame can be written as:

$$M_{suction} = 0.3*[-(z_B B - z_G W)\sin\theta - (x_B B - x_G W)\cos\theta] \tag{12}$$

4.1.1.4 Control Force: - Additional Buoyancy provided by the Inflating System

For the sunken vessel resting on the seafloor, the vessel weight is balanced by both the buoyancy and the ground reaction. Additional force required to lift the vessel should overcome both the in-water object weight and the ground reaction. This force, described in terms of the buoyancy, could be provided by the volume of gas inside the lift bags. The gas-generating system (solid, liquid or cryogenic pressurised system) is used such that the produced gas is pumped into the lift bags at a desired flow rate using pipes for a stable ascent.

The variation of volume with respect to time in the lift bags is accounted by considering the flow rate of filling gas inside the lift bags as follows:

Therefore, the control parameter is:

$$u_c = \frac{dV}{dt} = \dot{V} = f \tag{13}$$

Where f *is* the gas flow rate (m^3/s).

Consequently, the additional buoyancy provided by the lift bags can be written as:

$$B_a = (\rho - \rho_g)gV \quad (14)$$

The components of additional buoyancy for heave mode in body fixed frame can be written as:

$$B_{ah} = (\rho - \rho_g)gV\cos\theta \quad (15)$$

Similarly, the components of additional buoyancy per unit time for the pitch mode can be written as:

$$B_{ap} = -z_B(\rho - \rho_g)gV\sin\theta - x_B(\rho - \rho_g)gV\cos\theta \quad (16)$$

4.1.2 Kinematic Relations

The kinematic relations are used to transform the motion variables from local to global coordinate systems. The kinematic relations for heave and pitch can be obtained from Fossen [36] and Fossen [37]:

The simplified kinematic relations for heave and pitch motions are (u, v, p, r, Φ=0):

$$\dot{z} = w\cos\theta \quad (17)$$

$$\dot{\theta} = q \quad (18)$$

4.1.3 Development of State-Space Model

By accounting the components of hydrostatic, hydrodynamic, suction break out and additional buoyancy force components, the equation of motion for heave mode can be rewritten from Eq. (1) as:

I.e by integrating Eqs. (4), (6), (11) & (15) in Eq. (1),

$$m\left(\dot{w}-x_G\dot{q}-z_Gq^2\right)=(B-W)\cos\theta+Z_{\dot{w}}\dot{w}+Z_{\dot{q}}\dot{q}+Z_w w+Z_q q+0.3(B-W)\cos\theta+(\rho-\rho_g)gV\cos\theta \quad (19)$$

Similarly equation of motion for pitch mode can be modified from Eq. (2) by integrating Eqs. (5), (7), (12) & (16) as:

$$I_{yy}\dot{q}+m\left[z_G(wq)-x_G\dot{w}\right]=-(z_BB-z_GW)\sin\theta-(x_BB-x_GW)\cos\theta+M_{\dot{w}}\dot{w}+M_{\dot{q}}\dot{q}+M_w w+M_q q+$$
$$0.3*[-(z_BB-z_GW)\sin\theta-(x_BB-x_GW)\cos\theta]-z_B(\rho-\rho_g)gV\sin\theta-x_B(\rho-\rho_g)gV\cos\theta \quad (20)$$

For small values of pitch angle, it is assumed that $\sin\theta = \theta$ and $\cos\theta=1$. Imposing linearization about an equilibrium point (i.e. discarding q^2 term) and neglecting the products of small motions or coupled terms (i.e. neglecting *wq* term), the equations of motion for heave and pitch mode can be rewritten from Eqs. (19) & (20) as:

$$m\left(\dot{w}-x_G\dot{q}\right)=1.3(B-W)+Z_{\dot{w}}\dot{w}+Z_{\dot{q}}\dot{q}+Z_w w+Z_q q+(\rho-\rho_g)gV \quad (21)$$

$$I_{yy}\dot{q}+m\left[-x_G\dot{w}\right]=-1.3(z_BB-z_GW)\theta-1.3(x_BB-x_GW)+M_{\dot{w}}\dot{w}+M_{\dot{q}}\dot{q}+M_w w+M_q q+$$
$$-z_B(\rho-\rho_g)gV\theta-x_B(\rho-\rho_g)gV \quad (22)$$

Kinematic relation for heave mode can be modified from Eq. (17) as:

$$\dot{z}=w \quad (23)$$

Eqs. (21) & (22) can be rearranged as:

$$(-mx_G-Z_{\dot{q}})\dot{q}+(m-Z_{\dot{w}})\dot{w}=Z_w w+Z_q q+1.3(B-W)+(\rho-\rho_g)gV \quad (24)$$

$$(I_{yy} - M_{\dot{q}})\dot{q} + (-mx_G - M_{\dot{w}})\dot{w} = M_w w + M_q q - 1.3(z_B B - z_G W)\theta \\ -1.3(x_B B - x_G W) - z_B(\rho - \rho_g)gV\theta - x_B(\rho - \rho_g)gV \quad (25)$$

Eqs. (24) & (25) along with kinematic relations in Eqs. (23) & (18) to form the state space model as:

$$\begin{bmatrix} -mx_G - Z_{\dot{q}} & 0 & m - Z_{\dot{w}} & 0 \\ I_{yy} - M_{\dot{q}} & 0 & -mx_G - M_{\dot{w}} & 0 \\ 0 & 0 & 0 & 1 \\ 0 & 1 & 0 & 0 \end{bmatrix} \begin{bmatrix} \dot{q} \\ \dot{\theta} \\ \dot{w} \\ \dot{z} \end{bmatrix} = \begin{bmatrix} Z_q & 0 & Z_w & 0 \\ M_q & -1.3*(z_B B - z_G W) & M_w & 0 \\ 0 & 0 & 1 & 0 \\ 1 & 0 & 0 & 0 \end{bmatrix} \begin{bmatrix} q \\ \theta \\ w \\ z \end{bmatrix} + \begin{bmatrix} (\rho - \rho_g)*g \\ -(\rho - \rho_g)*g*x_B \\ 0 \\ 0 \end{bmatrix} [V(t)] \quad (26)$$

Which has the form,

$$[M_0]\{\dot{x}_s\} = [A_0]\{x_s\} + [B_0]\{u_c\} \quad (27)$$

Where,

$$[M_0] = \begin{bmatrix} -mx_G - Z_{\dot{q}} & 0 & m - Z_{\dot{w}} & 0 \\ I_{yy} - M_{\dot{q}} & 0 & -mx_G - M_{\dot{w}} & 0 \\ 0 & 0 & 0 & 1 \\ 0 & 1 & 0 & 0 \end{bmatrix} \quad (28)$$

$$[A_0] = \begin{bmatrix} Z_q & 0 & Z_w & 0 \\ M_q & -1.3*(z_B B - z_G W) & M_w & 0 \\ 0 & 0 & 1 & 0 \\ 1 & 0 & 0 & 0 \end{bmatrix} \quad (29)$$

$$\{B_0\} = \begin{bmatrix} (\rho - \rho_g)*g \\ -(\rho - \rho_g)*g*x_B \\ 0 \\ 0 \end{bmatrix}, \quad \{x_s\} = \begin{bmatrix} q \\ \theta \\ w \\ z \end{bmatrix}, \quad u_c = \dot{V}(t) = f \quad (30\text{-}32)$$

Where x_s is the state vector and u_c is the control vector.

Eq. (27) can be reduced in the form,

$$\{\dot{x}_S\} = [A]\{x_S\} + [B]\{u_C\} \tag{33}$$

Which is the State Dependant Riccati Equation (SDRE), in which [A] is the system matrix and [B] is the input matrix, which are given by

$$[A] = [M_0]^{-1}[A_0],\ [B] = [M_0]^{-1}[B_0] \tag{34}$$

The effect of uncertainty and external disturbance that would cause the system to deviate from the equilibrium point should be accounted in the system modeling for the accurate performance. Therefore, Eq. (33) can be modified as:

$$\{\dot{x}_S\} = [A]\{x_S\} + [B]\{u_C\} + \mathrm{d}\,(\mathrm{t}) \tag{35}$$

In which, *d(t)* is the unknown function representing the model uncertainty and external disturbances arises mainly due to wind, current, waves or voyage etc. They are normally unknown, but possibly bounded.

4.2 Secondary model: Automated Purge Valve Modeling

According to section 4.1.1.3, the lift force required to extract an object from sea bottom is typically about 1.3 times the wet weight. This implies that, soon after the suction break out, excessive buoyancy is present within the lift bags that cause a sudden increase in vertical speed. Also, during the ascent through water column, the lift bags experience a decrease in pressure with respect to the variation in depth. This decrease in pressure causes the volume of gas inside the lift bags to expand, resulting in an increase in buoyant force [32, 61, 111]. The automated purge valve is designed to eliminate the vertical acceleration experienced by the lift bags during

the ascent by restricting the expansion of gas through the valves. As the lift bag ascends, the expanded gas is purged through the valve in a controller manner to compensate for gas expansion by which, constant buoyancy can be always maintained. A microprocessor can be used to sample the pressure at predetermined intervals by which the change in pressure over each interval can be calculated, which is then interpolated by a PID control algorithm to find the ascent velocity and then the actual depth. Opening or closing of valves are carried out accordingly with system commands that will alter the amount of gas purged [33].

The pressure at any sea depth can be calculated based on the fundamentals of fluid mechanics as follows:

$$p_{abs} = \rho g h + p_{atm} \tag{36}$$

Where,

p_{abs} is the absolute pressure in N/m^2, ρ is the density of sea water = 1025 kg/m^3, g is the acceleration due to gravity = 9.81 m/s^2, h is the water depth in m, p_{atm} is the atmospheric pressure = 1.01325 bar = 101325 N/m^2

Assuming constant temperature (Isothermal process) and for a non flow system, the expansion of gas inside the lift bags is according to Boyle's law as:

$$p_1 v_1 = p_2 v_2 \tag{37}$$

In which, P_1 is the initial absolute pressure in N/m^2, V_1 is the initial volume in m^3

P_2 is the final absolute pressure in N/m^2, V_2 is the final volume in m^3.

Therefore, final volume,

$$V_2 = \frac{p_1 V_1}{p_2} \tag{38}$$

Note

If we are considering a flow process, then steady flow energy equation is to be accounted for calculating the change in volume. For more detail refer Nag [84].

The density of gas in the lift bag for different depths during the ascent can be calculated as:

According to Characteristic Gas Equation,

$$pV = mRT \tag{39}$$

Therefore,

$$p = \frac{m}{V}RT = \rho RT \tag{40}$$

i.e.

$$\rho_{gas} = \frac{p_{abs}}{RT} \tag{41}$$

Where R is the characteristic gas constant, for air = 286.9 J/kg.K and T is the absolute temperature assuming a constant value say 290 K.

The exponential increase in buoyancy force with respect to the gas expansion is according to:

$$B = (\rho - \rho_{gas}) \times V_2 \times g \tag{42}$$

Where *B* is the buoyant force in N.

The equation of motion in vertical direction can be written as:

$$(m + m_a)\dot{w} = 1.3(B - W) - \frac{1}{2}\rho c_d A_{bag} w^2 \tag{43}$$

Where, m_a is the added mass, A_{bag} is the area of bag surface perpendicular to motion and c_d is the drag coefficient=0.1.

By integrating the above equation with time provides the velocity of ascent. Further integrating the velocity with time provides the depth position at each point in time. Note that for initial calculations, drag force is assumed to be zero.

The pressure difference between the gas inside the top of lift bag and outside water is found as;

$$dp_{bag} = \frac{B}{A_{bag}} \tag{44}$$

The purge velocity can be found by equating pressure head and kinetic head according to Bernoulli's theorem as,

$$\frac{dp_{bag}}{\rho g} = \frac{v^2{}_{purge}}{2g} \tag{45}$$

Therefore,

$$v_{purge} = \sqrt{\frac{2dp_{\text{bag}}}{\rho_{gas}}} \tag{46}$$

Volume air purged through valves is obtained as:

$$V_{purge} = v_{purge} \times A_{purge} \times dt \tag{47}$$

Here area of purge valve opening 'A_{purge}' is the desired control parameter. *dt* is the time interval between system responses.

Now the present volume of gas inside the bag is estimated by subtracting the previous volume of gas inside the bag to the gas purged during the last time interval.

i.e.

$$V_{bag} = V_2 - V_{purge} \tag{48}$$

In which, V_{bag} is the present volume of gas inside the lift bag, V_2 is the previous volume of gas inside the bag and V_{purge} is the purge volume.

With this, new buoyancy can be evaluated as,

$$B = (\rho - \rho_{gas}) \times \mathrm{V}_{\mathrm{bag}} \times g \tag{49}$$

Now the iteration goes back to the Eq.43 and continues. This is the way an automatic purge valve works according to the excess buoyancy available after suction break out and to the pressure difference between the gas inside the lift bags and surrounding sea water pressure for a stable ascent.

5 Design of Primary Controller by Conventional Approach

For a complex under water nonlinear operations like marine salvage involving uncertainty and external disturbances, it is not possible to completely describe the system dynamics in a mathematical form. Due to the coupled nature of underwater dynamics, it is really difficult to design a control system fully based on the developed mathematical equations. Therefore the remaining possibility is to decouple the system dynamics based on some suitable assumptions and design a control system, which is capable of handling non linearity, system modeling errors, insensitiveness to parameter variations (i.e. mainly variation in hydrodynamic coefficients and suction breakout force) and external disturbance etc. Therefore the relative effectiveness of various control systems as a primary controller for regulating the gas flow rate is investigated in this chapter.

The function of the primary controller is to regulate the flow rate of filling gas inside the lift bags according to the buoyancy requirement in accordance with the hydrostatic force due to weight, buoyancy and suction breakout, hydrodynamic forces and uncertainty arises due to external disturbance such as wind, current or voyage etc for a safe and stable salvage operation.

Initially it is proposed to design conventional classic controllers like PD, PID and SMC for attaining the desired functionalities and later trying to integrate those with artificial intelligence techniques to get the optimum performance.

Note that in this section of the thesis there is also an active but not optimized purge gas controller. This results in the primary controller feeding air into the balloons whilst the purge controller is releasing gas. This is overcome by having a supervisory controller, over the primary inlet and secondary purge controllers, as described in Section 8.

5.1. Proportional Derivative Controller (PD)

Because of the simpler structure, at the beginning a proportional derivative controller (PD) is selected as the primary controller to regulate the gas flow rate. PD controller is a linear control technique consists of two basic terms: proportional term (k_p) and derivative terms (k_d). Proportional term determines the reaction to the current error (e), here the error is multiplied by a constant k_p. Derivative term determines the control action to the rate at which error is changing ($\dot{e}$), the first derivative is calculated and multiplied by a constant k_d.

The control law for the PD controller is formulated as [37]:

$$u = k_p e - k_d \dot{e} = k_p (z_{com} - z) - k_d (w) \quad (50)$$

Where, u is the control vector, z_{com} is the commanded or target depth, z is the actual depth from sea bottom and w is the heave velocity.

Figure 11 shows the SIMULINK block diagram of the PD controller for regulating the gas flow rate. The state space model for the proposed SIMULINK model for linear deterministic system is calculated based the equation Eq. (33).

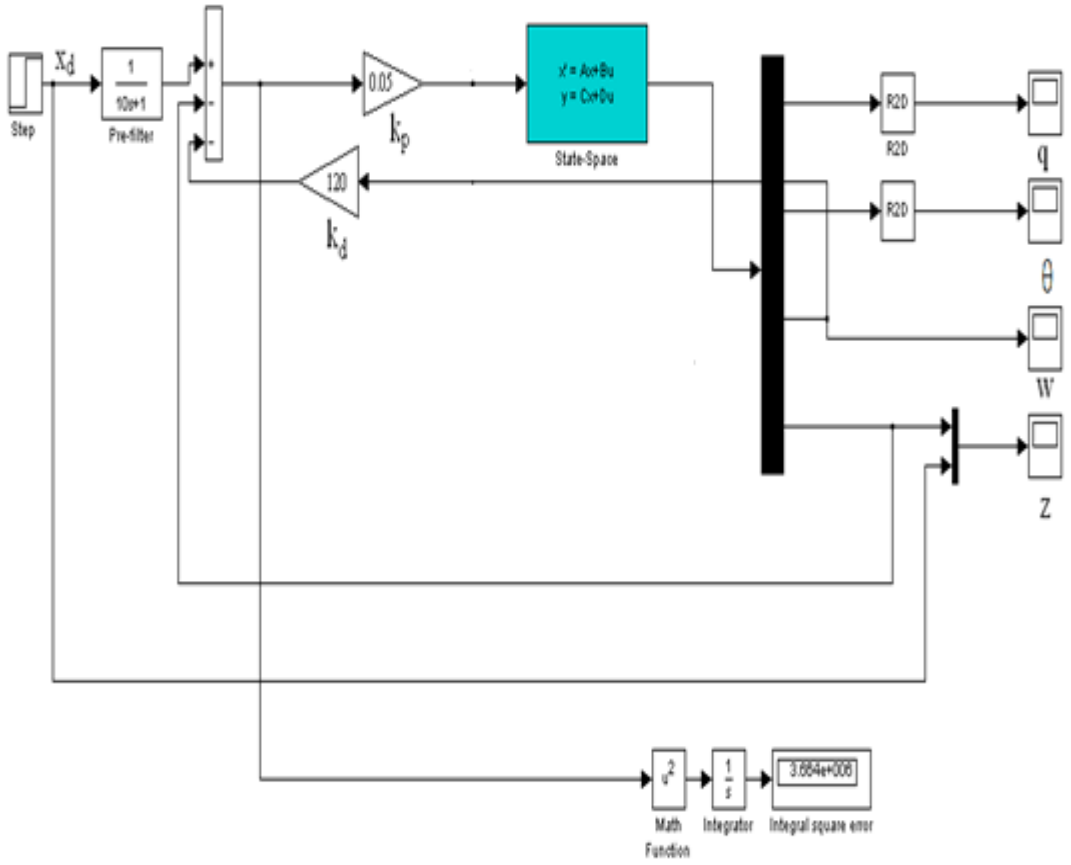

Figure 11: SIMULINK block diagram of the PD Controller for regulating the gas flow rate [91]

The response of the PD controller is investigated by conducting numerical simulations on a small-scale pontoon model in MATLAB [99] & SIMULINK [103]. The pontoon is a rectangular-shaped structure with watertight compartments for internal deployment of lift bags and gas generating system. External lift bags are also provided for achieving the desired lift. Normally internal bags are placed inside the vessel to make sure that centre of buoyancy C_B is above the centre of gravity C_g for stability. The lift bag diameter and length are 1.129 m & 1.8 m respectively and the maximum space inside a single compartment for the installation of a gas generator including piping is 0.29 m in diameter and 2 m in length [119]. Figure 12 exemplifies the installation of inflating system inside a single pontoon compartment.

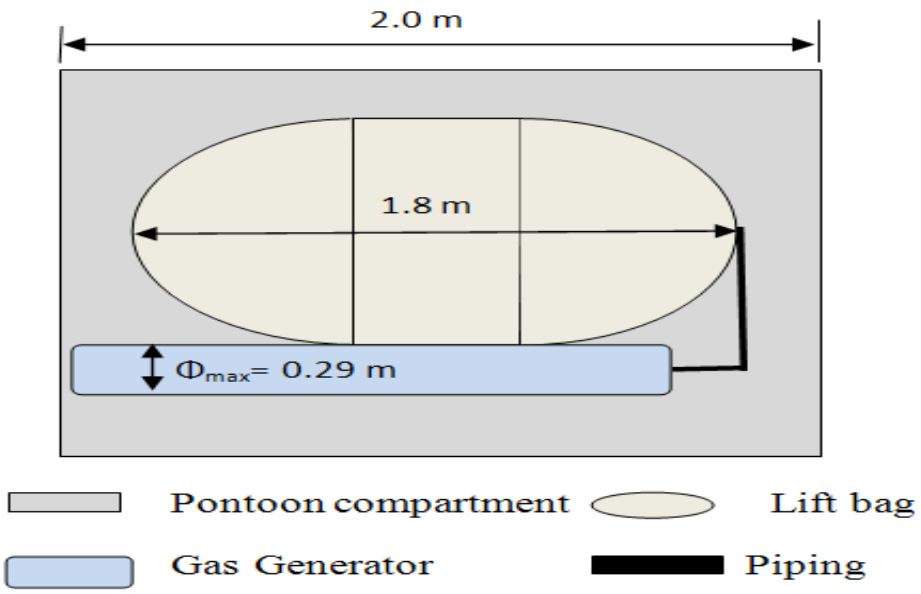

Figure 12: Pontoon compartment with inflating system [119]

The weight, length, breadth and mass moment of inertia about Y_b axis of the pontoon model are 9320 kg, 6m, 3m and 1481.31 kgm^2 respectively. The hydrodynamic coefficients used in the simulation are $Z'_{\dot{w}}$ = -0.0157, $Z'_{\dot{q}}$ = -0.00041, Z'_w =-0.043938, Z'_q =-0.017455, $M'_{\dot{w}}$ = -0.00053, $M'_{\dot{q}}$ = -0.00079, M'_w =-0.011175 and M'_q =-0.01131 respectively [36-37, 80, 96].

Simulation is initially performed for a target depth of 50 m from sea bottom. According to Section 4.1.1.3, the break out force for the pontoon model can be estimated as 103341.68 N (of the order of 10^5). According to Foda [35], for the estimated break out force, the break out time can be obtained as 100 sec. The minimum volume of gas required for breakout for a depth of 50 m (i.e. sea bottom is at 50 m from sea surface) is calculated based on the hydrostatic principles as 10.35 m^3 (see Appendix A). As the volume of one single inflated lift bag is 1.8 m^3, a total of 6 lift bags are required for the inflation. The buoyancy force provided by all lift bags are considered as a whole in the rigid body modeling approach.

For the desired performance, the PD controller is optimally tuned by trial and error method to obtain the proportional constant, $k_p = 0.05$ and derivative constant, $k_d = 120$. Simulated responses are presented in Figures 13-17.

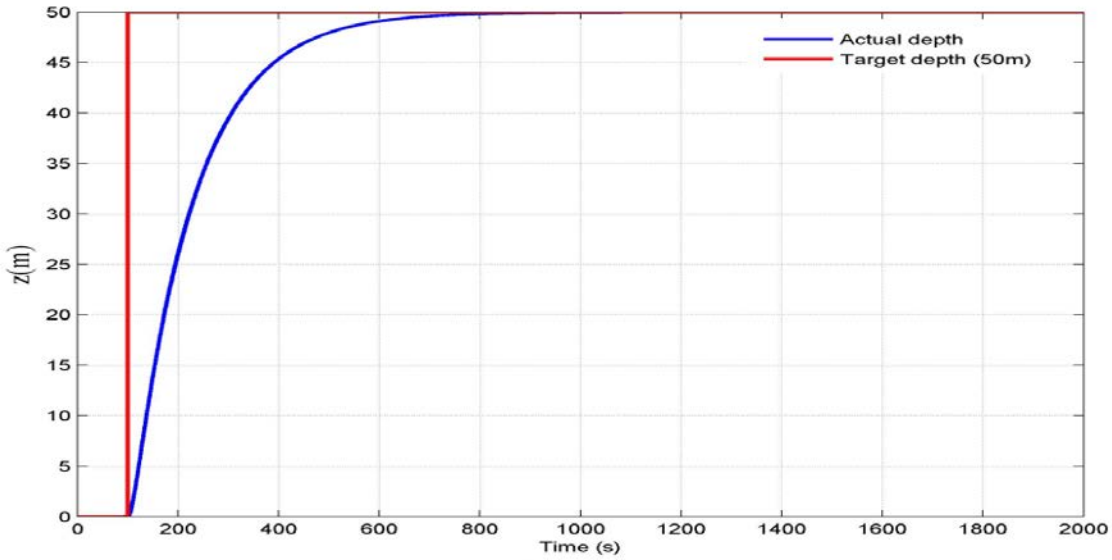

Figure 13: Variation of ship vertical position from sea bottom (50 m)

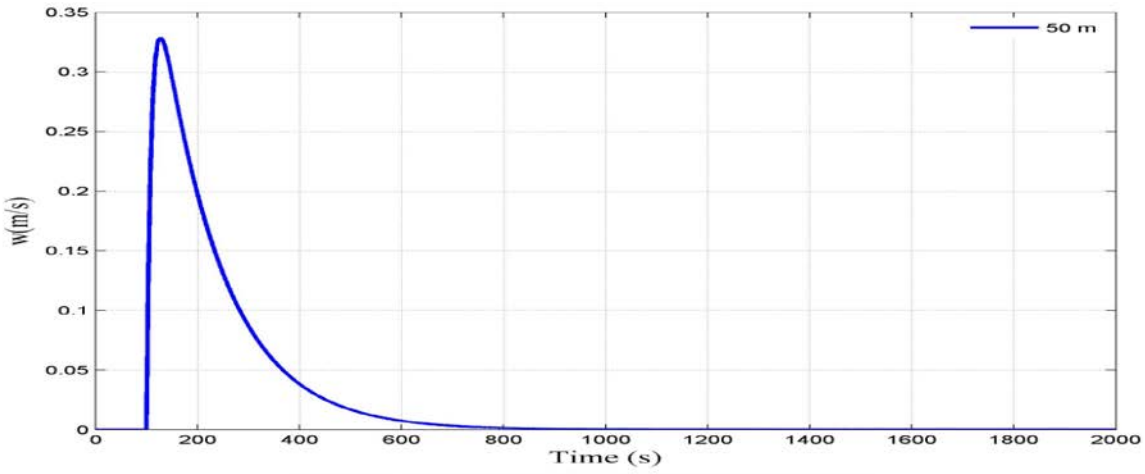

Figure 14: Variation of ship ascent velocity (50 m)

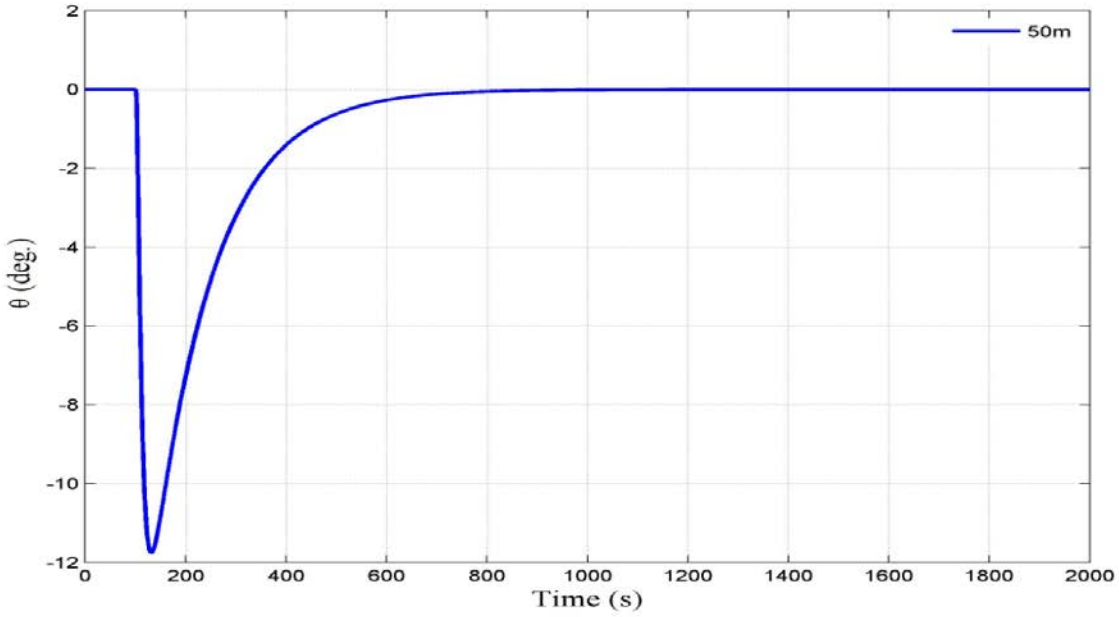

Figure 15: Variation of ship pitch angle (50 m)

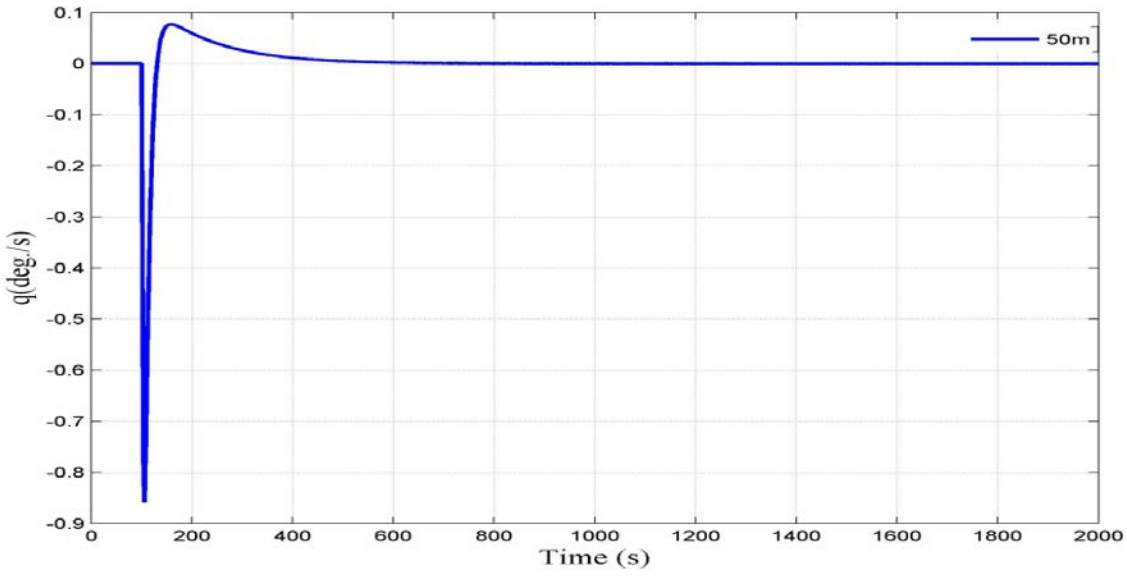

Figure 16: Variation of ship pitch rate (50 m)

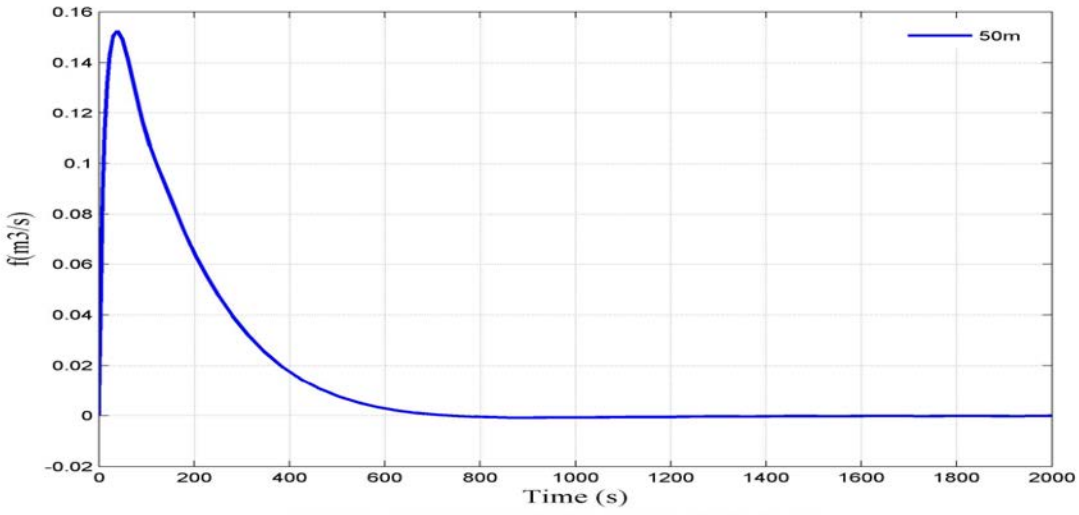

Figure 17: Variation of gas flow rate (50 m)

It is observed form Figure 13 that by properly tuning the PD controller, the system attains the steady state condition, i.e. reaching the target depth in 800 s without any overshoot. It is also noted from Figure 13 that after reaching the target depth, even if the simulation time is increased, it has no effect on the system performance. Figure 14 shows that the maximum value of ascent velocity is found to be 0.33 m/s – being within the required range (<0.6 m/s) [12, 61, 65], which is quite feasible for a stable salvage operation. When the vessel reaches the commanded depth, the PD controller reduces the ascent velocity to almost zero value. The depth rate and ascent velocity responses reveal similar trend to the results of Nicholls-Lee et al. [86].

From Figure 15, the pitch angle is found to increase with time, reaching a maximum value and thereafter decreasing. The maximum value of pitch angle is found to be about 11.8 degrees (<15 degrees) [12, 65], which implies that the motion is stable. Similar to ascent velocity in Figure 14, the pitch angle in Figure 15 initially increases to a higher value after the break out and reduces when the payload reaches the commanded depth. This is due to the reason that the controller generates pitch angle commands as per the depth error. At the beginning, the depth error is large thereby the controller produces a higher value of pitch angle to eliminate this error. Figure 16 shows that how the pitch rates become nearly equal to zero when the pontoon reaches the

required position. It is seen from Figure 17 that the controller sets initial flow rate value as 0.15 m^3/s for the suction breakout and soon after the break out period, it reduces flow rate significantly for the desired performance. Once the target depth is fulfilled, the controller further reduces the flow rate to almost zero value.

From the initial simulation results for 50 m depth, it is realized that the PD controller is good enough for controlling the depth and pitch motions without any overshoot and having less steady state error. The performance of the PD controller is further evaluated by conducting simulation for higher target depths say 100 m & 150 m from sea bottom with the same tuned coefficients (k_p = 0.5 & k_d = 120). The obtained responses are presented in Figures 18-22 for 100 m depth and Figures 23-27 for 150 m respectively.

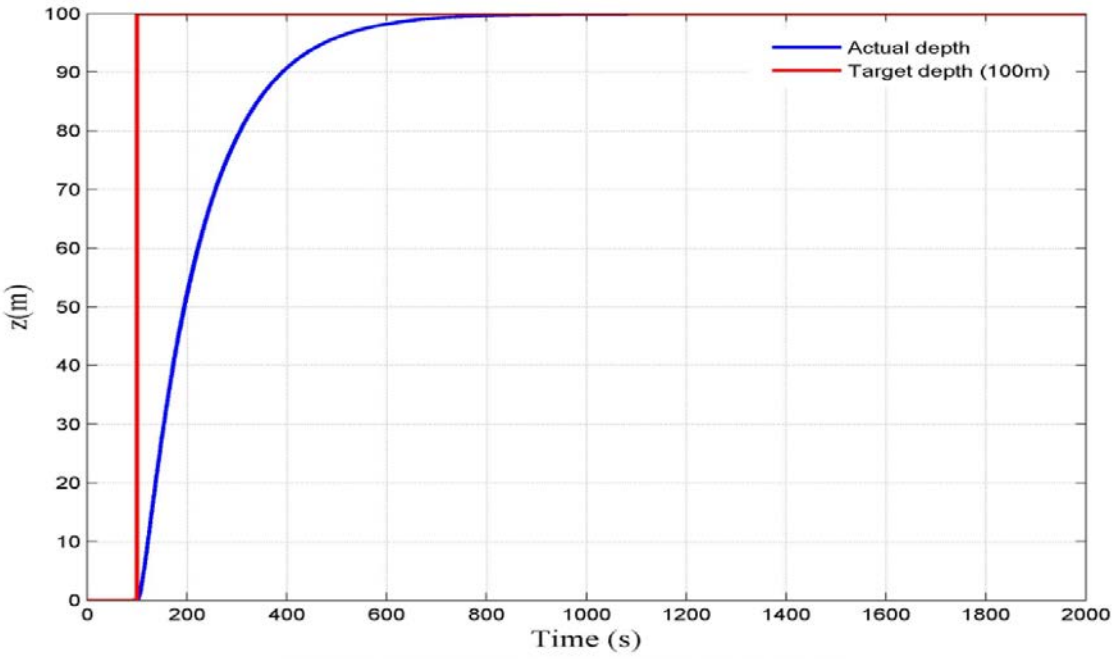

Figure 18: Variation of ship vertical position from sea bottom (100 m)

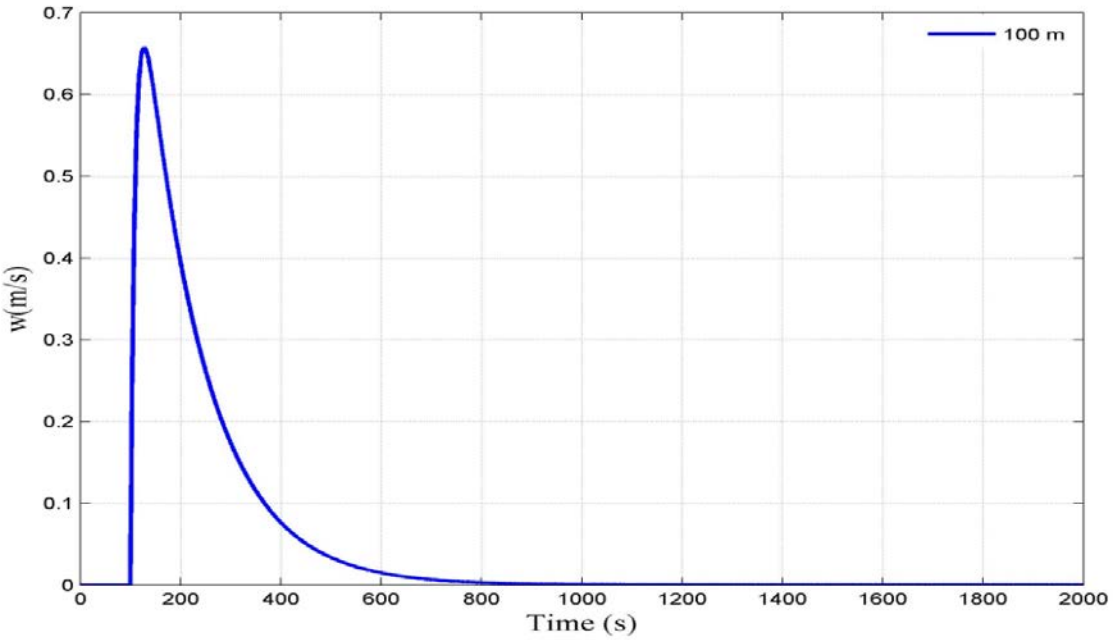

Figure 19: Variation of ship ascent velocity (100 m)

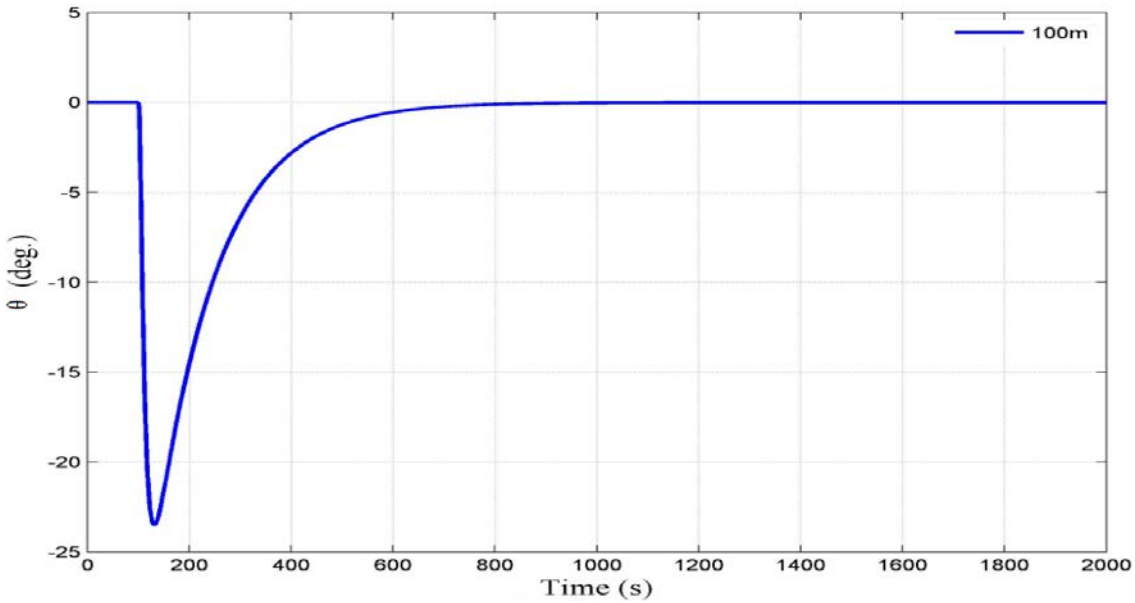

Figure 20: Variation of ship pitch angle (100 m)

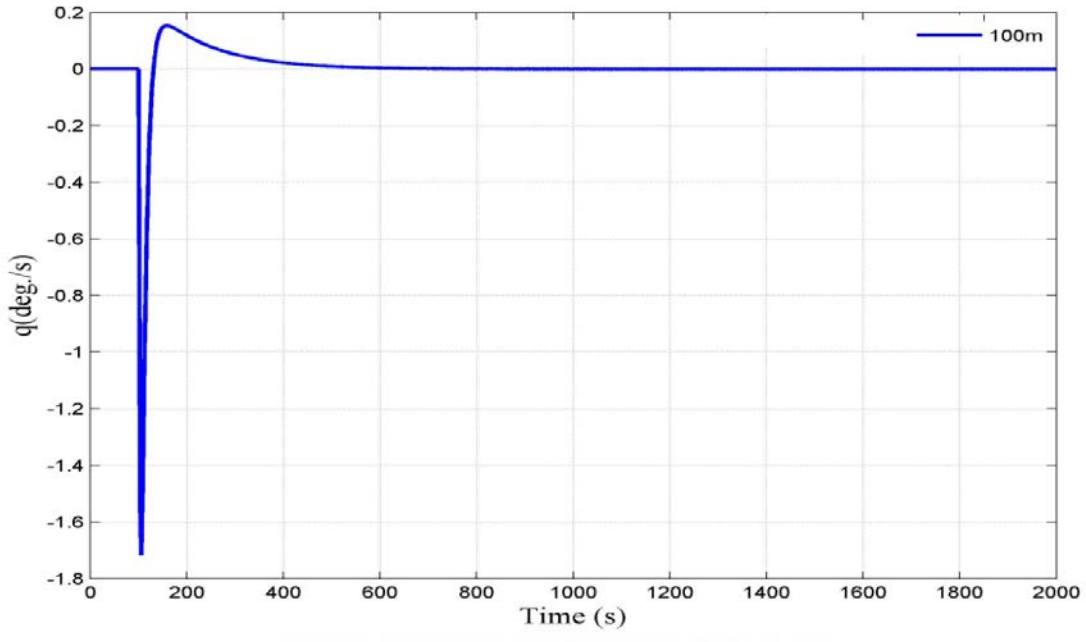

Figure 21: Variation of ship pitch rate (100 m)

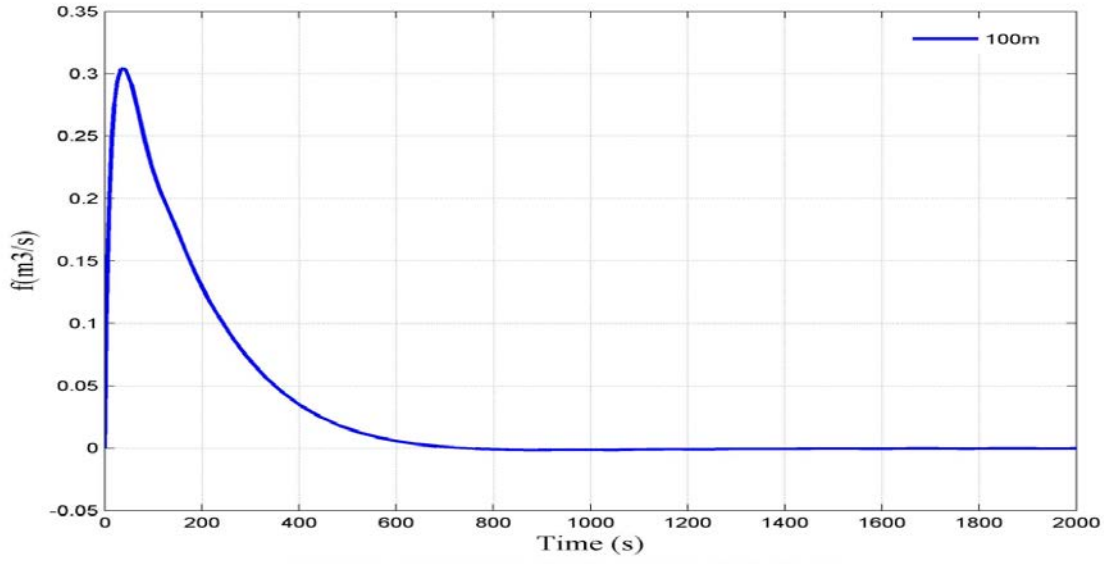

Figure 22: Variation of gas flow rate (100 m)

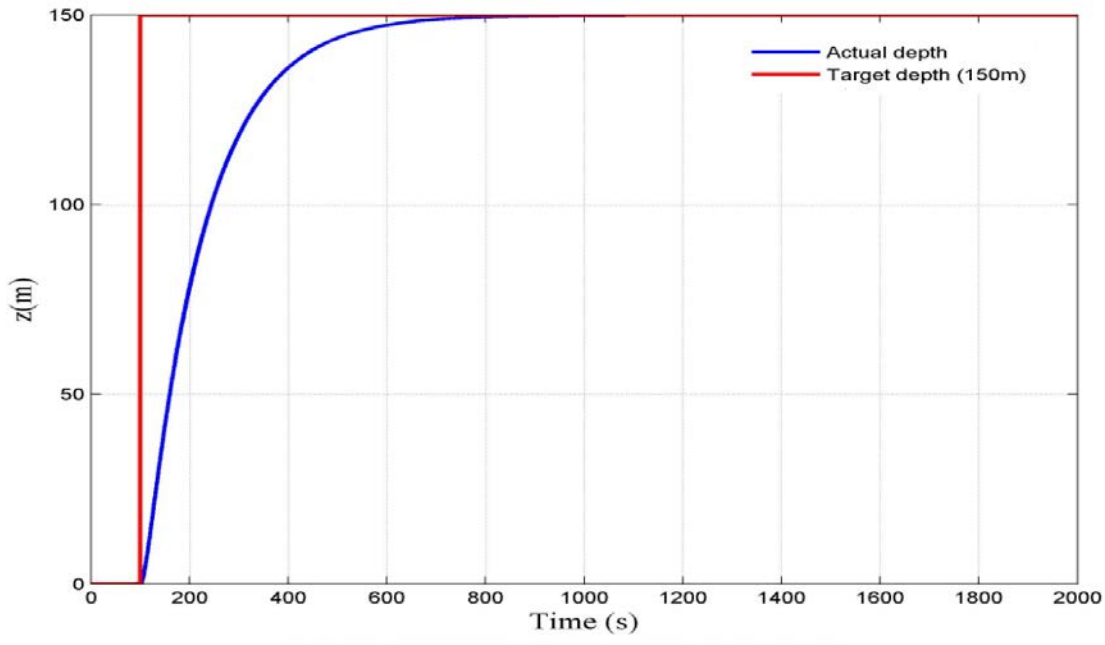

Figure 23: Variation of ship vertical position from sea bottom (150 m)

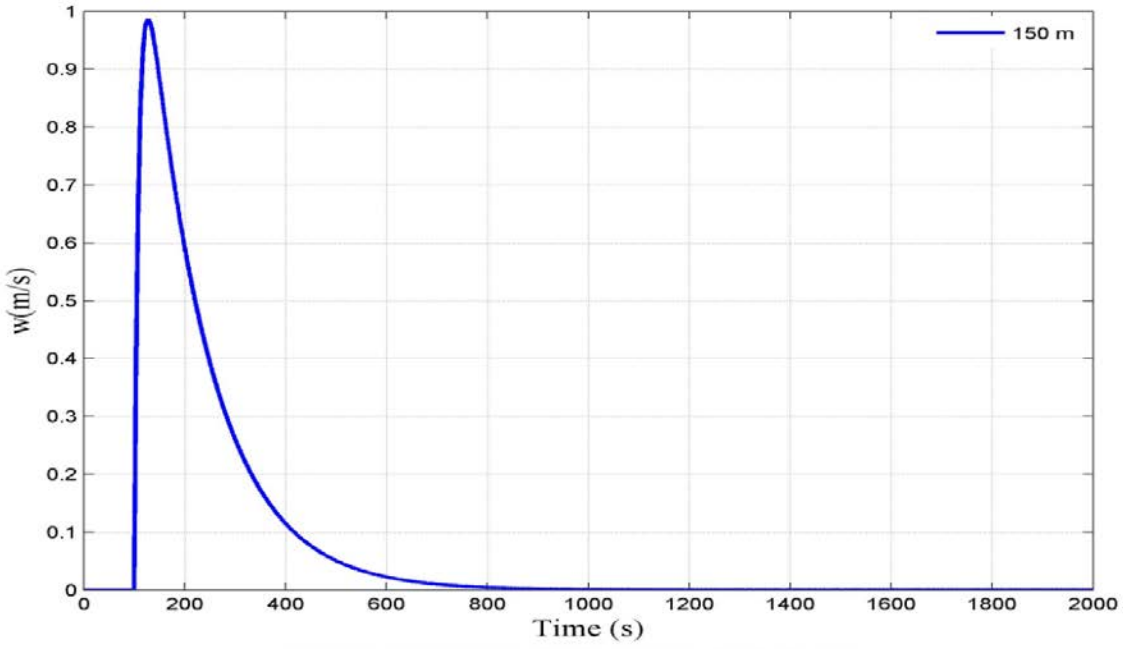

Figure 24: Variation of ship ascent velocity (150 m)

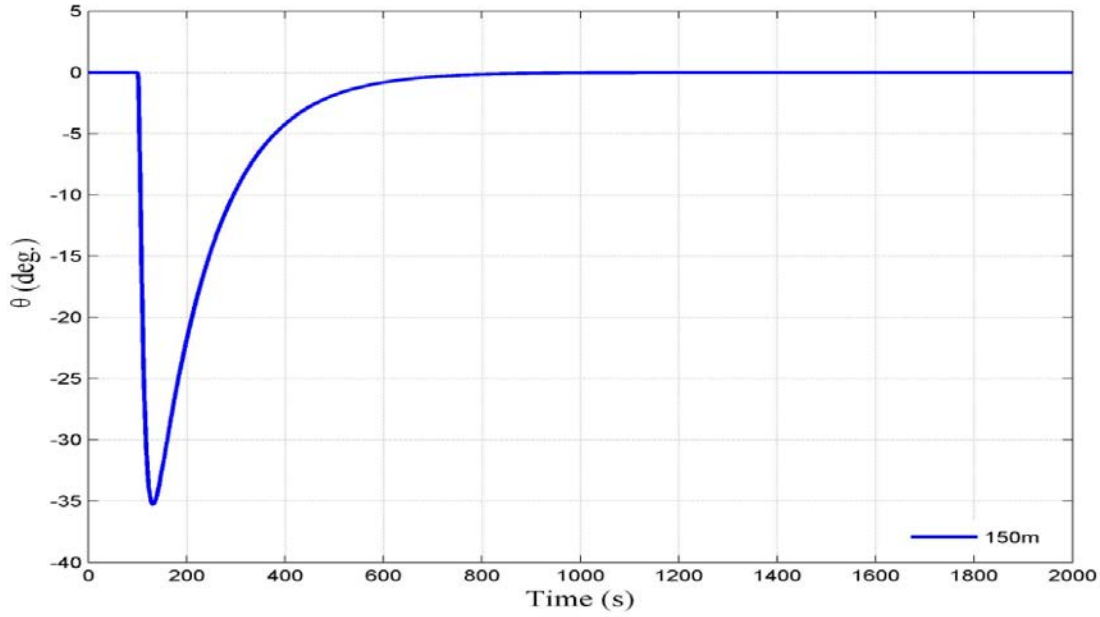

Figure 25: Variation of ship pitch angle (150 m)

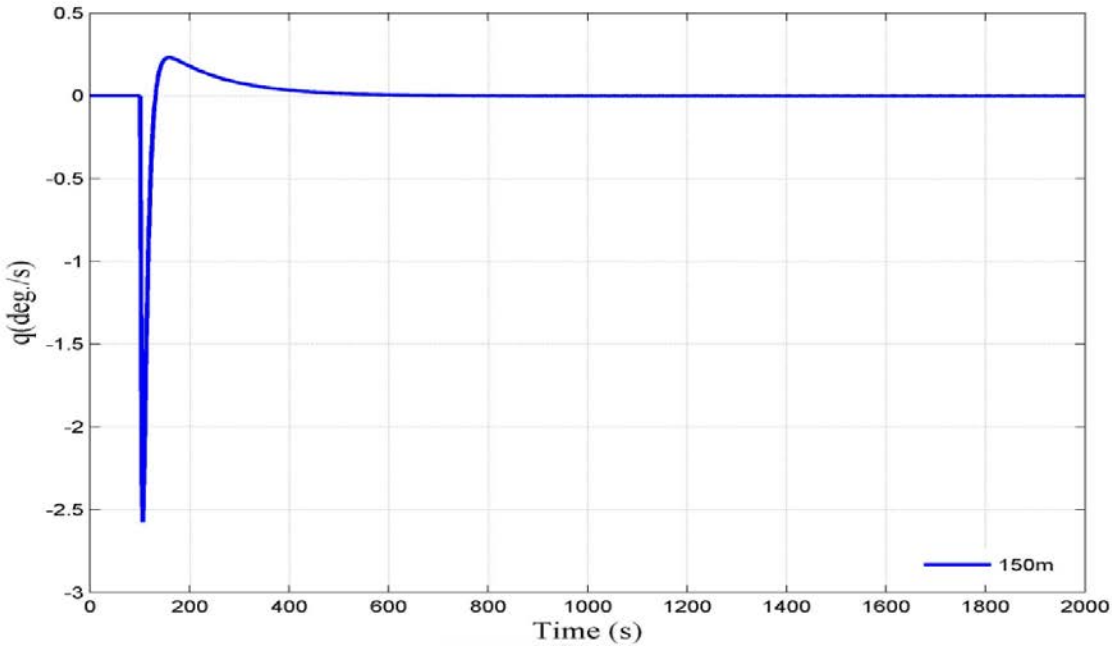

Figure 26: Variation of ship pitch rate (150 m)

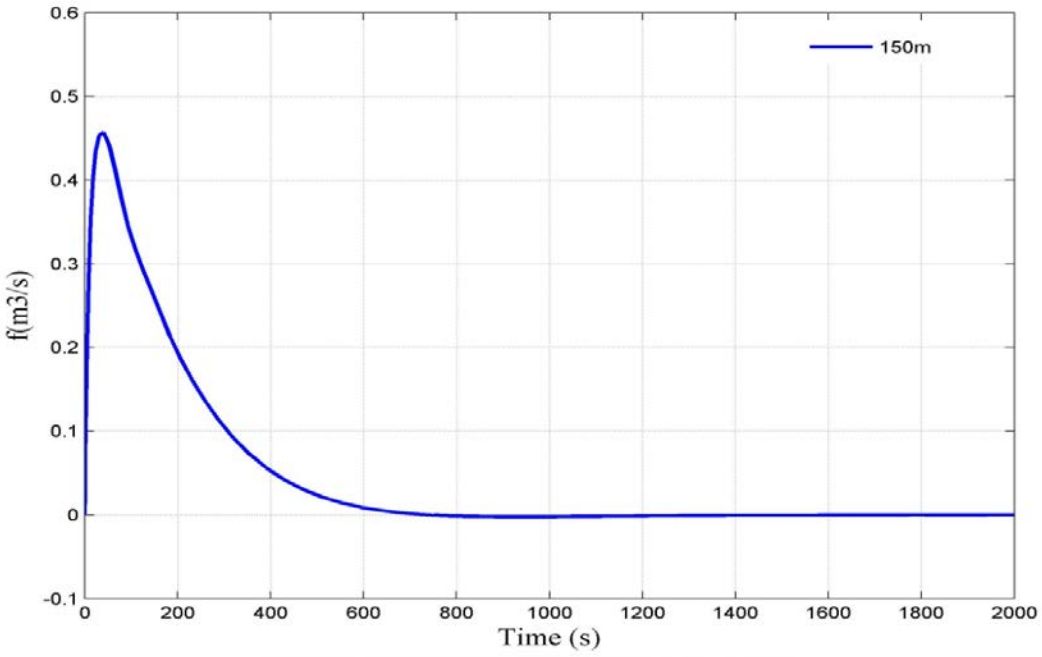

Figure 27: Variation of gas flow rate (150 m)

It is seen from Figures 18 & 23 that, with the same tuned parameters (k_p = 0.18 & k_d = 60), the PD controller is able to reach the commanded depths (i.e. 100 m & 150 m) without any overshoot and having less steady state error in the same reaching time (i.e. 800 s) as for 50 m water depth. But the Figures 19 & 24 reveals that the maximum ascent velocity for both the cases are 0.65 m/s and 0.99 m/s, which are beyond the stable limit (> 0.6 m/s). This much higher value of ascent velocity leads to the effect of drag force on the system, which may damage the lift bag adversely. The maximum value of pitch angle for both cases are found from Figures 20 &25 to be 24^0, & 35^0 respectively (> 15 degrees), they are totally unacceptable for a stable salvage operation. Higher values of pitch angle often cause the lift slings to break loose from the payload and hence results in a buoyancy loss and cause further damage to the system. Figures 21 & 26 shows that the pitch rates for 100 m & 150 m having the same trend as before for 50 m water depth, but they are of much higher value. Flow rates for both cases are initially fixed at 0.3 m^3/s & 0.46 m^3/s for suction break out and reduces considerably after break out as presented in

Figures 22 & 27. However it is seen that the PD control action is not able to regulate the depth and pitch motions within the stable region.

Remarks

The numerical simulation results using PD controller as the primary controller for regulating the gas flow rate shows that the controller is suitable for regulating the depth and pitch motions for smaller target depths with no overshoot and having less steady state error by properly tuning the controller. But, for higher depths with the same tuned coefficients, the performance of the controller is very poor as the ascent velocity and pitch angle goes beyond the stable region. Remembering the fact, that for complex underwater operations like marine salvage it is really difficult to retune the controller coefficients frequently for the desired performance, it is required to choose some other controller techniques for meeting the desired functionalities.

5.2 Proportional Integral and Derivative Controller (PID)

As the results obtained using PD controller for regulating the gas flow rate is not satisfactory due to the higher values of ascent velocity and pitch angle, especially for higher water depths, now a PID controller is chosen as the primary controller for regulating the gas flow rate.

PID is a linear control methodology with a very simple control structure as shown in Figure 28. It is a closed loop control system which consists of three basic terms: proportional, integral and derivative terms. Proportional term determines the reaction to the current error; i.e. to handle an immediate error, the error is multiplied by a constant k_p. Integral term determines the reaction to the sum of the current and past error values; i.e. the integral part works to learn from the past, the error is integrated and multiplied by a constant k_i. Derivative term determines the control action to the rate at which error is changing; i.e. the derivative part works to predict the future, the first derivative is calculated and multiplied by a constant k_d. A PID controller is trying to eliminate the error between the desired output and the actual output value by generating a control action such as an actuation signal that drives the plant [4, 63, 74]. A PID controller is called a PI, PD or P controller in the absense of the respective control actions.

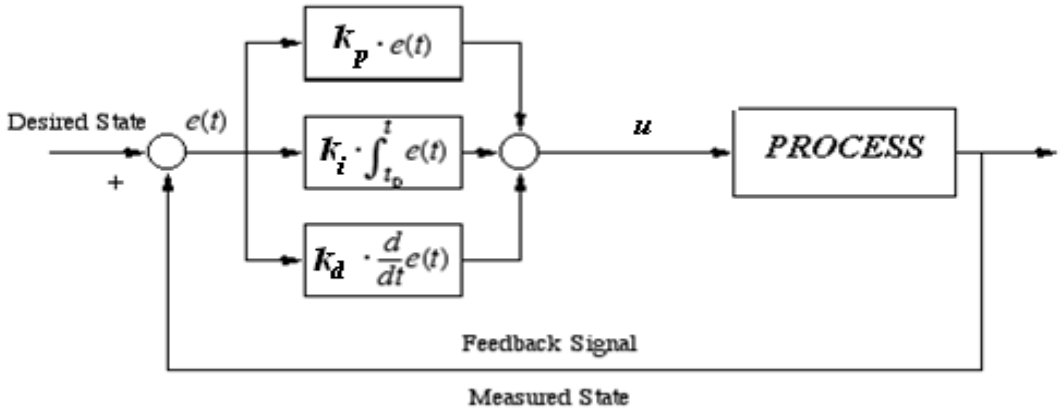

Figure 28: PID controller with plant control structure [4, 63]

The PID control law is formulated as:

$$u = k_p.e + k_i \int e.dt + k_d.\frac{de}{dt} \quad (51)$$

Where u is the control action, e is the error signal, k_p, k_i and k_d are proportional, integral and derivative gains respectively.

Table 1: The effect of increasing coefficients [63, 74]

	Rise Time	**Overshoot**	**Settling Time**	**Steady State Error**
$\boldsymbol{k_p}$	Decrease	Increase	Small change	Decrease
$\boldsymbol{k_i}$	Decrease	Increase	Increase	Remove
$\boldsymbol{k_d}$	Small change	Decrease	Decrease	Small change

Table 1 explains the effect of increasing coefficients in the PID controller response. The proportional term improves the rise time of the response and slightly improves the steady-state error. However, the proportional term can induce oscillations if the gain value is too high. The inclusion of the integral term improves the permanent action as it eliminates the steady-state error. The derivative term can be used to improve the transient response by damping unwanted overshoots. Nevertheless, it must be used with caution as it amplifies any existent noise in the signal. The SIMULINK block diagram of the proposed PID controller for regulating the gas flow rate is shown in Figure. 29.

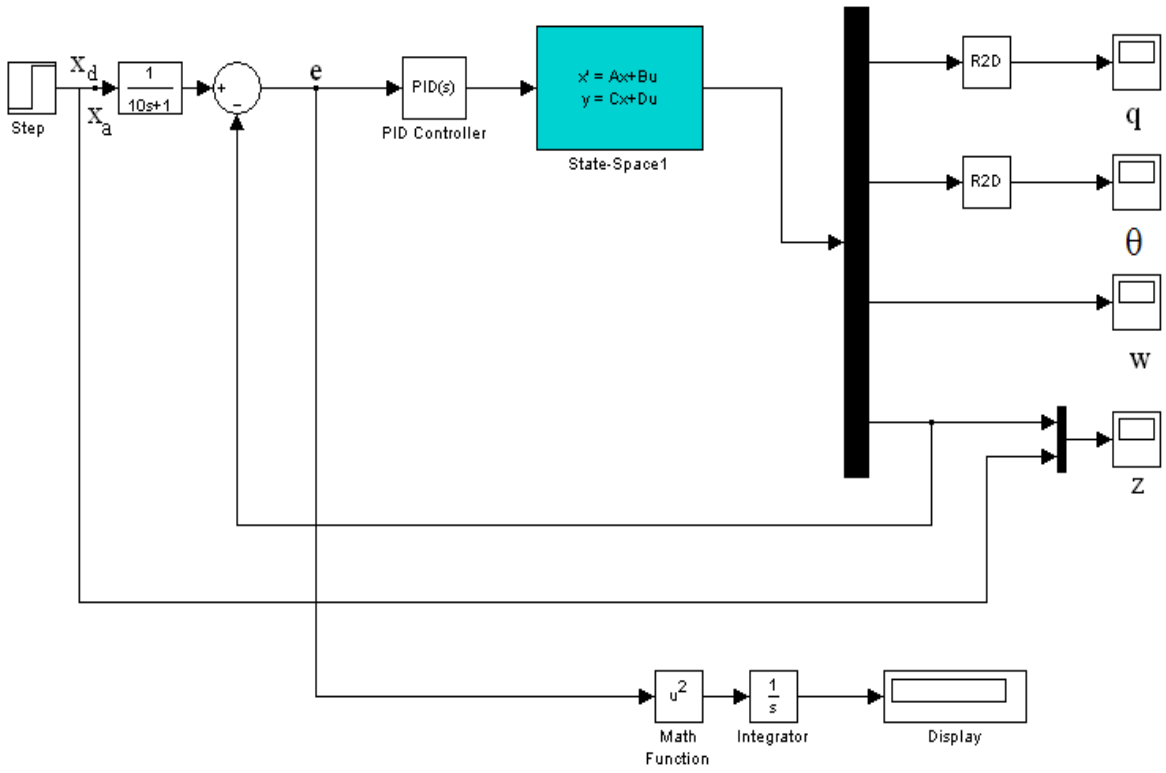

Figure 29: SIMULINK block diagram of the PID Controller for regulating the gas flow rate

The performance of the PID controller is analyzed by conducting simulation for three target depths 50 m, 100 m & 150 m from sea bottom with the same value of gain constants. PID coefficients are found online by using SIMULINK PID tuner. The obtained responses are shown in Figures 30-38. Depth controller results are produced separately for the three target depths, just to show how the system reaches the target depth with the controller commands as shown in Figures 30-32.

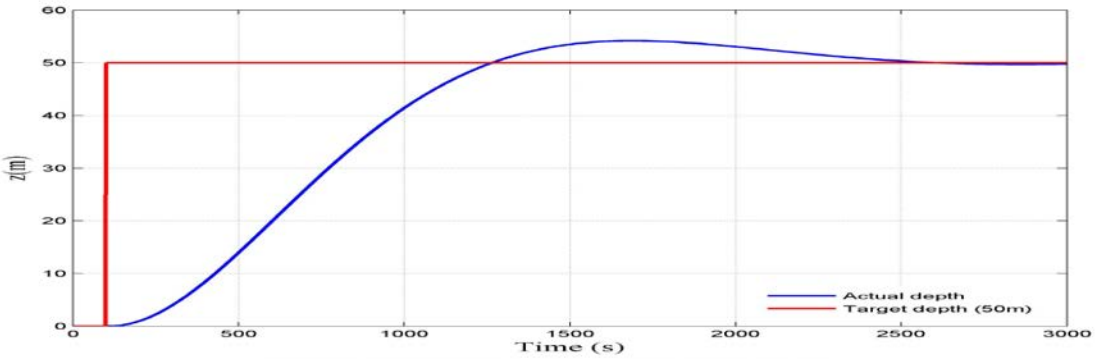

Figure 30: Variation of ship vertical position from sea bottom (50 m)

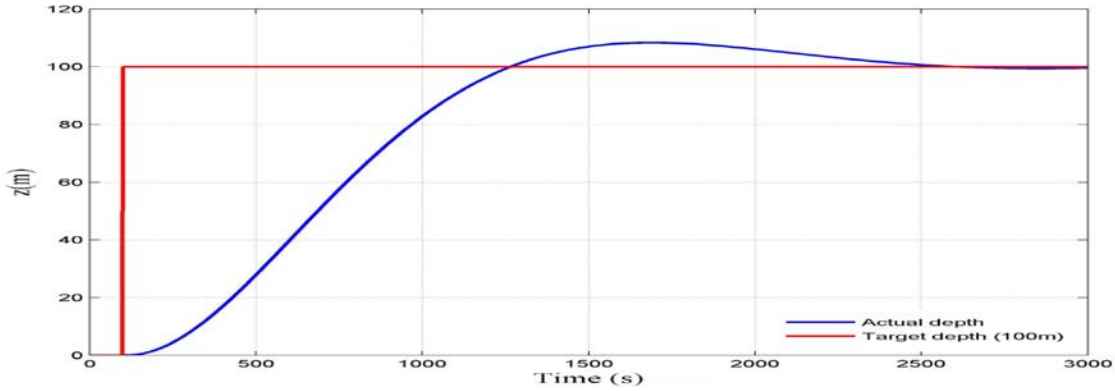

Figure 31: Variation of ship vertical position from sea bottom (100 m)

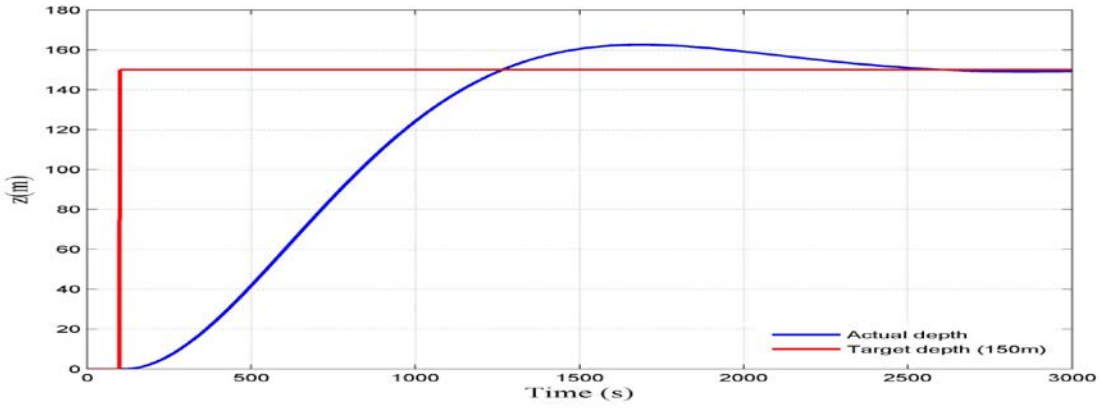

Figure 32: Variation of ship vertical position from sea bottom (150 m)

Figures 30-32 shows that there is considerable overshoot present in all the three cases, even though the controller is properly tuned, which may be due to the presence of the integral action in PID controller. Also it is observed that, the presence of integral action makes the settling time more for the proposed controller (2500 s for all the three cases) in comparison with the PD controller, where it is only 800s.

The variation of ascent velocity, pitch angle and pitch rate for the three commanded depths with time are presented in Figures 33-35. From Figure 33, the maximum value of ascent velocity for the three target depths are found to be 0.09, 0.18 & 0.28 m/s, which are well below 0.6 m/s. This implies that the ascent is stable, though an overshoot is present with the controller. Due to the presence of overshoot, the ascent velocity falls below zero value to reduce the error and to make the system to drive towards steady state.

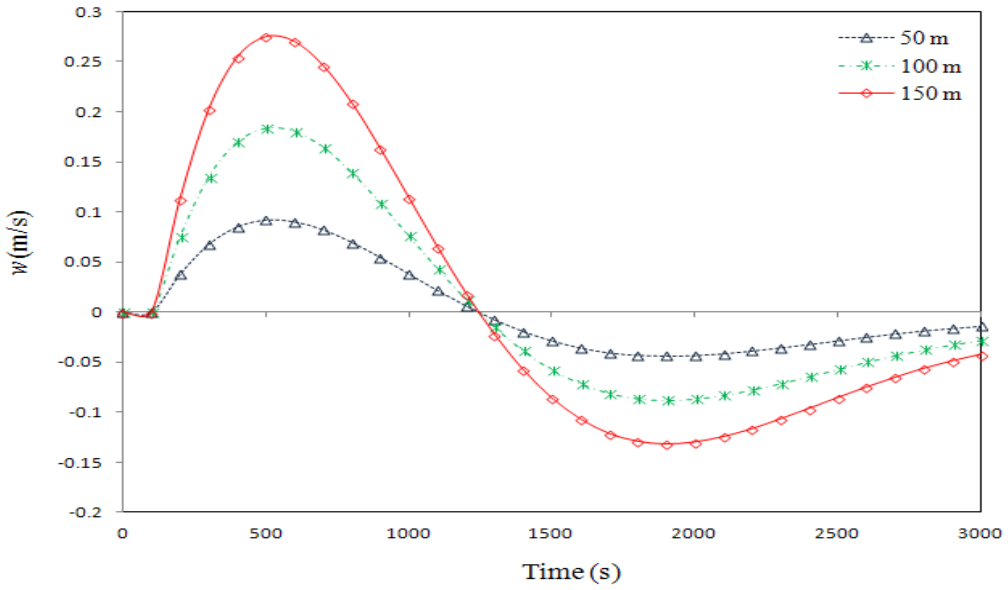

Figure 33: Variation of ship ascent velocity (50m, 100m & 150 m)

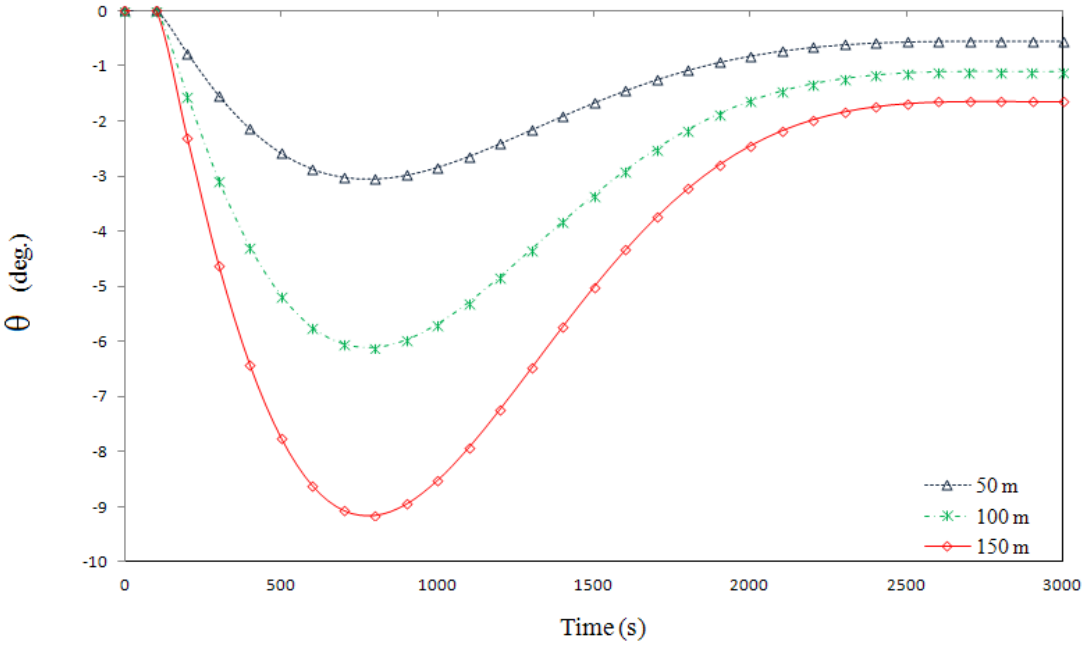

Figure 34: Variation of ship pitch angle (50m, 100m & 150 m)

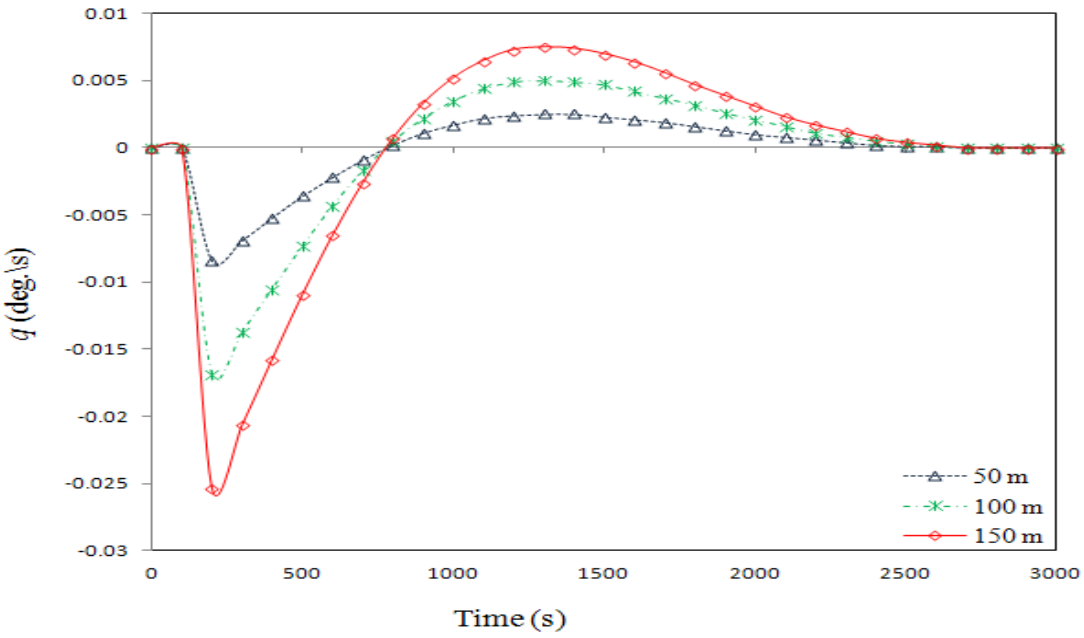

Figure 35: Variation of ship pitch rate (50m, 100m & 150 m)

Figure 34 shows that the maximum value of pitch angle for the three target depths are 3^0, 6^0 and 9.2^0 respectively, which are within the safe range ($<15^0$). Hence it is realized that the PID controller is able to control the pitch motion even for higher water depths for the linear deterministic model with the addition of integral term compared to the PD controller. Pitch rates for the three cases follow the same trend as the results obtained with the PD controller as shown in Figure 35.

The variation of control parameter, i.e. flow rate of filling gas inside the lift bags for the three target depths are displayed separately for better visibility in Figures 36-38. In all the three cases, after the suction break out (i.e. 100s), the controller reduces the initial flow rate value significantly and finally reaches zero as soon as the pontoon reaches the commanded depths.

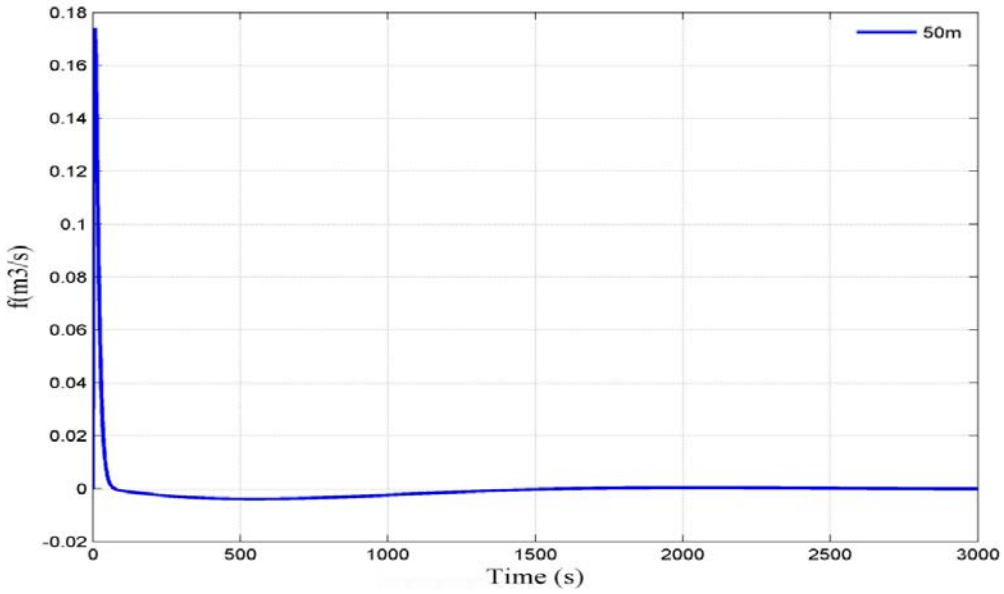

Figure 36: Variation of gas flow rate (50 m)

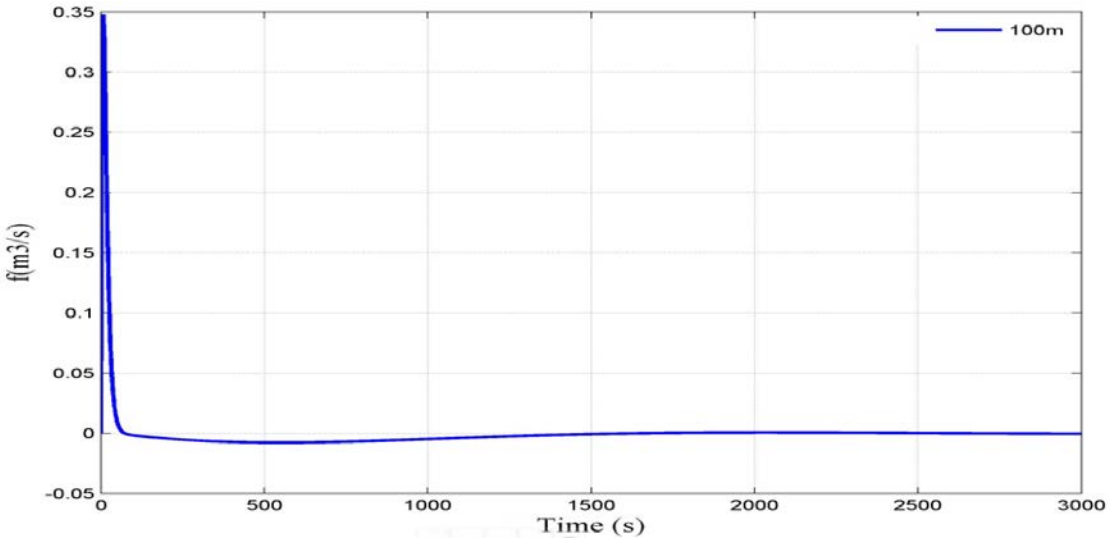

Figure 37: Variation of gas flow rate (100 m)

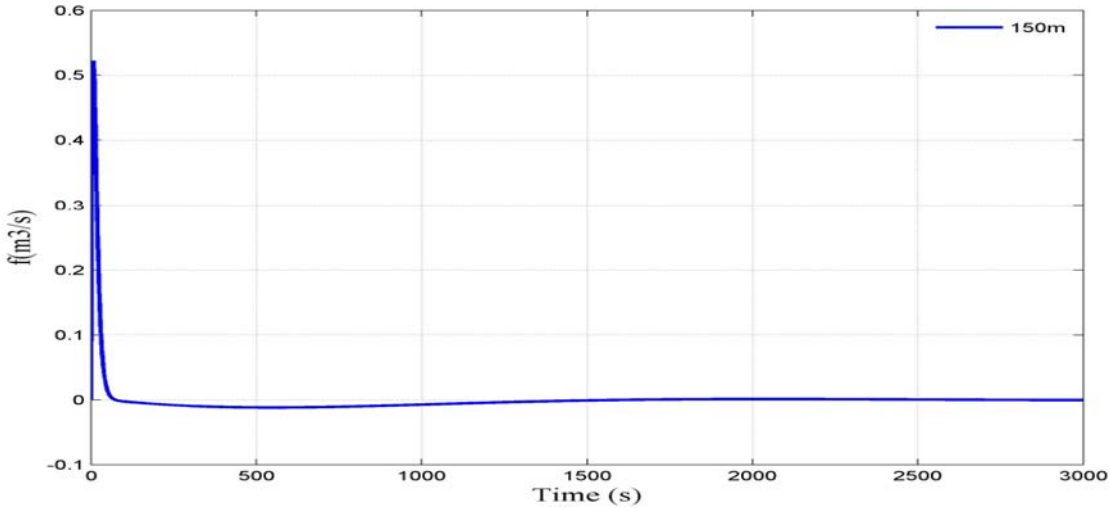

Figure 38: Variation of gas flow rate (150 m)

From the simulation, it is understood that the proposed PID controller is suitable for controlling the heave and pitch motions within the stable region even for higher water depths with the same tuned settings, though slight overshoot is present with the system. The presence of integral action

resulting to an overshoot as well as increase the settling time, at the same time, it is effective in regulating the state variables within the stable region along with proportional and derivative terms. The performance of the PID controller is further investigated by conducting case studies regarding sensitivity analysis and by considering the effect of external disturbance.

Case 1: Sensitivity Analysis: - Variation in break out force

A preliminary sensitivity analysis is carried out by considering the effect of variation in breakout force on the trajectory of simulation. According to Section 4.1.1.3, the total break out lift force is estimated to be in the range of 1.05-1.45 times the wet weight. For the pontoon model, which is calculated to be in the range 8508.5 kgf - 11749.83 kgf (see Appendix A). These lower and higher values of break out force are accounted in the simulation for a target depth of 100 m from sea bottom. From the simulation response (Figures 39-43), it is found that there is no significant variation in response trajectories except that there is slight change in breakout time due to this variation. Break out time for the 8508.5 kgf is found to be 80 s, whereas for 11749.83 kgf, it is 112s.

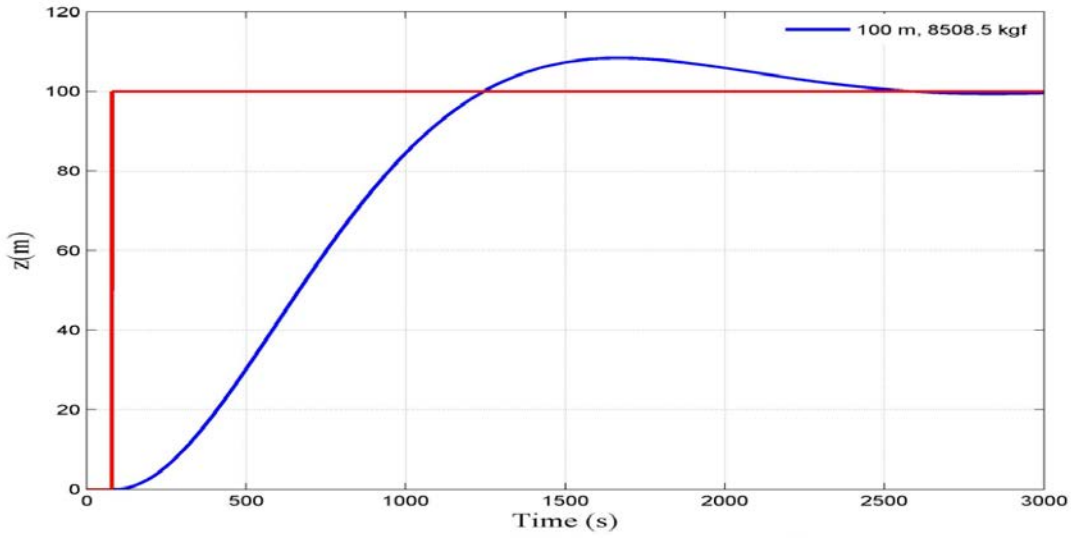

Figure 39: Variation of ship vertical position from sea bottom (100 m, 8508.5kgf)

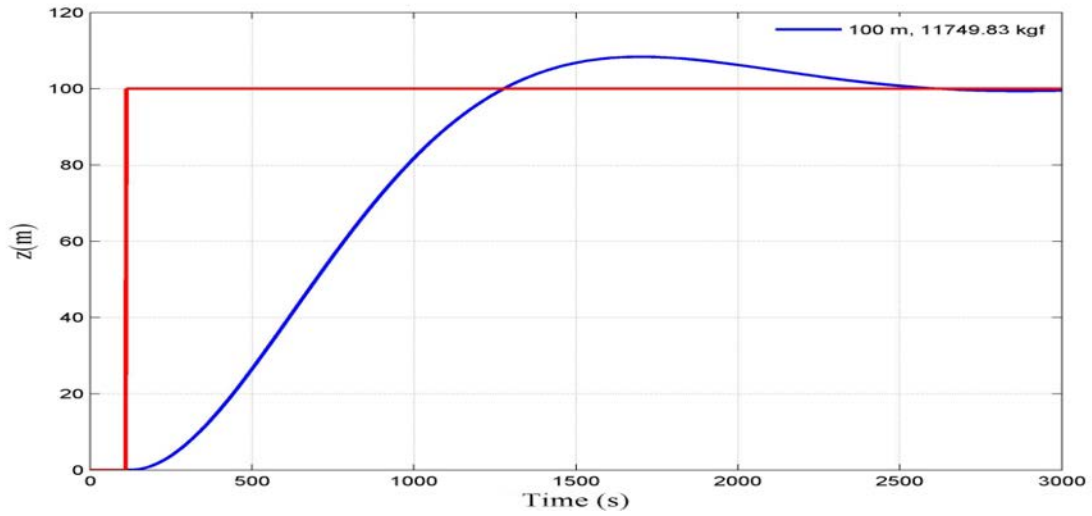

Figure 40: Variation of ship vertical position from sea bottom (100 m, 11749.83kgf)

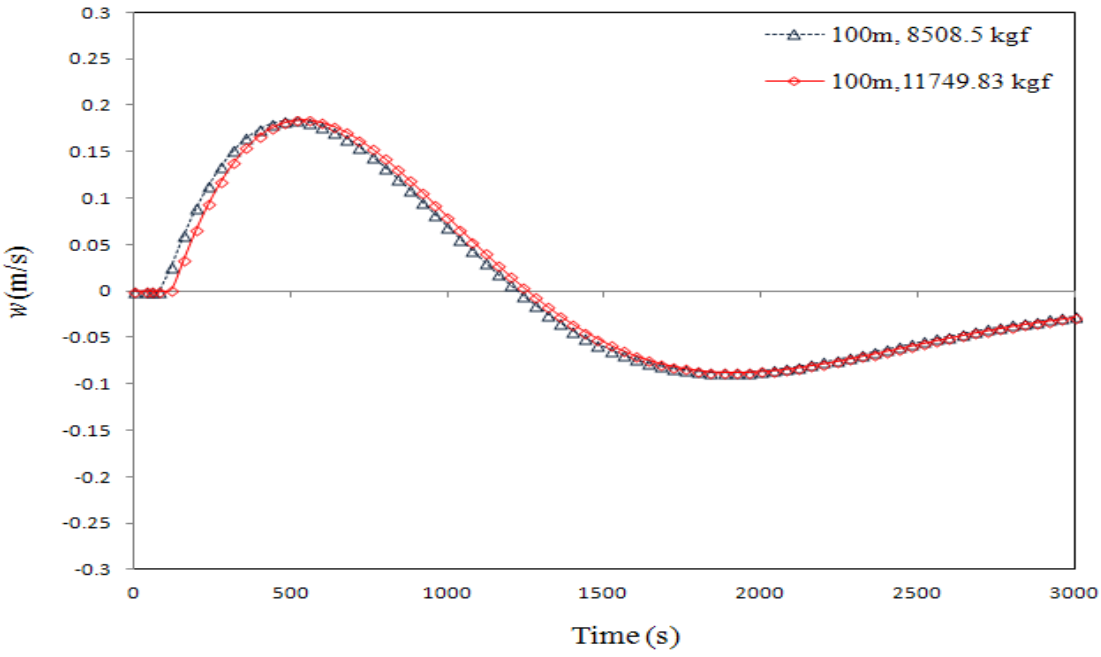

Figure 41: Variation of ship ascent velocity (100 m)

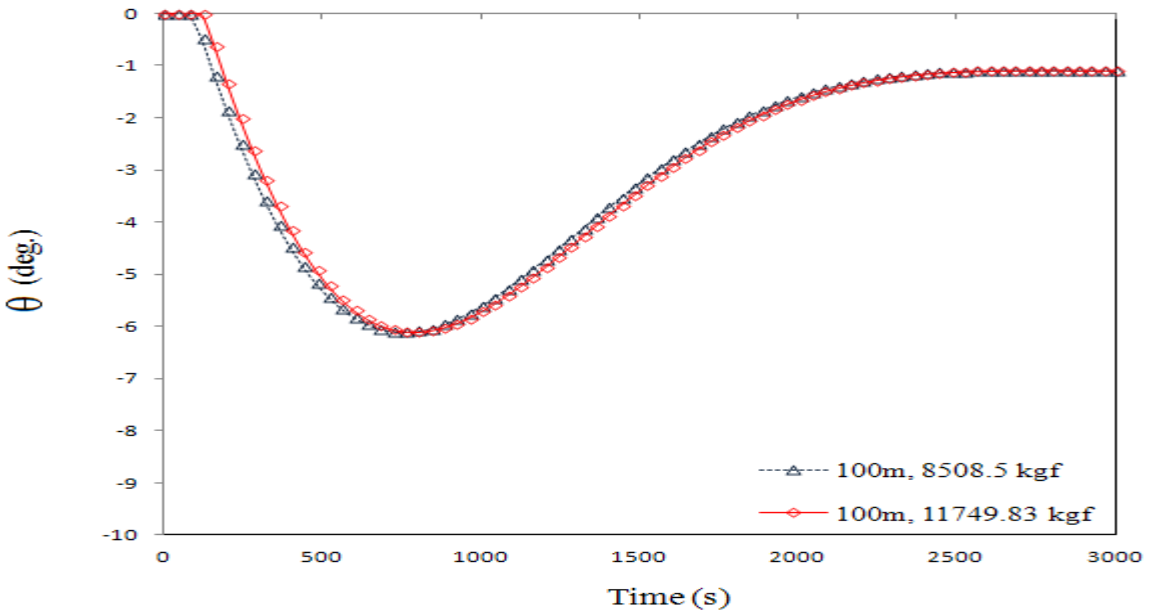

Figure 42: Variation of ship pitch angle (100 m)

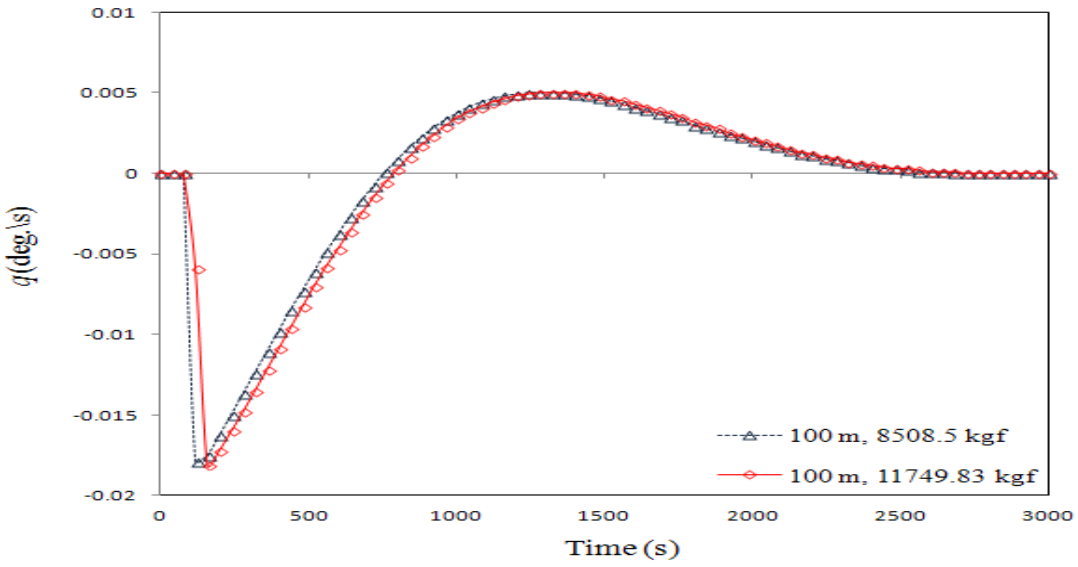

Figure 43: Variation of ship pitch rate (100 m)

Case 2: Sensitivity Analysis: - Variation in hydrodynamic coefficients.

As it is really difficult to exactly determine the hydrodynamic coefficients for the given pontoon model, a 50% variation in hydrodynamic coefficients obtained from literature are considered to be taking place. Simulation is performed by considering this variation in system dynamics with the proposed PID controller for a target depth of 100 m.

50% variation in hydrodynamic coefficients (denoted as '0.5 hc') results in a considerable change in state space model and the obtained simulation response, as presented in Figures 44-48, reveals that it is required to retune the PID controller for obtaining the desired response, which is not feasible for a marine salvage operation as manual retuning is difficult to carry out underwater.

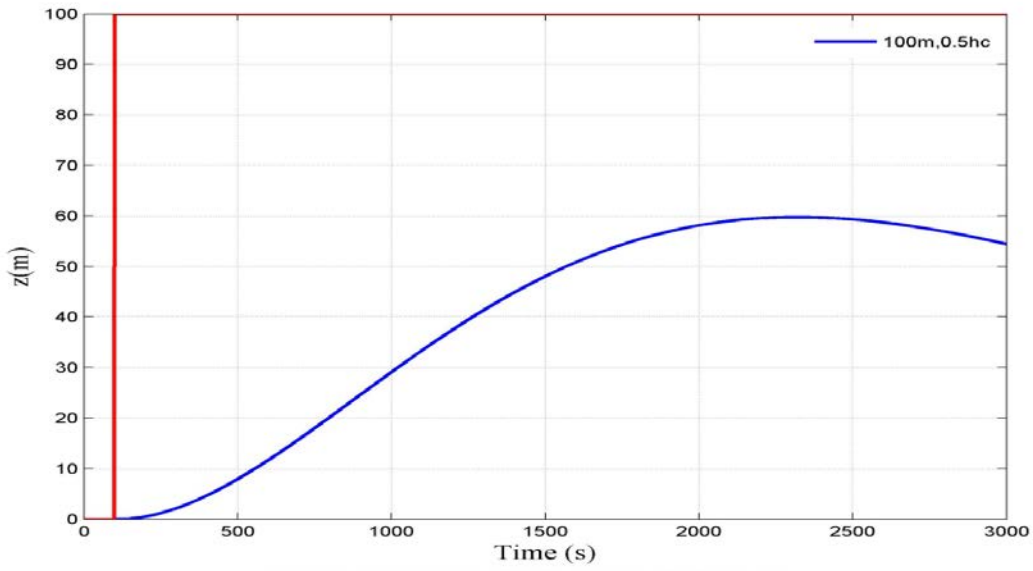

Figure 44: Variation of ship vertical position from sea bottom (100 m)

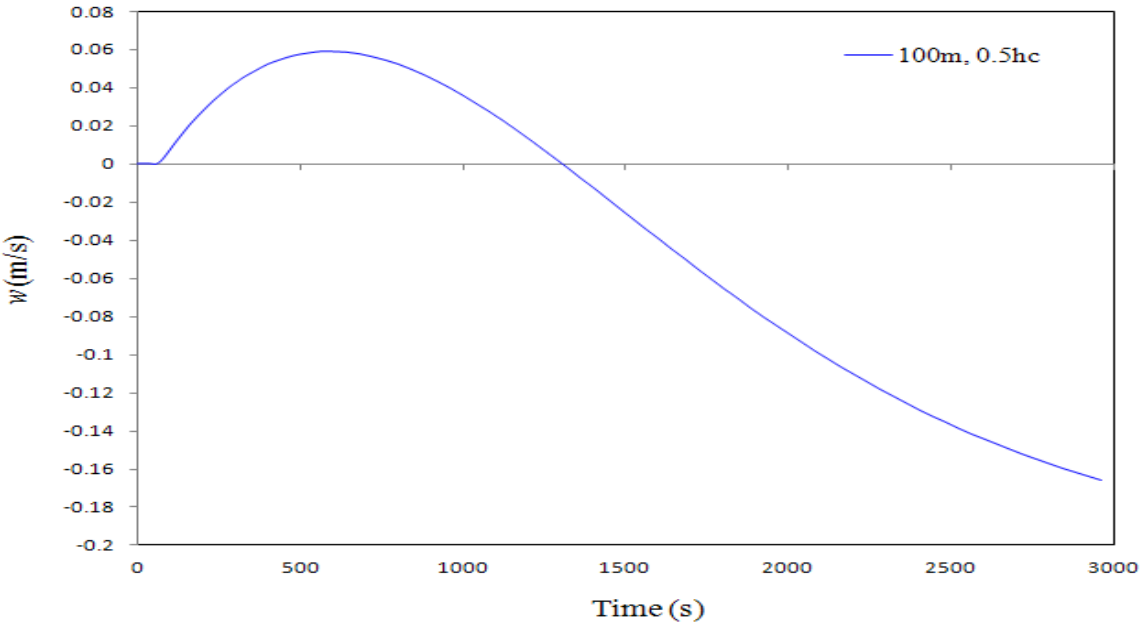

Figure 45: Variation of ship ascent velocity (100 m)

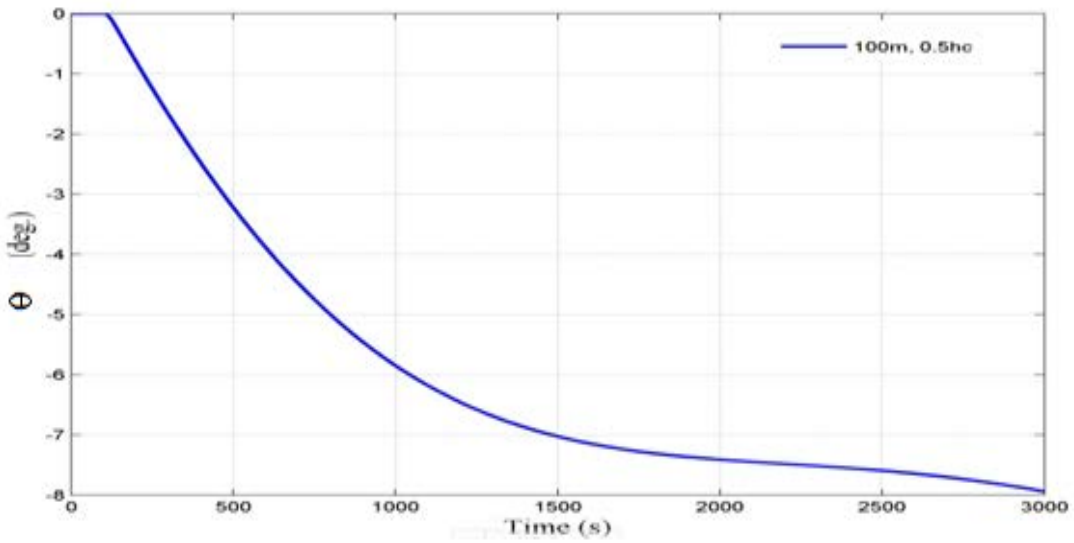

Figure 46: Variation of ship pitch angle (100m)

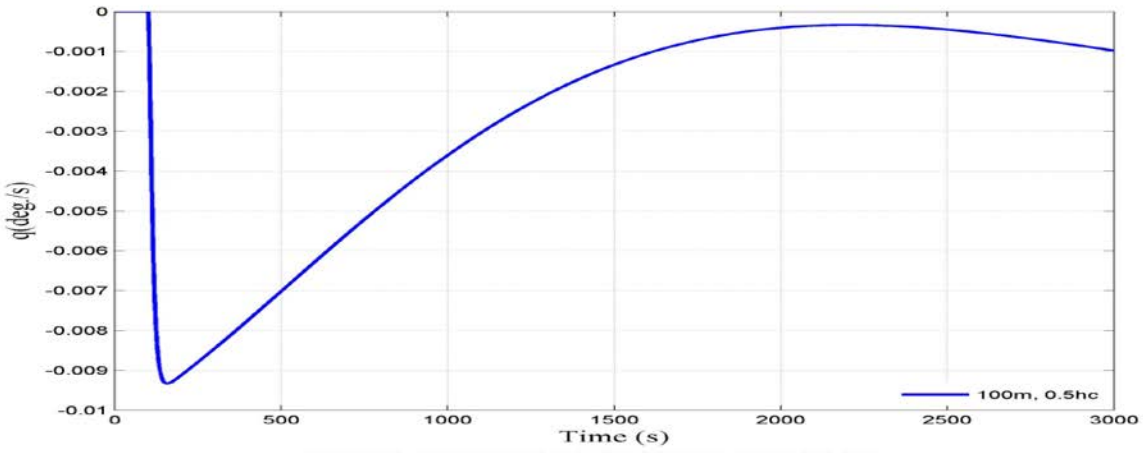

Figure 47: Variation of ship pitch rate (100m)

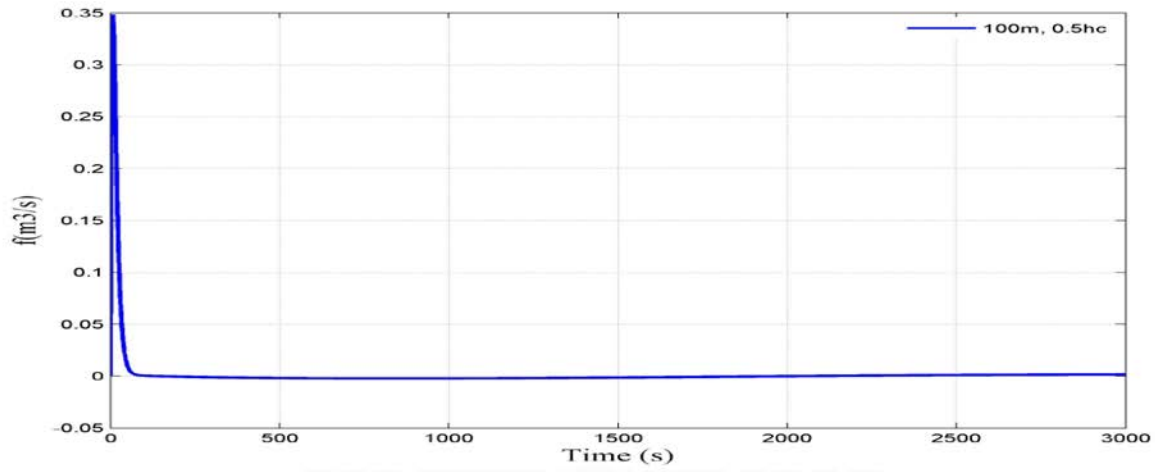

Figure 48: Variation of gas flow rate (100 m)

From the simulation results (Figures 44 - 48), it is understood that the performance of the PID controller is considerably degraded for the 50% variation in hydrodynamic coefficient values. Figure 44 shows that the controller is not capable of lifting the payload to the commanded depth under the effect of this variation in hydrodynamic coefficients. Pitch angle in Figure 46 is found to increase with time, which is not a good trend. Hence, it is realized that the proposed PID controller is not suitable for handling the parameter variations and they are very sensitive to the changes in system dynamics.

Case 3: Sensitivity Analysis: - Effect of external disturbances and uncertainty

In a marine salvage operation, there will be always chances of external disturbances occurring due to wind, current or voyage and uncertainties such as loss of buoyancy due to any lift bag failure, a sudden increase in added mass, volume of trapped air escaping etc. It is really difficult to predict it accurately.

In our simulation system, the external disturbance and parameter uncertainties are modeled as [36]:

$$d(t) = 0.05 + 0.25\cos(3\pi t) \quad (52)$$

The effect of external disturbances and uncertainties (denoted as 'ed') on the performance of PID controller is investigated by conducting numerical simulations for 100 m target depth in which the state space model is modified according to the Eq. 35 for calculating the state space model. The simulation results are plotted in Figures 49-53.

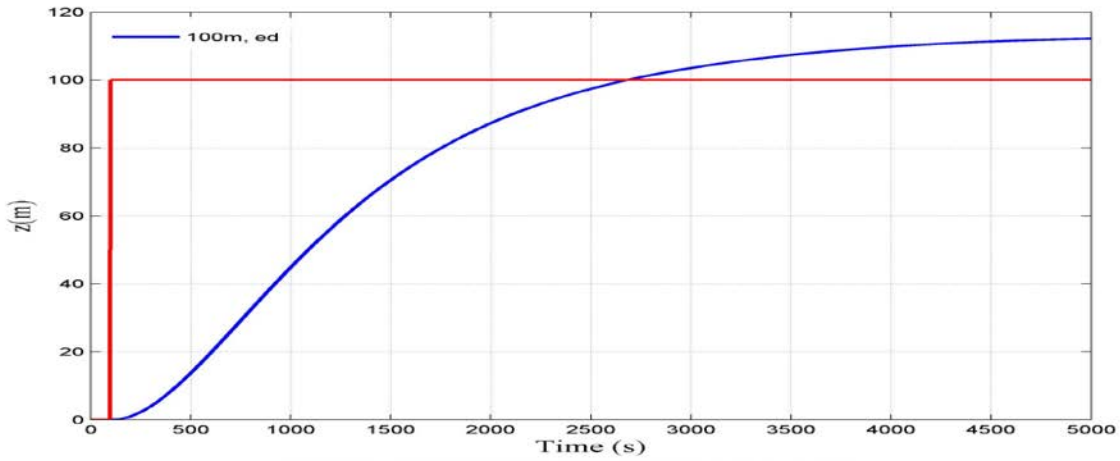

Figure 49: Variation of ship vertical position from sea bottom (100 m)

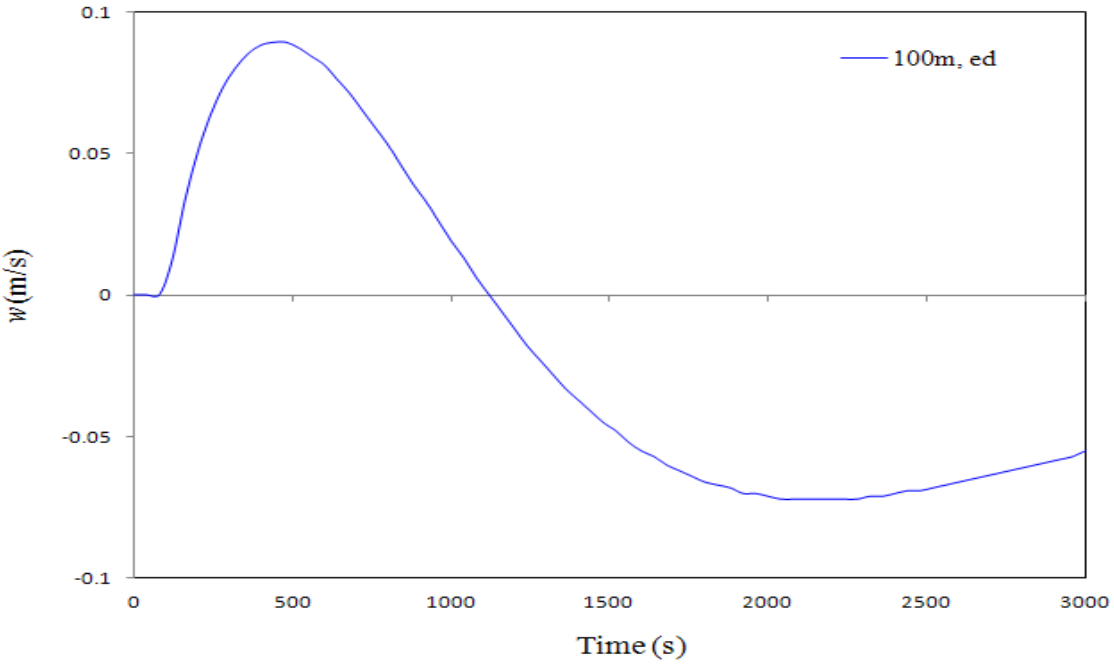

Figure 50: Variation of ship ascent velocity (100 m)

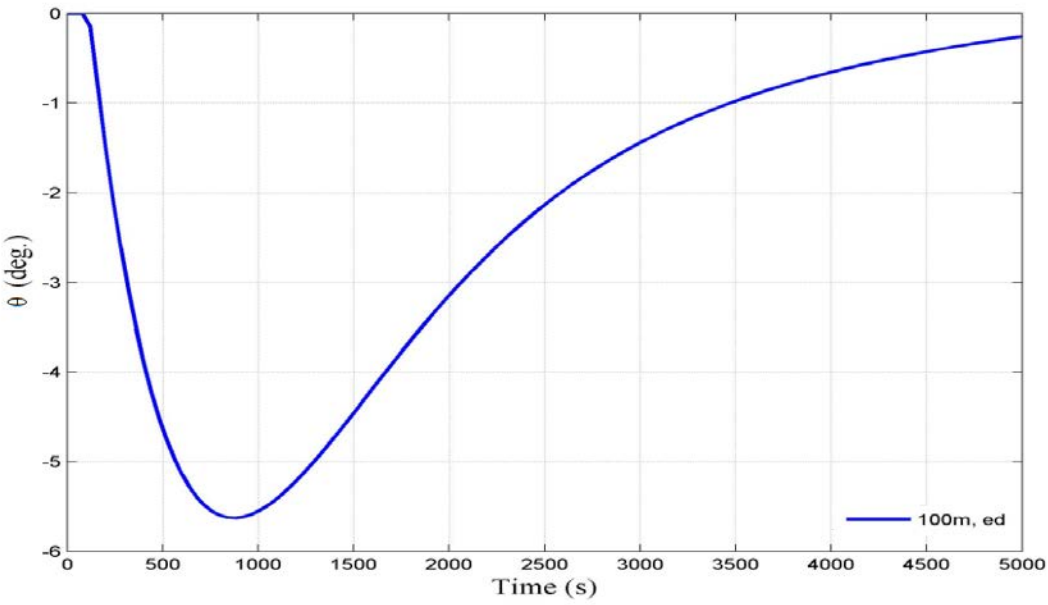

Figure 51: Variation of ship pitch angle (100m)

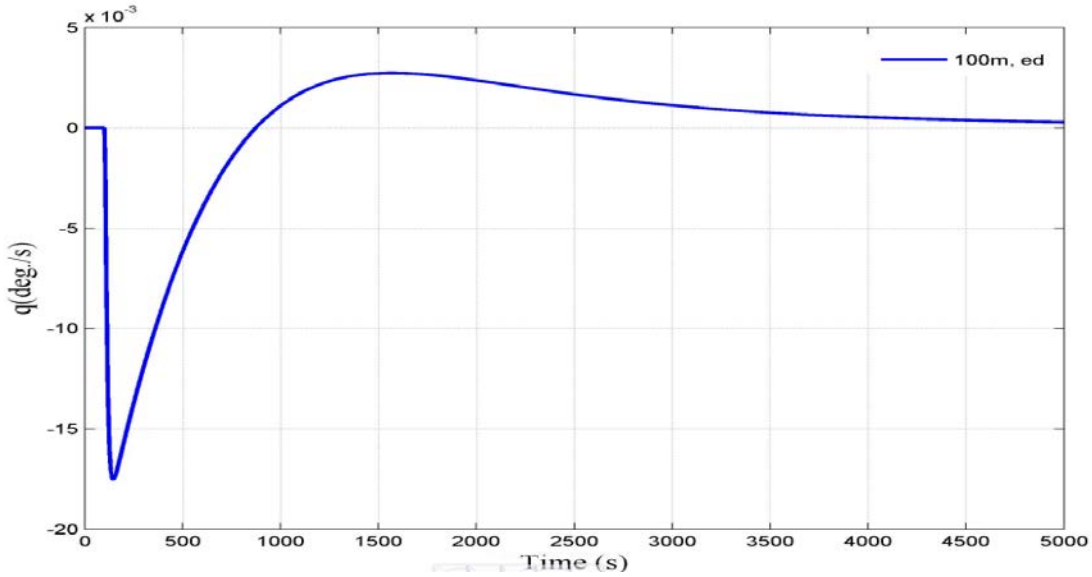

Figure 52: Variation of ship pitch rate (100m)

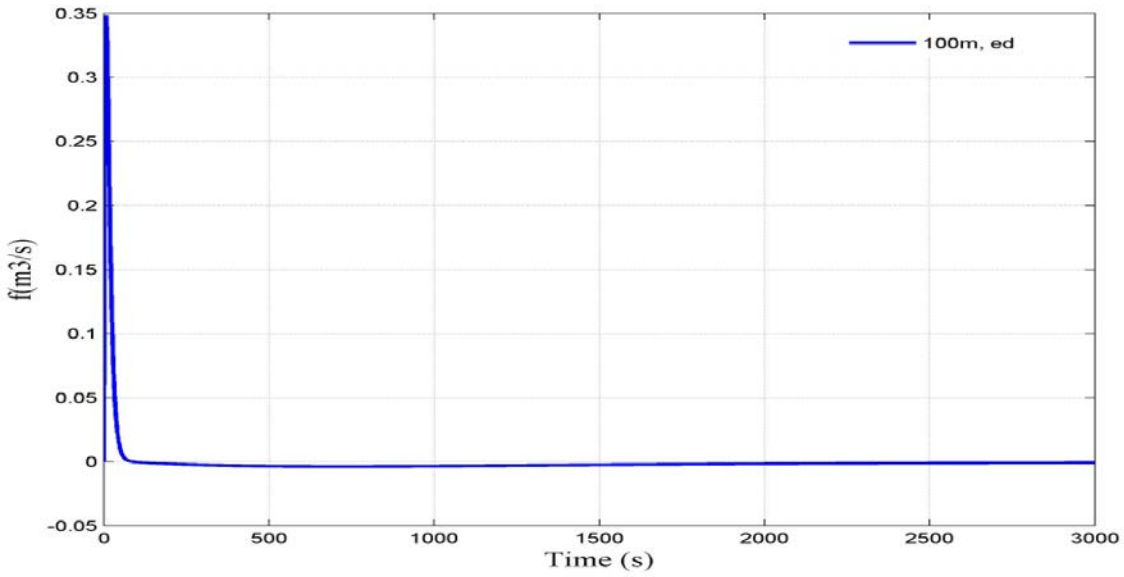

Figure 53: Variation of gas flow rate (100 m)

Figure 49 shows that due to effect of external disturbances, the system deviates from its equilibrium point and the payload reaches higher depth as the PID controller is not able to attain steady state. Even if the payload reaches the commanded depth, the ascent velocity in Figure 50

is not converging to zero. This implies that the proposed PID controller is not capable of handling external disturbances. Pitch response from Figures 51 & 52 shows satisfactory results with the PID controller. From Figure 53, it is understood that the controller action for the modified state space model is almost similar to the case without external disturbances for 100m.

Case 4: Sensitivity Analysis: - Sensor Failure.

Suppose, in worst situations, there can be chances of sensor failure (denoted as 'sf') in marine salvage operations, which might occur due to strong currents or voyage of other ships etc. The behavior of the PID controller in such situation is investigated by conducting open loop simulation for 100 m. The obtained responses are plotted in Figures 54-57.

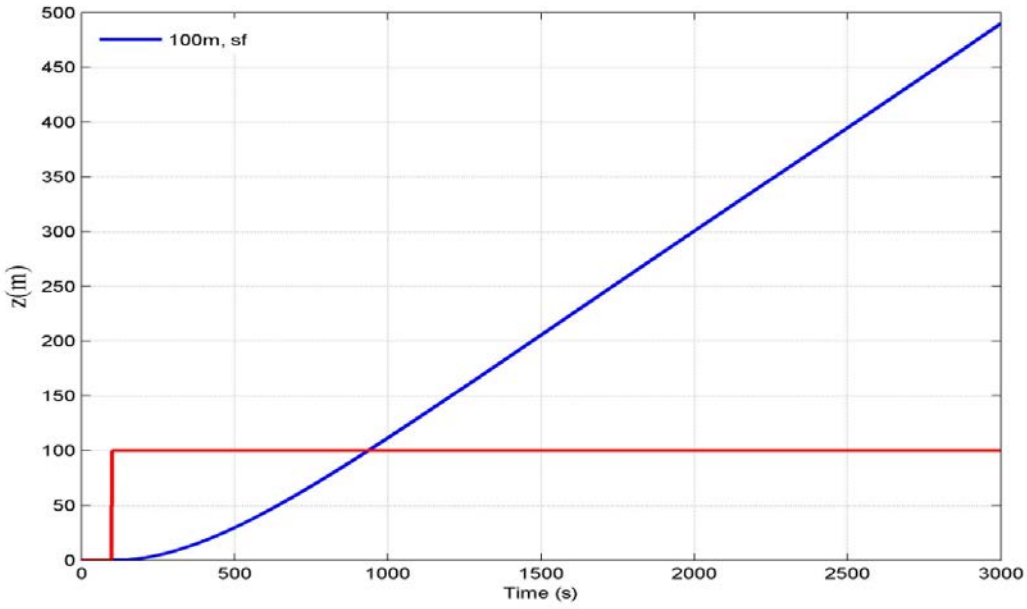

Figure 54: Variation of ship vertical position from sea bottom (100 m)

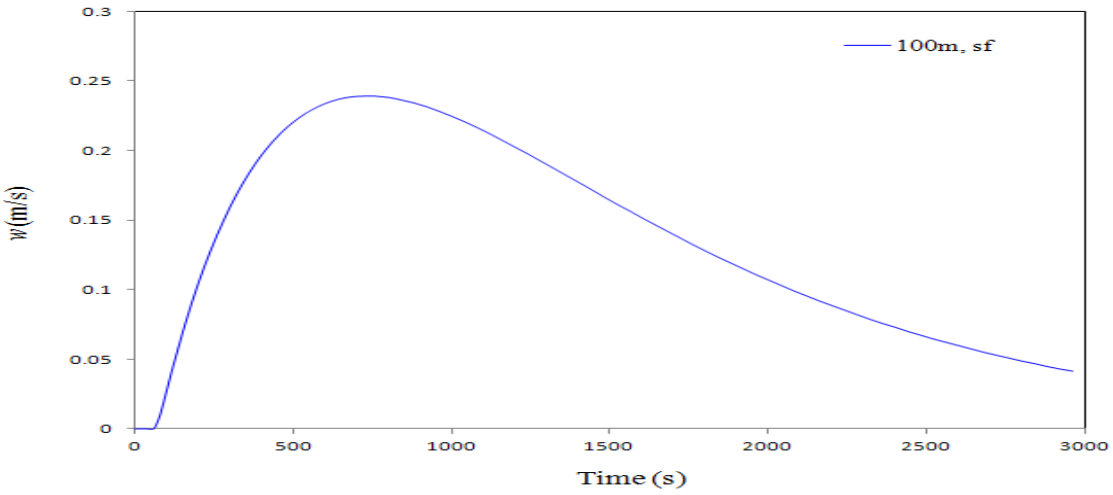

Figure 55: Variation of ship ascent velocity (100 m)

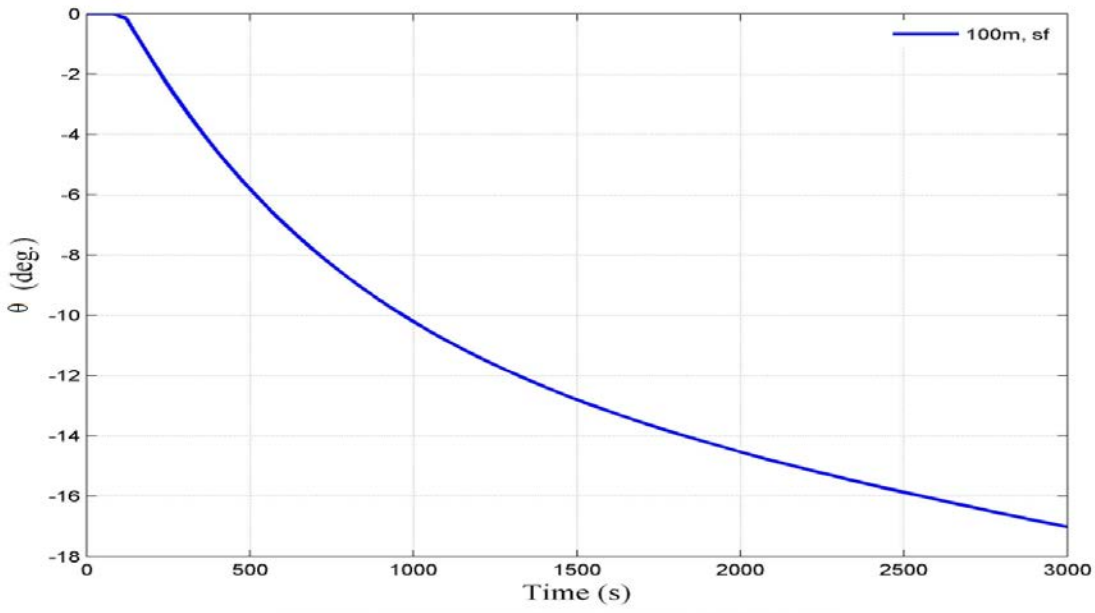

Figure 56: Variation of ship pitch angle (100m)

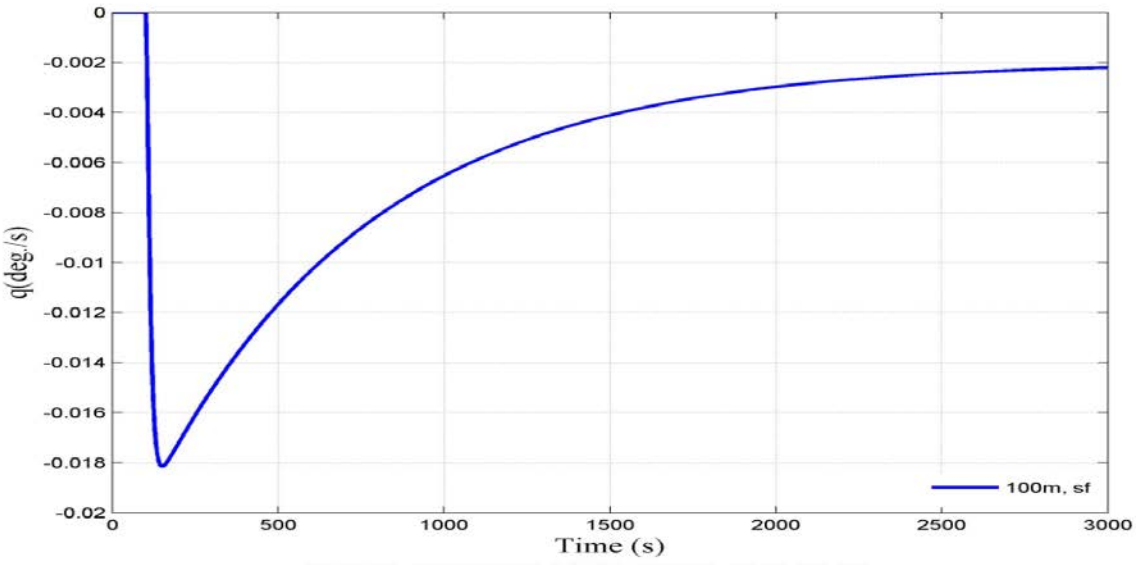

Figure 57: Variation of ship pitch rate (100m)

From Figure 54, it is found that the system is completely unstable as the payload reaches nearly 480 m due to the feedback sensor failure. As sensor fails, the controller cannot be able to track the reference trajectory and the payload reaches higher positions abruptly by losing the control action. Also the pitch angle, in Figure 56, is found to go on increasing with time and to reaching high values, which implies the chance of lift bags to loose free from payload and breach the surface of water too fast and cause damage to the hull and risks to divers and crew members. This reveals that for a complex underwater operation like marine salvage, a closed loop control system is mandatory. Therefore, the only solution is to avoid such situations by providing better protection to the controller components.

Remarks

From the case studies, it is found that PID controller gives satisfactory results for almost all water depths by approximating a linear deterministic model with considerable overshoot, where as in the presence of parameter variations, non linearity and external disturbances, good results are not guaranteed. This is due to the fact that the PID controller is using a linear control law, which is not suitable for non linear undeterministic dynamics. In the case of the disturbance

change, the performance of the PID controller is considerably degraded because it uses constant gains although operation conditions are changing. It is also noted that for salvage operations, a closed loop control system is mandatory to achieve the desired performance, therefore it is important to try to avoid failure in controller components especially sensor failure as it significantly affects the performance of the controller.

5.3 Conventional Sliding Mode Controller (CSMC)

From the simulation studies, it is understood that the well-developed linear classic controllers like PD & PID fails in satisfying performance requirements especially when changes in the system and environment occur during the salvage operation. Therefore now it is required to adopt a control system, which is capable of handling non linearity, parameter variations and external disturbances with good robustness. A sliding mode controller (SMC) is selected as the primary controller for regulating the flow rate of filling gas inside the lift bags according to buoyancy requirement so that the system attains stability in diving plane. This selection was made due to the following reasons [3, 12, 15, 22, 34, 36-38, 49-50, 58-60, 65, 68, 80-81, 104-106, 109, 126, 131, 139-140, 145,149-150]:

- SMC compensates for nonlinear behaviours
- SMC provides robustness to uncertainty
- SMC is straightforward to implement

In a closed loop control system, the function of the controller is to make the state variable x_s follow the desired state x_d with a prescribed dynamic characteristic in the presence of uncertainty and disturbances. The state variable error is defined as [12, 65,139]:

$$e = x_d - x_s = z_{com} - z \tag{53}$$

Or in general, the state variable error vector can be written as

$$\tilde{e} = (e, \dot{e}, \ddot{e} ..... e^{(n-1)})^T \quad (54)$$

Where n is the order of the system. In the development of sliding mode controller, a sliding surface (σ) is to be created from a linear combination of the state variable errors such as position, velocity and acceleration. The aim is to drive the system to the sliding surface and ultimately to the condition $\sigma = 0$ while making sure that the state variables are always reducing. The sliding surface σ can be defined for an n^{th} order system as [12, 49-50, 65, 80-81, 105]:

$$\sigma = (\frac{d}{dt} + \lambda)^{n-1} e \quad (55)$$

Therefore, for a second order nonlinear system (n = 2), the corresponding sliding surface would be defined as:

$$\sigma = \dot{e} + \lambda e \quad (56)$$

Where λ is the slope of the sliding surface. Then, the Lypunov method can be used to formulate the control law (u_c), which is further developed by defining a positive definite function , $V(\sigma) > 0$ where the derivative of this function for all times greater than zero is negative. By defining a positive definite Lyapunov function's derivative as negative, we guarantee that the sliding surface (σ) is always reducing [37, 65, 139-140].

Let the Lypunov function,

$$V(x_s) = \frac{1}{2}[\sigma(x_s)]^2 \quad (57)$$

The scalar function $\sigma(x_s)$ is the weighted sum of the errors in the states x_s [12, 65].

$$\sigma(x_s) = s^T x_s \quad (58)$$

The time derivative of Lypunov function $V(x_s)$ should be negative in order to provide stability [12, 37, 49-50],

$$\dot{V}(x_s) = \sigma\dot{\sigma} < 0 \tag{59}$$

This can be accomplished if,

$$\sigma\dot{\sigma} = -\eta^2|\sigma| \tag{60}$$

The term η^2 is an arbitrary positive quantity, selected to ensure that $\dot{V}$ is negative even in the presence of modeling errors and disturbances. Therefore,

$$\dot{\sigma} = -\eta^2\frac{|\sigma|}{\sigma} = -\eta^2 sgn(\sigma) \tag{61}$$

Where $sgn(\sigma)$ is the signum function that is discontinuous across the sliding surface provided to ensure stability and is given by [12, 37, 65]:

$$sgn(\sigma) = \begin{cases} 1, & \text{if } \sigma > 0 \\ 0 & \text{if } \sigma = 0 \\ -1, & \text{if } \sigma < 0 \end{cases} \tag{62}$$

From Eqs. (58) and Eqs. (33),

$$\dot{\sigma} = s^T\dot{x}_s = s^T\left[Ax_s + Bu_c\right] \tag{63}$$

Combining Eqs. (61) and (63), we can write

$$\dot{\sigma} = s^T\dot{x}_s = s^T\left[Ax_s + Bu_c\right] = -\eta^2 sgn(\sigma) \tag{64}$$

By solving the above equation, the control law u_c is obtained as:

$$u_c = -\left[s^TB\right]^{-1}s^TA - \left[s^TB\right]^{-1}\eta^2 sgn(\sigma) \tag{65}$$

In which the first term describes the nonlinear state feedback whereas the second term represents the switching control law. A control law of the form (Eq. 65) guarantees the stability for nonlinear systems whereas the discontinuous term (*sgn (σ)*) results in undesirable chattering around the sliding point. It can be avoided by smoothing the control law with in a thin boundary layer around the sliding surface. This can be achieved by choosing a boundary layer thickness Φ_b and replacing the discontinuous *signum* function by a continuous *saturation* function (*sat* (σ/Φ_b)) [3, 12, 37, 65, 106, 139-140]. This *saturation* function has the same end points as the *signum* function, however the function has a more gradual transition towards zero value as $\sigma \rightarrow 0$. Next, the control law u_c can be written after linearization and smoothing as [22, 49-50, 65, 72, 127, 139]:

$$u_C = -\left[s^T B\right]^{-1} s^T A x_S - \left[s^T B\right]^{-1} \eta sat\left(\sigma / \Phi_b\right) \tag{66}$$

Where

$$sat\left(\sigma / \Phi_b\right) = \begin{cases} \text{sgn}\ (\sigma) & |\sigma| > \Phi \\ \sigma / \Phi_b & |\sigma| \le \Phi \end{cases} \tag{67}$$

The values of *A* and *B* can be obtained from Eq. (34). By further letting $k = [s^T B]^{-1} s^T A$, Eq. (66) becomes:

$$u_C = -kx_S - \left[s^T B\right]^{-1} \eta sat(\sigma / \Phi_b) \tag{68}$$

The gain vector *k* can be calculated in MATLAB using the pole placement method [12, 65]. Figure 58 represents the SIMULINK block diagram of the conventional sliding mode controller for regulating the gas flow rate.

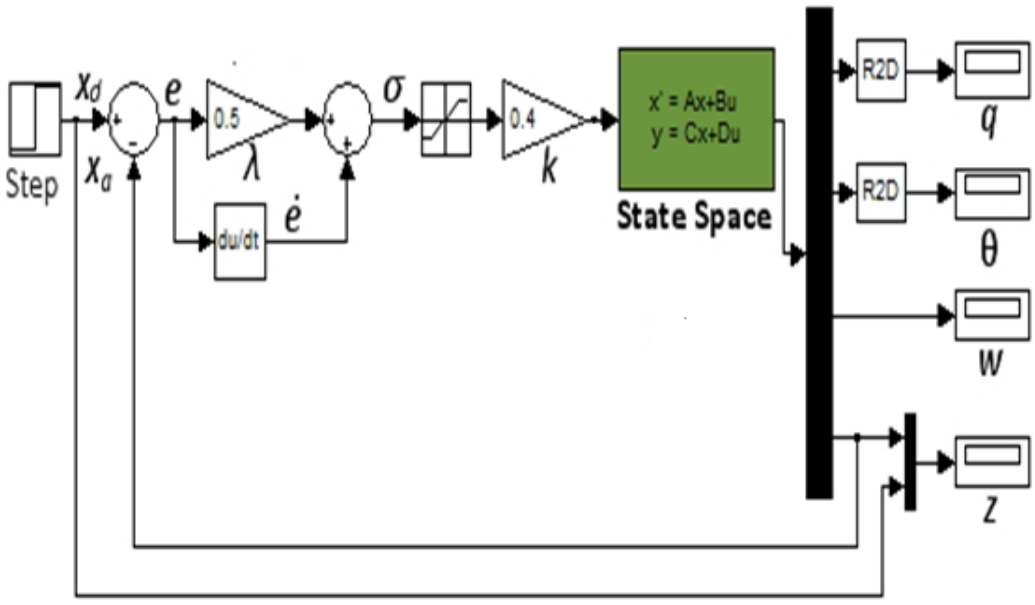

Figure 58: SIMULINK block diagram of the Conventional Sliding Mode Controller (CSMC) for regulating the gas flow rate

Simulations are initially performed on the pontoon model for target depths of 50 m, 100 m & 150 m from sea bottom. The obtained vertical dynamic responses and the variation of control parameter are plotted in Figures 59-67. From Figures 59-61, it is found that in all the three cases, the payload reaches the respective commanded depths without any overshoot by properly tuning the sliding mode controller. The rise time required for the SMC to reach steady state is nearly equal to that of PD controller. After reaching the desired depth, even if the simulation time is increased, it has no effects on the system performance due to the controller action. The settling time required in all the three cases are exactly same and equals to 1500 s. Figure 62 shows that there is a steep increase in the value of ascent velocity soon after the suction break out, while it reduces significantly due to the sliding mode controller action. The maximum value of ascent velocity is found be 0.45 m/s- being within the required range (< 0.6 m/s). This implies how the pontoon motion is stable. When the vessel reaches the commanded depth, the controller reduces

the ascent velocity to almost zero value in all the three cases. While conducting simulations, it is noted that for higher target depths (see 150m case) with the same tuned settings, the peak of the response become flat instead of sharp to make the depth rate or ascent velocity within the stable region. With the use of non linear control law, the performance of SMC is found to be much better than the PD and PID controller for regulating the depth rate and pitch motion even for higher water depths.

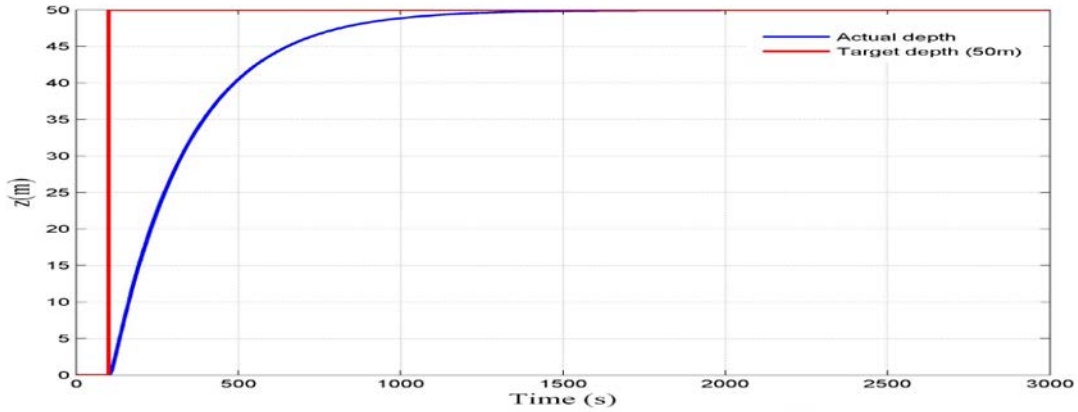

Figure 59: Variation of ship vertical position from sea bottom (50 m)

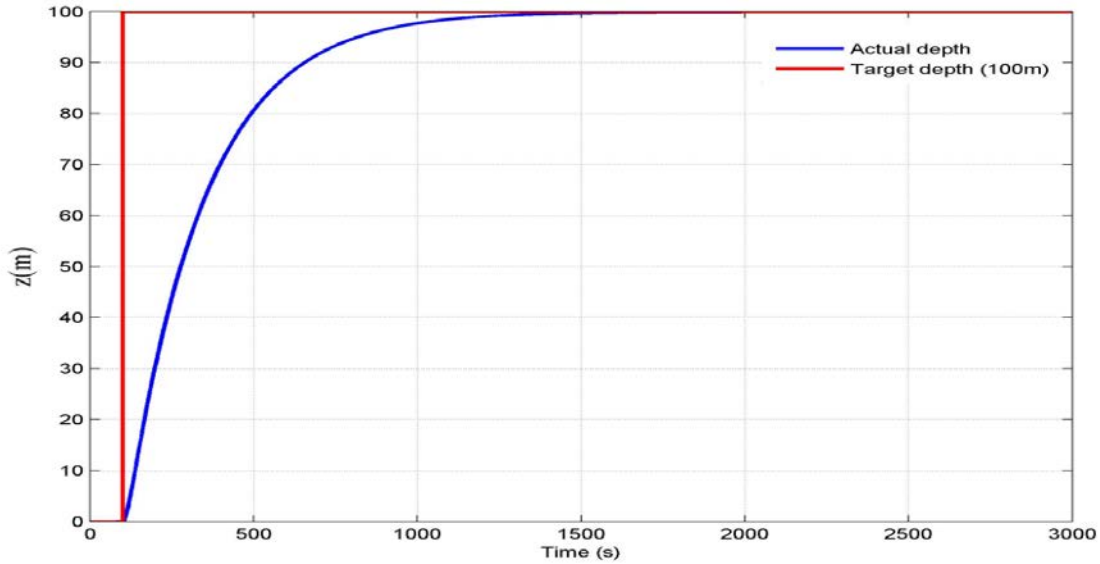

Figure 60: Variation of ship vertical position from sea bottom (100 m)

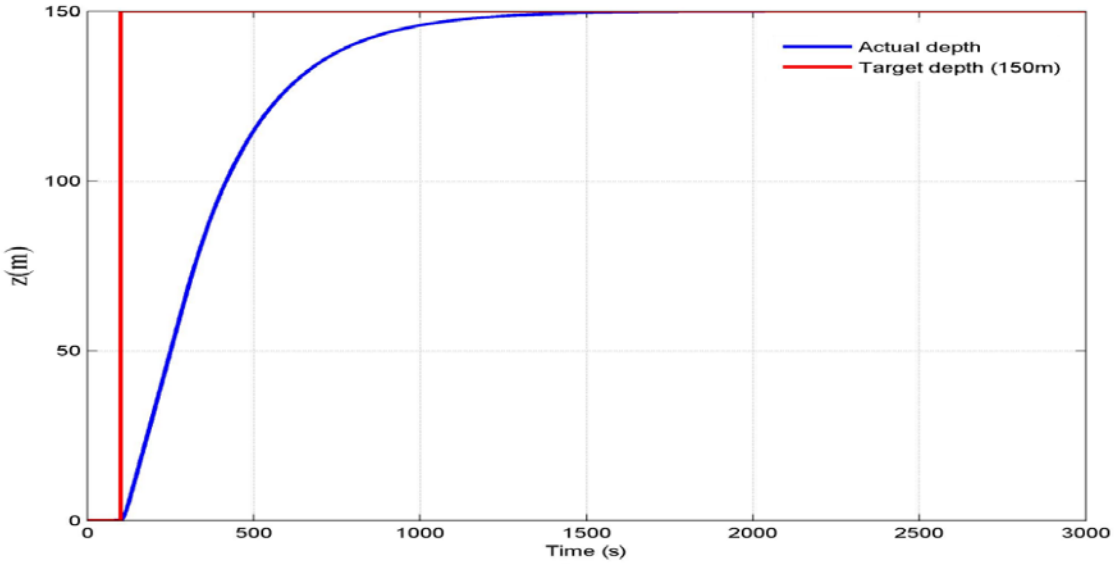

Figure 61: Variation of ship vertical position from sea bottom (150 m)

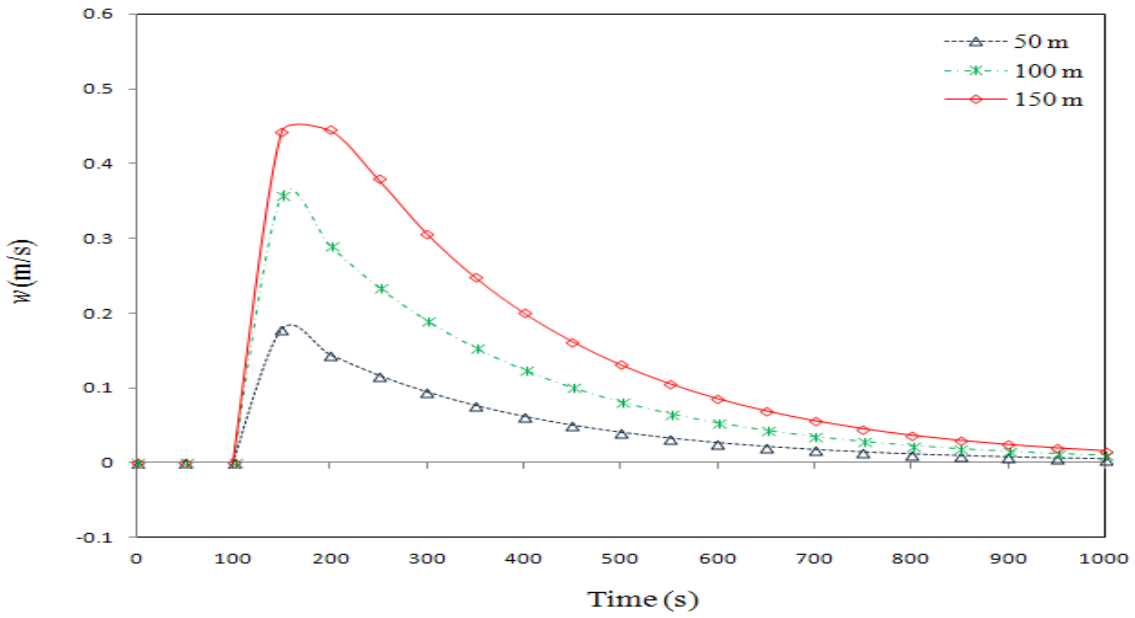

Figure 62: Variation of ship ascent velocity for 50 m, 100 m & 150 m

Similar to the ascent velocity in Figure 62, the pitch angle in Figure 63 increases soon after break out, reaching a maximum value and thereafter decreasing. The maximum value of pitch angle is found to be about 12 degrees, which is within the required limit (< 15 deg.). Nevertheless, the pitch angle becomes almost zero, when the pontoon reaches, the commanded depth due to the fact that the controller generates pitch angle commands as per the depth error. Similar to the response curve for ascent velocity in Figure 62, the peak of the pitch angle response curve in Figure 63 becomes flat instead of sharp for higher water depths (see 150 m case) with the same tuned settings to make sure that the response never goes beyond the stable region (i.e. > 15 deg.). The variations in pitch rate for the three target depths are produced in Figures 64. It is noted that the pitch rates for all three target depths reaches a higher value after breakout and thereafter decreasing and finally attains zero value, when the pontoon reaches the target depth.

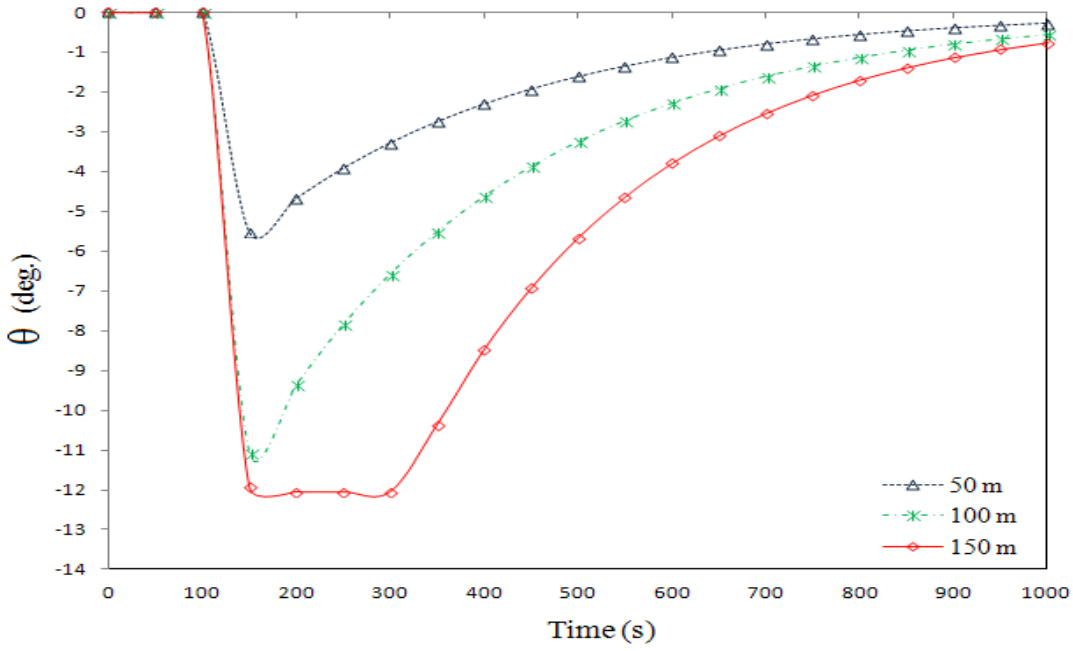

Figure 63: Variation of ship pitch angle for 50m, 100m & 150 m

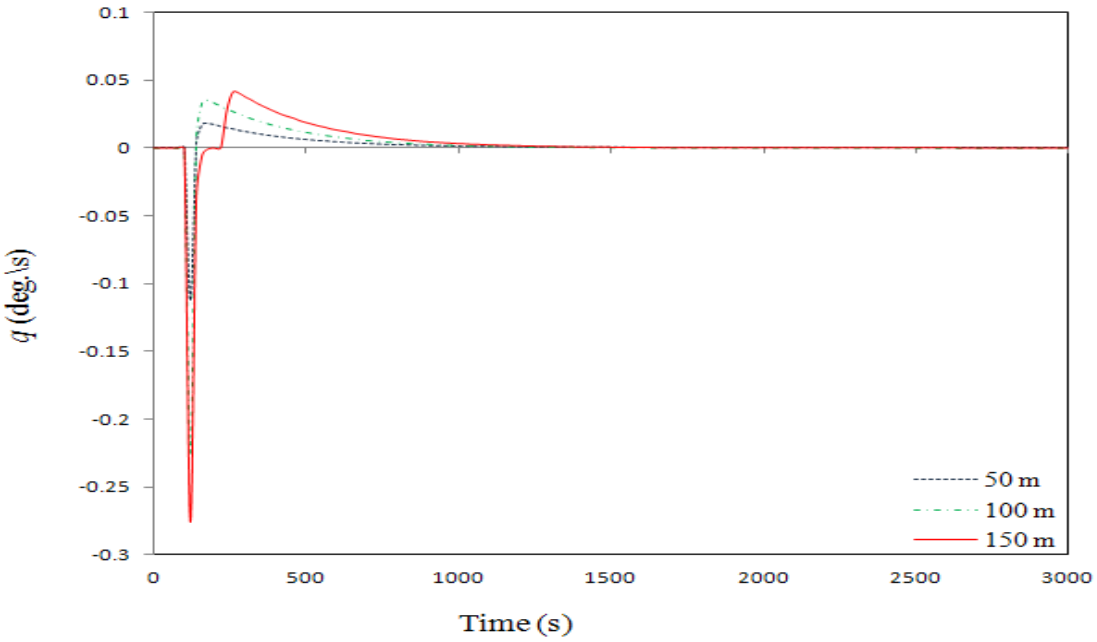

Figure 64: Variation of ship pitch rate for 50, 100 & 150 m

For better visibility, gas flow rates for the three target depths are presented separately as shown in Figures 65-67. Initially for all the three target depth cases, the controller sets the flow rate to a higher value 0.096, 0.1 and 0.108 m^3/s to reach the additional buoyancy to overcome the suction break out force and to achieve the desired depths. It is seen that soon after the break out, the SMC reduces the flow rate significantly to reduce the ascent rate. Once the target depth is fulfilled, the controller further reduces the flow rate to almost zero value.

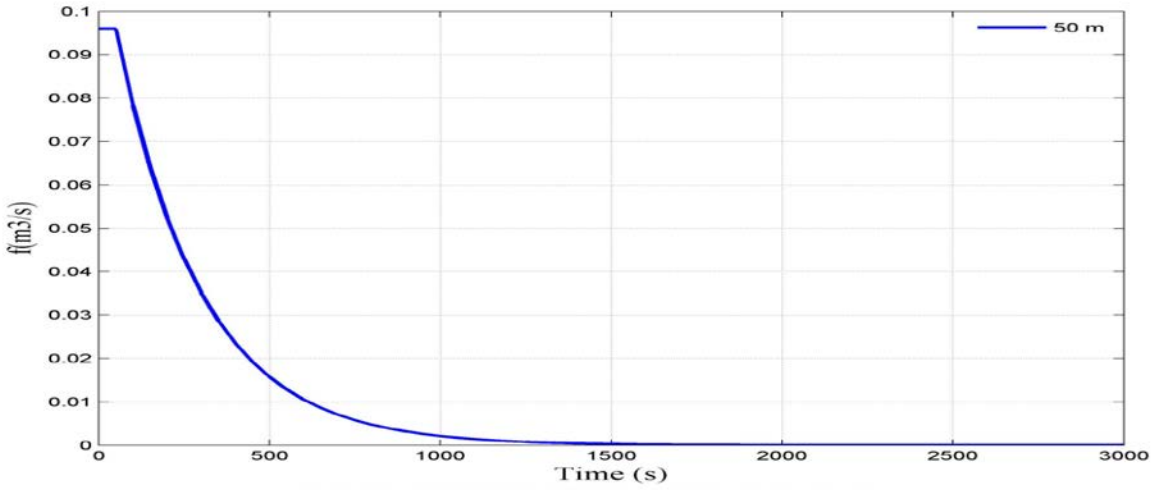

Figure 65: Variation of gas flow rate (50m)

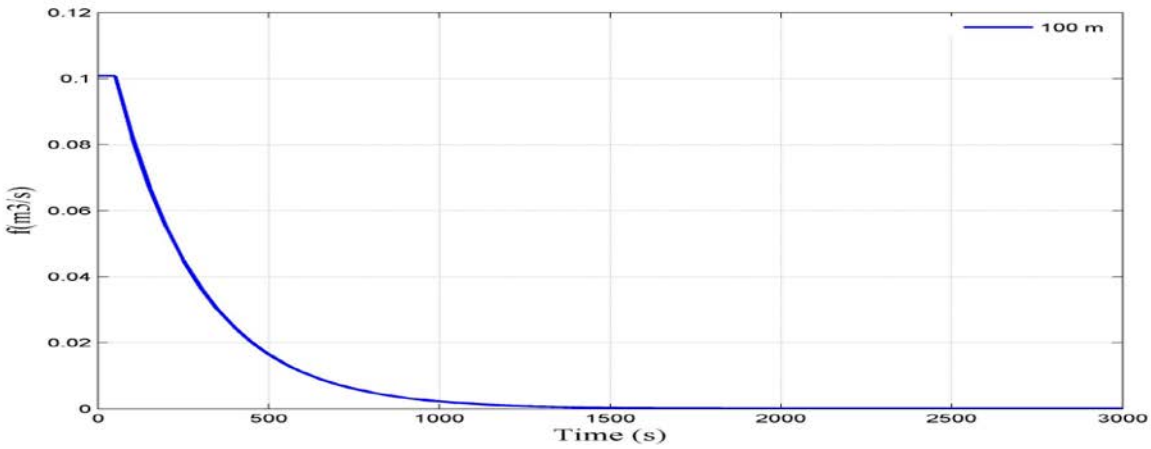

Figure 66: Variation of gas flow rate (100m)

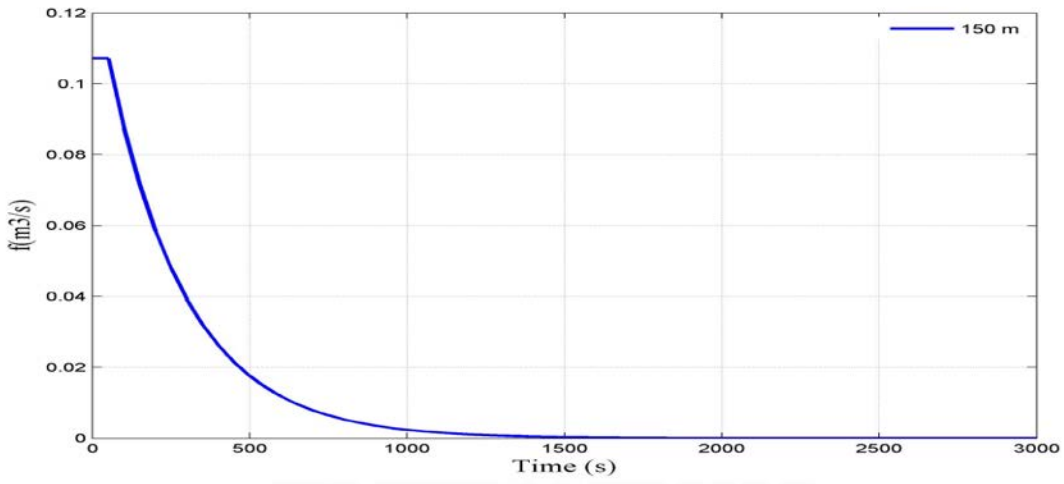

Figure 67: Variation of gas flow rate (150m)

From the simulation, it is understood that the proposed SMC is suitable for controlling the heave and pitch motions without overshoot, moderate settling time and having no steady state error even for higher water depths with the same tuned settings in comparison with PD and PID controllers, which is the most important requirement in a salvage operation. This is mainly due to the reason that the SMC uses a non linear control law, where as PD & PID controllers use a linear one. Also, it is proved that the designed SMC is capable of handling non linear salvage dynamics with the assumption of a linearised state space model, which implies the supremacy of SMC in comparison with PD and PID controllers. During the simulation, the most difficult task faced by the author is how to tune the controller precisely (i.e. to find the controller gain and slope of the sliding surface) for the optimum performance. The performance of the SMC is further investigated by conducting case studies including sensitivity analysis and considering the effect of external disturbance.

Case 1: Sensitivity Analysis: - Variation in break out force

As discussed earlier, a preliminary sensitivity analysis is carried out by considering the effect of variation in breakout force on the trajectory of simulation. The lower and higher values of total break out lift force (8508.5 kgf & 11749.83 kgf) are accounted in the simulation for a target depth of 100 m from sea bottom. From the simulation response (Figures 68-74), it is found that there is no significant variation in response trajectories where as there is considerable change in initial gas flow rate value to make sure that the pontoon breaks free from sea bed within the same time (i.e. 100s).

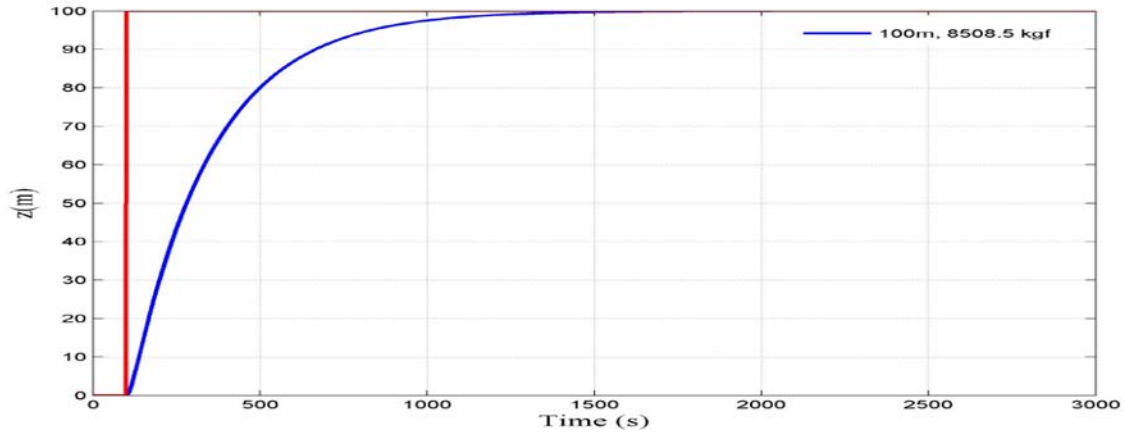

Figure 68: Variation of ship vertical position from sea bottom (100 m, 8508.5kgf)

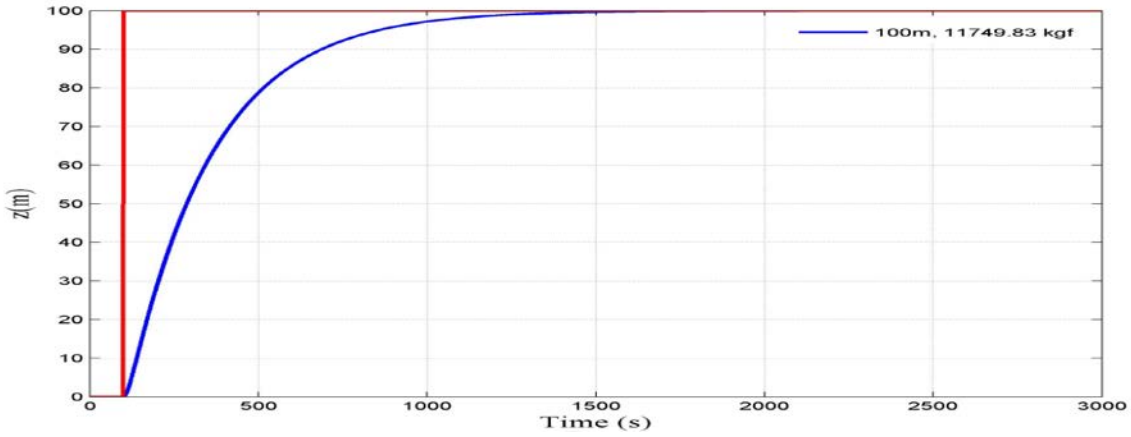

Figure 69: Variation of ship vertical position from sea bottom (100 m, 11749.83kgf)

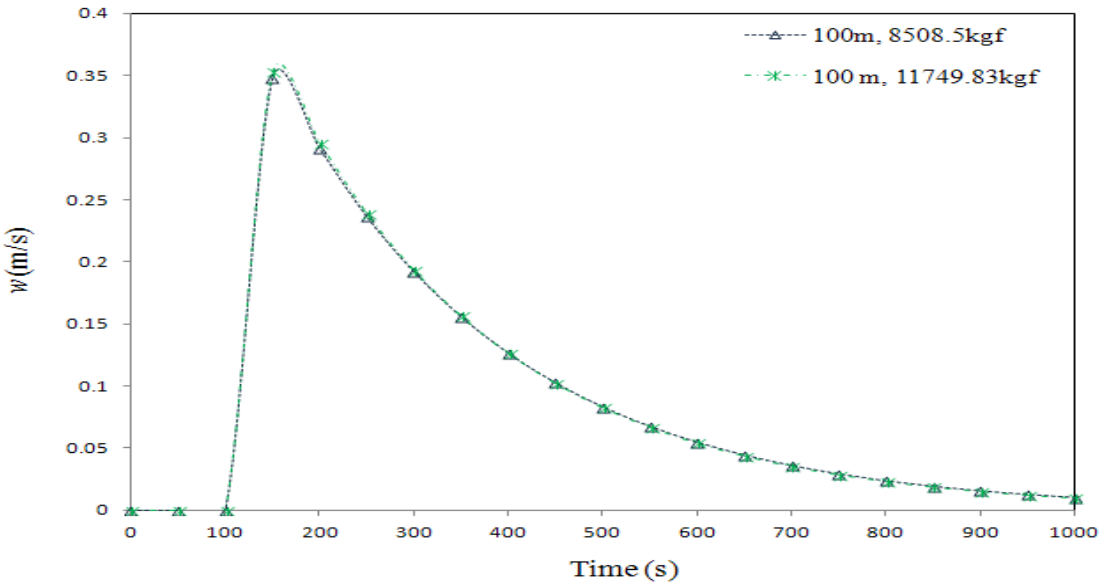

Figure 70: Variation of ship ascent velocity (100 m)

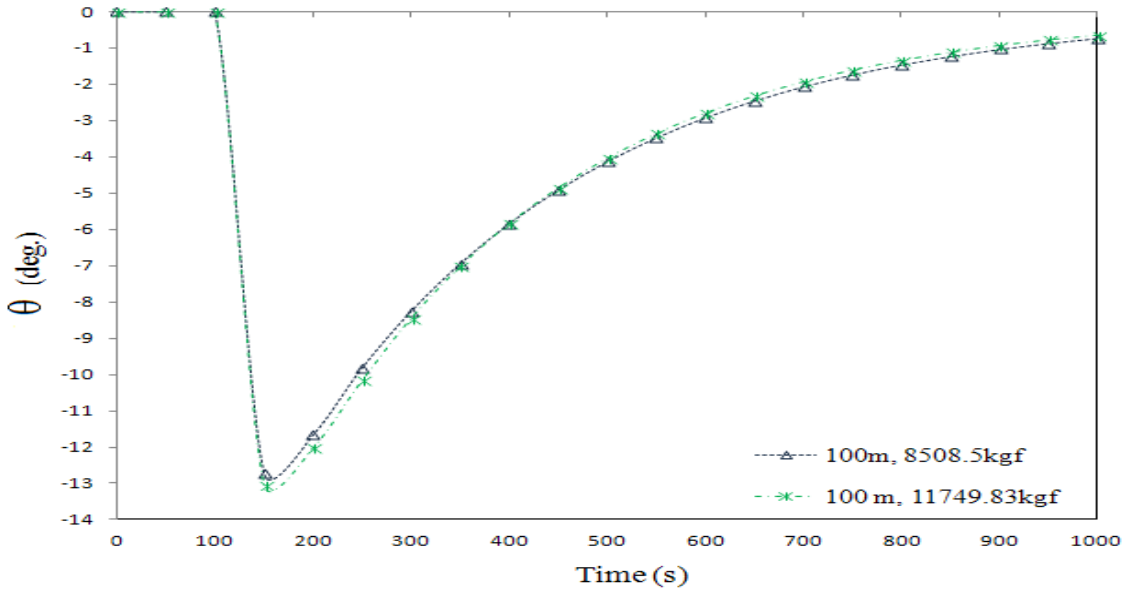

Figure 71: Variation of ship pitch angle (100 m)

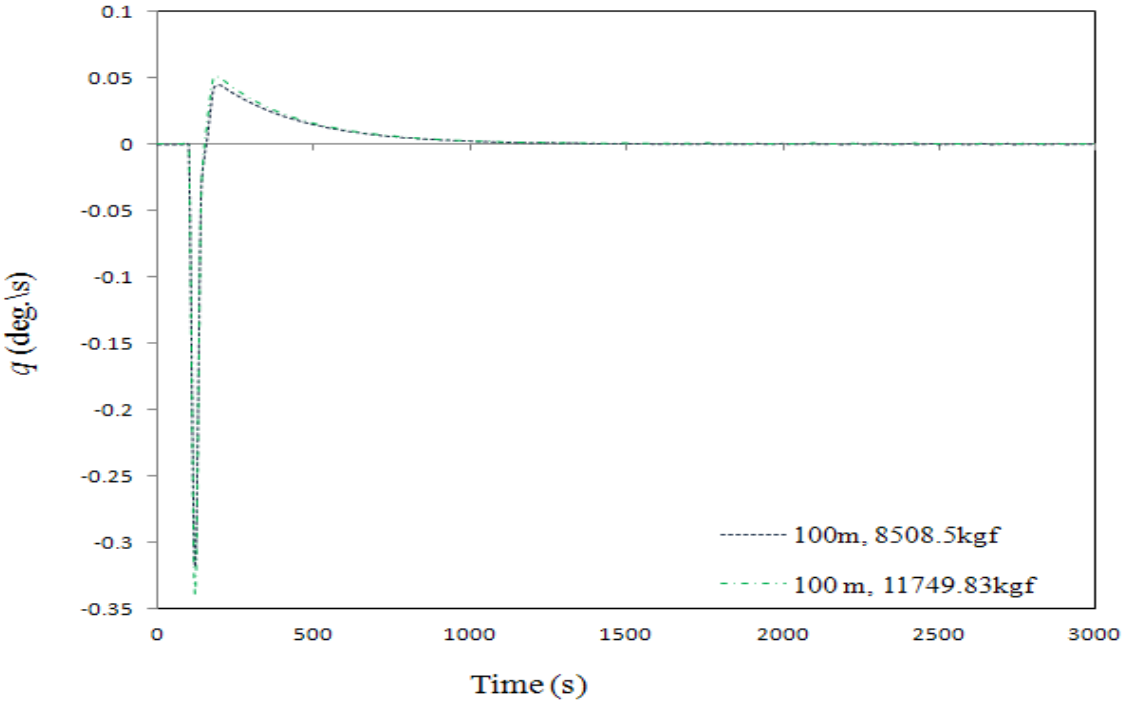

Figure 72: Variation of ship pitch rate (100 m)

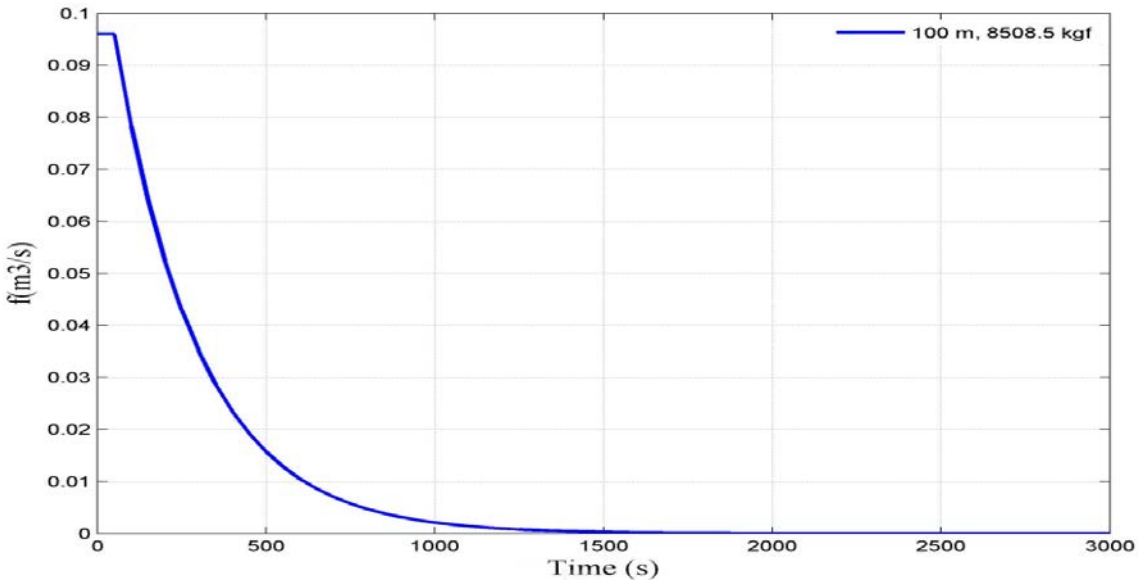

Figure 73 Variation of gas flow rate (100 m, 8508.5 kgf)

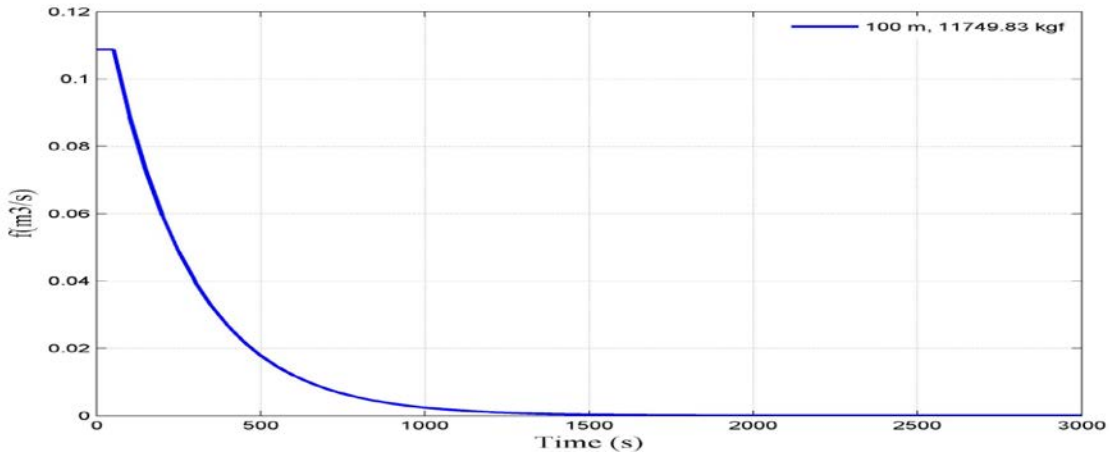

Figure 74: Variation of gas flow rate (100 m, 11749.83kgf)

Case 2: Sensitivity Analysis: - Variation in hydrodynamic coefficients.

A sensitivity analysis is performed with the proposed SMC by allowing a 50 % variation in hydrodynamic coefficients used in the simulation program. Simulation is carried out by considering this variation for a target depth of 100 m from sea bottom on the pontoon model. From the simulation results (Figures 75-79), it is found that SMC is still able to maintain hydrodynamic stability throughout the ascent even with this 50% variation in hydrodynamic coefficients. Figure 75 shows that the reaching time for attaining the target depth decreases from 1500s (see Figure 60) to nearly 900s due to this variation. There is no significant variation in response trajectories, except the maximum value of pitch angle reduces from 12^0 to 8^0.

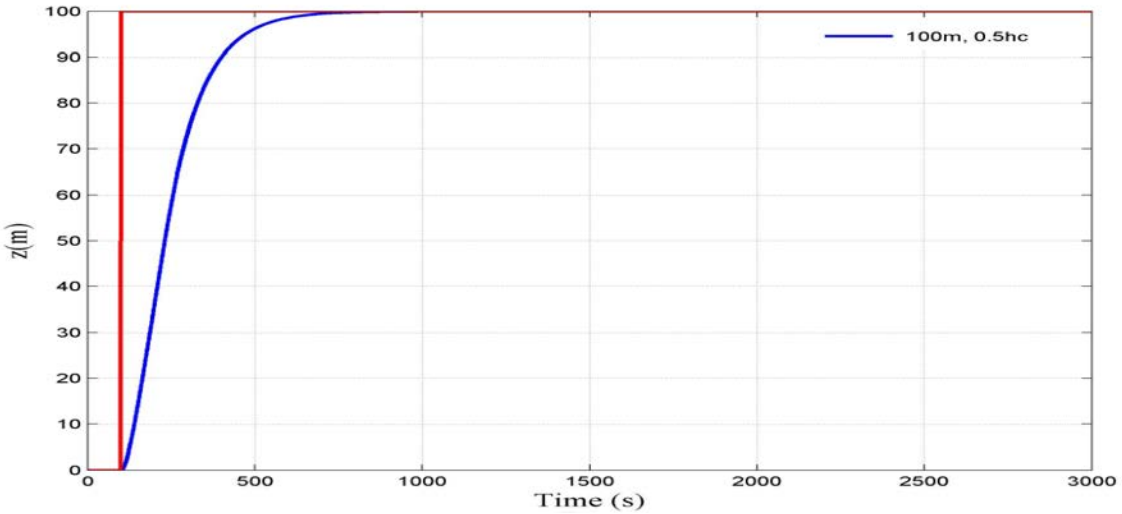

Figure 75: Variation of ship vertical position from sea bottom (100 m)

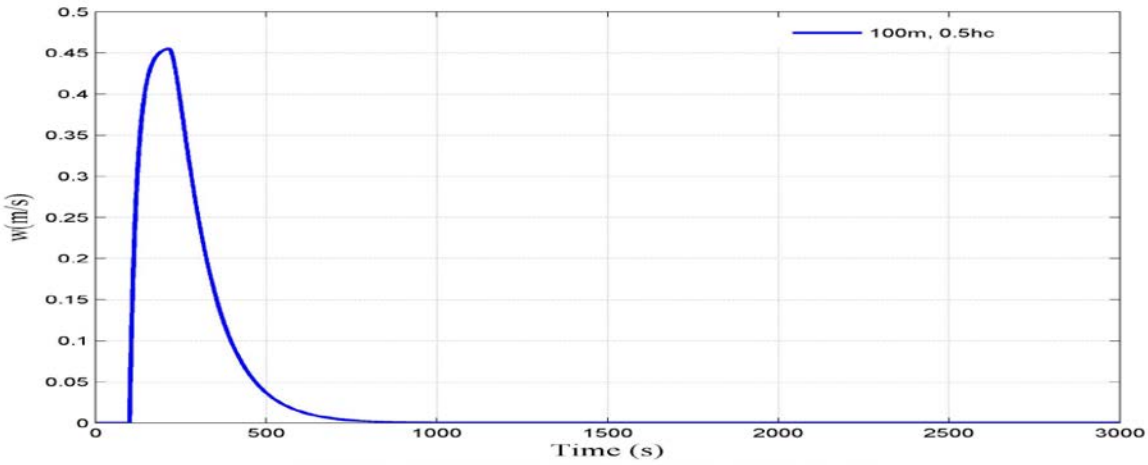

Figure 76: Variation of ship ascent velocity (100 m, 0.5hc)

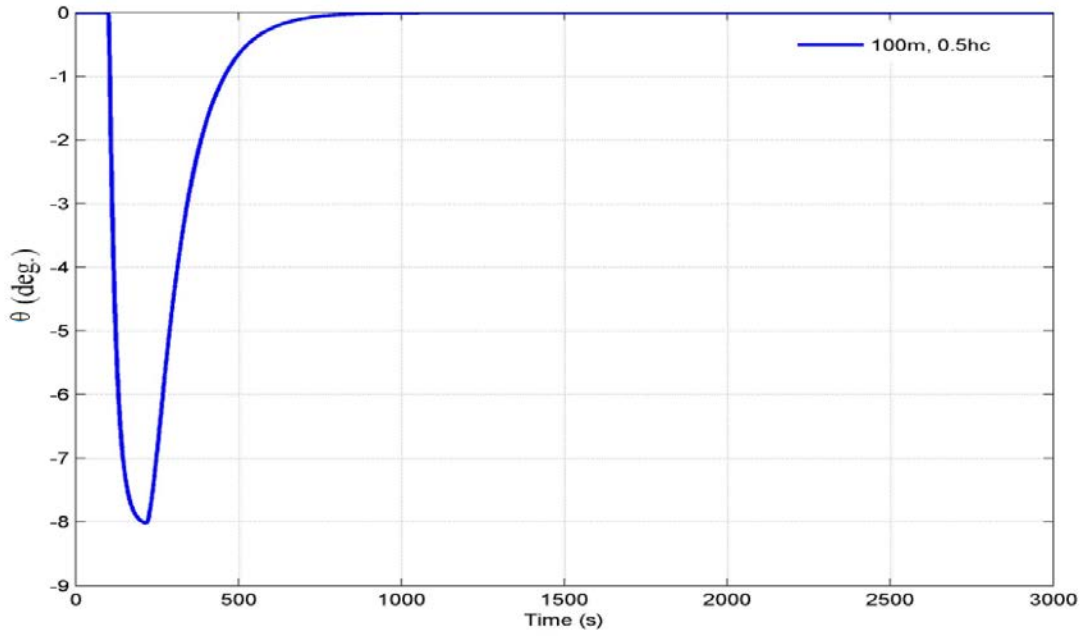

Figure 77: Variation of ship pitch angle (100 m, 0.5hc)

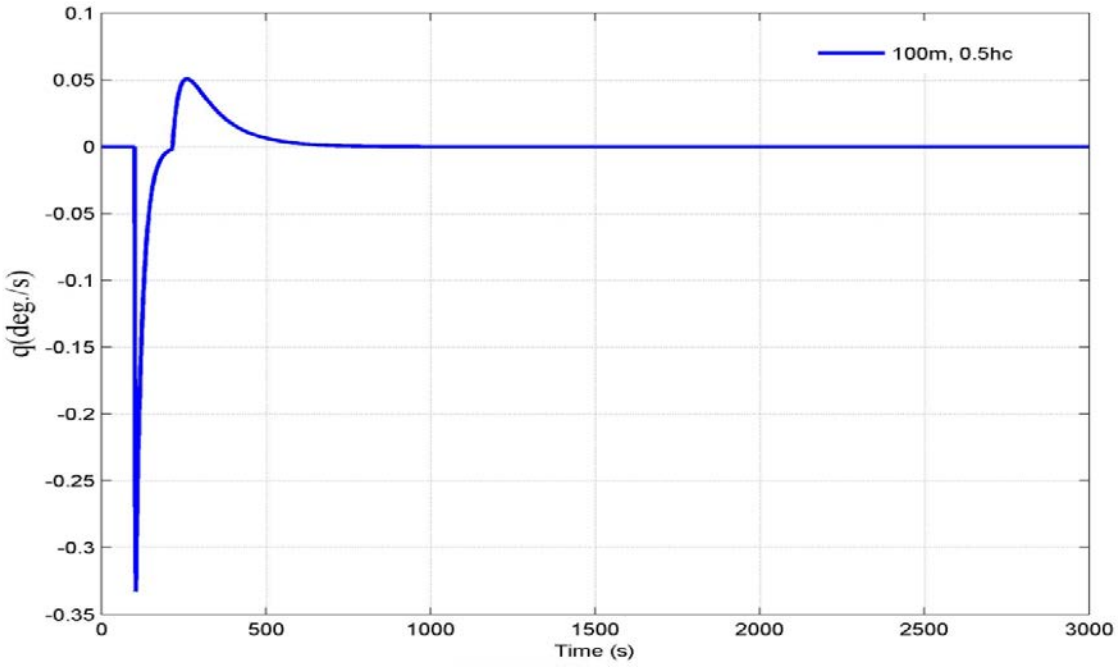

Figure 78: Variation of ship pitch rate (100 m, 0.5hc)

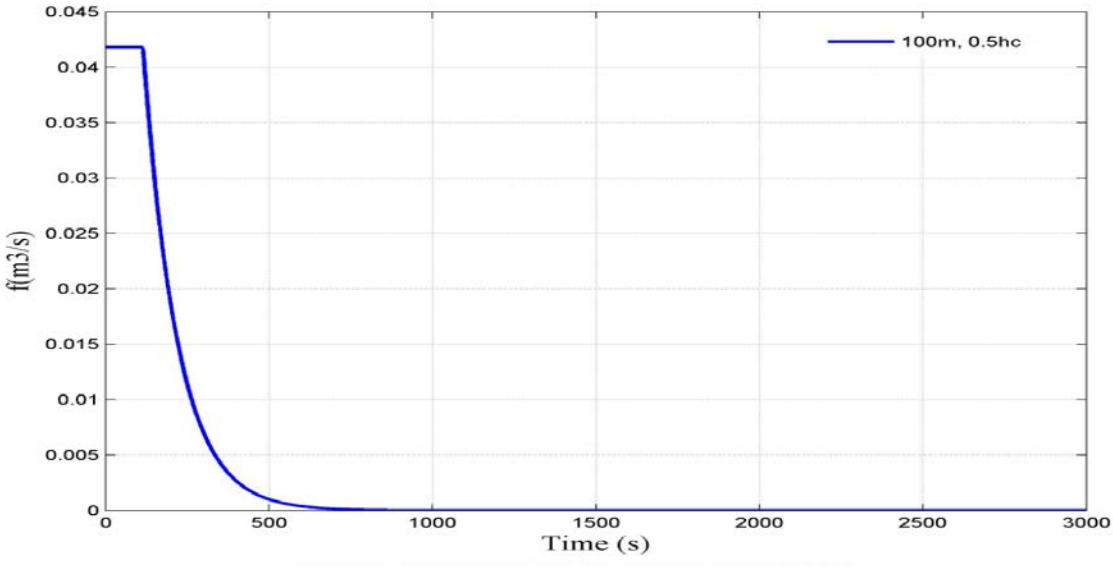

Figure 79: Variation of gas flow rate (100 m, 0.5hc)

Case 3: Effect of External Disturbance and Uncertainty

External disturbances and uncertainties are modeled according to the Eq.52 and included in the system dynamics as per Eq. (35). By considering this effect, simulation is carried out on the pontoon model for a commanded depth of 100 m. The obtained simulation responses are plotted in Figures 80-84. From Figure 80, it is seen that due to the effect of external disturbances, the payload takes more time to reach the commanded depth (1800 s) in comparison with the model without disturbances (1500 s). This is due to the reason that conventional SMC uses constant sliding surface slope and control gains throughout the simulation irrespective of the change in system dynamics due to external disturbances, which is one of the minor drawbacks of conventional sliding mode controllers. It is also noted that the pontoon reaches the commanded depth without overshoot and less steady state error. Figures 81-82 shows that both heave velocity and pitch angle are stable. This shows that the designed SMC is capable of handling external disturbance and uncertainty with system robustness even with the same tuned settings while compared with PD and PID controllers. From the simulation, it is observed that with the use of a variable structure controller like SMC for regulating the gas flow rate, the entire process is quasi-

static (changes take place in infinitely small manner) or in mechanical equilibrium, i.e. the controller switches from one equilibrium state to another equilibrium state, thus stability can be ensured. This verifies the supremacy of SMC in comparison with other controllers like PD, PID, Fuzzy Logic and Neural Network for handling non linear underwater problems involving uncertainty and external disturbances.

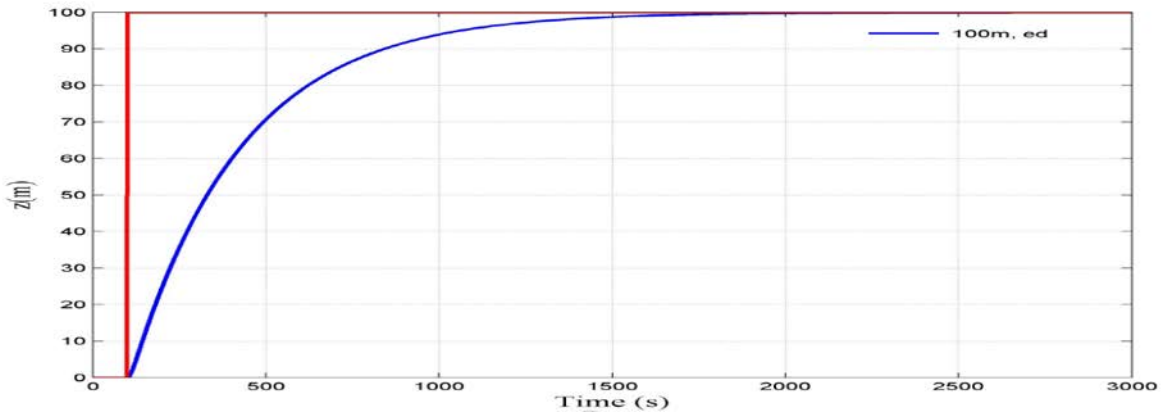

Figure 80: Variation of ship vertical position from sea bottom (100 m, ed)

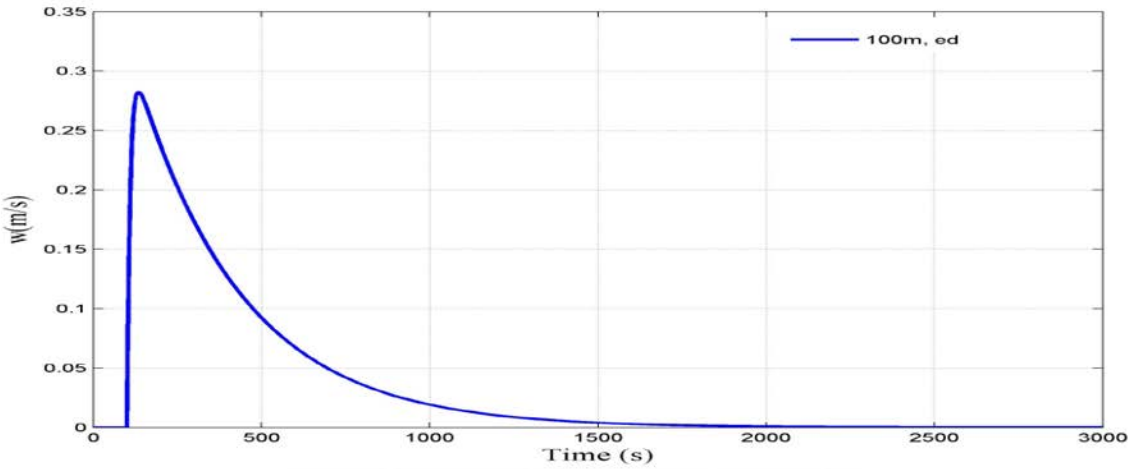

Figure 81: Variation of ascent velocity (100 m, ed)

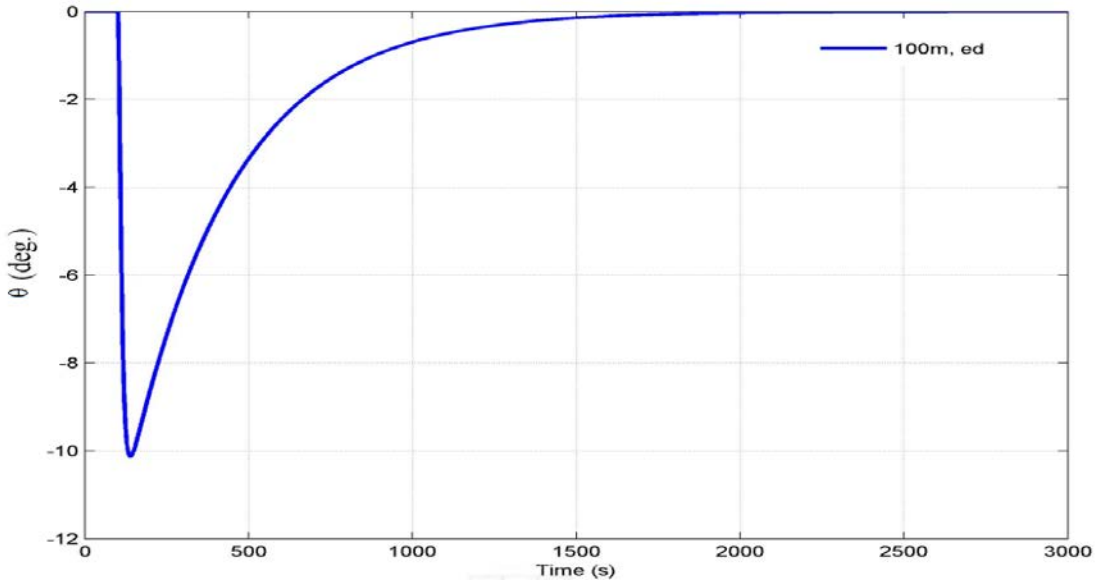

Figure 82: Variation of ship pitch angle (100 m, ed)

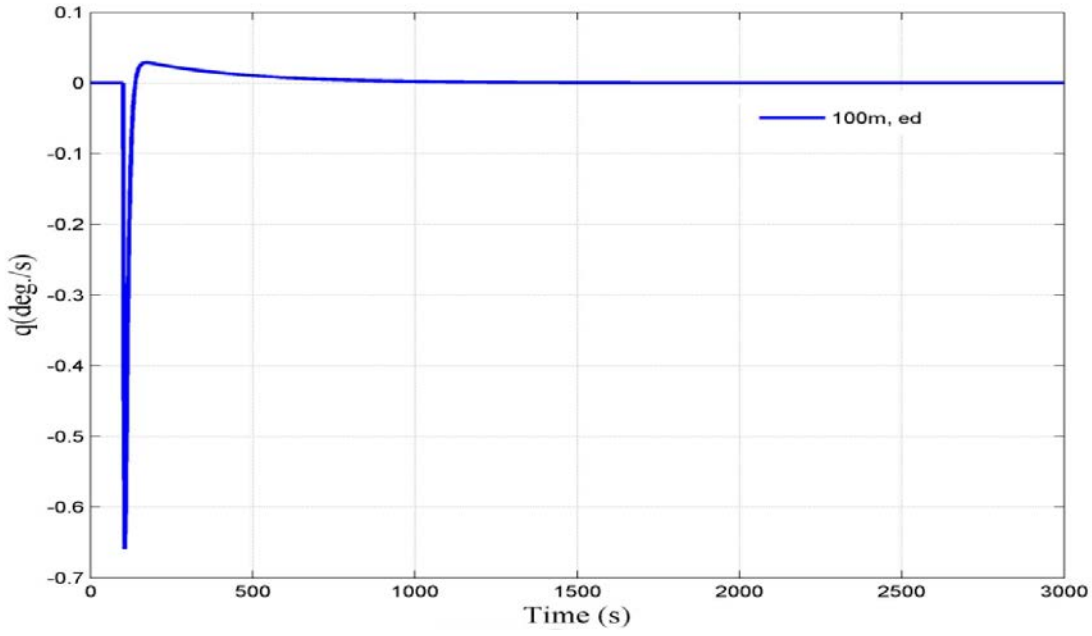

Figure 83: Variation of ship pitch rate (100 m, ed)

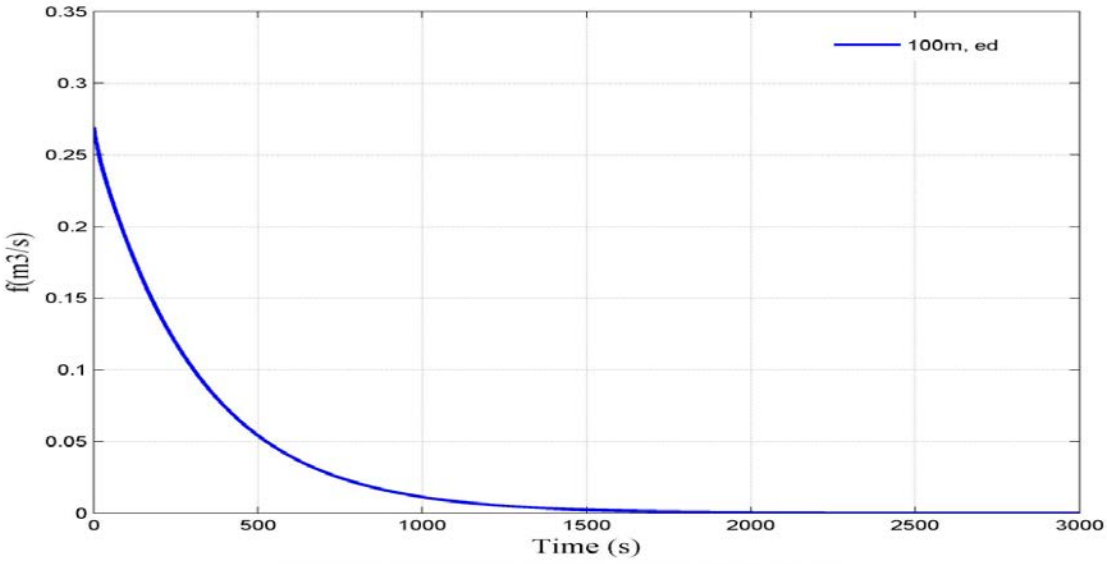

Figure 84: Variation of gas flow rate (100 m, ed)

Drawbacks of CSMC: - Chattering

It is found that the proposed CSMC is capable of handling non linearity, parameter variations and uncertainty arises due to external disturbances with good robustness, while maintaining hydrodynamic stability in diving plane for the linear state space model in comparison with PD & PID controllers. In the presence of external disturbances, the performance of the CSMC slightly degraded as it uses constant sliding surface slope and controller gain throughout the simulation irrespective of the variation in system dynamics. While performing simulation, the main difficulty faced is how to tune the controller precisely for the desired optimum performance. This operation is normally carried out by trail and error method, which is cumbersome. A constant higher value of controller gain often leads to well known chattering due to high frequency switching as shown in Figures. 85-89 that may results in high heat losses in electrical circuits and premature wear in actuators.

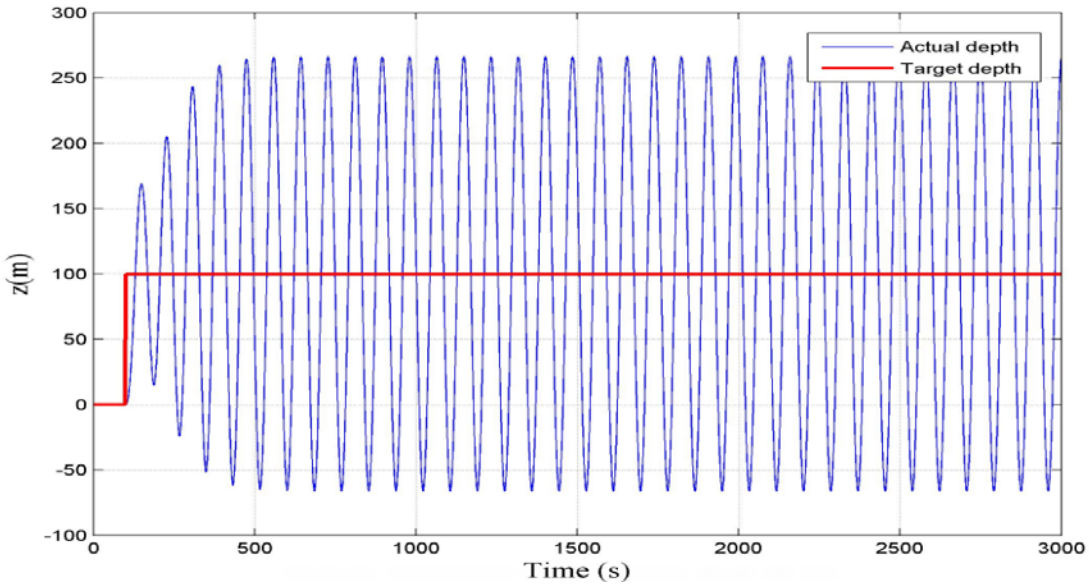

Figure 85: Variation of ship vertical position from sea bottom (100 m)

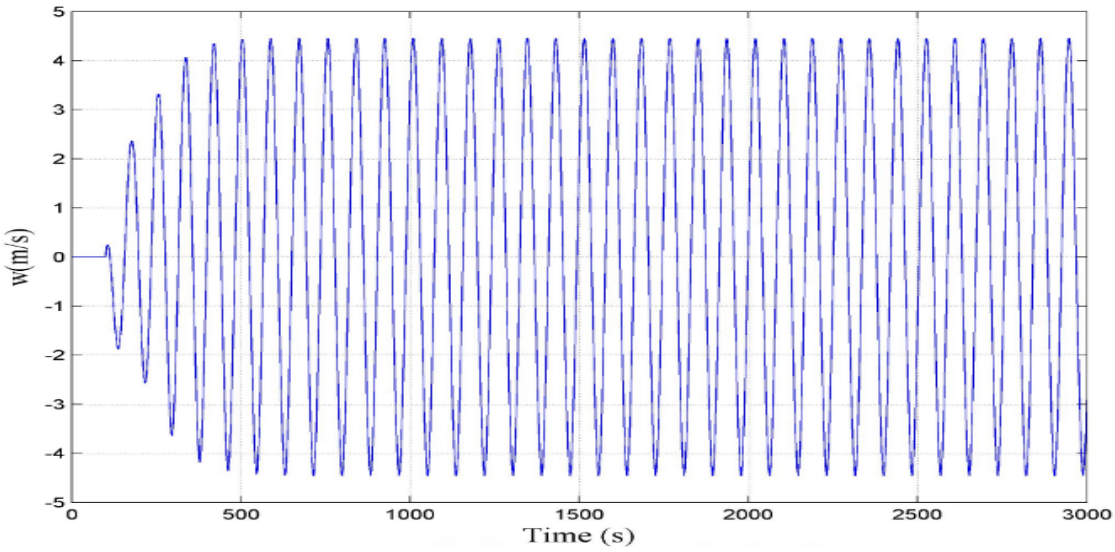

Figure 86: Variation of ascent velocity (100 m)

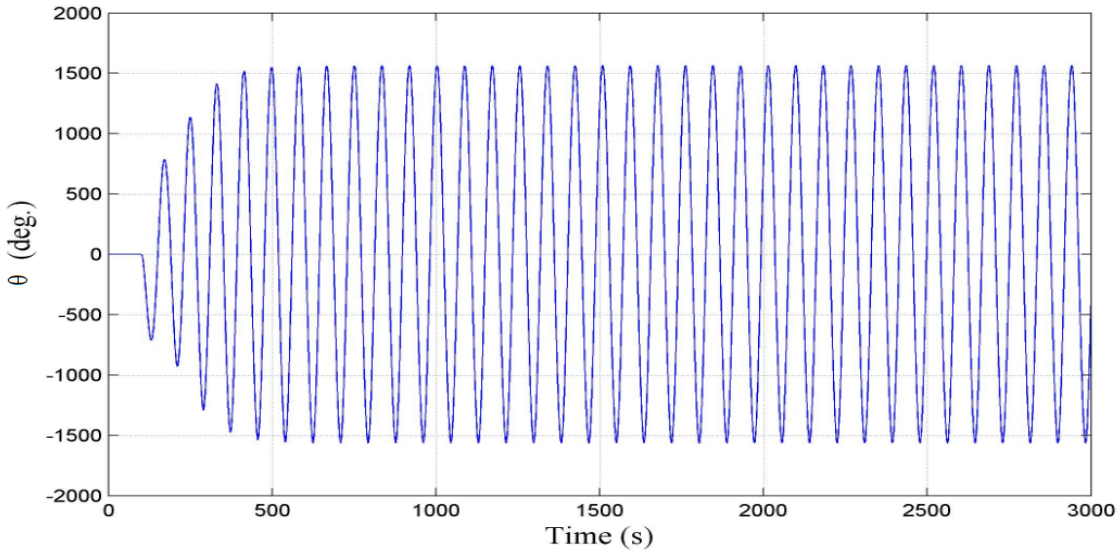

Figure 87: Variation of ship pitch angle (100 m)

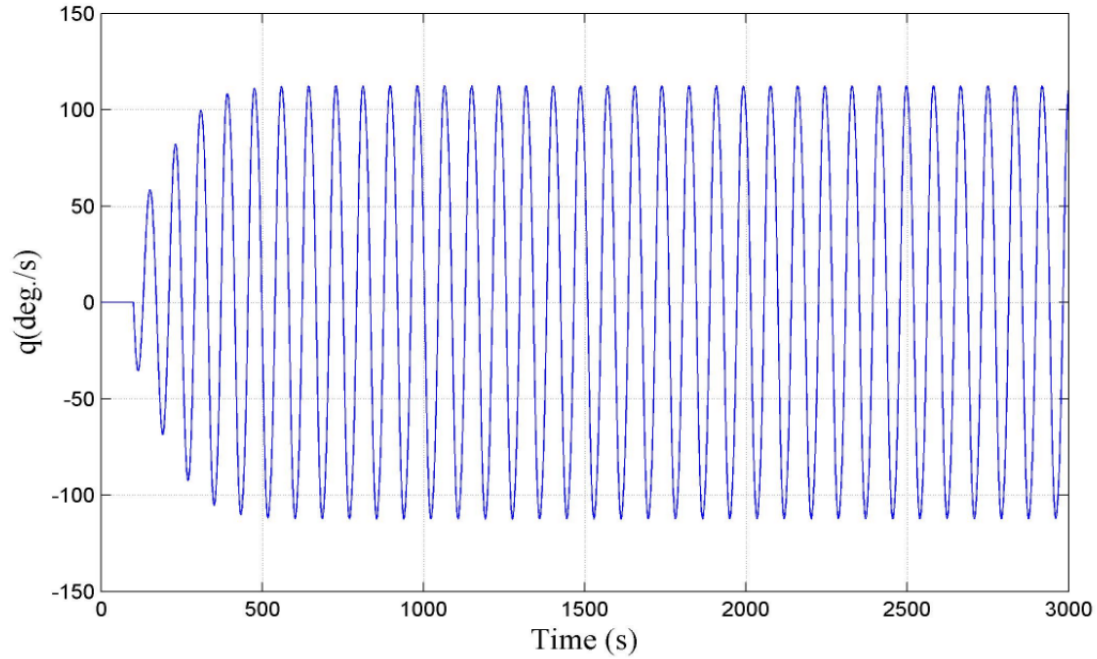

Figure 88: Variation of ship pitch rate (100 m)

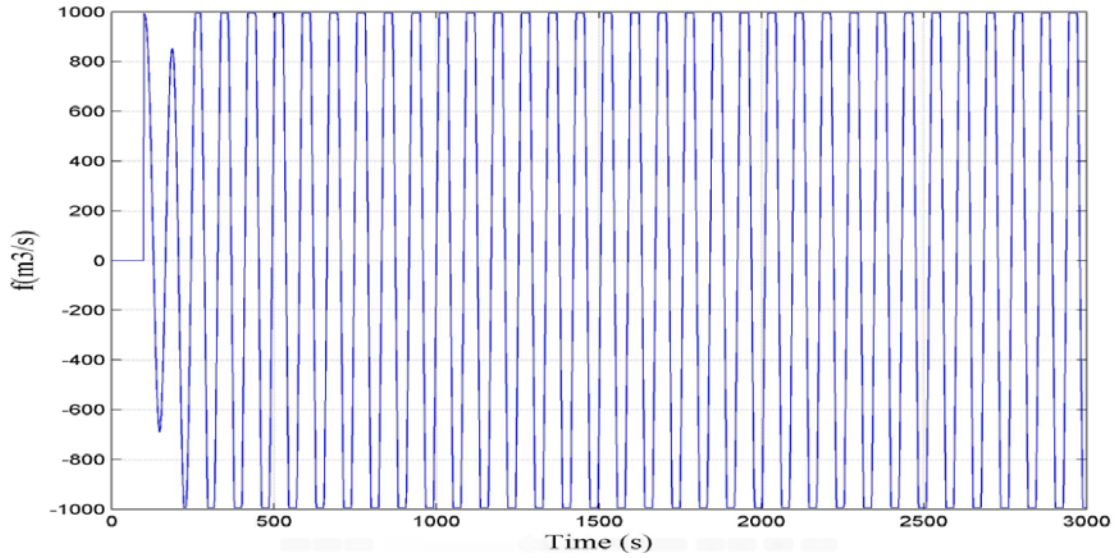

Figure 89: Variation of gas flow rate (100 m)

Clearly this level of chattering would be totally unacceptable as it would waste a large amount of gas. Can you not get less chatter?

5.4 Concluding Remarks

In this chapter, the relative efficacies of PD, PID and CSMC are investigated as a primary controller for regulating the volume flow rate of filling gas inside the lift bags for a safe and stable ascent. The obtained numerical simulation results highlight the following findings.

- PD controller: is suitable for regulating the depth and pitch motions for smaller target depths with no overshoot and having less steady state error. But, for higher commanded depths with the same tuned coefficients, the performance of the controller is very poor as the ascent velocity and pitch angle goes beyond the stable region.

- PID controller: gives satisfactory results for all most all target depths by approximating a linear deterministic model with considerable overshoot, where as in the presence of

parameter variations, non linearity and external disturbances, good results are not guaranteed.

- CSMC: is capable of handling non linearity, parameter variations and uncertainty arises due to external disturbances with good robustness, while maintaining hydrodynamic stability in diving plane for almost all commanded depths by approximating a linear state space model in comparison with PD & PID controllers. Tuning effort and chattering are the two major draw backs of CSMC.

- For salvage operations, a closed loop control system is mandatory to achieve the desired performance, therefore try to avoid failure in controller components especially sensor failure as it significantly affects the performance of the controllers.

6 Modification of Primary Controller by Artificial Intelligence

The proposed CSMC shows good robustness with the linear state space model and able to maintain hydrodynamic stability in diving plane even in the presence of parameter variations, external disturbances and uncertainty. The major problem associated with the CSMC is tuning effort and that may leads to well known 'chattering'. It is noted that under the effect of external disturbance and uncertainty, even though the system is stable, there is slight degradation in the system performance, which may be due to the CSMC using a constant values of sliding surface slope (λ) and controller gain (k) throughout the process irrespective of the change in system dynamics. *Since it is almost impossible to manually retune the control parameters under water, it is highly desirable to have controllers capable of self-adjusting their control parameters (i.e. adaptive controllers) when the overall performance degrades due to any uncertainties or any system failure.* From the literature review, it is found that the performance of CSMC can be considerably improved by integrating it with fuzzy logic to become an adaptive non linear controller called a fuzzy sliding mode controller.

6.1 Design of a Fuzzy Sliding Mode Controller

In a sliding mode controller, the states switch between the stable and unstable trajectories until the state variables reach the sliding surface. The phase trajectory of a sliding mode controller can be divided into two stages: the reaching and the sliding mode. The reaching or hitting phase is the trajectory starting from the given initial conditions of the sliding surface and tending towards the sliding surface; then the sliding mode starts once the state variables converge to the sliding surface. When the state variables are in the sliding mode, the system remains on the sliding surface and the states go to the origin while the system is insensitive to parameter variations or

external disturbances. That is the controller works effectively in the sliding mode. On the contrary, when the system acts in the reaching mode, tracking errors cannot be directly controlled, hence the system becomes sensitive to parameter variations. This implies that the robustness of the sliding mode controller resides in its sliding phase rather than the reaching phase, owing to the fact that the conventional sliding mode controllers uses fixed (invariant) sliding surfaces. Conventional sliding mode controllers with predetermined fixed slope (λ) degrade the dynamic performance of the system during the reaching mode; i.e. the controllers with minimum values of slope (λ_{min}) lead to a slower error convergence but better tracking performance, whereas controllers with maximum values of slope (λ_{max}) lead to a faster error convergence along which the tracking accuracy can be degraded. In addition, finding the optimum value of slope for the given controller is a complicated task [142]. Thus, a very important task in sliding mode controller design is to continuously change the slope of the sliding surfaces based on the state errors and their derivatives. This task is accomplished by using a Fuzzy Logic Controller (FLC) that continuously computes the slope of the sliding surface according to the values of state error and its derivatives. The chattering can also be effectively eliminated by this approach [11, 17, 27-29, 75, 88, 120, 135-136, 141-142, 148]. Another difficulty faced by the control engineers in sliding mode controller design is how to tune the controller effectively for a desired performance. Normally, this operation is carried out by a trial and error but this is cumbersome and time consuming. A constant high value of controller gain often leads to chattering. This problem can be overcome by adaptively tuning the controller by another FLC that computes the controller gain k based on the sliding surface σ and its variation [1, 10, 46-47, 52]. Hence, it is found that the performance of the conventional sliding mode controller can be effectively improved by using the FLC for continuously computing the slopes of the sliding surface instead of a constant sliding surface and also adaptively tuning the controller gain (k) by another FLC.

6.1.1 Design of Two Input Fuzzy Sliding Mode Controller (TIFSMC)

In this section, the performance of the conventional sliding mode controller is improved by using two conventional or two input fuzzy logic controllers TIFLC1 and TIFLC2, as shown in Figure

90. The first TIFLC1 is used for computing the slope of the sliding surface dynamically according to the system states such as error and change in error so that the tracking performance can be improved, thus maintaining the robustness throughout the process. The second TIFLC2 then calculates the controller gain adaptively with respect to the sliding surface σ and its derivative $\dot{\sigma}$, thereby eliminating the complex process of tuning and reduces chattering.

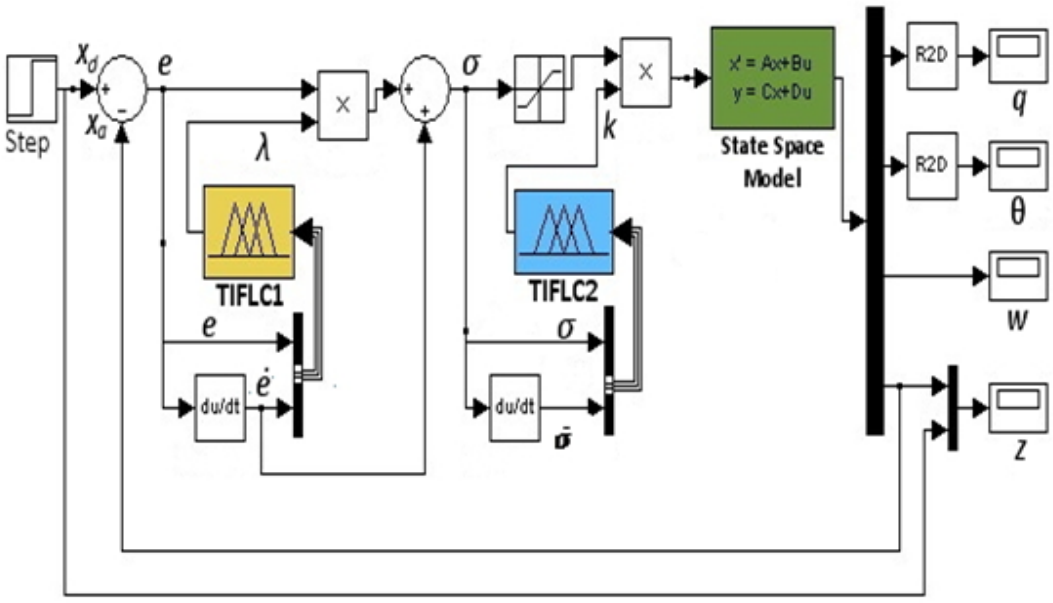

Figure 90: SIMULINK block diagram of a Two Input Fussy Sliding Mode Controller (TIFSMC) for regulating the gas flow rate

TIFLC1 computes the value of λ dynamically based on the system error (e) and change of error ($\dot{e}$) so that the tracking performance of the system can be improved. The combination of trapezoidal and triangular membership functions (μ) are used for modeling the input variables e & $\dot{e}$ as shown in Figures 91(a). The shapes of all membership functions for the output λ are chosen being triangular, fully-overlapping and fully-symmetric, as shown in Figure 91(b). Seven linguistic sets have been chosen as NB, NM, NS, ZE, PS, PM, PB for the inputs and VVS, VS, S, M, B, VB, VVB for the outputs, where the abbreviations N stands for negative, P positive, ZE zero, B big, M medium, S small and V very, respectively. It is assumed that the input variables

are normalized within a universe of discourse (UOD) of [-1 1] during the process of fuzzification [88]. Two dimensional fuzzy rules for computing λ are designed in such a way that the values of λ are always positive in order to satisfy the conditions of stability [135-136, 142]. These seven linguistic sets lead to 49 fuzzy rules as shown in Table 2. Figure 92 graphically represents the input-output relation (i.e. fuzzy control surface) or the variation of sliding surface with error states for the TIFLC1.

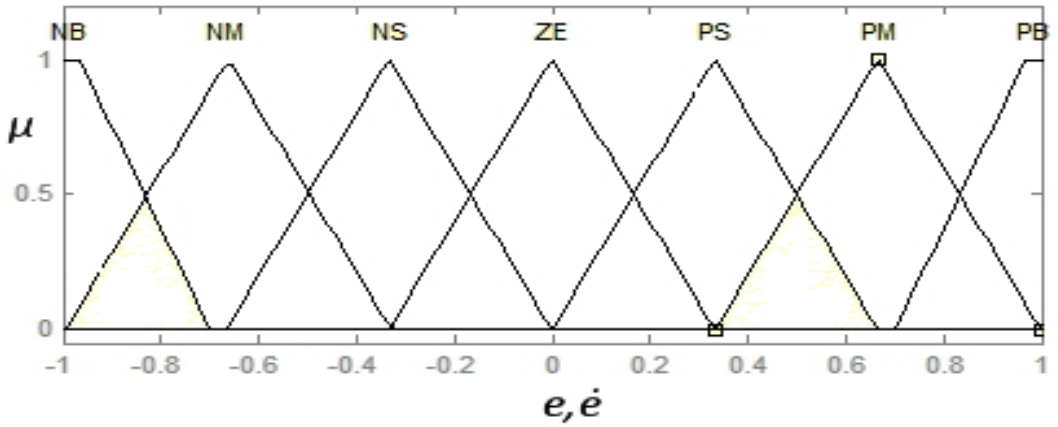

(a)

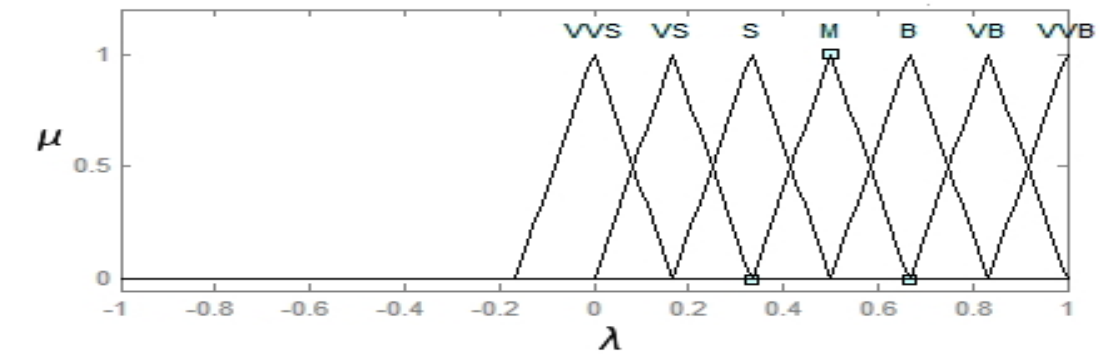

(b)

Figure 91: (a) TIFLC 1 input membership functions (b) output membership functions

Table 2. Two- dimensional fuzzy rule table to compute λ

e(t)	*ė(t)*						
	NB	**NM**	**NS**	**ZE**	**PS**	**PM**	**PB**
NB	**M**	**S**	**VS**	**VVS**	**VS**	**S**	**M**
NM	**B**	**M**	**S**	**VS**	**S**	**M**	**B**
NS	**VB**	**B**	**M**	**S**	**M**	**B**	**VB**
ZE	**VVB**	**VB**	**B**	**M**	**B**	**VB**	**VVB**
PS	**VB**	**B**	**M**	**S**	**M**	**B**	**VB**
PM	**B**	**M**	**S**	**VS**	**S**	**M**	**B**
PB	**M**	**S**	**VS**	**VVS**	**VS**	**S**	**M**

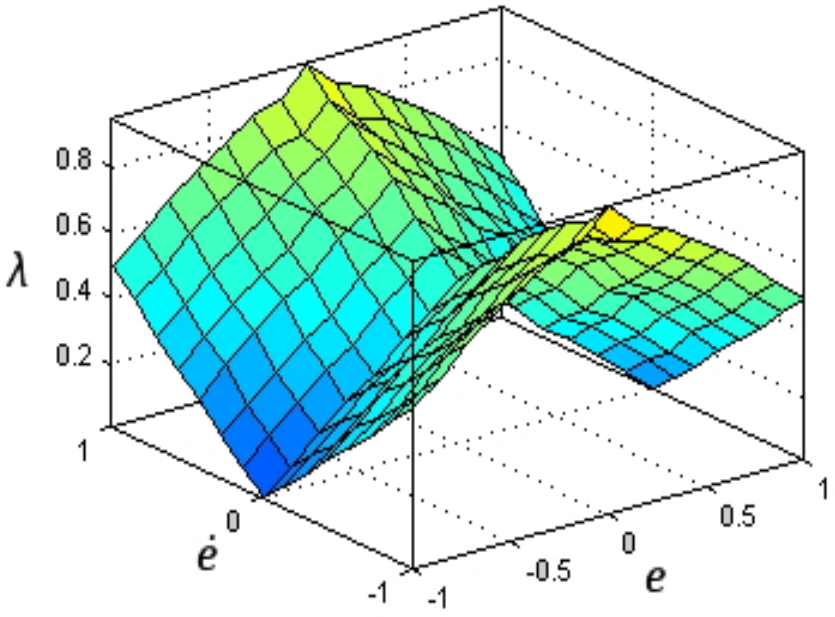

Figure 92: Variation of sliding surface with error states

The controller TIFLC2 computes the controller gain (k) dynamically based on the sliding surface σ and its derivative $\dot{\sigma}$ by which chattering can be avoided. For simplicity, the triangular, fully overlapping and fully symmetrical membership functions are used for representing the input/output variables. Fuzzy rules are selected in such a way that the control gain k is always maintained to positive values in order to satisfy the Lyapunov stability condition as shown in Table 3. Figure 93 shows the three dimensional representation of the input-output relation (i.e. fuzzy control surface) or the adaptive tuning of control gain with sliding surface error states of TIFLC2.

Table 3. Two dimensional fuzzy rules to compute k

$\sigma(t)$	$\dot{\sigma}(t)$						
	NB	**NM**	**NS**	**ZE**	**PS**	**PM**	**PB**
NB	**M**	**B**	**VB**	**VVB**	**VB**	**B**	**M**
NM	**S**	**M**	**B**	**VB**	**B**	**M**	**S**
NS	**VS**	**S**	**M**	**B**	**M**	**S**	**VS**
ZE	**VVS**	**VS**	**S**	**M**	**S**	**VS**	**VVS**
PS	**VS**	**S**	**M**	**B**	**M**	**S**	**VS**
PM	**S**	**M**	**B**	**VB**	**B**	**M**	**S**
PB	**M**	**B**	**VB**	**VVB**	**VB**	**B**	**M**

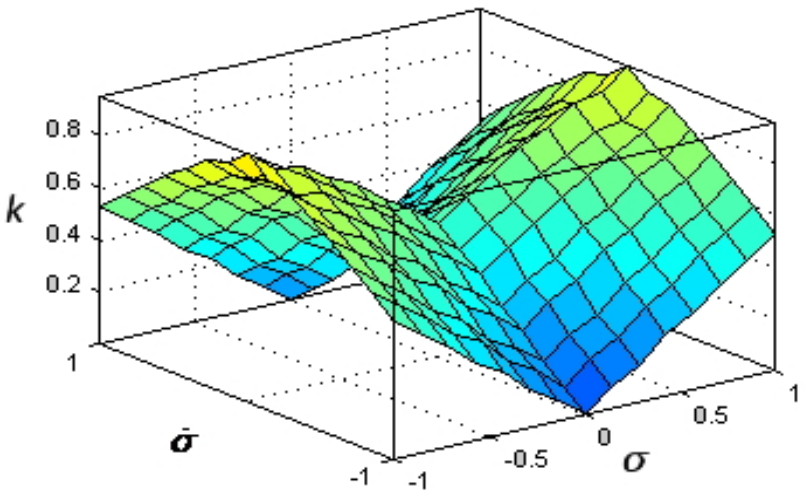

Figure 93: Adaptive tuning of control gain with sliding surface error states

6. 1. 2 Design of Single Input Fuzzy Sliding Mode Controller (SIFSMC)

The design procedure of the TIFSMC is complicated due to the involvement of large number of fuzzy rules and parameters to be tuned. The TIFSMC requires the process of fuzzification, rule inferences, defuzzification process that involved extensive computation which leads to the requirement of high performance computing. As a remedy to this problem, a SIFSMC was recently proposed by various researchers to reduce the large number of fuzzy rules, hence minimum computational time and less tuning effort [141]. The SIFSMC allows the control surface to represent in a 2-D form, i.e. approximation as a linear or piecewise linear surface irrespective of the 3-D surface by which the number of tuning parameters can be considerably

reduced. In the SIFSMC, the single fuzzy input variable (e_d) is defined as the absolute magnitude difference between the state error (e) and its derivative (e_{dot}) [141].

$$e_d(t) = \left| e(t) - \dot{e}(t) \right| \tag{69}$$

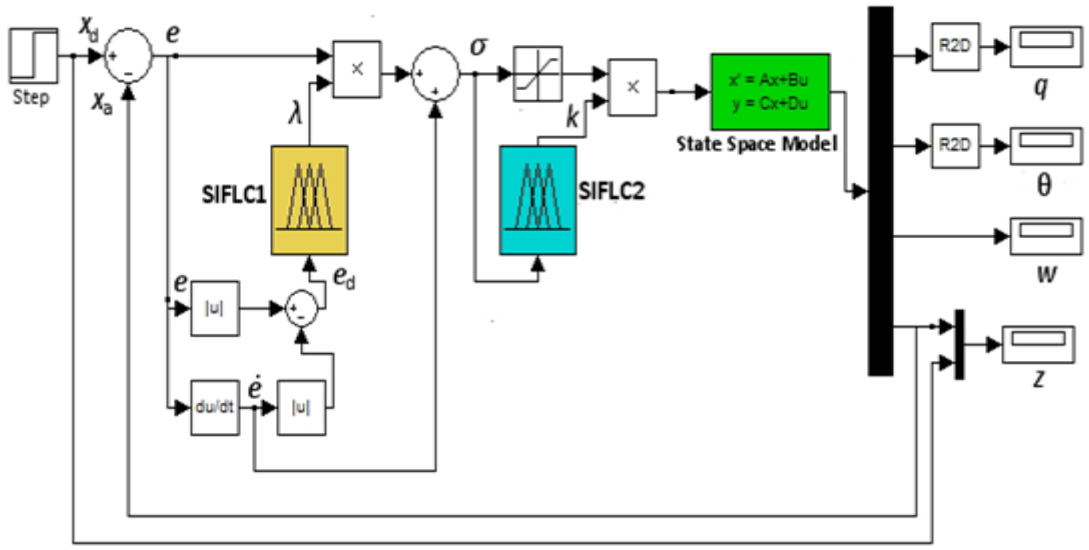

Figure 94: SIMULINK block diagram of a Single Input Fuzzy Sliding Mode Controller (SIFSMC) for regulating the gas flow rate

The SIMULINK block diagram of a SIFSMC for regulating the flow rate of filling gas inside the lift bags is shown in Figure 94. The SIFLC1 dynamically computes the sliding surface slope (λ) according to the fuzzy input variable e_d. Similar to the previous case, both the triangular and trapezoidal membership functions are used for modeling the input variable e_d, while the triangular membership functions are used for representing the output λ. One dimensional fuzzy rules are formulated based on the work of Yorgancioglu & Komurcugil [141]. Table 4 shows that the fuzzy rules are considerably reduced from 49 to 7 in comparison with the TIFLC1 (see Table 2). As it is a single input- single output system, the input-output relation or dynamic variation of sliding surface with error state can be approximated as a straight line as shown in Figure 95.

Table 4: One dimensional fuzzy rules to compute λ

Rule No	One dimensional fuzzy rules
1	If (e_d is NB) then (λ is VVB)
2	If (e_d is NM) then (λ is VB)
3	If (e_d is NS) then (λ is B)
4	If (e_d is ZE) then (λ is M)
5	If (e_d is PS) then (λ is S)
6	If (e_d is PM) then (λ is VS)
7	If (e_d is PB) then (λ is VVS)

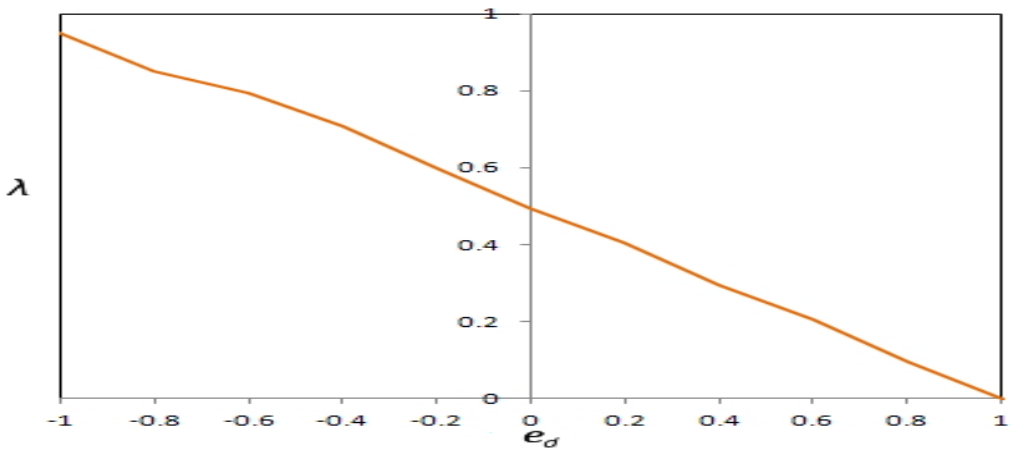

Figure 95: Variation of sliding surface slope with e_d

The fuzzy logic controller SIFLC2 computes the controller gain adaptively based on the sliding surface σ. The triangular, fully symmetrical and fully overlapping membership functions are used for modeling both input and output variables. Table 5 represents the

1-D fuzzy rule table to compute the gain *k* that considerably reduced from 49 to 7 compared to TIFLC 2 (see Table 3). Figure 96 represents the fuzzy control surface or the adaptive tuning of control gain with sliding surface.

Table 5 One dimensional fuzzy rules to compute *k*

Rule No	One dimensional fuzzy rules
1	If (σ is NB) then (k is VVS)
2	If (σ is NM) then (k is VS)
3	If (σ is NS) then (k is S)
4	If (σ is ZE) then (k is M)
5	If (σ is PS) then (k is B)
6	If (σ is PM) then (k is VB)
7	If (σ is PB) then (k is VVB)

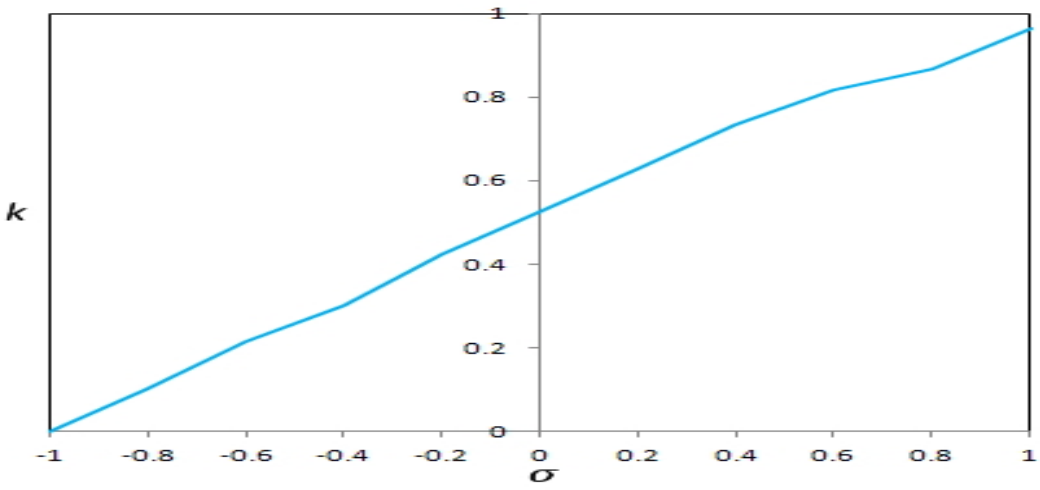

Figure 96: Adaptive tuning of control gain with sliding surface

6.2 Comparison with Conventional Sliding Mode Controller

The performance of the TIFSMC and SIFSMC over CSMC is investigated by performing simulation on the pontoon model for a higher target depth say 300 m. The obtained responses are shown in Figures 97-101.

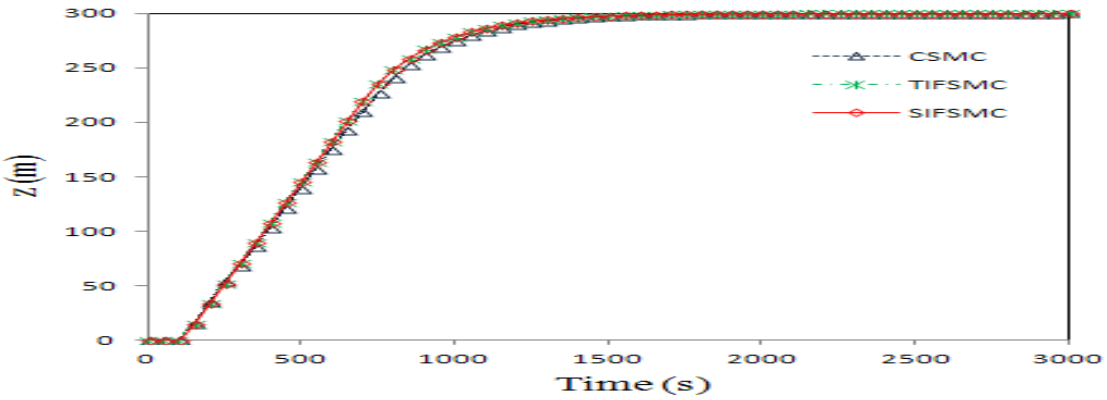

Figure 97: Variation of ship vertical position from sea bottom (300m)

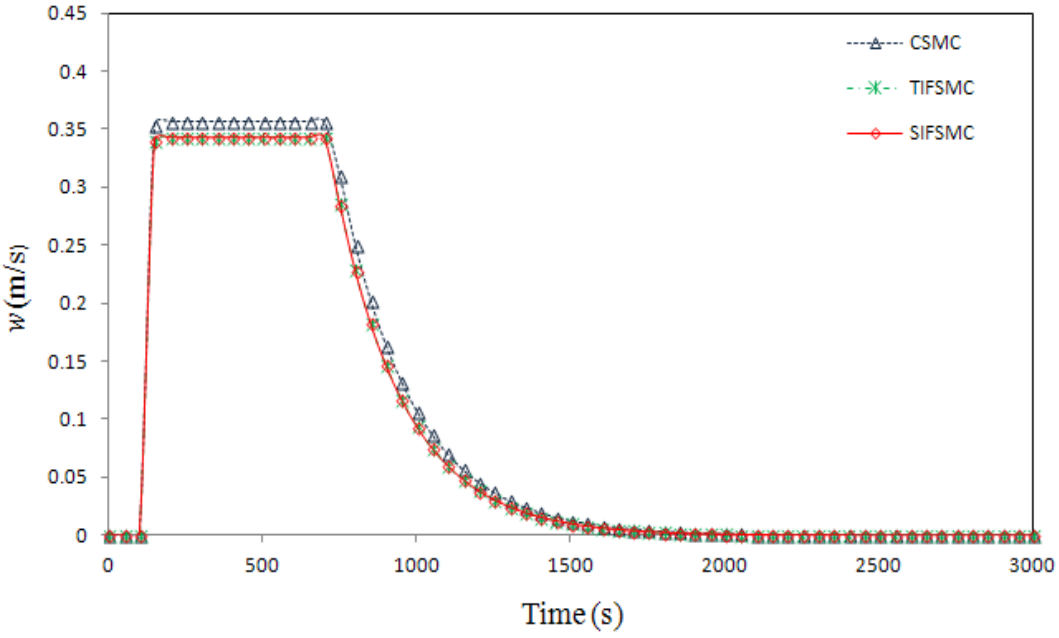

Figure 98: Variation of ship ascent velocity (300 m)

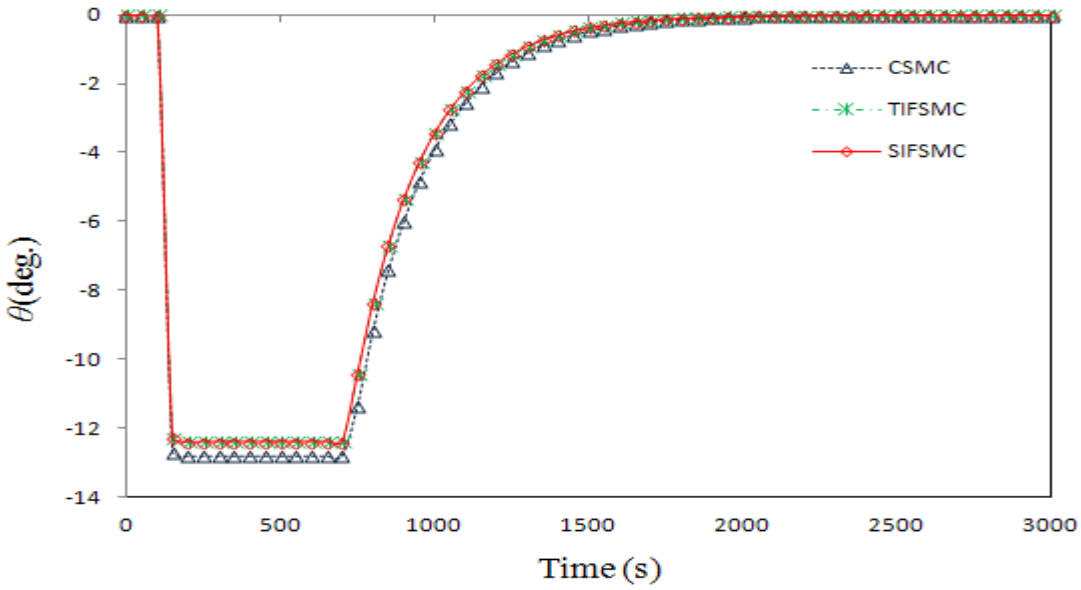

Figure 99: Variation of ship pitch angle (300m)

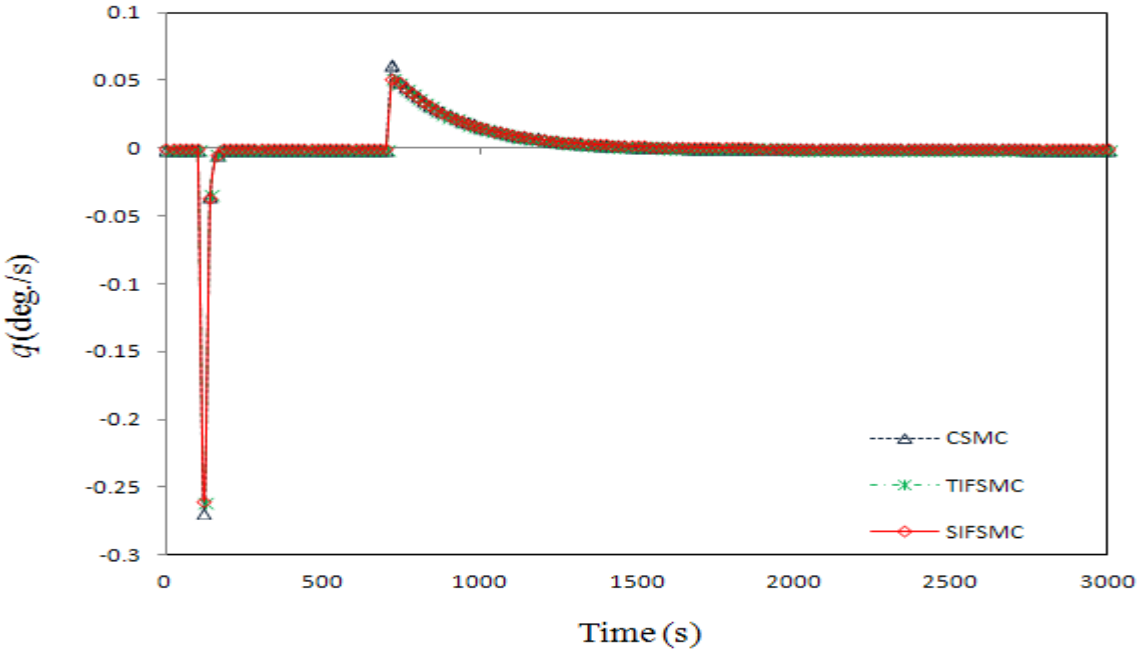

Figure 100: Variation of ship pitch rate (300m)

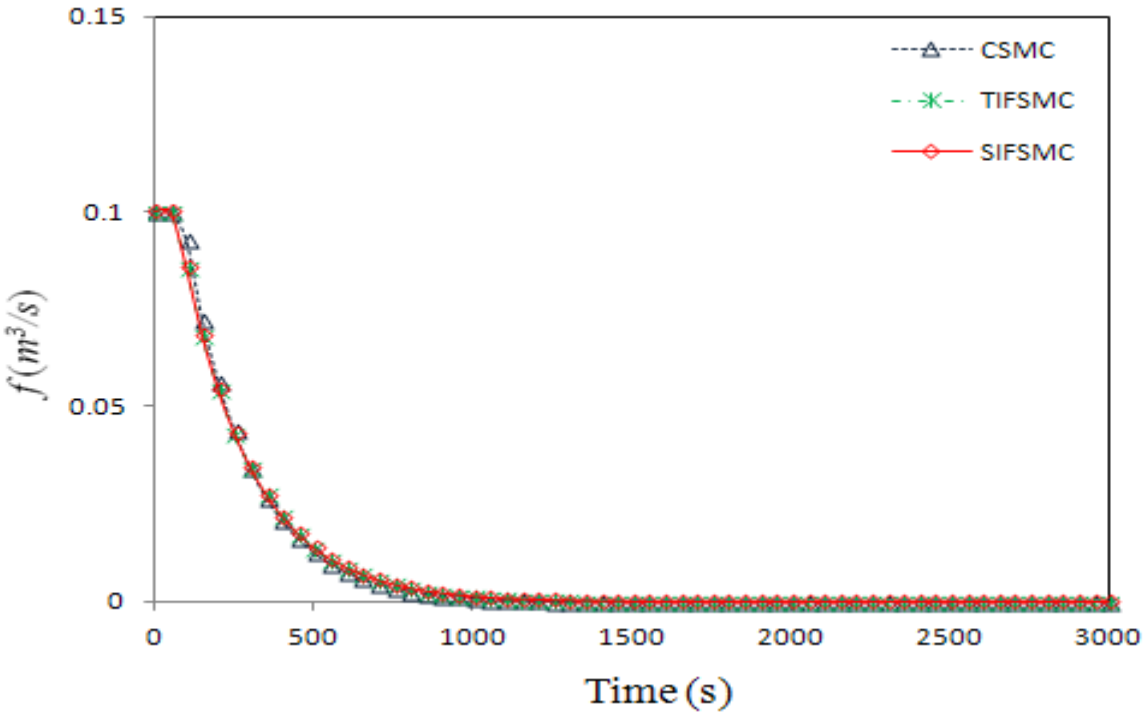

Figure 101: Variation of gas flow rate (300m)

Overall, all three controllers show good performance over the system. In all the three cases the pontoon reaches the target depth in 1600s. The most important thing while conducting simulation is after designing the SIFSMC, the tuning process (i.e. to determine the slope of the sliding surface λ & control gain *k)* become very easy and standardized by simply looking the 1-D fuzzy control surfaces of SIFSMC as shown in Figures 95 & 96 and hence chattering can be considerably avoided. This is the highest advantage as far as control engineering is concerned while maintaining the robustness property of SMCs. But, it is better to remember that, for designing a SIFSMC, firstly it is required to design CSMC as the base, then extended it to TIFSMC and finally simplified to SIFSMC. When Figures 97 is considered, the slow response of the CSMC is further improved by continuously varying the sliding surface slope and online tuning the controller gain so that the steady state error is considerably reduced. Figure 98 & 99 shows how all the three controllers maintains ascent velocity and pitch angle within the stable region by flattening the peak curve instead of a sharp one for higher commanded water depths in comparison with lower target depths. This verifies the supremacy of SMCs over PD & PID

controllers especially for higher water depths. It is observed that FSMCs are free from chattering due to high frequency switching as inherently seen with CSMCs. The rise time produced by all controller models are nearly the same, but the time required for the state variables to attain the steady state condition is lesser in FSMCs than the CSMC. In all cases, the state variables attain their steady state, indicating how the dynamic system is stable throughout the process. The percentage of overshoot is negligible with all controllers. Since it is difficult to visually observe the comparative performance of these controllers, the Integral Absolute Error (IAE) and Integral of Time multiplied Absolute Error (ITAE) and steady state error (e_{ss}) are considered during the simulations, which are given in Table 6. It is found that both FSMCs show about 30% of improvement in the IAE index compared to the CSMC. In addition, in terms of the transient response, both FSMCs better perform. For the TIFSMC, the above transient performance is obtained after a lengthy complex tuning process of fuzzification, defuzzification and inference of 49 rules. If these processes had not been properly tuned, unsatisfactory results would have been produced by the TIFSMC. Irrespective of the 3D control surface of TIFSMC in Figures 92 and 93, SIFSMC requires only two parameters to be tuned; slope of the linear control surface and the break point as shown in Figures 95 and 96. Table 6 shows the computational time required for the two FSMCs. It is seen that SIFSMC is two orders of magnitude faster than TIFSMC. This is due to the reduction in linguistic fuzzy rules from 49 to 7 for both the FLCs. Finally, it is worth emphasizing that the SIFSMC can be implemented using a much slower and low cost processor with minimum tuning effort.

Table 6 Performance measures for the three controllers

	CSMC	TIFSMC	SIFSMC
IAE	2.68	0.804	0.78
ITAE	5.20	0.790	0.716
e_{ss}	0.08	0.02	0

Table 7 Comparison of computational time

Controller	Computational time (s)
CFSMC	500
SIFSMC	4

From the simulation results, it is found that, there is no significant visible difference between the performances of CSMC, TIFSMC & SIFSMC for the linear deterministic state space model under normal conditions. But with the development of SIFSMC, the tuning process become standardized and hassle free and hence the well known chattering problem present with SMCs can be avoided. The performance of the TIFSMC & SIFSMC over CSMC is further evaluated by considering the effect of external disturbances and uncertainties in the system modeling.

Effect of External Disturbance and Uncertainty

As explained earlier external disturbances and uncertainties are modeled according to the Eq.52 and included in the system dynamics as per Eq. (35). By considering this effect, simulation is carried out on the pontoon model for a commanded depth of 300 m. The obtained simulation responses are plotted in Figures 102-106.

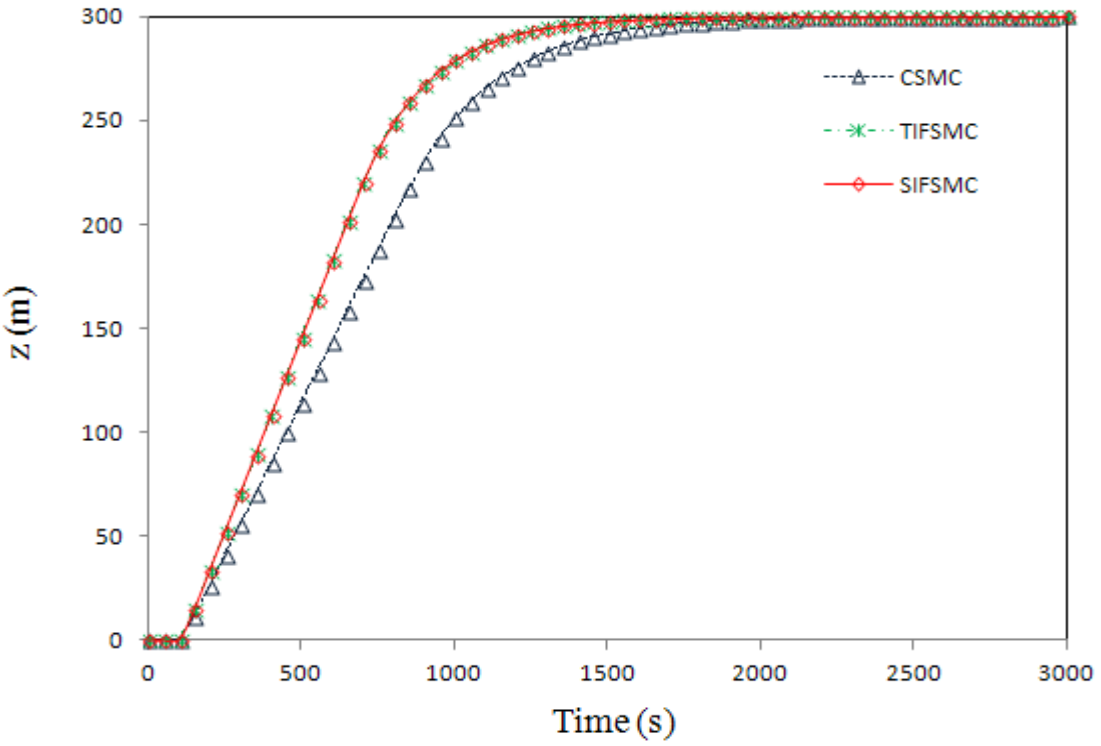

Figure 102: Variation of ship vertical position from sea bottom (300m)

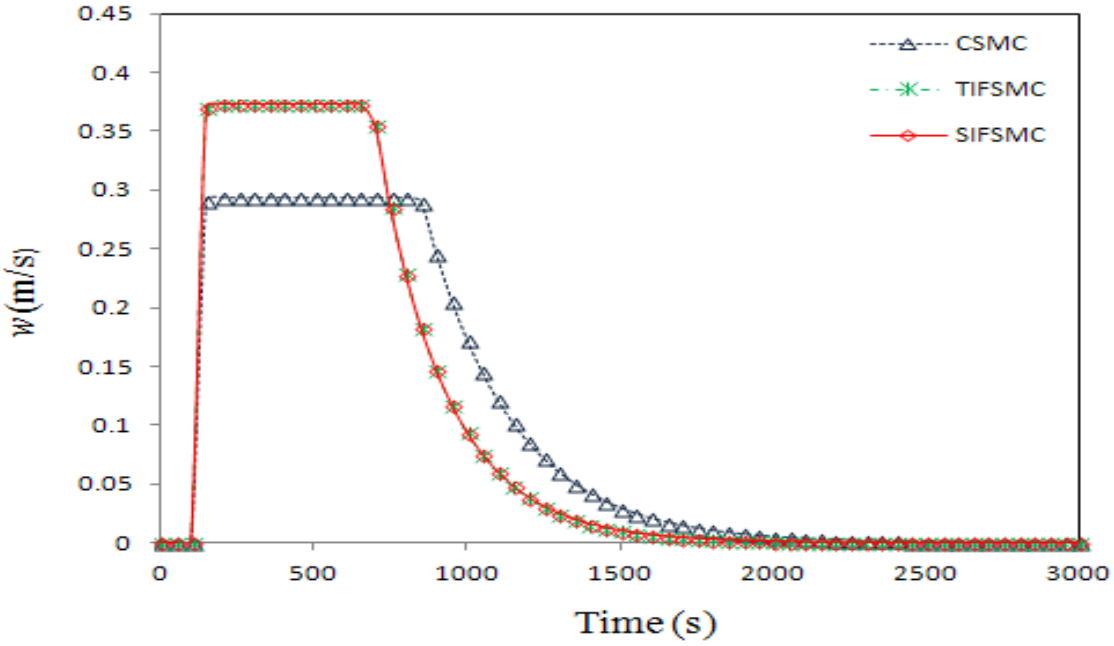

Figure 103: Variation of ship ascent velocity (300m)

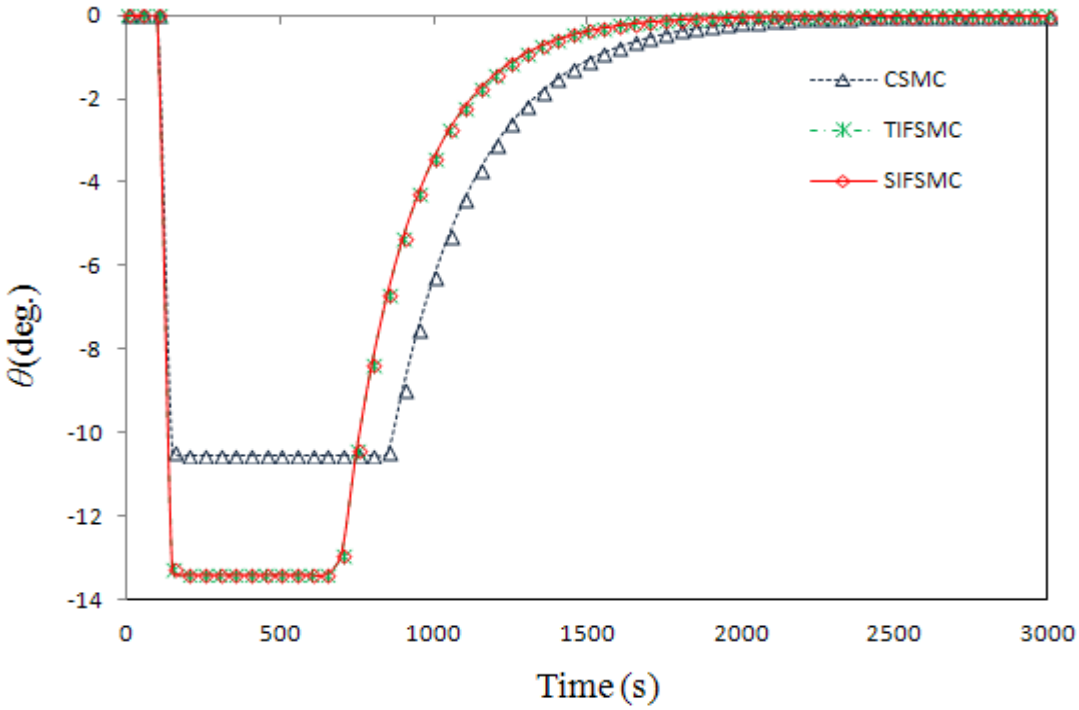

Figure 104: Variation of ship pitch angle (300m)

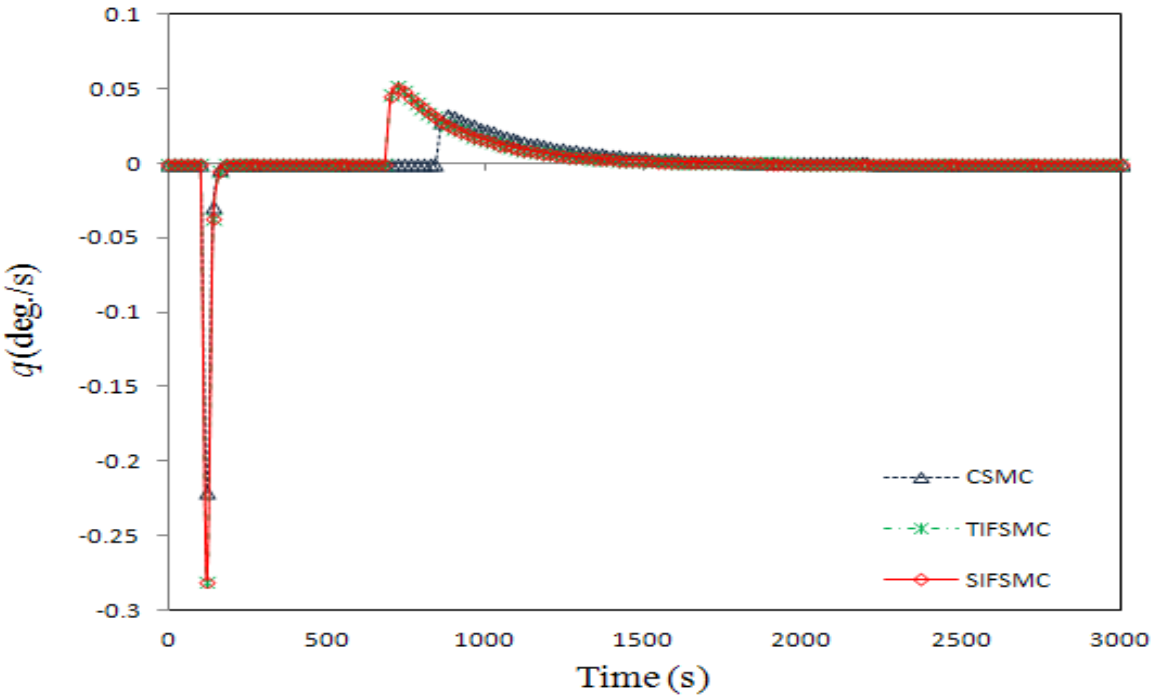

Figure 105: Variation of ship pitch rate (300m)

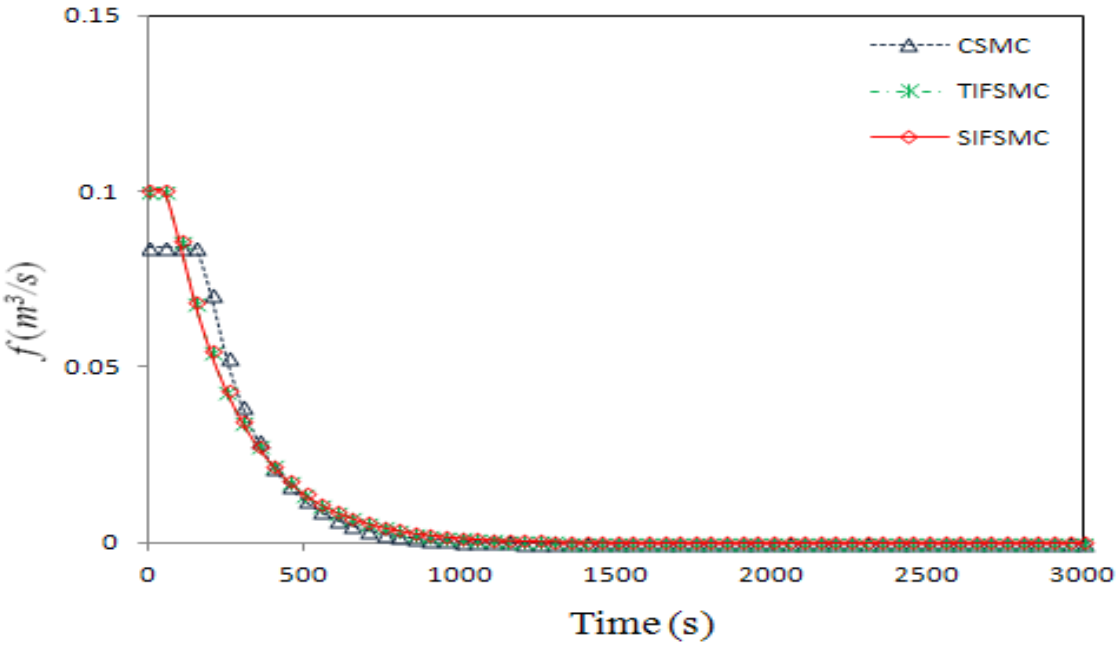

Figure 106: Variation of gas flow rate (300m)

From the response plots, it is observed that all the three controllers maintain hydrodynamic stability even in the presence of uncertainty due to external disturbances. By comparing the simulation response of the system with and without external disturbances, i.e. by comparing Figures 102-106 with Figures 97-101, it is noted that both FSMCs are less sensitive to external disturbances compared with CSMC. Figure 102 shows that under the effect of external disturbances, the CSMC takes more time to reach the commanded depth (2000s) in comparison with TIFSMC & SIFSMC, where it is only 1600s. These are due to the reason that CSMC uses constant sliding surface slope (λ) and control gain (k) throughout the simulation irrespective of the change in system dynamics due to external disturbances. Hence it is realized that for a complex non linear underwater operations like marine salvage, where there is always possibility of sudden change in system environment, uncertainty and external disturbances, it is better to adopt a non linear adaptive controllers like TIFSMC & SIFSMC for regulating the gas flow rate, in which SIFSMC is the optimum choice due to less tuning effort and computational time.

6.3 Concluding Remarks

In this chapter, a new controller design is implemented that brings together the advantages of both fuzzy logic and sliding mode controllers. A conventional sliding mode controller (CSMC) is first designed and then its performance is improved by extending to TIFSMC & then simplified to SIFSMC. *With the development of SIFSMC, the tuning process become standardized and hassle free and hence the well known chattering problem associated with SMCs can be avoided.* It is found that both FSMCs show 30% of improvement in the tracking performance when compared to the CSMC, while maintaining its robustness. It is also noted that both FSMCs are less sensitive to external disturbances and uncertainties in comparison with CSMC. The responses obtained by the SIFSMC are the same as those obtained by the TIFSMC, with the former involving a much less tuning effort and computational time. *Therefore, an adaptive controller like SIFSMC proves to be the preferred option amongst the considered controllers as the primary controller for regulating the gas flow rate.*

7. Design of Secondary Controller

In this chapter a secondary controller is proposed to regulate the area of purge valve opening fitted with lift bags in accordance with the excess buoyancy available after suction breakout and according to the variation in pressure difference between the gas inside the lift bags and surrounding sea water pressure for a stable ascent.

Consider the problem of lifting the pontoon model lying at sea bottom, which is at a distance of 300 m from sea surface. Total breakout lift force required for the pontoon is calculated as 10.67 m^3 (see Appendix A). As the volume of one single inflated lift bag is 1.8 m^3, a total of 6 lift bags are required for inflation. The buoyancy force provided by all 6 lift bags are taken together in the rigid body modeling. During the ascent, as the water depth decreases (i.e. distance from sea bottom increases), there is considerable decrease in surrounding sea water pressure as shown in Figure 107.

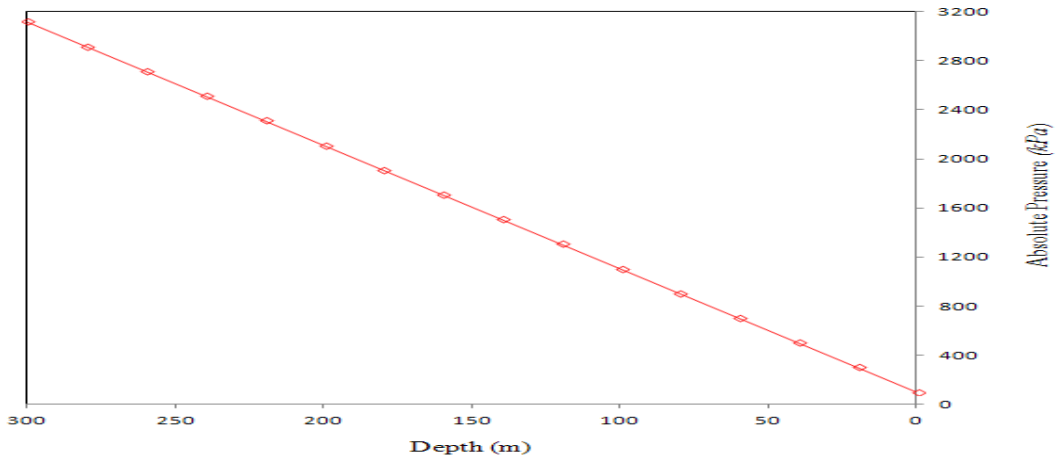

Figure 107: Decrease in sea water pressure during the ascent

Figure 107 shows that the decrease in sea water pressure is linearly with respect to the variation in depth. At sea surface the absolute pressure is same as the atmospheric pressure. Suppose, if there is no purging, the total expansion of gas inside the lift bags according to this decrease in surrounding sea water pressure is plotted in Figure 108. This expansion of gas results to an exponential increase in buoyancy force as shown in Figure 109, which leads to an unpredictable acceleration during the ascent. The excess buoyancy available after suction breakout also causes a sudden increase in acceleration after the breakout.

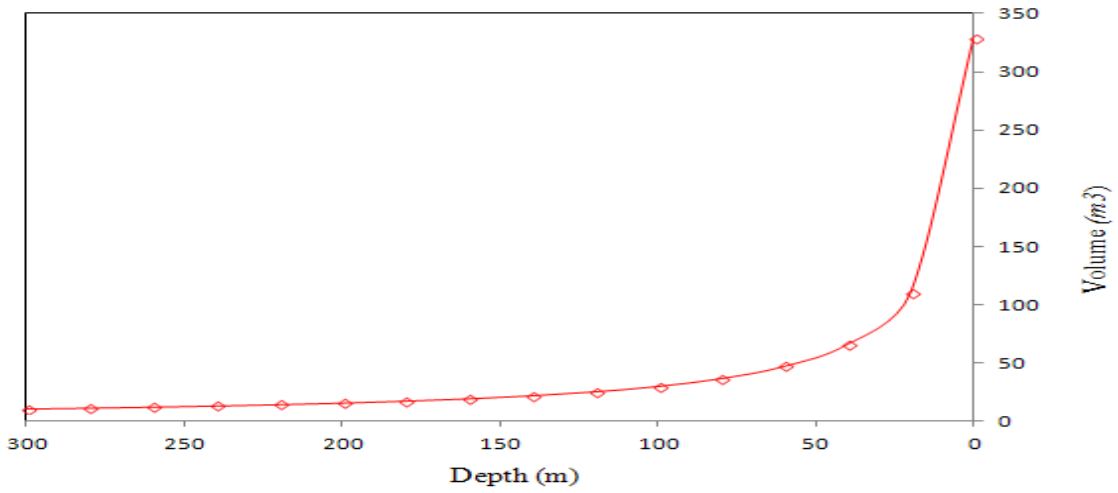

Figure 108: Total expansion of gas inside the lift bags during the ascent

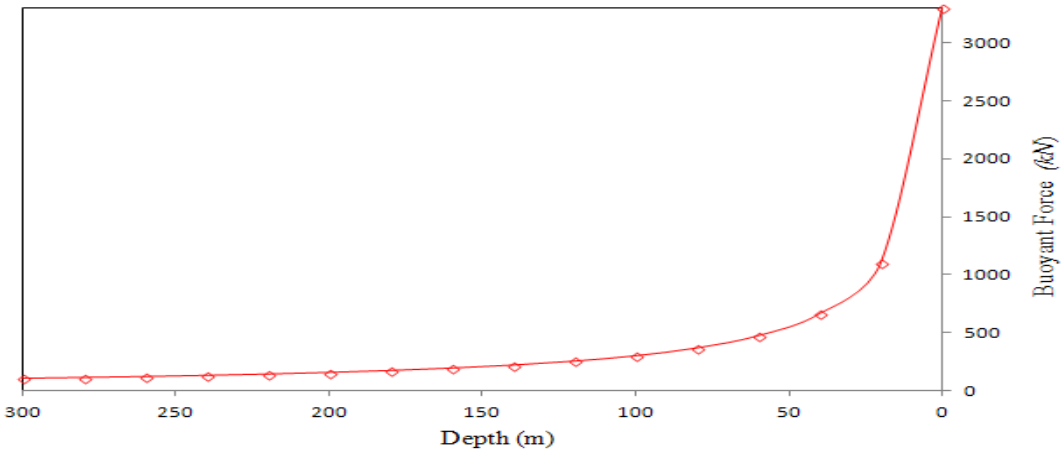

Figure 109: Increase in buoyancy force during the ascent

Hence, in order to reduce the excess buoyancy available after the suction breakout and to avoid the unpredictability in the acceleration due to the expansion of gas during the ascent, purge valves are provided at the top of the lift bags. The function of the secondary controller is to regulate the area of purge valve opening in accordance with the excess buoyancy available after suction break out and according to the variation in pressure difference between gas inside the lift bag and surrounding sea water pressure for a stable ascent. A PID controller is proposed for achieving this purpose.

7.1 Proportional Integral and Derivative Controller (PID)

A PID controller is selected as the secondary controller to regulate the purge valve opening as explained in Farrell & Wood [32]. Explanation of the working components of a PID controller is given in Section 5.2. Purge valve modeling is already carried out in Section 4.2.

In order to simulate the properties of purge valve's actual response, an equation is formulated as discussed in Section 4.2 to take the PID control response and translates that into a purge area size.

$$V_{purge} = v_{purge} \times A_{purge} \times dt \tag{70}$$

In which,

$A_{purge} = [PID]$ = area of valve opening in m^2 (control parameter)

V_{purge} = volume of air purged (m^3)

dt = time interval

Here the purge valve opening is controlled according to the feedback obtained from sensors based on the system error. The error is the difference between desired depth and actual depth.
i.e.

$$e = z_{com} - z \quad (71)$$

Where z_{com} is the commanded depth and z is the actual depth.

The control law is formulated as:

$$[PID]=k*(P + I + D) \quad (72)$$

In which,

$$P = p * e_1 \quad (73)$$

$$I = i*((e_1 + e_0)/t + I_0) \quad (74)$$

$$D = d*(e_1 - e_0)/dt \quad (75)$$

Where,
P = proportional control response, I = integral control response, D = derivative control response, k = control response gain constant, p = proportional constant, i = integral constant, d = derivative constant, e_1 = instantaneous error, e_0 = previous error measured, I_0 = cumulative integral response, dt = time interval between system response, t = total time.

The performance of the automated purge valve using PID controller is investigated by conducting simulation for the lifting of pontoon model lying at sea bottom having distance 250m, 300m & 350 m from sea surface using lift bags. The obtained responses are shown in Figures 110-113.

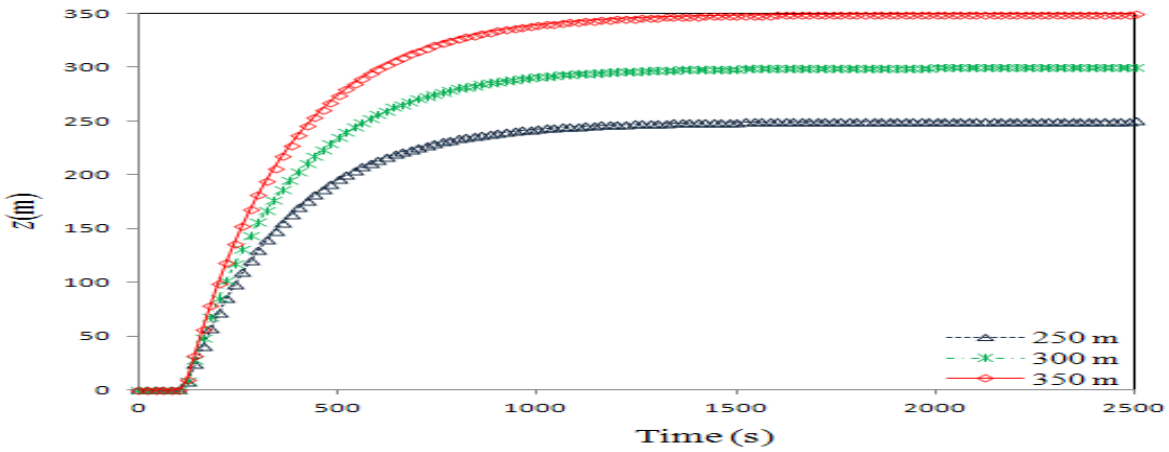

Figure 110: Variation of ship vertical position from sea bottom

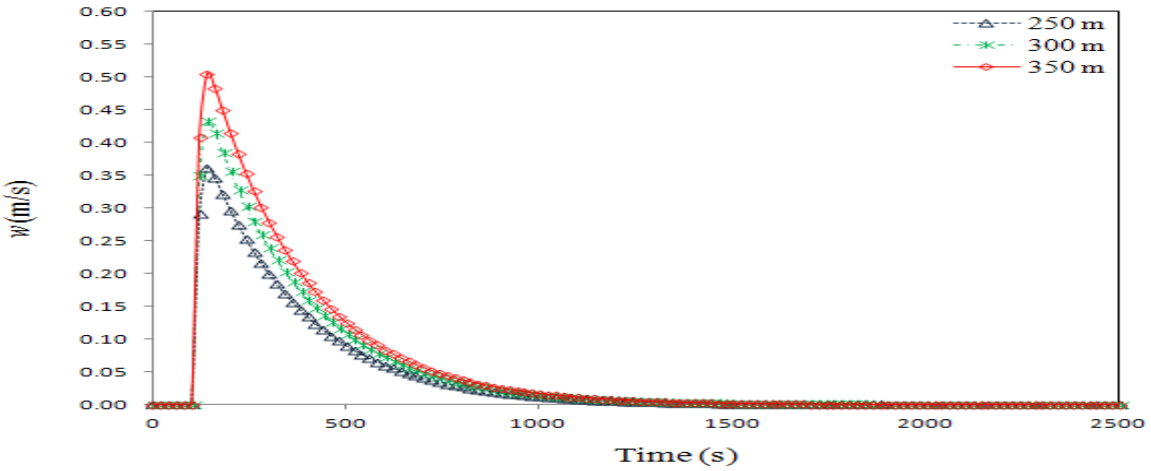

Figure 111: Variation of ship ascent velocity

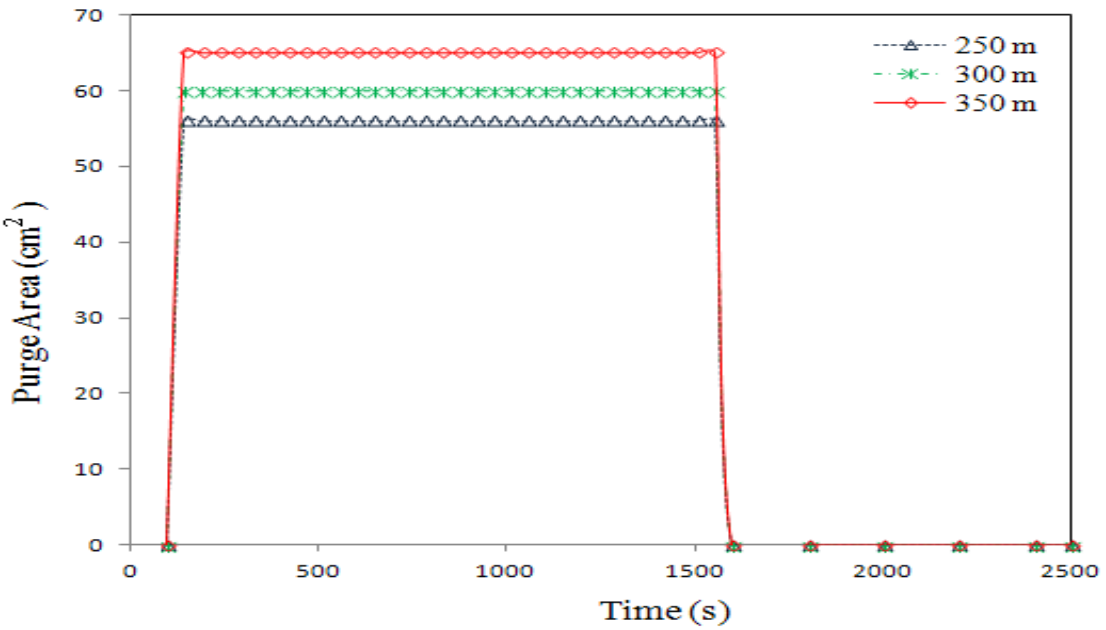

Figure 112: Variation in purge area (control parameter)

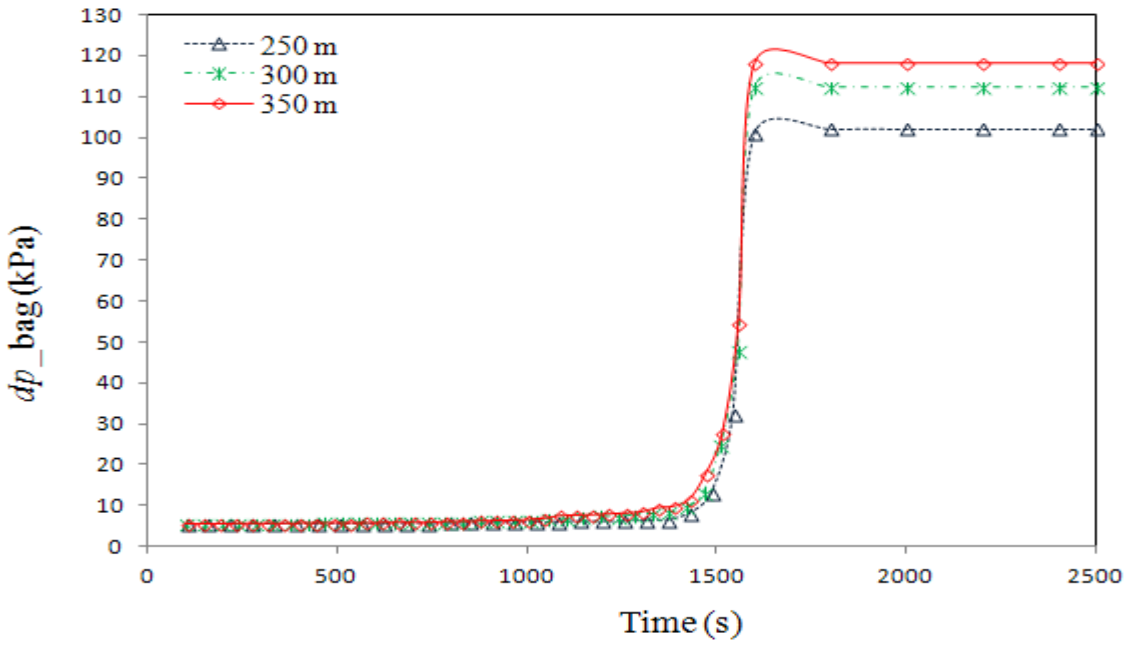

Figure 113 Variation of gas pressure inside the lift bags.

Figure 110 shows that in the all the three cases, the vessel reaches the target depths without any overshoot by properly tuning the PID controller. The maximum value of ascent velocity among the three target depths is found from Figure 111 to be 0.5 m/s (<0.6 /s), which implies that the ascent is stable. Figure 112 shows how the controller regulates the purging of gas through valves in accordance with the excess buoyancy available after breakout and to the variation in pressure difference between gas inside the lift bags and surrounding sea water pressure for a stable ascent. The purge area suddenly increase from 0-60 cm^2 for reducing the excess buoyancy available after suction breakout and thereafter remains a constant value for handling the increase in buoyancy due to the expansion of gas inside the lift bags and finally reduces zero after the pontoon reaches the commanded depths. From Figure 113, the variation of gas pressure inside the lift bags is found to be in the range 5-120 kPa.

7.2 Concluding Remarks

In this chapter, a PID controller is designed as the secondary controller for regulating the purging of gas through the valves in accordance with the excess buoyancy available after suction breakout and to the pressure difference between gas inside the lift bags and surrounding sea water pressure for a stable ascent. PID controller is found to be effective in maintaining the ascent velocity within the stable region by properly tuning the control coefficients.

8. Design of Supervisory Controller

For maintaining hydrodynamic stability in a salvage operation using buoyant systems, a SIFSMC is selected as the primary controller for regulating the flow rate of filling gas inside the lift bags and a PID controller is chosen as the secondary controller to regulate the purging of gas through the valves fitted on the lift bags. Now for a stable salvage operation, it is required to monitor or switch between these two sub controllers by a supervisory controller as per the depth error and depth rate. In such situations, the only possibility is to choose an intelligent controller such as fuzzy logic controller (FLC) as the supervisory controller for monitoring the primary and secondary controllers as shown in Figure 114.

FLC issues system commands to effect the changes in depth, while also regulating the pitch angle of the vehicle. Due to the non linear nature of fuzzy mathematics, it can be applied for marine salvage problems. But the problem associated with FLC is how to generate the linguistic fuzzy rules for meeting the desired functionalities.

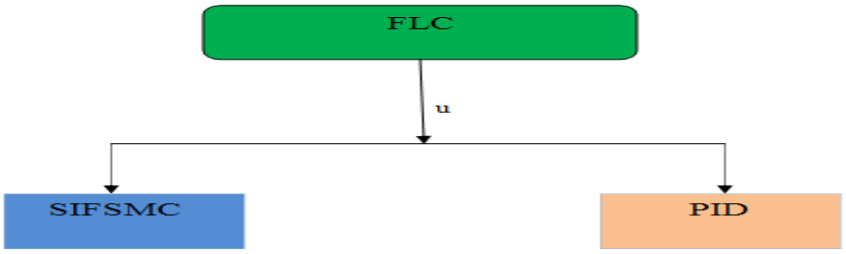

Figure 114: Design of a Fuzzy logic controller for monitoring two control subsystems

In Fuzzy logic controllers, the controlling action is through artificial intelligence i.e. linguistic expressions (fuzzy rules) based on the knowledge of operator or salvor. The majority of the FLCs use a two dimensional rule base (2D) that is derived from the error and derivative of error

according to the system state and its derivative. FLCs are designed with respect to a phase plane determined by the state error (e) and its derivatives ($\dot{e}$). The general heuristic approach in designing FLCs is to separate the phase plane into two semi planes with a diagonal line. Positive control outputs are placed in one semi plane and negative control outputs are located in the other. The magnitude of the control output is proportional to the distance from the diagonal line and that forms a diagonal symmetric rule table; i.e. when the system states are far from the diagonal, the controller signal is big and vice versa. Absolute values of control input change proportionally with respect to the distance of the representative point from the diagonal line. The diagonal line can be treated as a switching line, which is similar to the sliding line of an SMC [24, 64, 73, 88, 97, 147].

The benefits of the fuzzy logic controller are [24, 88, 147]:

- Simplicity, by not requiring a dynamic model, which leads to the rapid development of a working design
- better matching of the control strategy and complexity with performance objectives and limitations
- easy modification of the controller through the use of linguistic fuzzy rules

Based on the experience learned while conducting numerical simulations on primary and secondary controllers, a supervisory fuzzy logic controller is designed by utilizing MATLAB Fuzzy Logic toolbox [42] and integrated in SIMULINK as shown in Figure 115. Here inputs to the FLC are the depth error (z_e) and depth rate (w). Depth error is defined as the commanded depth minus the measured depth. The output or control variable is 'u' which regulates the buoyancy with respect to the depth error and depth rate. After carrying out the stability check using different kinds of membership functions, *Gaussian* membership functions are finally used for representing the input and output variables as shown in Figures 116-117. Using a trial and error approach, the best inference mechanism to use in this case seems to be the *prod-probor*

method. Because of simplicity and availability of the graphical user interface (GUI) in MATLAB, the Mamdani inference engine is employed for designing the FLC that uses the *minimum* operator for a fuzzy implication and *max-min* operator for composition The defuzzification technique used is found using a trial and error and *centroid* method is the one which provides least integral square error. Table 8 shows fuzzy rule base consists of 49 rules for computing the output variable, which are formulated based on the author's experience in performing numerical simulation using depth error and depth rate as the system states and change in volume of gas inside the lift bag as the output. The definition of fuzzy control actions are defined in Table 9.

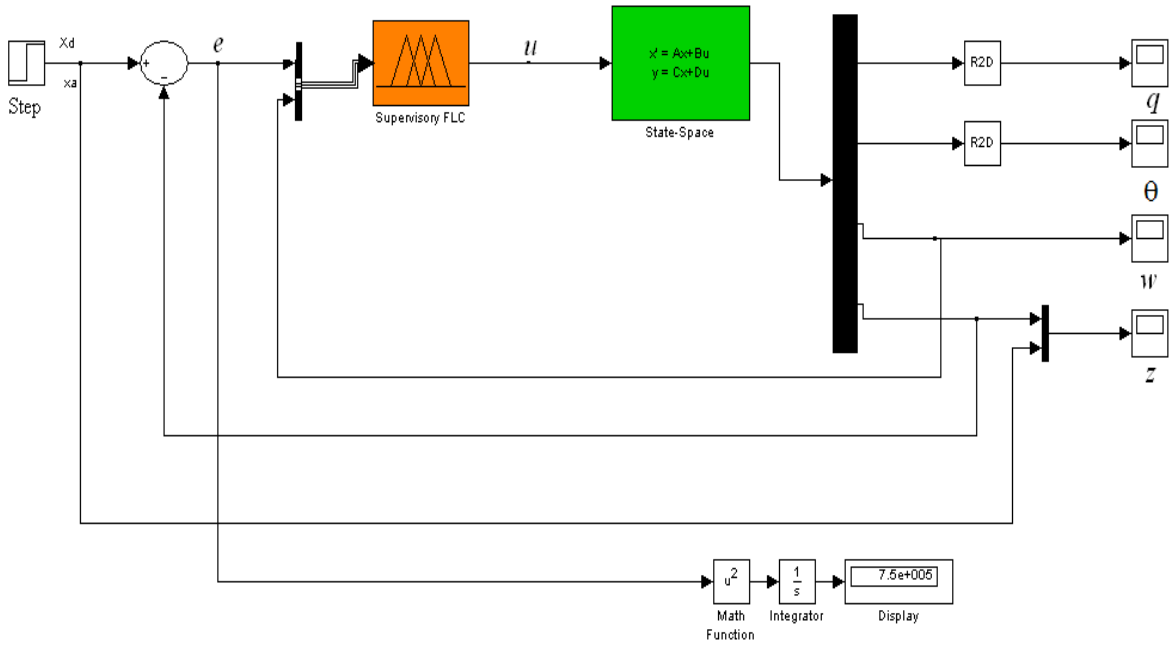

Figure 115: SIMULINK block diagram of a supervisory FLC for marine salvage

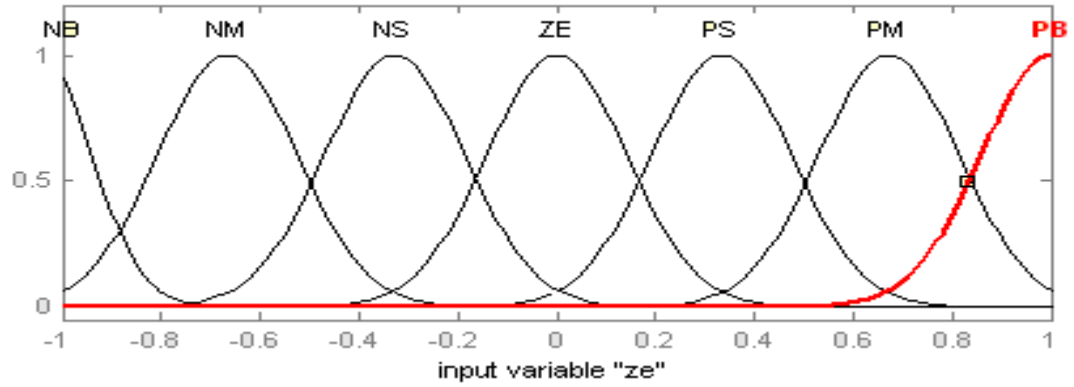

Figure 116 (a): Membership functions for the input variable z_e

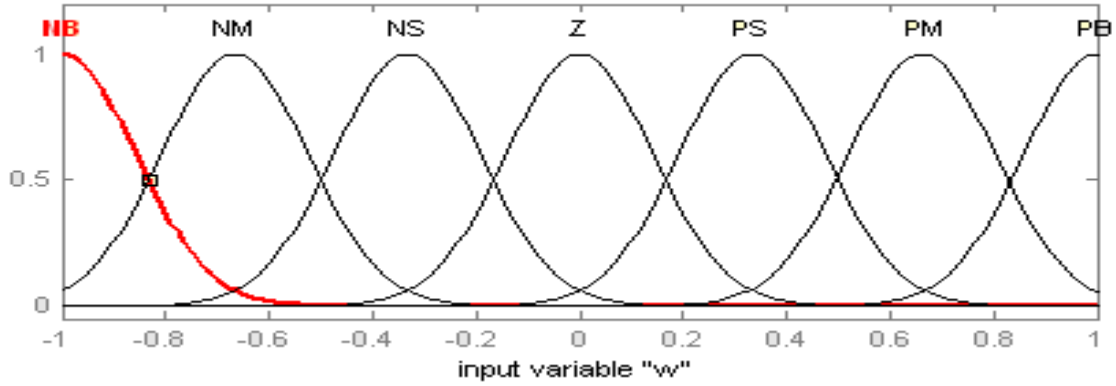

Figure 116 (b): Membership functions for the input variable '*w*'

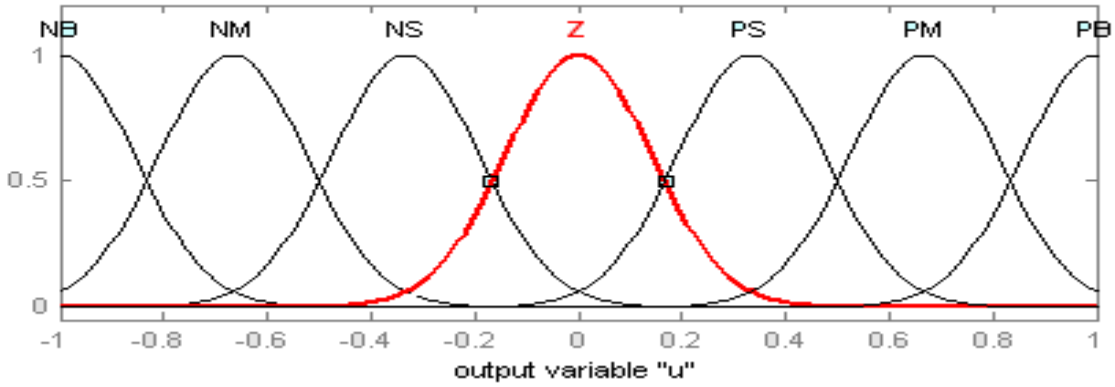

Figure 117: Membership functions for the output variable '*u*

Table 8. Two dimensional fuzzy rules to compute *u*

Z_e	W						
	NB	NM	NS	ZE	PS	PM	PB
PB	Z	PS	PM	PB	PB	PB	PB
PM	NS	Z	PS	PM	PB	PB	PB
PS	NM	NS	Z	PS	PM	PB	PB
ZE	NB	NM	NS	Z	PS	PM	PB
NS	NB	NB	NM	NS	Z	PS	PM
NM	NB	NB	NB	NM	NS	Z	PS
NB	NB	NB	NB	NB	NM	NS	Z

The variation of control action '*u*' with respect to the depth error (z_e) and depth rate (*w)* is shown in Figure 118. Positive value of *u* implies filling gas inside the lift bags, where as negative value implies taking gas or purging gas out from the bags. Thus by the combined action of filling gas in to the lift bag and by regulating the purging of gas through the valves in accordance with the depth error and its derivative, a stable ascent can be ensured.

The performance of the supervisory fuzzy logic controller is investigated by performing simulation on the pontoon model, which is lying at sea bottom 250 m, 300 m & 350 m below the sea surface and the obtained responses are plotted in Figures 119-123.

Table 9: Definition of fuzzy output control action

Output ‘*u*’	Meaning	Control Action
Z	Zero	Both Primary and Secondary controllers are off
PS	Positive Small	Small rate of filling gas in to the lift bag : operating primary controller
PM	Positive Medium	Medium rate of filling gas in to the lift bag : operating primary controller
PB	Positive Big	Large rate of filling gas in to the lift bag : operating primary controller
NS	Negative Small	Small purging of gas from lift bag: operating secondary controller
NM	Negative Medium	Medium purging of gas from lift bag : operating secondary controller
NB	Negative Big	Large rate of purging gas from lift bag: operating secondary controller.

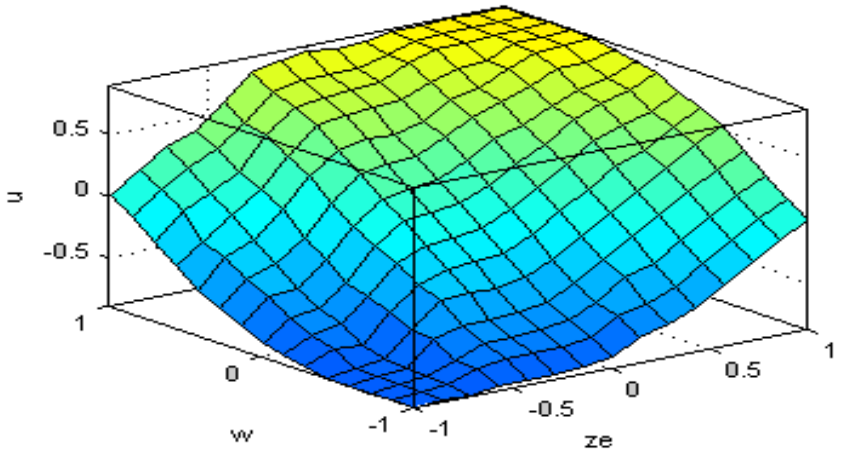

Figure 118: Variation of control action with depth error and depth rate

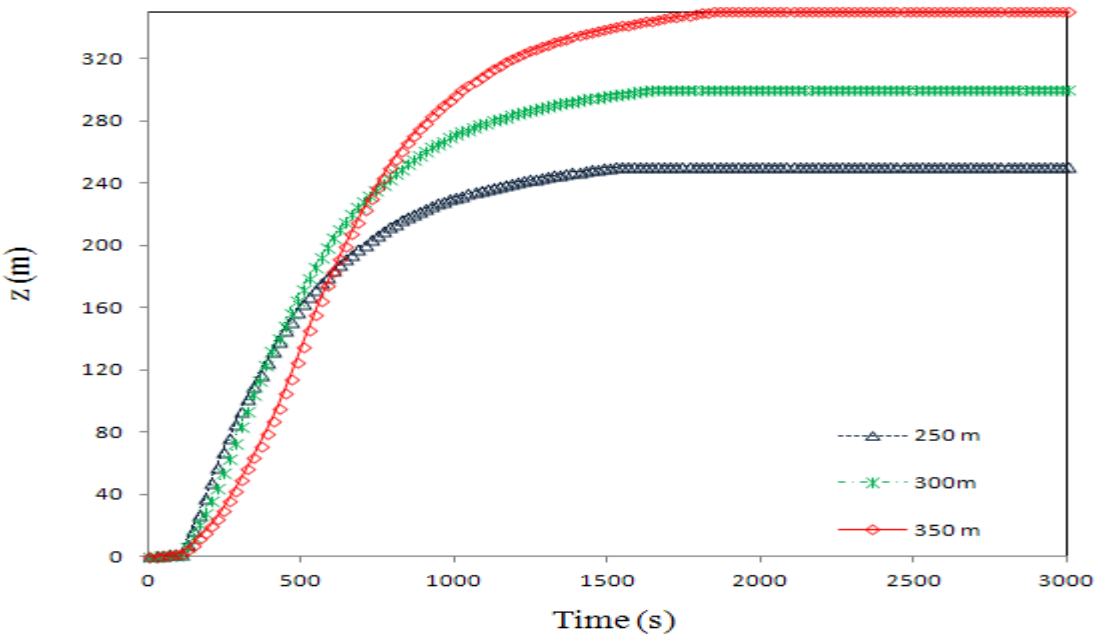

Figure 119: Variation of ship vertical position from sea bottom

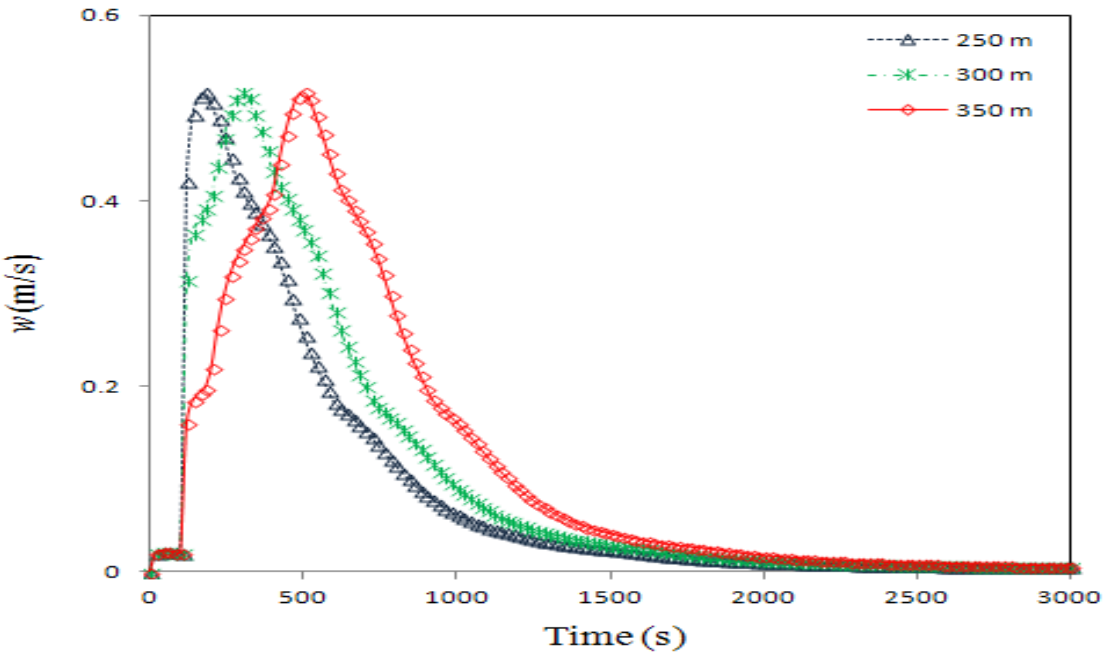

Figure 120: Variation of ship ascent velocity

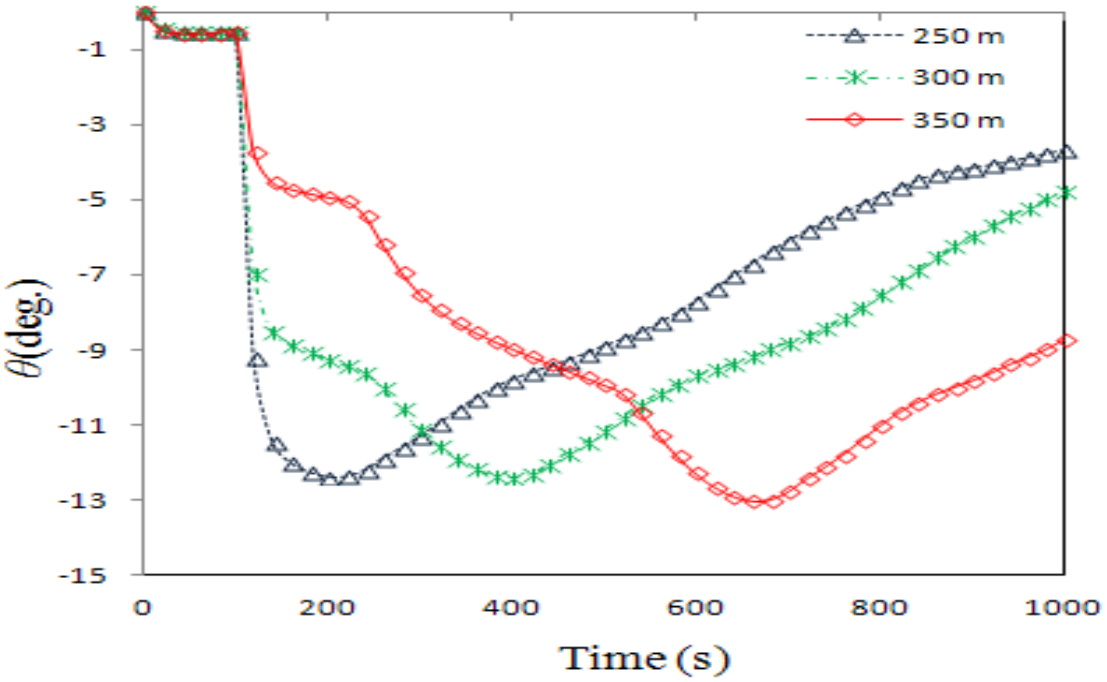

Figure 121: Variation of ship pitch angle

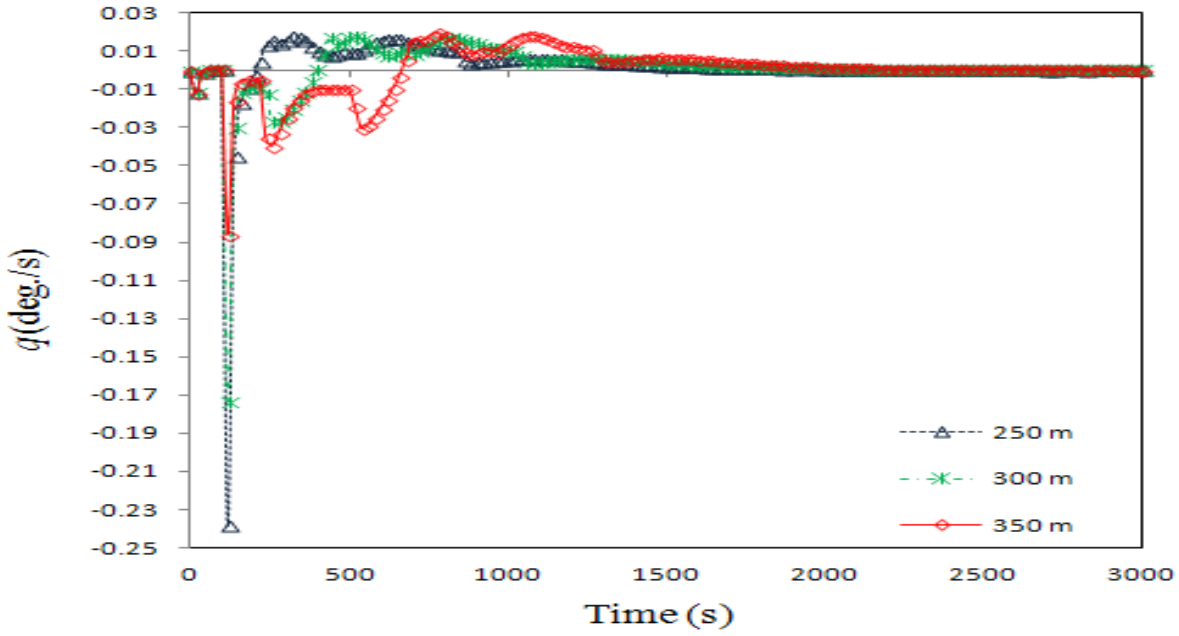

Figure 122: Variation of ship pitch rate

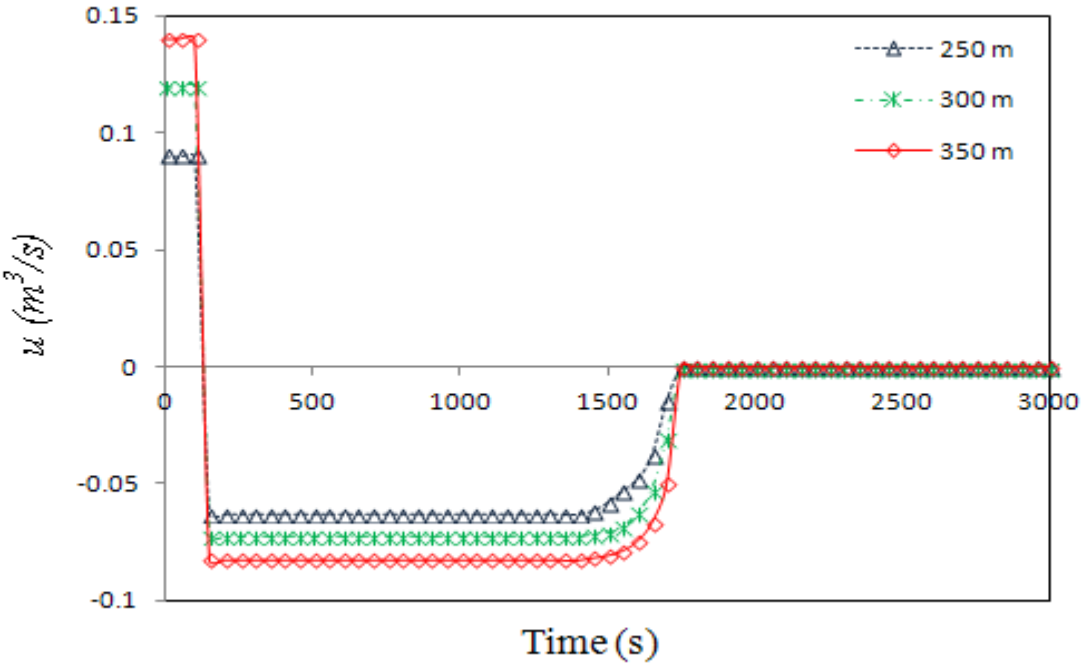

Figure 123: Net flow rate (at local pressure) in and out of lift bags

Figure 119 shows that in all the three cases the pontoon reaches the target depth in 1600s with no overshoot and less steady state error. The maximum value of ascent velocity among the three target depths is found from Figure 120 to be 0.45 m/s (<0.6 m/s), which leads to the conclusion that the controller is capable to maintain ascent velocity within the stable range for even higher water depths. From Figure 121, the maximum value of pitch angle for the three cases are found to be 13^0, which shows that pitch is stable (< 15^0). Pitch rates for the three case approaches zero when the pontoon reaches the commanded depth as shown in Figure 122. Figure 123 shows how the fuzzy control action regulates the volume inside the lift bags according to the depth error and depth rate for a stable ascent. It is noted that the controller initially sets positive flow rate for suction breakout and after the suction breakout (i.e.100 s), the controller reduce the flow rates to negative value in order to overcome the excess buoyancy available and thereafter maintains a

constant value for handling the variation in additional buoyancy due to the expansion of gas inside the lift bags with respect to the decrease in depth and finally reaches zero value after the pontoon reaches the commanded depth. From the simulation studies it is found that the proposed supervisory FLC is suitable for maintaining hydrodynamic stability for even higher commanded depths by suitably designing the fuzzy membership functions, scaling factors and linguistic fuzzy rules.

8.1 Concluding Remarks

A supervisory fuzzy logic controller is designed to monitor or switch between the primary and secondary controllers as per the depth error and depth rate for a stable ascent. From the simulation studies, it is found that the proposed supervisory FLC is able to maintain hydrodynamic stability for even higher water depths without overshoot and less steady state error. This is because the FLC uses a non linear control law that is developed based on the author's experience in conducting numerical simulations on primary and secondary controllers and also due to the stability analysis by using different combinations of fuzzy membership functions and scaling factors by the trial and error method. Thus the supervisory fuzzy logic controller becomes adaptable for a safe and stable salvage operation.

9 Extending to Flexible Body Modeling & Control

In the rigid body modeling & control approach, the state space model is created by considering the total additional buoyancy provided by all lift bags together and the responses are available for the whole motion of the payload. But in actual practice, lift bags are located at different locations on the vessel and their location significantly affects the hydrodynamic and control responses. Whilst rigid body modeling can be extended to include the response of individual lift bags and to control them separately, i.e. to use multiple controlled lift bags to ensure both hydrodynamic and structural stability, it cannot deal with more complicated lifts, such as a flexible pipeline. Although it continues to consider the case of ship salvage, this chapter extends the theory to allow for this possibility. For meeting these objectives, the rigid body modeling & control approach is extended to a detailed flexible beam modeling & control.

In the flexible body modeling & control approach, the vessel or payload is modeled as an Euler-Bernoulli beam with free – free boundary conditions as shown in Figure 124. Initially free vibration analysis or eigen value analysis of the vessel is carried out in MATLAB using analytical and finite element method to obtain the natural frequencies (eigen values) and mode shapes (eigen vectors) and the obtained responses are compared. By looking the mode shapes, the optimum location of lift bags on the vessel can be determined. Within the controller it is not possible to integrate the coupled motions equation of motion, so it is required to convert from physical to principal coordinates. For that, the eigenvectors are normalized with respect to mass and the equation of motion is developed in principal coordinates, after defining the nodal forces and moments. Nodal forces and moments can be determined from the hydrostatic, hydrodynamic, suction breakout and additional buoyancy force components as explained in Section 4.1.1.1- 4.1.1.4. The uncoupled equations of motion in principal coordinates are transformed in to a state space form. The modal contributions of individual modes are analyzed

according to their dc gain/peak gain value to define which ones having the greatest contribution. Finally efficacies of modal reduction techniques such as '*modred*' (both 'mdc' & 'del' sub functions) methods with *sorted* / *unsorted* modes are used to obtain a smallest state space model (4*4) that accurately represents the pertinent flexible body dynamics. Later supervisory fuzzy logic controller is integrated with the flexible state space model of each lift bags to obtain the controlled stable responses.

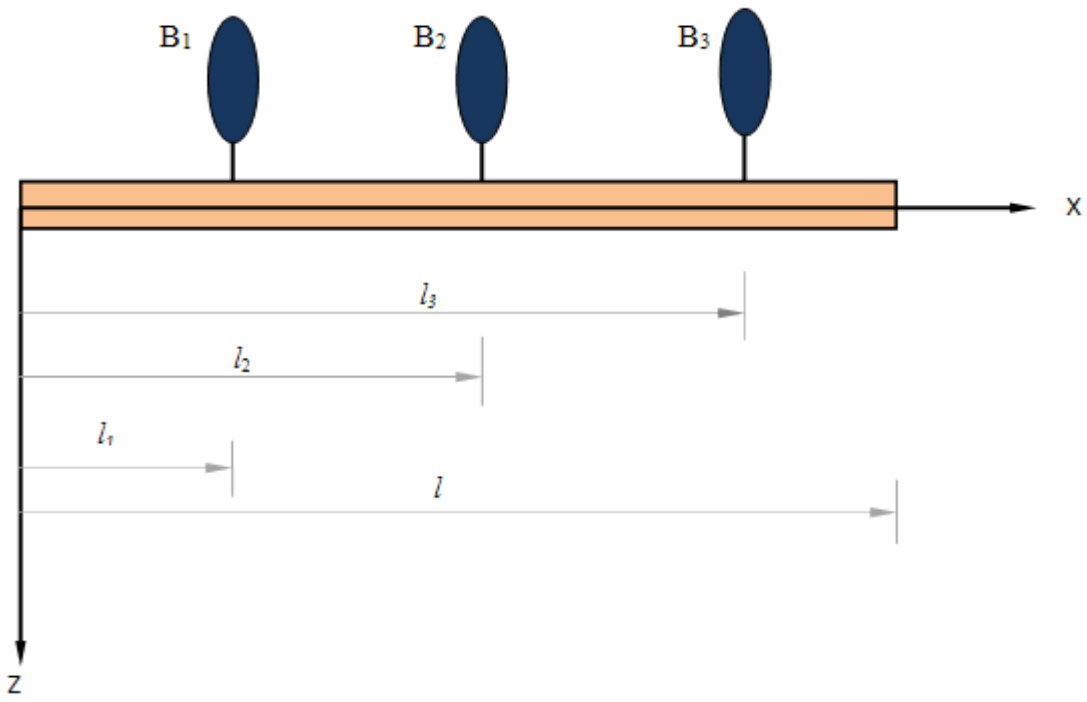

Figure 124: Concept of a beam model with lift bags for marine salvage

9.1 Euler-Bernoulli Equation

The Euler-Bernoulli equation for the transverse vibration of a beam within the X-Z plane is given by [2, 21, 71, 94],

$$\frac{\partial^2}{\partial x^2}\left[EI\frac{\partial^2 z}{\partial x^2}\right]+\rho A\left[\frac{\partial^2 z}{\partial t^2}\right]=F\left(x,t\right) \tag{76}$$

In which, *z (x, t)* is the deflection at location *x* along the beam at time *t*, *E* –Young's modulus or modulus of elasticity of the beam material, *I* – Second moment of area of the beam cross section about the neutral axis, *m* - Mass per unit length = ρA. Where ρ is the density of the material and *A* is the cross sectional area of the beam.

F(x, t) is the force excitation on the beam, which is a function of both space & time, can be represented as the summation of all the point forces [112],

$$F\left(x,t\right)=\sum_{i=1}^{r} f_i(x,t) \tag{77}$$

In which *r* is the total number of input forces. $f_i(x, t)$ is the set of point forces $f_i(t)$ located at $x=l_i$, which can be expressed as a distributed force per unit length according to

$$f_i\left(x,t\right)=F_i(t)\delta(x-l_i) \tag{78}$$

Where $\delta(x-l_i)$ is the Dirac Delta function for i = 1, 2….r and $F_i(t)$ is the universally distributed force per unit length.

For the beam with free-free boundary conditions, the shear force and bending moment at the two ends are zero [21],

i.e.

$$\left.\frac{\partial^2 z(x,t)}{\partial x^2}\right|_{x=0} = 0, \qquad \left.\frac{\partial^2 z(x,t)}{\partial x^2}\right|_{x=l} = 0, \tag{79}$$

$$\left.\frac{\partial^3 z(x,t)}{\partial x^3}\right|_{x=0} = 0, \qquad \left.\frac{\partial^3 z(x,t)}{\partial x^3}\right|_{x=l} = 0, \tag{80}$$

In Euler-Bernoulli beam theory, the assumption is plane cross section of the beam remains plane and normal to the neutral axis before and after the bending. i.e. Euler-Bernoulli beam theory neglects rotational inertia and deformation due to shear forces.

9.1.1 Analytical Solution

The natural frequencies of the vessel for any mode of vibration can be found using analytical method as [21],

$$f_n = \frac{1}{2\pi}\left[\frac{(kl)_n}{l}\right]^2 \sqrt{\frac{EI}{\rho A}} \tag{81}$$

Where, f_n is the natural frequency for any mode of vibration in hz and l is the length of the vessel.

The value of $(kl)_n$ can be obtained by solving the equation $coshklcoskl = 1$ as shown in Table 10.

Table 10 Graphical solution of *coshklcoskl*=1

$(kl)_1$	$(kl)_2$	$(kl)_3$	$(kl)_4$	$(kl)_5$	$(kl)_6$
0	4.73	7.853	10.996	14.137	17.279

Therefore, by substituting the various values of $(kl)_n$ in Eq. (81), the respective natural frequencies for any mode of vibration can be found. The value $(kl)_1 = 0$ is disregarded as it does not give rise to an oscillatory motion.

The mode shapes at number of positions (x/l) along the length of the beam can be obtained by,

$$Z_n\left\{\frac{x}{l}\right\} = D\left[\left(\cosh(kl)_n\left\{\frac{x}{l}\right\} + \cos(kl)_n\left\{\frac{x}{l}\right\}\right) - \left(\frac{\cosh(kl)_n - \cos(kl)_n}{\sinh(kl)_n - \sin(kl)_n}\right)\left(\sinh(kl)_n\left\{\frac{x}{l}\right\} + \sin(kl)_n\left\{\frac{x}{l}\right\}\right)\right] \quad (82)$$

In order to plot the vibration profiles, the value of Z is calculated at number of points along the beam and the resulting profile is then normalized.

See Appendix B for the detailed derivation of analytical solution of an Euler-Bernoulli beam with free-free boundary conditions.

9.1.2 Finite Element Solution

For a beam with free-free boundary conditions, the displacement $z(x, t)$ can be represented as [53],

$$z = z_0 e^{-i\omega t} \tag{83}$$

Where z_0 is the amplitude and ω is the natural frequency of vibration.

Therefore,

$$\dot{z} = z_0 e^{-i\omega t} \times -i\omega \tag{84}$$

$$\ddot{z} = z_0 e^{-i\omega t} \times -i\omega \times -i\omega = -\omega^2 z \tag{85}$$

Substituting Eq. (85) in Eq. (76), the eigenvalue problem is obtained as,

$$\frac{\partial^2}{\partial x^2}\left[EI \frac{\partial^2 z}{\partial x^2} \right] - \rho A \omega^2 z = 0 \tag{86}$$

The above eigenvalue problem in differential form can be converted to finite element formulation as [8, 53, 79]:

$$-\omega_i^2 \left[M \right] \{ z_i \} + \left[K \right] \{ z_i \} = 0 \tag{87}$$

i.e.

$$\left[\left[K\right]-\omega_i^2\left[M\right]\right]\{z_i\}=0 \tag{88}$$

Therefore,

$$\left|\left[K\right]-\omega_i^2\left[M\right]\right|=0 \tag{89}$$

Where,

ω_i is the eigenvalue or natural frequencies of the beam and z_i is the eigenvector or mode shape of the beam, which can be obtained from eigenvalue analysis in MATLAB. *[M]* - Mass matrix of the system, *[K]* - Stiffness matrix of the system, which can be calculated based on finite element principles as shown below:

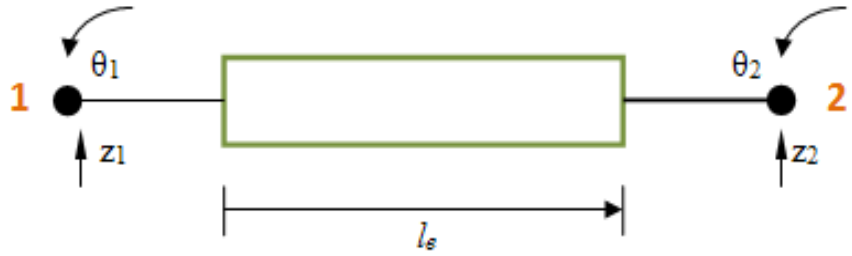

Figure 125: Two DOF beam element

A 2D prismatic homogeneous isotropic beam element is shown in Figure 125 [16, 53, 77-78, 137]. The longitudinal axes of the element lies along the *X* axis. The element has a constant moment of inertia I_e, modulus of elasticity *E*, density ρ, length l_e and area of cross section A_e . Beam element is considered with two nodes at its ends. Each node is having two dof. I.e. the translation in *Z* axis (heave) and rotation about *Y* axis or *XZ* plane (pitch).

Degree of freedoms of the element can be expressed as:

$$u_e = [z_1, \theta_1, z_2, \theta_2]^T \quad (90)$$

The displacement function can be approximated as:

$$z(x,t) = z_1(t)\psi_1(x) + \theta_1(t)\psi_2(x) + z_2(t)\psi_3(x) + \theta_2(t)\psi_4(x) \quad (91)$$

Where the shape functions $\psi_1(x)$, $\psi_2(x)$, $\psi_3(x)$ and $\psi_4(x)$ are obtained by applying boundary conditions at the corresponding nodes as [16, 67]:

$$\psi_1(x) = 1 - \frac{3x^2}{l_b^2} + \frac{2x^3}{l_b^3} \quad (92)$$

$$\psi_2(x) = x - \frac{2x^2}{l_b} + \frac{x^3}{l_b^2} \quad (93)$$

$$\psi_3(x) = \frac{3x^2}{l_b^2} - \frac{2x^3}{l_b^3} \quad (94)$$

$$\psi_4(x) = \frac{-x^2}{l_b} + \frac{x^3}{l_b^2} \quad (95)$$

Strain energy of the element is [16, 53]:

$$S.E = \int_0^{l_e} \frac{EI_e}{2}\left(\frac{\partial^2 z}{\partial x^2}\right)^2 dx = \frac{1}{2} u_e{}^T [K]_e u_e \quad (96)$$

Therefore, the consistent stiffness matrix is obtained as [16],

$$\left[K\right]_e^{ij} = \int_0^{l_e} EI\psi_i''(x)\psi_j''(x)dx = EI\int_0^{l_e} \begin{bmatrix} \frac{6}{l_e^2}+\frac{12x}{l_e^3} \\ -\frac{4}{l_e}+\frac{6x}{l_e^2} \\ \frac{6}{l_e^2}-\frac{12x}{l_e^3} \\ -\frac{2}{l_e}+\frac{6x}{l_e^2} \end{bmatrix} \begin{bmatrix} \frac{6}{l_e^2}+\frac{12x}{l_e^3} & -\frac{4}{l_e}+\frac{6x}{l_e^2} & \frac{6}{l_e^2}-\frac{12x}{l_e^3} & -\frac{2}{l_e}+\frac{6x}{l_e^2} \end{bmatrix} dx \quad (97)$$

After integrating,

$$\left[K\right]_e = \frac{EI_e}{l_e^3}\begin{bmatrix} 12 & 6l_e & -12 & 6l_e \\ 6l_e & 4l_e^2 & -6l_e & 2l_e^2 \\ -12 & -6l_e & 12 & -6l_e \\ 6l_e & 2l_e^2 & -6l_e & 4l_e^2 \end{bmatrix} \quad (98)$$

Kinetic Energy of the element can be expressed as [16]:

$$K.E = \int_0^{l_e} \frac{\rho A_e}{2}\left(\frac{\partial z}{\partial t}\right)^2 dx = \frac{1}{2}\ \dot{u}_e^{\,T}\left[M\right]_e \dot{u}_e \quad (99)$$

The consistent mass matrix is obtained as [16, 53]:

$$\left[M\right]_e^{ij} = \int_0^{l_e} \rho A_e\psi_i(x)\psi_j(x)dx = \rho A_e\int_0^{l_e} \begin{bmatrix} 1-3\frac{x^2}{l_e^2}+2\frac{x^3}{l_e^3} \\ x-2\frac{x^2}{l_e}+\frac{x^3}{l_e^2} \\ 3\frac{x^2}{l_e^2}-2\frac{x^3}{l_e^3} \\ -\frac{x^2}{l_e}+\frac{x^3}{l_e^2} \end{bmatrix} \begin{bmatrix} 1-3\frac{x^2}{l_e^2}+2\frac{x^3}{l_e^3} & x-2\frac{x^2}{l_e}+\frac{x^3}{l_e^2} & 3\frac{x^2}{l_e^2}-2\frac{x^3}{l_e^3} & -\frac{x^2}{l_e}+\frac{x^3}{l_e^2} \end{bmatrix} dx \quad (100)$$

After integrating,

$$[M]_e = \frac{\rho A_e l_e}{420}\begin{bmatrix} 156 & 22l_e & 54 & -13l_e \\ 22l_e & 4l_e^2 & 13l_e & -3l_e^2 \\ 54 & 13l_e & 156 & -22l_e \\ -13l_e & -3l_e^2 & -22l_e & 4l_e^2 \end{bmatrix} \quad (101)$$

9.2 Equation of motion in Principal Coordinates

The general equation of motion for a multi degree of freedom forced vibration system in physical coordinates is,

$$M\ddot{z} + C\dot{z} + Kz = F \quad (102)$$

Here the mass, damping and stiffness matrices are non diagonal matrices. Therefore the above equation leads to *n* coupled second order differential equations. As it is not possible to integrate controller techniques with coupled motions, the equation of motion needs to be uncoupled. Therefore, it is required to transform equation of motion from physical coordinates to principal coordinates. For that, firstly the eigenvalue problem is solved using FEM (see Section 9.1.2) so that the eigenvectors are obtained as $z_m(1)$, $z_m(2)$, $z_m(3)$……..$z_m(n)$. Then the eigenvectors are normalized with respect to mass in order to obtain identity mass matrix and diagonal stiffness matrix consists of square of eigenvalues as diagonal elements [5, 7, 14, 19-20, 48, 53, 62, 66-67, 85, 93, 102].

Normalized eigenvector [48],

$$z_{ni} = \frac{z_{mi}}{[z_{mi}^T M z_{mi}]^{1/2}} = \frac{z_{mi}}{q_i} \quad (103)$$

Where q_i is defined as [48]:

$$q_i = \left[\sum_{k=1}^{n} m_k z_{mki}^2 \right]^{1/2} \quad (104)$$

Then the modal matrix of the system is defined as,

$$[z_n] = [z_n(1) \;\; z_n(2) \;\; \ldots\ldots\ldots \; z_n(n)] \quad (105)$$

According to superposition principle, with the assumption of proportional damping, the solution of Eq. (102) can be expressed as a linear combination of normal modes as [48, 67]:

$$z(t) = [z_n] z_p(t) \text{ or } z_p(t) = [z_n]^{-1} z(t) \quad (106)$$

Where $z_p(t)$ is the vector of amplitudes of different vibration modes in principal coordinates (or simply amplitudes of different vibration modes), $z(t)$ is the displacement in physical coordinates or vector of physical cartesian coordinates of the beam nodes and z_n is the modal matrix or matrix of modal shape vectors (displacement of beam nodes) normalized with respect to mass for each vibration mode.

Therefore, the equation of motion in principal coordinates can be written as [5, 14, 48, 53, 67, 134, 138],

$$\ddot{z}_{pi}(t) + 2\zeta_i \omega_i \dot{z}_{pi}(t) + \omega_i^2 z_{pi}(t) = F_{pi}(t) \quad (107)$$

Where,

$F_{pi}(t) = [z_n]^T F_i(t)$ is the vector of force in principal coordinates, ζ is the critical damping and i denote the number of modes, i.e. i =1, 2……..n.

Therefore,

$$F_{pi}(t)=\left[z_n\right]^T F_i(t)=\begin{bmatrix} z_{n1}(l_1) & ..... & z_{n1}(l_c) & z_{n1}(l_{c+1}) & ..... & z_{n1}(l_n) \\ ..... & ..... & ..... & ..... & ..... & ..... \\ z_{nc}(l_1) & ..... & z_{nc}(l_c) & z_{nc}(l_{c+1}) & ..... & z_{nc}(l_n) \\ z_{nc+1}(l_1) & ..... & z_{nc+1}(l_c) & z_{nc+1}(l_{c+1}) & ..... & z_{nc+1}(l_n) \\ ..... & ..... & ..... & ..... & ..... & ..... \\ z_n(l_1) & ..... & z_n(l_c) & z_n(l_{c+1}) & ..... & z_n(l_n) \end{bmatrix} * F_i(t) \quad (108)$$

Where $z_{ni}(l_j)$ represents modal shape at mode *i* location 'l_j'. $F_p(t)$ is the force in principal coordinates and $F_i(t)$ represents the excitation force in the physical system.

Thus a set of *n* uncoupled second order differential equations are obtained from the set of *n* coupled second order differential equations.

9.3 Development of State Space Model

In order to integrate the controller, it is required to represent the system of equations in principal coordinates to a state space form. By modeling the equation of motion in principal coordinates, *n coupled* second order differential equations are transformed in to *n uncoupled* second order differential equations. These *n* uncoupled second order differential equations can be written in a state space model as 2*n* first order differential equations having the following form [48, 53]:

$$\dot{x} = Ax + Bu \quad (109)$$

$$y = Cx + Du \quad (110)$$

In which, *x* is the state vector, *u* the control vector, *y* the output vector, *A* the system matrix, *B* the input matrix, *C* the output matrix and *D* the direct transmission matrix of the system.

For example, suppose we are considering only the first three modes, then the equations of motion in principal coordinates can be written from Eq. (107) as:

$$\ddot{z}_{p1} + 2\zeta_1\omega_1\dot{z}_{p1} + \omega_1^2 z_{p1} = F_{p1} \quad (111)$$

$$\ddot{z}_{p2} + 2\zeta_2\omega_2\dot{z}_{p2} + \omega_2^2 z_{p2} = F_{p2} \quad (112)$$

$$\ddot{z}_{p3} + 2\zeta_3\omega_3\dot{z}_{p3} + \omega_3^2 z_{p3} = F_{p3} \quad (113)$$

Let,

$z_{p1} = z_1$ is the amplitude of vibration mode 1, then $\dot{z}_{p1} = z_2$ (114)

$z_{p2} = z_3$ is the amplitude of vibration mode 2, then $\dot{z}_{p2} = z_4$ (115)

$z_{p3} = z_5$ is the amplitude of vibration mode 3, then $\dot{z}_{p3} = z_6$ (116)

Therefore,

$$\dot{z}_1 = z_2 \quad (117)$$

$$\dot{z}_2 = \ddot{z}_{p1} = -\omega_1^2 z_{p1} - 2\zeta_1\omega_1\dot{z}_{p1} + F_{p1} = -\omega_1^2 z_1 - 2\zeta_1\omega_1 z_2 + F_{p1} \quad (118)$$

$$\dot{z}_3 = z_4 \quad (119)$$

$$\dot{z}_4 = \ddot{z}_{p2} = -\omega_2^2 z_{p2} - 2\zeta_2\omega_2\dot{z}_{p2} + F_{p2} = -\omega_2^2 z_3 - 2\zeta_2\omega_2 z_4 + F_{p2} \quad (120)$$

$$\dot{z}_5 = z_6 \quad (121)$$

$$\dot{z}_6 = \ddot{z}_{p3} = -\omega_3^2 z_{p3} - 2\zeta_3\omega_3\dot{z}_{p3} + F_{p3} = -\omega_3^2 z_5 - 2\zeta_3\omega_3 z_6 + F_{p3} \quad (122)$$

Eqs. (117-122) can be written in matrix form as:

$$\begin{bmatrix} \dot{z}_1 \\ \dot{z}_2 \\ \dot{z}_3 \\ \dot{z}_4 \\ \dot{z}_5 \\ \dot{z}_6 \end{bmatrix} = \begin{bmatrix} 0 & 1 & 0 & 0 & 0 & 0 \\ -\omega_1^2 & -2\xi_1\omega_1 & 0 & 0 & 0 & 0 \\ 0 & 0 & 0 & 1 & 0 & 0 \\ 0 & 0 & -\omega_2^2 & -2\xi_2\omega_2 & 0 & 0 \\ 0 & 0 & 0 & 0 & 0 & 1 \\ 0 & 0 & 0 & 0 & -\omega_3^2 & -2\xi_3\omega_3 \end{bmatrix} \begin{bmatrix} z_1 \\ z_2 \\ z_3 \\ z_4 \\ z_5 \\ z_6 \end{bmatrix} + \begin{bmatrix} 0 \\ F_{p1} \\ 0 \\ F_{p2} \\ 0 \\ F_{p3} \end{bmatrix} u_c \tag{123}$$

This is the form $\dot{x} = Ax + Bu$, where the system matrix A is made up of each eigenvalue and damping for each mode [48, 53, 134].

$$A = \begin{bmatrix} 0 & 1 & .... & .... & .... \\ -\omega_1^2 & -2\xi_1\omega_1 & .... & .... & .... \\ .... & .... & .... & .... & .... \\ ..... & .... & .... & 0 & 1 \\ .... & .... & .... & -\omega_n^2 & -2\xi_n\omega_n \end{bmatrix} \quad \text{or} \qquad A = \begin{bmatrix} 0 & I \\ -\omega_i^2 & -2\xi_i\omega_i \end{bmatrix} \tag{124}$$

Input matrix B is made up of applied force at the nodes.

$$B = \begin{bmatrix} 0 \\ F_{p1} \\ 0 \\ F_{p2} \\ .... \\ F_{pn} \end{bmatrix} \qquad or \qquad B = \begin{bmatrix} 0 \\ F_{pi} \end{bmatrix} = \begin{bmatrix} 0 \\ z_n^T F_i \end{bmatrix} \tag{125}$$

State vector x consists of amplitudes of vibration and its derivatives for each mode in principal coordinates,

$$x = \begin{bmatrix} z_{pi} \\ \dot{z}_{pi} \end{bmatrix} \tag{126}$$

Suppose we are interested in three displacements and three velocities as system output, then the output matrix equation can be written from Eq. (110) as:

$$y_p = Cz = \begin{bmatrix} y_{p1} \\ y_{p2} \\ y_{p3} \\ y_{p4} \\ y_{p5} \\ y_{p6} \end{bmatrix} = \begin{bmatrix} 1 & 0 & 0 & 0 & 0 & 0 \\ 0 & 1 & 0 & 0 & 0 & 0 \\ 0 & 0 & 1 & 0 & 0 & 0 \\ 0 & 0 & 0 & 1 & 0 & 0 \\ 0 & 0 & 0 & 0 & 1 & 0 \\ 0 & 0 & 0 & 0 & 0 & 1 \end{bmatrix} \begin{bmatrix} z_1 \\ z_2 \\ z_3 \\ z_4 \\ z_5 \\ z_6 \end{bmatrix} \tag{127}$$

(As there is no state by pass, direct transmission matrix D=0)

Output vector in physical coordinates can be obtained by transformation from principal coordinates as [48]:

$$z = z_n y_p = \begin{bmatrix} z_1 \\ \dot{z}_1 \\ z_2 \\ \dot{z}_2 \\ z_3 \\ \dot{z}_3 \end{bmatrix} = \begin{bmatrix} z_{n11} & 0 & z_{n12} & 0 & z_{n13} & 0 \\ 0 & z_{n11} & 0 & z_{n12} & 0 & z_{n13} \\ z_{n21} & 0 & z_{n22} & 0 & z_{n23} & 0 \\ 0 & z_{n21} & 0 & z_{n22} & 0 & z_{n23} \\ z_{n31} & 0 & z_{n32} & 0 & z_{n33} & 0 \\ 0 & z_{n31} & 0 & z_{n32} & 0 & z_{n33} \end{bmatrix} \begin{bmatrix} y_{p1} \\ y_{p2} \\ y_{p3} \\ y_{p4} \\ y_{p5} \\ y_{p6} \end{bmatrix} = \begin{bmatrix} z_{n11}y_{p1} + z_{n12}y_{p3} + z_{n13}y_{p5} \\ z_{n11}y_{p2} + z_{n12}y_{p4} + z_{n13}y_{p6} \\ z_{n21}y_{p1} + z_{n22}y_{p3} + z_{n23}y_{p5} \\ z_{n21}y_{p2} + z_{n22}y_{p4} + z_{n23}y_{p6} \\ z_{n31}y_{p1} + z_{n32}y_{p3} + z_{n33}y_{p5} \\ z_{n31}y_{p2} + z_{n32}y_{p4} + z_{n33}y_{p6} \end{bmatrix} \tag{128}$$

9.3.1 Estimation of Individual Modal Contributions

In a model analysis problem, all the modes do not contribute significantly to the overall system behavior. In some problems, low frequency modes are important, whereas in some other cases high frequency modes are relevant. Therefore, while performing modal analysis, it is required to estimate the contributions of individual modes in the overall system behavior. Contributions of individual mode over the system behavior can be obtained from state space model as follows:

For the First mode (i=1), the state space model may be written from Eq. (123) as:

$$\begin{bmatrix} \dot{z}_1 \\ \dot{z}_2 \end{bmatrix} = \begin{bmatrix} 0 & 1 \\ -\omega_1^2 & -2\xi_1\omega_1 \end{bmatrix} \begin{bmatrix} z_1 \\ z_2 \end{bmatrix} + \begin{bmatrix} 0 \\ F_{p1} \end{bmatrix} u_c \tag{129}$$

Similarly, for the Second mode (i=2), the state space model can be written as:

$$\begin{bmatrix} \dot{z}_3 \\ \dot{z}_4 \end{bmatrix} = \begin{bmatrix} 0 & 1 \\ -\omega_2^2 & -2\xi_2\omega_2 \end{bmatrix} \begin{bmatrix} z_3 \\ z_4 \end{bmatrix} + \begin{bmatrix} 0 \\ F_{p2} \end{bmatrix} u_c \tag{130}$$

For the Third mode (i=3), the state space model can be written as:

$$\begin{bmatrix} \dot{z}_5 \\ \dot{z}_6 \end{bmatrix} = \begin{bmatrix} 0 & 1 \\ -\omega_3^2 & -2\xi_3\omega_3 \end{bmatrix} \begin{bmatrix} z_5 \\ z_6 \end{bmatrix} + \begin{bmatrix} 0 \\ F_{p3} \end{bmatrix} u_c \tag{131}$$

Suppose, we are only interested in displacements as outputs, then ouput vector can be

defined from Eq. (128) as:

$$z = \begin{bmatrix} z_1 \\ z_2 \\ z_3 \end{bmatrix} = \begin{bmatrix} z_{n11} & 0 & z_{n12} & 0 & z_{n13} & 0 \\ z_{n21} & 0 & z_{n22} & 0 & z_{n23} & 0 \\ z_{n31} & 0 & z_{n32} & 0 & z_{n33} & 0 \end{bmatrix} \begin{bmatrix} y_{p1} \\ y_{p2} \\ y_{p3} \\ y_{p4} \\ y_{p5} \\ y_{p6} \end{bmatrix} \quad (132)$$

9.4 Model Reduction Techniques

The structure or beam can vibrate with many modes. In the development of flexible state space model, *n uncoupled* second order differential equations are converted into 2*n* first order differential equations. Therefore the size of system matrix is twice the number of modes to be included in the analysis. Hence if large number of modes are included in the analysis, the process become cumbersome and leads to high computational time [48]. However all the modes do not contribute significantly to the overall responses. Hence it is sensible to use the important modes, that cause the maximum disturbances, and to develop a state space model that includes the most significant modes in the analysis at the same time it might account for the effect of eliminated modes in the remaining system. The objective of the modal reduction technique is to provide the smallest state space model that accurately represents the flexible system dynamics [48, 53, 66-67].

9.4.1 Sorting of Modes by dc gain approach

The common method for reducing the modal size is to simply truncate the higher frequency modes. This kind of elimination is not valid for all cases and leads to less desired accuracy. Therefore, accurate reduced models can be obtained by sorting the modes based on their

individual contribution to the overall response (see Section 9.31) and keeping only important modes. In other words, the size of the model can be reduced by discarding those modes, which do not contribute to the overall response. The contribution of each mode to the overall response is calculated in terms of 'dc gain' [48, 53, 62, 66, 137].

The transfer function for the displacement of the jth node due to a force applied at kth node for the ith mode is [48, 53]:

$$z_{jki} = \frac{z_{nji} z_{nki}}{s^2 + 2\zeta_i \omega_i s + \omega_i^2} = \frac{z_{ji}}{F_{ki}} \quad \text{(damped system)} \tag{133}$$

$$z_{jki} = \frac{z_{nji} z_{nki}}{s^2 + \omega_i^2} = \frac{z_{ji}}{F_{ki}} \quad \text{(undamped system)} \tag{134}$$

This is the contribution from i^{th} mode to the transfer function z_{jk}. Therefore total contribution is obtained by summing all such contributions from individual modes as:

$$z_{jk} = \sum_{i=1}^{m} \frac{z_{nji} z_{nki}}{s^2 + 2\zeta_i \omega_i s + \omega_i^2} = \frac{z_j}{F_k} \quad \text{(damped system)} \tag{135}$$

$$z_{jk} = \sum_{i=1}^{m} \frac{z_{nji} z_{nki}}{s^2 + \omega_i^2} = \frac{z_j}{F_k} \quad \text{(undamped system)} \tag{136}$$

Where, z_{nji} z_{nki} are the product of the j^{th} (output) row and k^{th} (input or force applied) row terms of i^{th} eigenvector. ω_i is the eigenvalue or resonant frequency of the i^{th} mode and m is the total number of modes to be included [48, 53].

The dc gain for each mode is obtained by substituting s=$j\omega$=0 in the Eqs. (133) & (134), which is same for both undamped and damped systems as:

i.e.

dc gain for i^{th} mode is,

$$\frac{z_{ji}}{F_{ki}} = \frac{z_{nji} z_{nki}}{\omega_i^2} \tag{137}$$

Peak gain of each mode is obtained at resonance. Therefore, substituting $s=j\omega_i$ in the Eq. (133), so that peak gain for i^{th} mode is obtained as [48, 53]:

$$peak\ gain = -\frac{j}{2\zeta_i}(\text{dc gain}) \tag{138}$$

The relationship between dc gain and peak gain of a mode is that dc gain term is dived by 2ζ and multiplied by '$-j$', which gives a 90 degree phase shift at resonance. ζ is the critical damping, which is typically small for mechanical structures and hence amplifies the response with a resonant peak [48, 53, 66].

$$\zeta_i = \frac{\alpha + \beta\omega_i^2}{2\omega_i} \tag{139}$$

In which α and β are the damping coefficients of mass and stiffness matrices respectively.

Note

If the same value of ζ is used for all modes (uniform damping), there is no difference in sorting the model using dc gain or peak gain. If the modes have different damping, then peak gain must be used to sort the modes for importance [48].

In the considered problem, the force and moments are distributed on the beam nodes, therefore it is required to define a composite forcing function or force vector, which consists of force applied to each node times the eigenvector value for that node. Therefore, for a single input system, the composite forcing vector will be (1 × ndof) × (ndof × nmodes) = (1×nmodes). Thus a composite force vector is obtained for each mode, which then multiplied element by element by the rows of the eigenvector matrix corresponding to nodal displacements [48].

9.4.2 Modred method

Though reduced models can obtained effectively by sorting of modes based on their dc gain value, still there is an error introduced due to neglecting the contribution of eliminated modes in the overall dc gain. The MATLAB function “modred” (MODel order REDuction) is introduced to eliminate this error, which is based on the assumptions that some modes being more important than other [48, 53]. This allows reducing size of the problem to that of the ‘important modes’. The Modred function has two options or sub functions; the ‘mdc’ (Matched DC gain) option reduces defined states by setting the derivatives of the state to be eliminated to zero and then solving for the remained states, which is analogous to Guyan reduction in that the low frequency effects of the eliminated states are included in the remaining states. The other option ‘del’ simply eliminates the defined states, typically associated with the higher frequency modes [48].

In the modred function, firstly it is required to define the states to be eliminated. The states to be eliminated can be defined as a vector of arbitrary states or as a continuous partition or block of states, from one index greater than the number of states to be kept to the total number of states. If the sorting is carried out according to dc gain or peak gain, the most important modes are separated from the less important modes and maintained. If unsorted states are used for the

modred method, higher frequency modes are eliminated while maintaining the lower frequency modes [48, 53, 62, 66-67].

Let z_k represents the modes to be kept and z_e represents the modes to get eliminated. Therefore state space model can be written as [48, 53]:

$$\begin{bmatrix} \dot{z}_k \\ \dot{z}_e \end{bmatrix} = \begin{bmatrix} A_{kk} & A_{ke} \\ A_{ek} & A_{ee} \end{bmatrix} \begin{bmatrix} z_k \\ z_e \end{bmatrix} + \begin{bmatrix} B_k \\ B_e \end{bmatrix} u \tag{140}$$

The output equation can be written as [48, 53]:

$$y = \begin{bmatrix} C_k & C_e \end{bmatrix} \begin{bmatrix} z_k \\ z_e \end{bmatrix} + Du \tag{141}$$

Expanding the state space equations in Eq. (140),

$$\dot{z}_k = A_{kk} z_k + A_{ke} z_e + B_k u \tag{142}$$

$$\dot{z}_e = A_{ek} z_k + A_{ee} z_e + B_e u \tag{143}$$

By the principle of ‘mdc’ sub function, setting the derivative of states to be eliminated as zero [48, 53]:

i.e.

$$\dot{z}_e = 0 \tag{144}$$

Therefore, solving for z_e in Eq. (143),

$$z_e = -A_{ee}^{-1} A_{ek} z_k - A_{ee}^{-1} B_e u \tag{145}$$

Substituting Eq. (145) in to Eq. (142) and grouping terms:

$$\dot{z}_k = A_{kk} z_k + A_{ke}(-A_{ee}^{-1}A_{ek} z_k - A_{ee}^{-1}B_e u) + B_k u = (A_{kk} - A_{ke}A_{ee}^{-1}A_{ek})z_k + (B_k - A_{ke}A_{ee}^{-1}B_e)u \quad (146)$$

The above equation can be rewritten as [48, 53]:

$$\dot{z}_{red} = A_{red} z_{red} + B_{red} u \quad (147)$$

Where,

$$A_{red} = (A_{kk} - A_{ke}A_{ee}^{-1}A_{ek}) \text{ and } B_{red} = (B_k - A_{ke}A_{ee}^{-1}B_e) \quad (148)$$

Similarly, expanding the output equation and substituting the value of z_e leads to:

$$y = C_k z_k + C_e z_e + Du = C_k z_k + C_e(-A_{ee}^{-1}A_{ek} z_k - A_{ee}^{-1}B_e u) + Du = (C_k - C_e A_{ee}^{-1}A_{ek})z_k + (D - C_e A_{ee}^{-1}B_e)u \quad (149)$$

The above equation can be rewritten as [48, 53]:

$$y_{red} = C_{red} z_{red} + D_{red} u \quad (150)$$

Where,

$$C_{red} = (C_k - C_e A_{ee}^{-1}A_{ek}) \text{ and } D_{red} = (D - C_e A_{ee}^{-1}B_e) \quad (151)$$

9.5 Results and Discussion

For carrying out the flexible body analysis and control, a Chemical Tanker is suitably taken as shown in Figure 126. Geometric particulars of the chemical tanker are given in Table 11. Initially modal analysis of the chemical tanker is performed, without the controller, to obtain the free vibration analysis and forced vibration analysis responses and supervisory fuzzy logic controller (see Chapter 8) is integrated later to obtain the controlled stable responses.

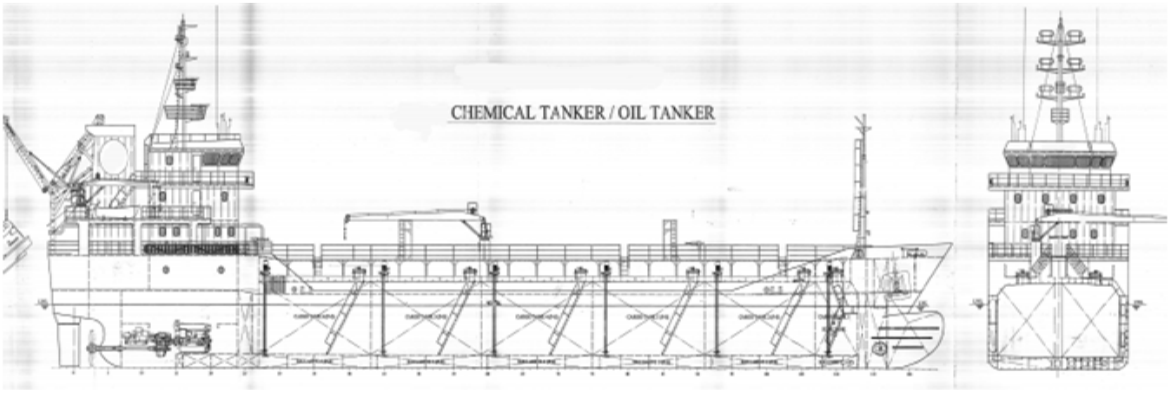

Figure 126: Chemical Tanker model [118]

Table 11 Geometric Particulars of the chemical tanker

Main Dimensions	
LOA	78.02 m
LBP	72.40 m
Breadth	12 m
Depth	5.4 m
Displacement	3200

9.5.1 Motion Responses without Controller

At the beginning, free vibration analysis or eigenvalue analysis of the tanker is carried out in MATLAB using both analytical and finite element method and the obtained responses such as eigen values (natural frequencies) and eigen vectors (mode shapes) are compared. Then the forced vibration analysis of the sunken chemical tanker using buoyant systems is carried out. For that, primarily it is required to estimate the nodal forces and moments. As a first step, we need to fix lift bags suitably on the vessel. Internal (cylindrical type) lift bags are placed inside the tanker (i.e. in ballast tanks) and external (parachute type) lift bags are attached outside. The position of external lift bags can be suitably located by looking the mode shape plots obtained from eigenvalue analysis. Nodal force and moments can be computed from Section 4.1.1.1-4.1.1.4. Then the eigenvectors are normalized with respect to mass and equation of motion is developed in principal coordinates after defining the nodal forces and moments. Then the modal contributions of individual modes are analyzed according to their dc gain/peak gain value to define which ones have greatest contribution. Finally effectiveness of various modal reduction techniques such as '*modred*' (both 'mdc' & 'del' sub functions) methods with *sorted* and *unsorted* modes are analyzed to obtain the smallest state space models of individual nodes or lift bags that accurately represents the pertinent system dynamics.

9.5.1.1 Free Vibration Analysis (Eigenvalue Analysis)

A two dimensional Euler- Bernoulli beam model with free - free boundary conditions is developed in MATLAB. Eigenvalue analysis is carried out by finite element method using different number of elements, a convergence check is also carried out and it is found that an 11 element beam model is the preferred one. Finite element modal analysis results (eigenvalues and eigenvectors) are compared with analytical solutions and it is seen that both are quite matching. Table 12 compares the eigenvalues of the 11 element tanker model from finite element and analytical solutions.

The mode shapes of the chemical tanker obtained from finite element free vibration analysis are shown in Figures 127-138, in which the first two modes are rigid body modes (heave and pitch) corresponding to zero frequency and rest of them are flexible modes. Note that, the eigenvectors are normalized with respect to unity for plotting. Figure.138 shows the resonant frequency corresponding to each mode.

Table 12 Comparison of resonant frequencies of the tanker

Mode No.	Resonant Frequency (Hz)		
	Analytical	FEM	% Difference
1	0	0	0
2	0	0	0
3	4.683	4.683	0
4	12.908	12.910	-0.015
5	25.305	25.321	-0.063
6	41.830	41.900	-0.167
7	62.487	62.711	-0.358
8	87.275	87.857	-0.667
9	116.194	117.480	-1.107
10	149.245	151.725	-1.662
11	186.427	190.485	-2.177

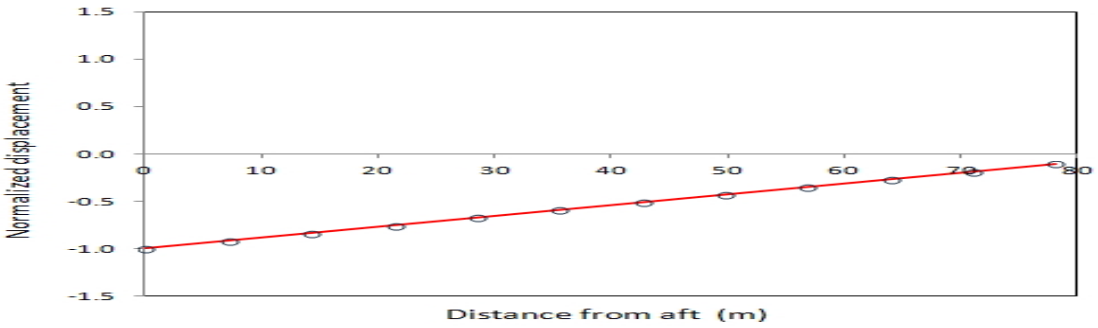

Figure 127: First rigid body (heave) response, 0 Hz.

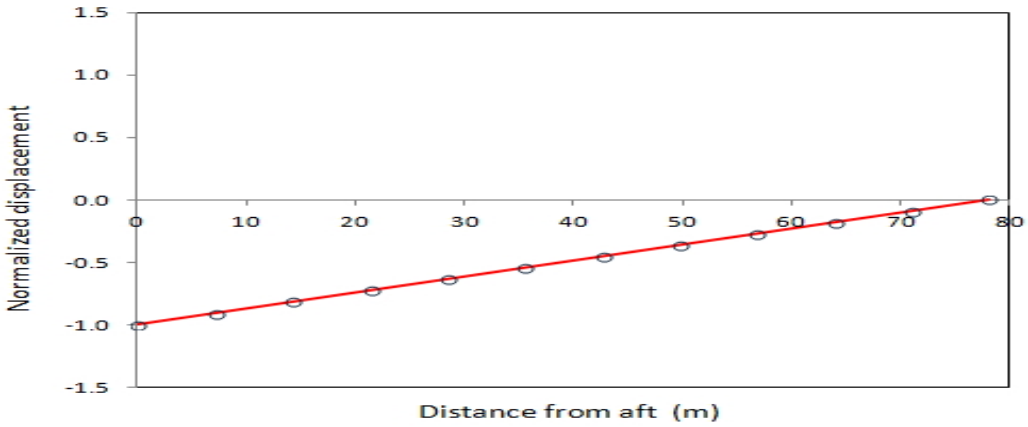

Figure 128: Second rigid body (pitch) response, 0 Hz.

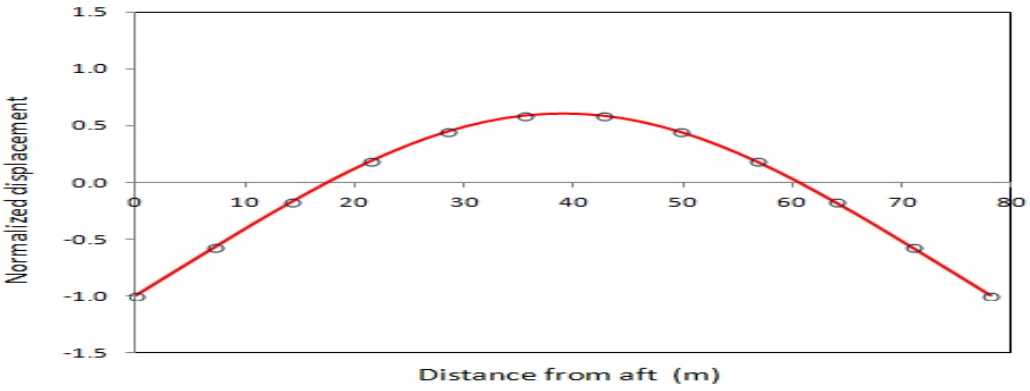

Figure 129: First flexible body response, 5 Hz.

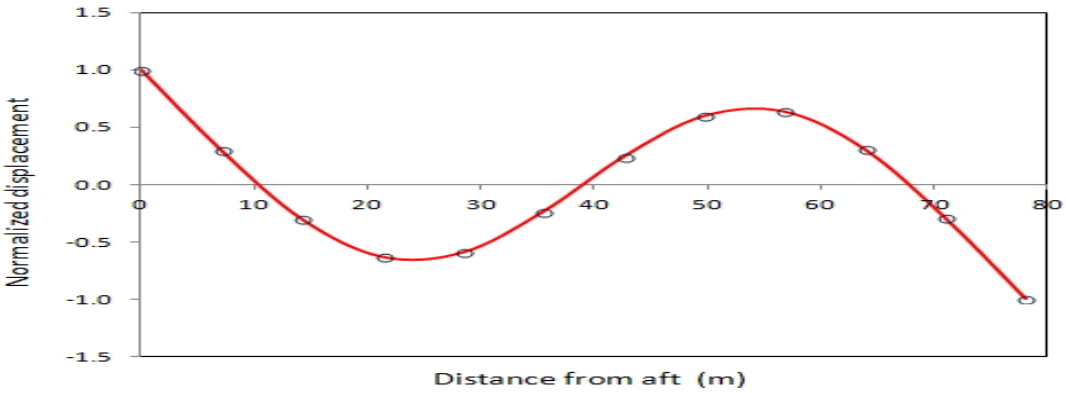

Figure 130: Second flexible body response, 13 Hz.

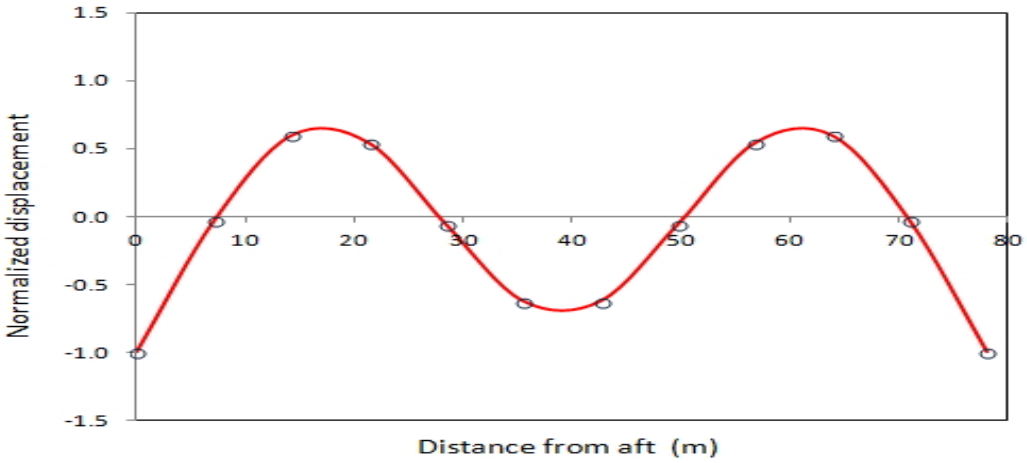

Figure 131: Third flexible body response, 25 Hz.

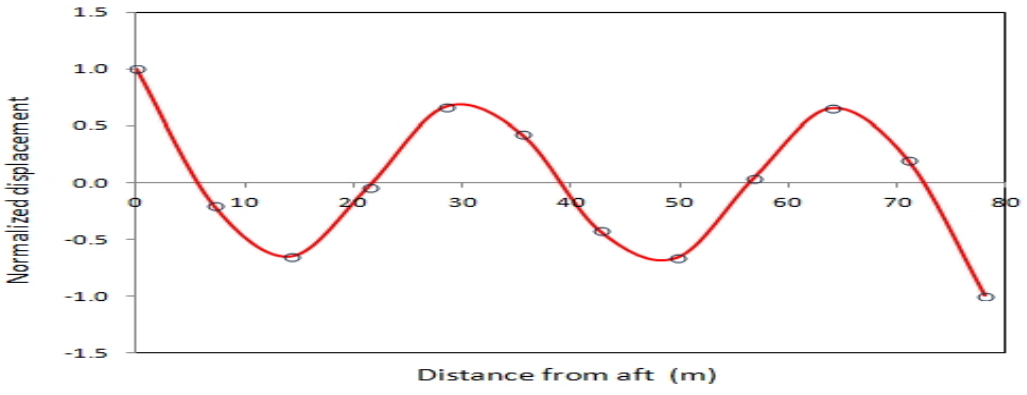

Figure 132: Fourth flexible body response, 42 Hz.

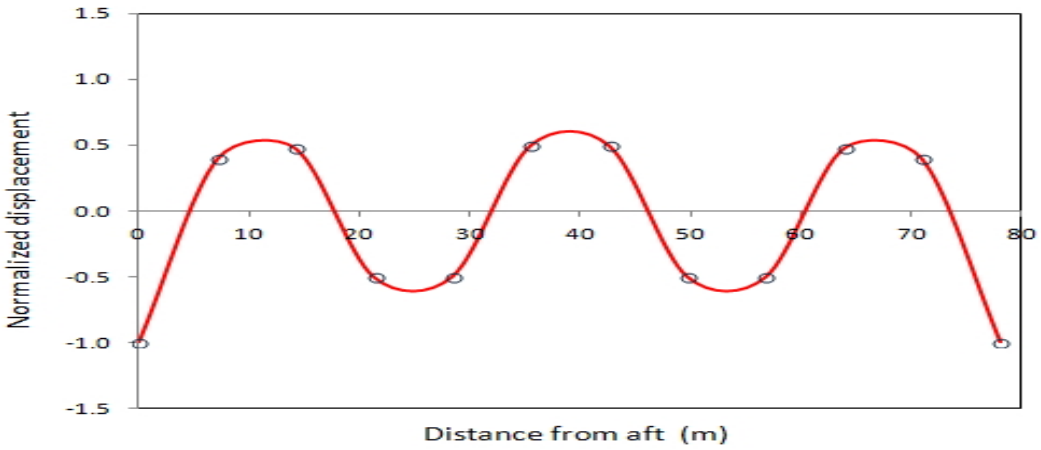

Figure 133: Fifth flexible body response, 63 Hz.

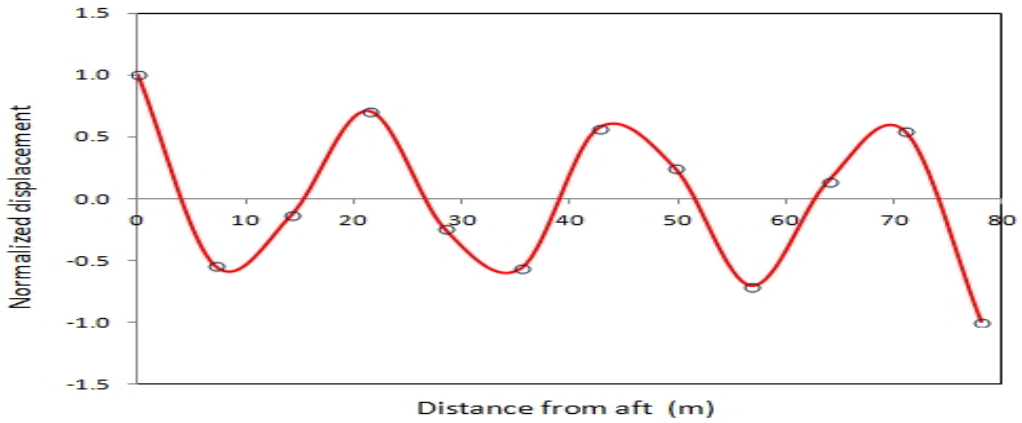

Figure 134: Sixth flexible body response, 88 Hz.

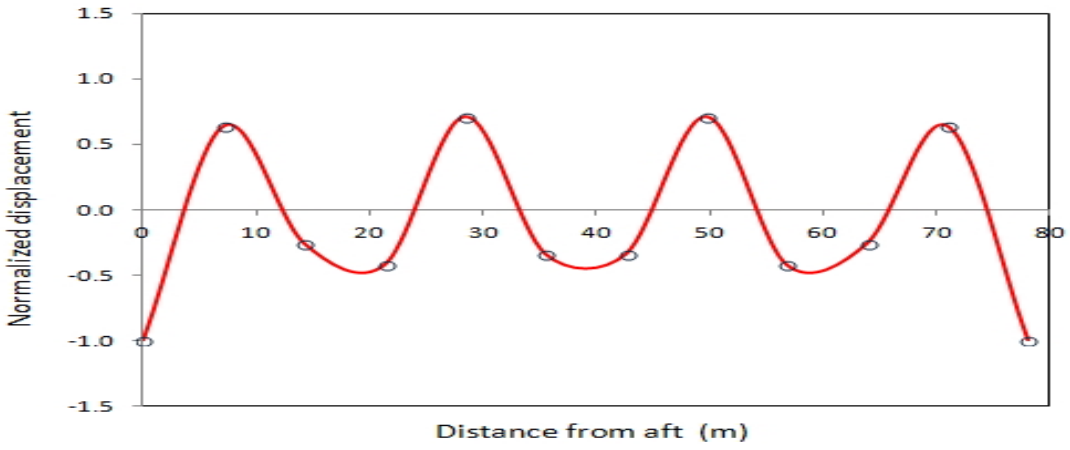

Figure 135: Seventh flexible body response, 117 Hz.

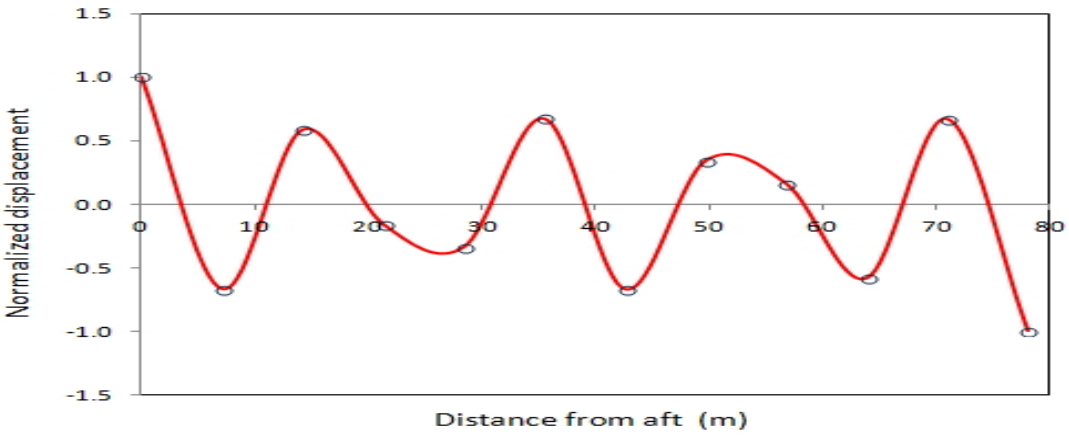

Figure 136: Eighth flexible body response, 152 Hz.

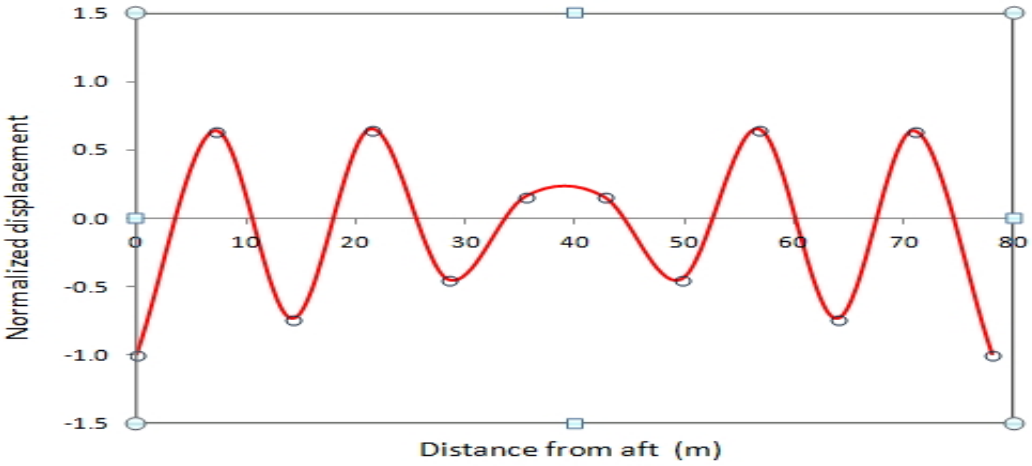

Figure 137: Ninth flexible body response, 190 Hz.

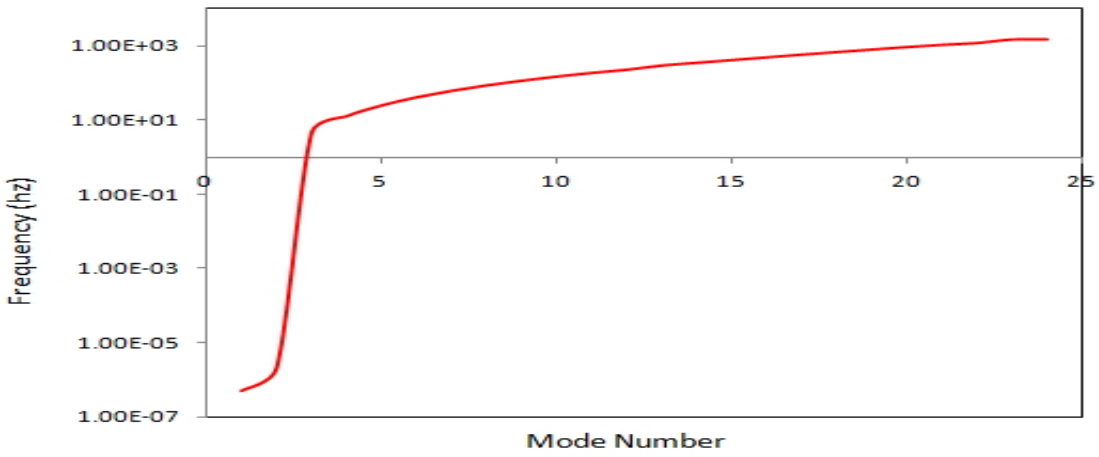

Figure 138: Resonant frequency versus mode number

9.5.1.2 Forced Vibration Analysis

In order to carry out the forced vibration analysis of the sunken chemical tanker, primarily it is required to carry out the force modeling, i.e. to define the nodal force and moments. For the chemical tanker salvage using buoyant systems, the major forces to be considered are hydrostatic force due to weight and buoyancy, suction break out force and the additional buoyancy provided by the inflating system (see section 4.1.1.1 – 4.1.1.4). Total lift force required to extract the sunken tanker from sea bottom is estimated to be 1.3 times the wet weight, which is equals to **3616.815** tonnes (see Appendix A).

Suppose if we are using lift bags [30] with 1.5m diameter and 18 m length that can displace **565 tonnes** with 2.8 bar working pressure.

Therefore number of lift bags required

= total lift force required/ lifting capacity of a lift bag

= 3616.815/565=6.40~ 7

Considering buoyancy losses, total **7** lift bags are required for inflating. Therefore additional buoyancy provided by lift bags= 7*565=3955 tonne, which is much higher than the total lift force required. Therefore for mathematical calculations, we are redesigning lift bags having lift capacity **517 tonnes** each so that in total they can offer 517*7=3619 tonne, which is equal to the lift force required.

Thus we are attaching two vertical parachute type lift bags externally on each side of the tanker and three cylindrical bags (internal) horizontally in the ballast tank to maintain hydrodynamic stability as shown in Figure 139. The positions of external lift bags can be located according to the eigenvalue or free vibration analysis of the chemical tanker (see Section 9.5.1.1). The lift bags can be attached at the "*node of a mode*", the point where the displacement is negligible. As we need to fix the four external bags, it is relevant to consider the **third** flexible mode response as plotted in Figure 133. From the response, it is seen that there are four "node of modes", which are at nodes 2, 5, 8 and 11. Therefore, the external lift bags can be fixed at node 2, 5, 8 & 11 respectively. Internal lift bags can be placed suitably on the ballast tanks of the tanker. Now it is required to define the nodal positions on the beam.

Nodal positions on the beam

The length of chemical tanker is 78 m and during the finite element free vibration analysis, the vessel length is divided in to 11 finite elements (i.e. 12 nodes), therefore, the length of each element = 78.02/11=7.09 m. Table 13 shows the location of beam nodes across the vessel length.

Table 13: Location of nodes from vessel aft

Node	Distance from aft (m)
1	0
2	7.09

3	14.185
4	21.28
5	28.37
6	35.46
7	42.56
8	49.65
9	56.74
10	63.83
11	70.93
12	78.02 (fore end)

From the chemical tanker GA (Figure 126), it is found that ballast tanks are situated at frame 27 to frame 113 and one longitudinal frame spacing is 0.57 m.

i.e. 27^{th} frame= 27*0.57=15.39 m from aft.

113^{th} frame = 113*0.57=64.41 m from aft.

Therefore, 3 internal lift bags can be placed horizontally between the length 15.39 m and 64.41 m from the aft end of the vessel as shown in Figure 140. In order to incorporate this in to the beam model, suitably internal lift bags are placed between node 3 and node 10 for a length of 49.645m**.**

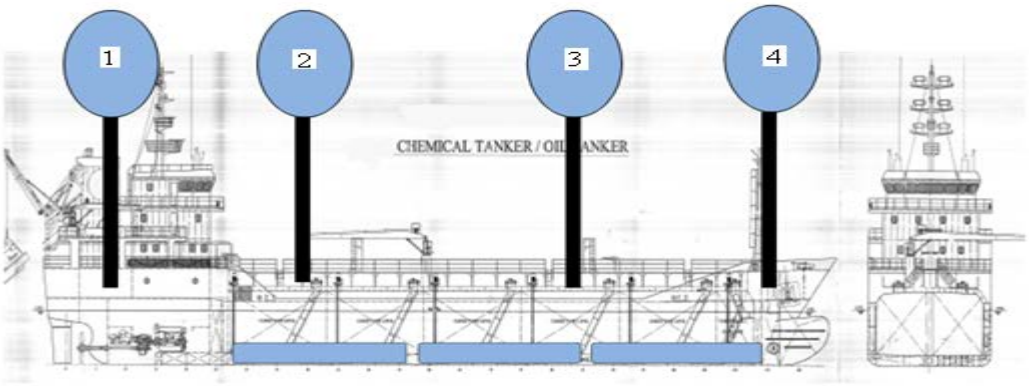

Figure 139: Arrangement of lift bags for the chemical tanker salvage

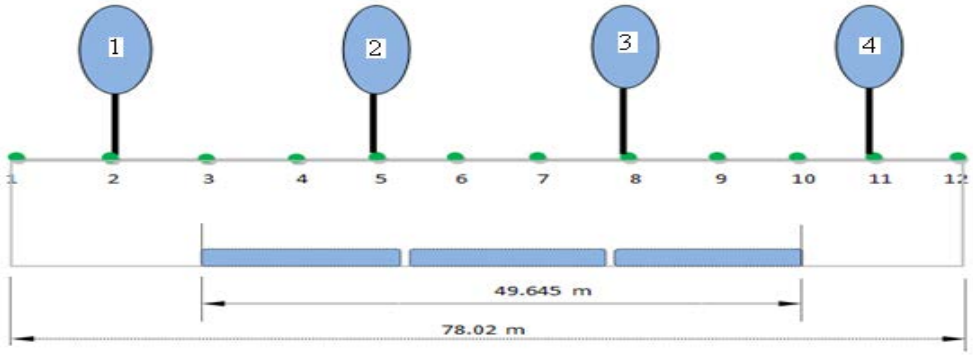

Figure 140: Arrangement of lift bags on beam nodes

9.5.1.2.1 Force Modeling

In the dynamics of raising sunken chemical tanker using buoyant systems, the major forces to be considered are hydrostatic force due to weight, buoyancy and suction breakout, hydrodynamic force and additional buoyancy provided by lift bags as explained in Section 4.1.1.1- 4.1.1.4.

According to Section 4.1.1.3, hydrostatic force acting downwards due to weight, buoyancy and suction breakout is 1.3 *(W-B)*, which is assumed to be uniformly distributed along the vessel length. Therefore, **1.3*(W-B)/l*** is the net hydrostatic force acting *downwards* at a particular beam node. Hydrodynamic force can be computed from Eqs. (6) & (7) of Section 4.1.1.2, which are also considered as uniformly distributed along the vessel length. Additional buoyancy provided by external or parachute type lift bags are taken as point loads where as buoyancy provided by internal or cylindrical type lift bags are treated as universally distributed load (UDL).

Nodal force and moments across the vessel length are computed according to classical strength of material's principles [95] and its values are given in Table 14. These values of exciting nodal force and moments need to put in the MATLAB program for obtaining the forced vibration analysis results.

Table 14: Nodal Forces and Moments

Node	Nodal Force (MN)	Nodal Moment (anticlockwise) (MN.m)
12 (fore end)	35.48 (↓)	0
11	27.19 (↓)	10.91
10	13.81 (↓)	9.20
9	12.77 (↓)	22.86
8	6.64 (↓)	44.03
7	10.66 (↓)	36.65
6	9.61 (↓)	36.61
5	3.48 (↓)	44.16
4	7.51 (↓)	23.26
3	6.45 (↓)	9.83
2	1.85 (↑)	11.44
1 (aft end)	0	0

9.5.1.2.1.1 Estimation of Shear Force and Bending Moments

Shear force and bending moment at any point on the vessel length are estimated from force modeling based on the principles of strength of materials [95] and its values are provided in Table 15.

Table 15: Shear force and bending moment at beam nodes

Node	Shear Force (MN)	Bending Moment (anticlockwise) (MN.m)
12	0	0
11	3.24 (↑)	10.91
10	1.40 (↑)	9.20
9	2.45 (↑)	22.86
8	3.51 (↑)	44.03
7	0.52 (↓)	36.65
6	0.54(↑)	36.61
5	1.59 (↑)	44.16
4	2.43(↓)	23.26
3	1.38 (↓)	9.83
2	1.84 (↑)	11.44
1	0	0

From Table 15, the longitudinal distribution of shear force and bending moment across the beam length is plotted in Figures 141 & 142 respectively. The maximum value of shear force is

3.51MN, which is at node 8 (i.e. at lift bag 3) and the bending moment is 44.16 MN.m at node 5 (i.e. at lift bag 2).

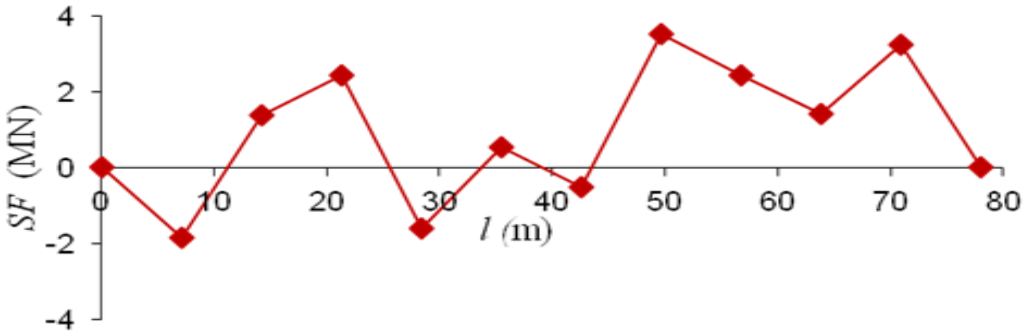

Figure 141: Longitudinal distribution of shear force

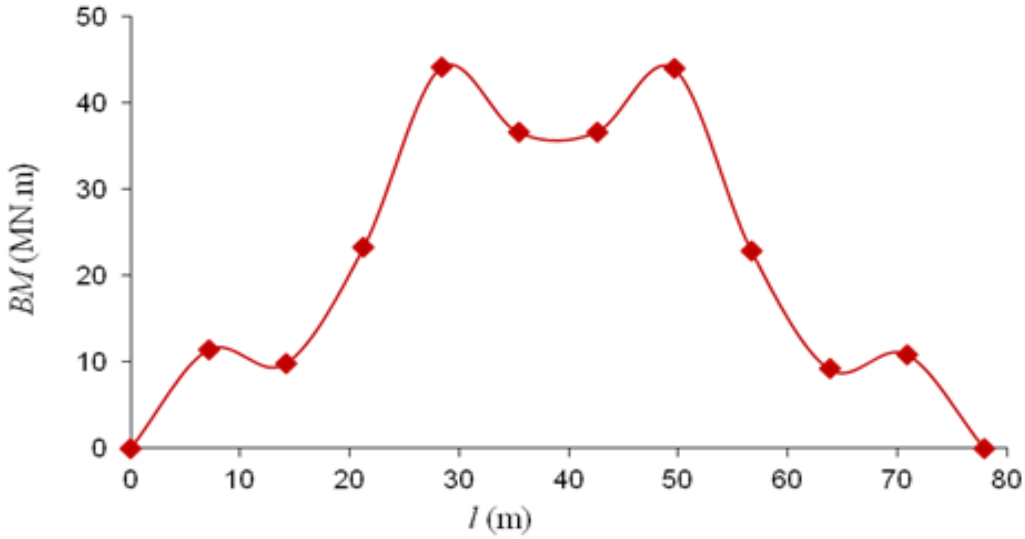

Figure 142: Longitudinal distribution of bending moment

9.5.1.2.2 Forced Vibration Analysis Responses

The first step in any modal analysis is to understand the resonant frequencies of the model. From Figure 143, it is found that the resonant frequencies of the tanker are within the order 10^0

to 10^4. As we are using 11 element beam, total 22 modes are considered for the analysis, out of which the first two modes are rigid body modes corresponding to 0 Hz frequency and rest are flexible modes. Now the sorting of modes are carried out by their 'dc gain' value to measure the individual modal contribution to the overall response. Figure 144 shows the low frequency gain for the first two rigid body modes (mode 1 & mode 2) and dc gains for all other modes versus mode number. The modes are sorted according to their dc gain in the order as:

1 2 3 4 6 8 7 9 11 12 10 14 18 13 20 19 22 17 16 21 15 5

As expected, it is observed that, for this problem, the first two rigid body modes are more important than the flexible modes.

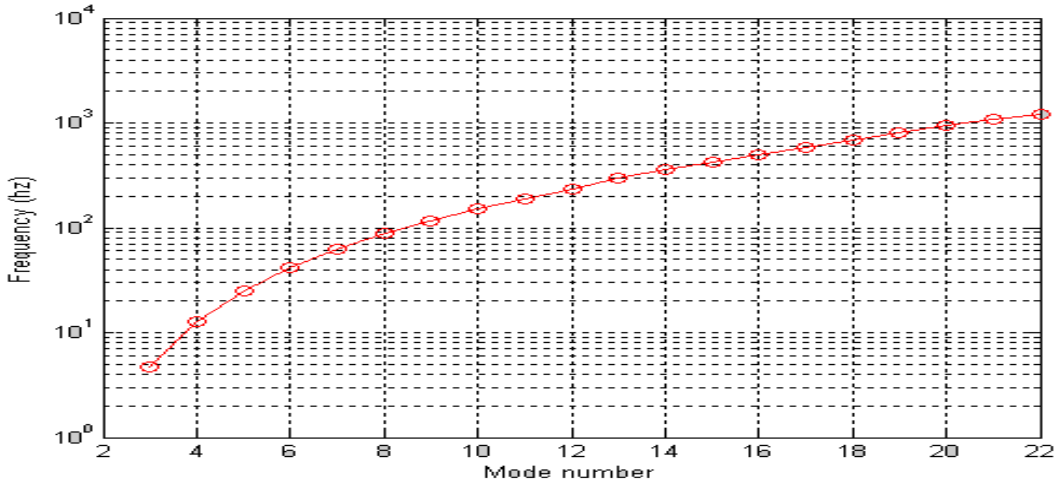

Figure 143: Resonant frequency versus mode number

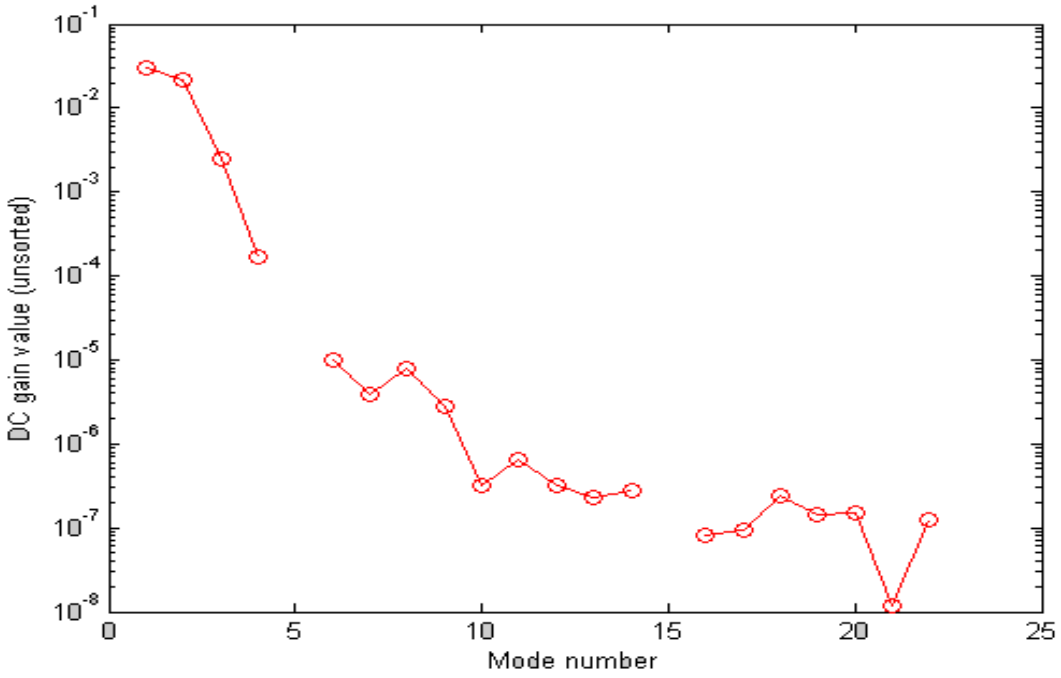

Figure 144: Unsorted dc gain value of each mode versus mode number

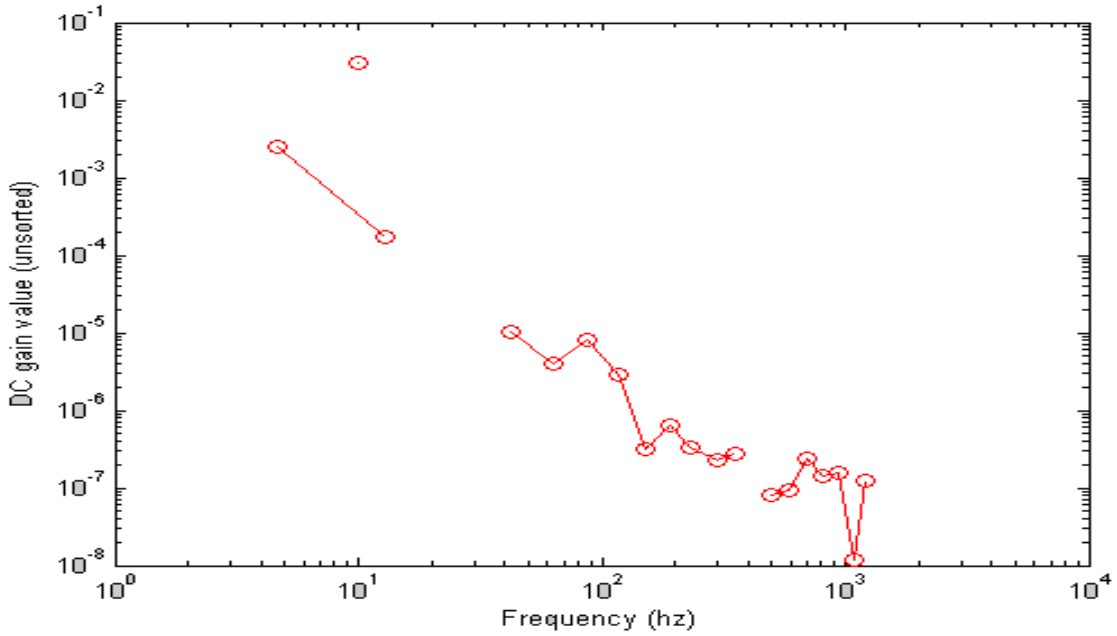

Figure 145: Unsorted dc gain value of each mode versus resonant frequency

Unsorted dc gain value of each mode versus its resonant frequency is shown in Figure 145. It is noted that as the frequency increases, the general trend is to have modes with lower dc gain values. Highest dc gain is obviously for the first two rigid modes.

Now modes are sorted according to their dc gain value and allocate index numbers from higher dc gain modes to lower dc gain modes as shown in Figure 146.

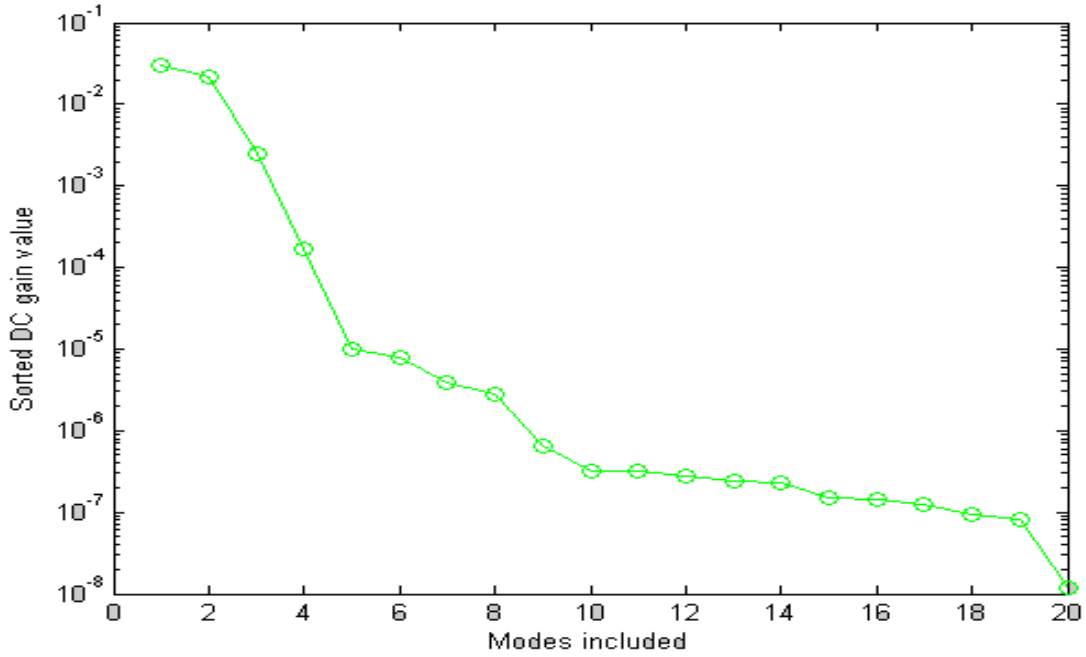

Figure 146: sorted dc value of each mode vs. number of modes

It should be noted that for hull bending effects the gain associated with hull curvature will be important and this should be taken into account when deciding frequency cut-off values.

9.5.1.2.2.1 Full and Reduced Model Responses

As controller needs to integrate with the smallest state space model, which accurately represents the flexible body dynamics, the responses obtained from various model reduction techniques using either sorted or unsorted modes with full model responses are compared in both frequency

and time domain. Finally state space models are developed using the optimum modal reduction technique.

In this section, three different sets of model matrices and eigenvalue vectors are defined. The first one uses all the modes and frequencies in their original unsorted form (i.e. full modal), which is mainly used to determine the frequency and time domain responses of the non reduced model for comparison. The second one (denoted with the "unsorted" suffices) uses only the number of modes specified by the user in their original unsorted order that is used to visualize the effects of a simple truncation of higher frequency modes without sorting or ranking. The third set (denoted with the "sorted" suffices) takes the number of modes specified by the user and sort and rank them according to their dc gain value and includes only modes with the highest dc gains. After that reduced models are obtained using 'modred' technique using both '*mdc*' and '*del*' sub functions, which are considering either unsorted modes or dc gain sorted modes as the important modes to be kept. Output can be determined in terms of heave displacement, heave velocity, pitch displacement and pitch rate at beam nodes by suitably defining the output matrix *C*. Initially the output matrix *C* is separated into displacement and velocity matrices and the heave and pitch responses are obtained by allocating corresponding row of the output matrix. Force modeling is carried out in such a way that the simulations are produced for the response of the tanker at the time of breakout.

9.5.1.2.2.1.1 Heave displacement

Heave displacement can be obtained for any node on the beam. In order to compare the various modal reduction techniques, initially responses are plotted for the lift bag 1 (i.e. node 2).

At the beginning, responses are obtained by simply using '*unsorted*' and '*sorted*' reduced models. The first six *unsorted* modes (modes 1-6, i.e. first two rigid bodes and first four flexible modes) are included and its frequency domain contributions are overlaid with the full model in Figure 147. From simulation, dc gain error relative to the full model is found to be +0.0796% because of discarding the dc gain contribution from high frequency eliminated modes.

In Figure 148, six *sorted* modes (modes 1-4, 6, 8) by dc gain approach are included and its individual contributions are depicted with full model. The dc gain error relative to full 22-mode model is -0.3429 %, which is due to discarding the contribution from other flexible modes.

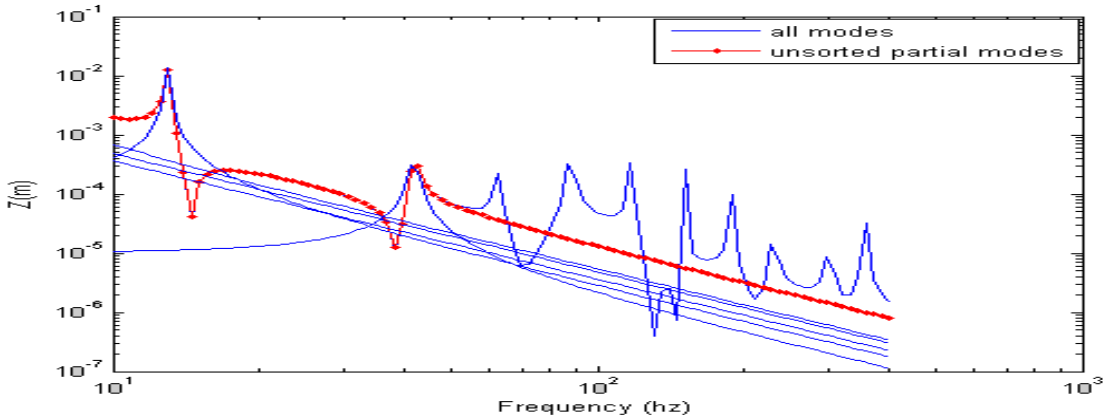

Figure 147: Heave displacement of lift bag 1- first 6 *unsorted* modes included

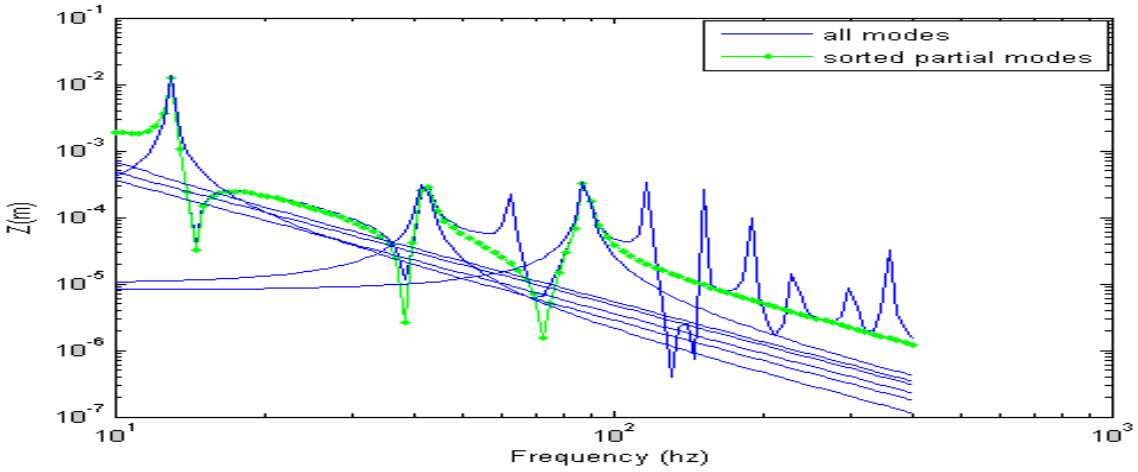

Figure 148: Heave displacement of lift bag 1- first 6 *sorted* modes included.

It is found that the response obtained from reduced models using '*unsorted*' and '*sorted*' methods tally very well with full model responses at lower frequencies, whereas for higher frequencies the responses from reduced models deviate from full model responses. This is due to

the discarding of higher frequency modes in the reduced system. Therefore it is better to adopt modal order reduction techniques to obtain an optimum reduced model.

Now the responses are taken using modal reduction technique such as '*modred-del*' and *modred-mdc*' using both *unsorted* and *sorted* models. In Figure 149, reduced models are obtained using '*modred-del*' option keeping first six *unsorted* modes; i.e. the first six low frequency modes are maintained in the model, whereas higher frequency modes are eliminated. The overall frequency response with six overlaid individual mode contributions is plotted. It is observed that at high frequencies reduced and full model responses attenuate with frequencies. The dc gain error relative to full model is +0.0796 because of eliminating the contribution from higher frequency modes. (Note, as discussed earlier, for hull flexure it is necessary to consider the contribution to curvature and this may require more nodes to be included.)

In Figure 150, reduced models are obtained using '*modred-del*' option keeping first six *sorted* modes (modes 1-4, 6, 8). The overall frequency response with six overlaid individual mode contributions is plotted. The dc gain error relative to full model is -0.3429 % because of eliminating the contribution from other flexible modes.

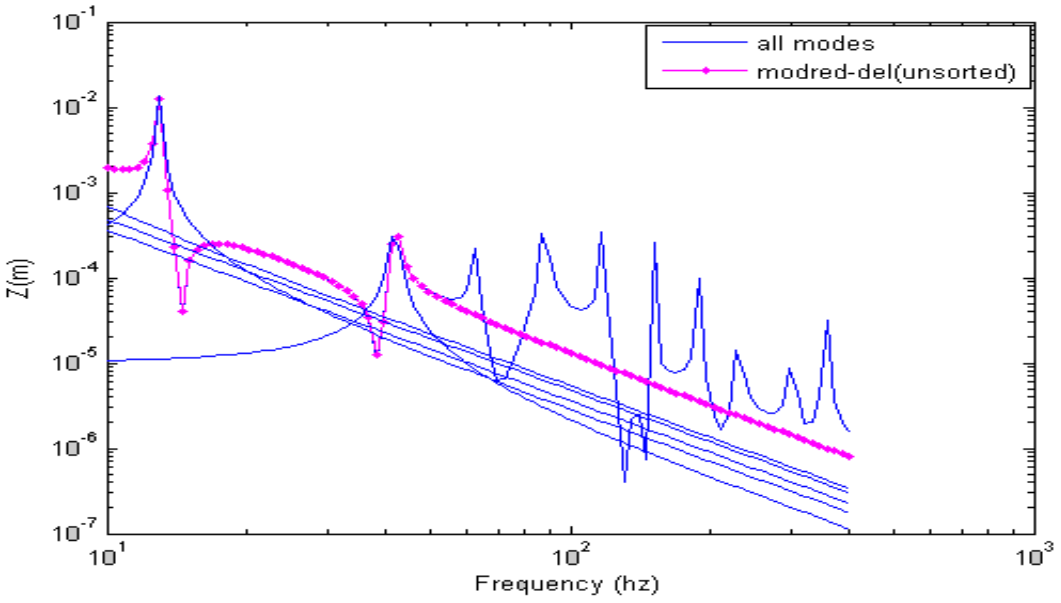

Figure 149: Heave displacement of lift bag 1- first 6 *unsorted* modes included: '*modred-del*'.

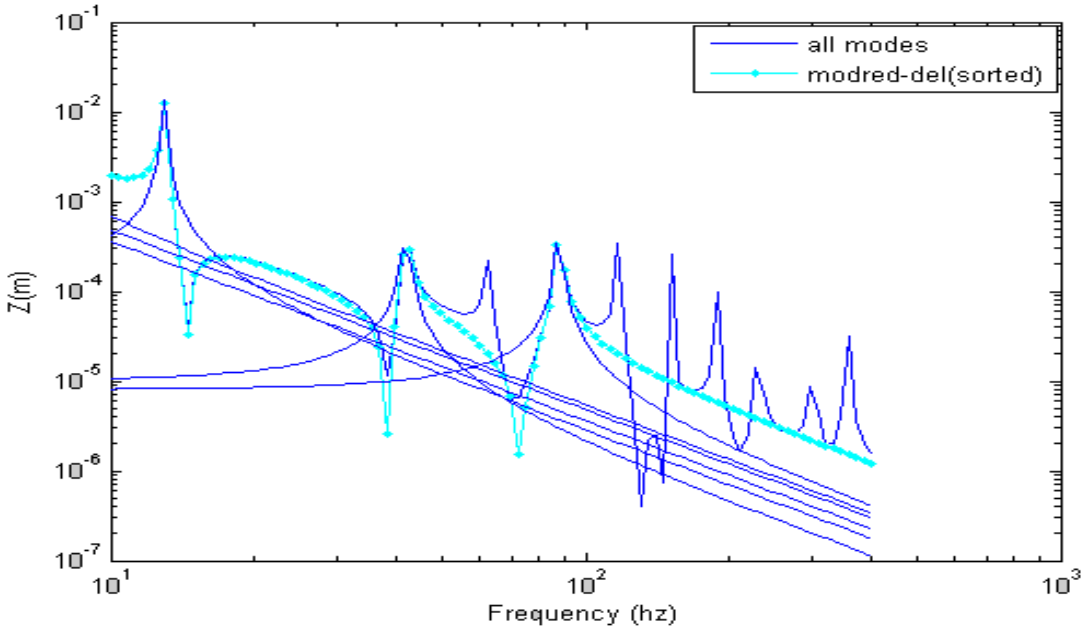

Figure 150: Heave displacement of lift bag 1- first 6 *sorted* modes included-'*modred-del*'

Now the responses are obtained using '*modred-mdc*' option. In Figure 151, reduced models are obtained using '*modred-mdc*' option keeping first six *unsorted* modes; i.e. the first six low frequency modes are maintained in the model, whereas remaining higher frequency modes are reduced. The overall frequency response with four overlaid individual mode contributions is plotted. The dc gain error relative to full model is found to be -0.00087794 %, which is a positive sign. This is due to the reason that in *modred-mdc* using *unsorted* modes, the low frequency effects of the eliminated states (i.e. high frequency modes) are included in the remaining states. Therefore, this method is found to be more convenient compared to other reduction methods.

In Figure 152, reduced models are obtained using '*modred-mdc*' option keeping first six *sorted* modes i.e. (modes 1-4, 6, 8). It is seen that the reduced model represents the overall contributions. The dc gain error relative to full model is found to be -0.0064 %, which implies that this method is less convenient compared to the previous one.

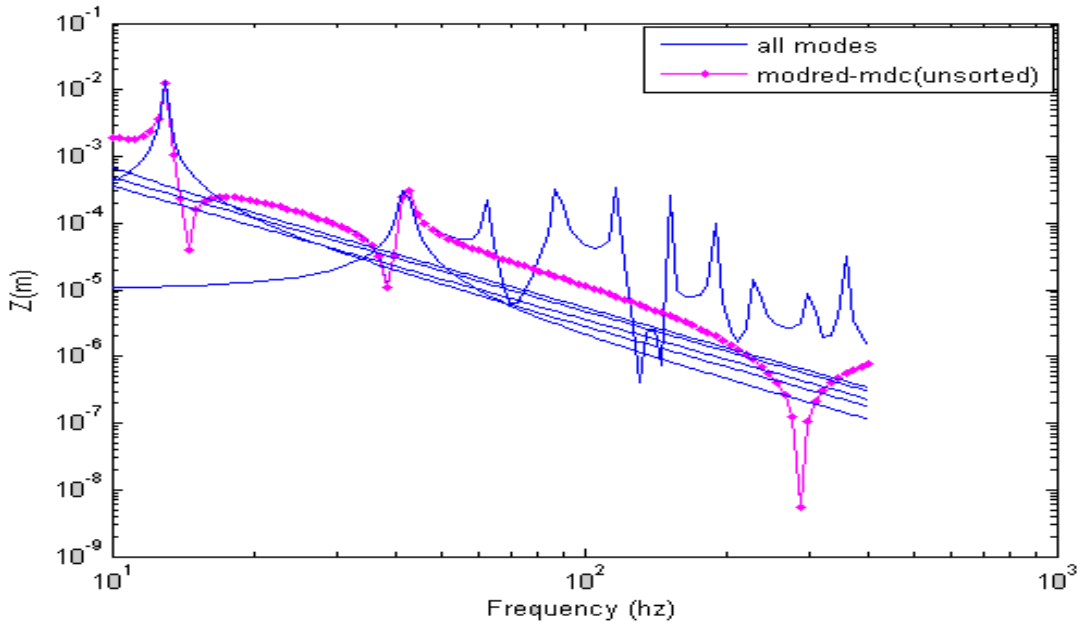

Figure 151: Heave displacement of lift bag1- first 6 *unsorted* modes included- '*modred-mdc*'

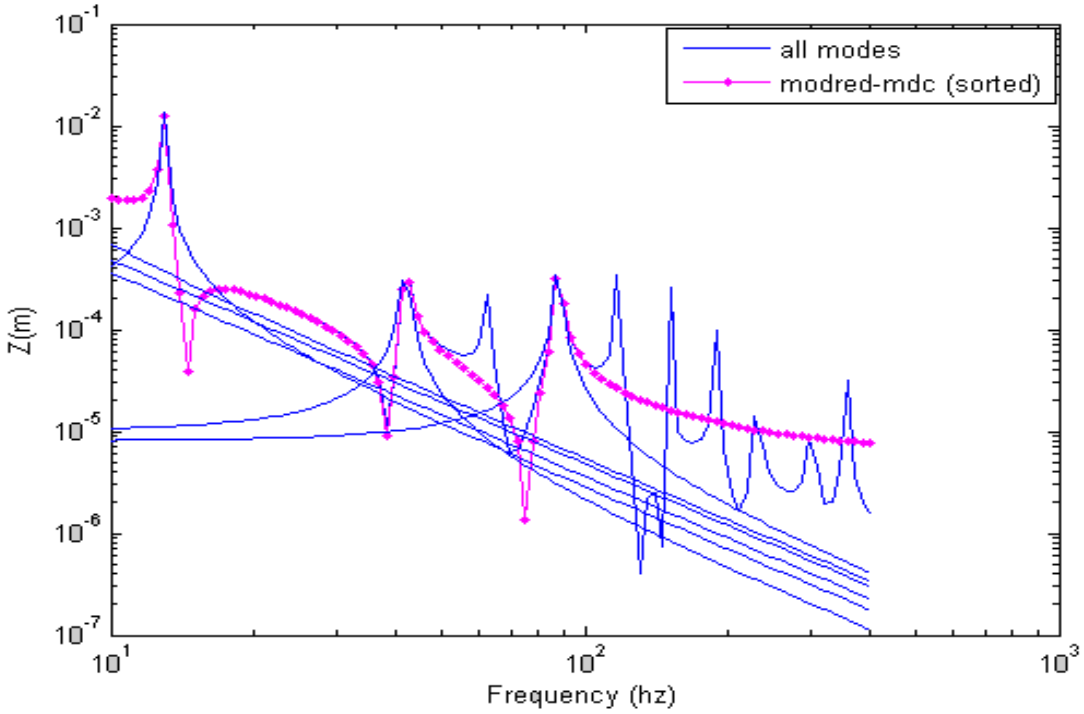

Figure 152: Heave displacement of lift bag1 - first 6 *sorted* modes included, 'm*odred-mdc'*

Now the responses of the tanker are found in time domain. The heave displacement of lift bag 1 at the time of breakout is plotted in time domain using various modal reduction techniques. Figure 153 shows the time domain response for the *full* model, *unsorted* reduced model and *sorted* reduced models. It is found that the response obtained from full model and reduced models are exactly same. Heave displacement is found to be increases with time. The peak error of *unsorted* reduced model and *sorted* reduced model in comparison with full model is -0.0023% and 0.0109 % respectively. This shows that *unsorted* model truncation is more suitable compared to *sorted* model truncation, which means that low frequency modes are more important in a marine salvage operation in comparison with higher frequency modes.

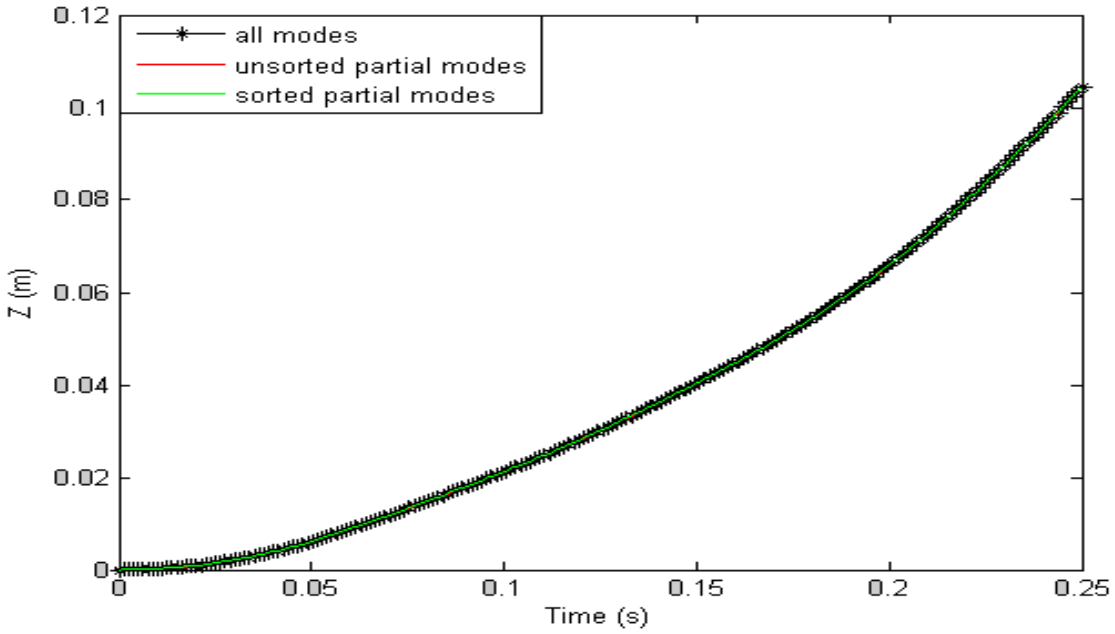

Figure 153: Heave displacement of lift bag 1 for all modes included, first 6 modes included-*unsorted* & *sorted* modal truncation

The time domain response of lift bag 1 for the full model, and two *unsorted* reduced models: -'*modred-del*' and '*modred-mdc*' options is presented in Figure 154. It is found that there is no visible difference in the transient response of the above models. The peak error of *unsorted* '*modred-del*' and '*modred-mdc*' options in comparison with full model is -0.0023% and 0.000072472% respectively. This implies that both reduction method responses are valid, though '*unsorted modred-mdc*' option is the most convenient one for modal order reduction as it includes the low frequency effects of the eliminated high frequency modes in the reduced model.

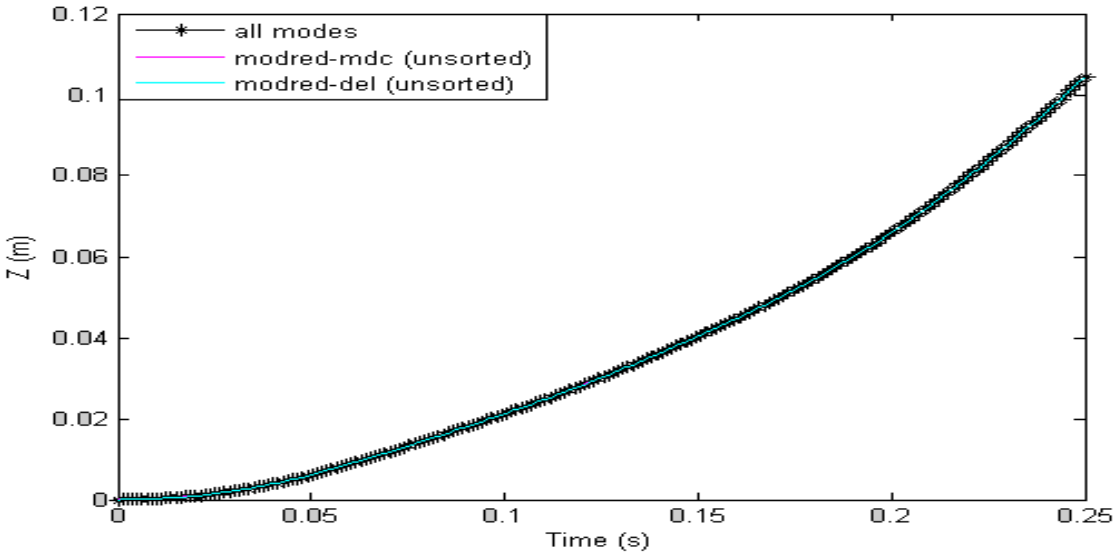

Figure 154: Heave displacement of lift bag 1 for all modes included, first 6 *unsorted* modes included-'*modred-mdc*' & '*modred-del'*

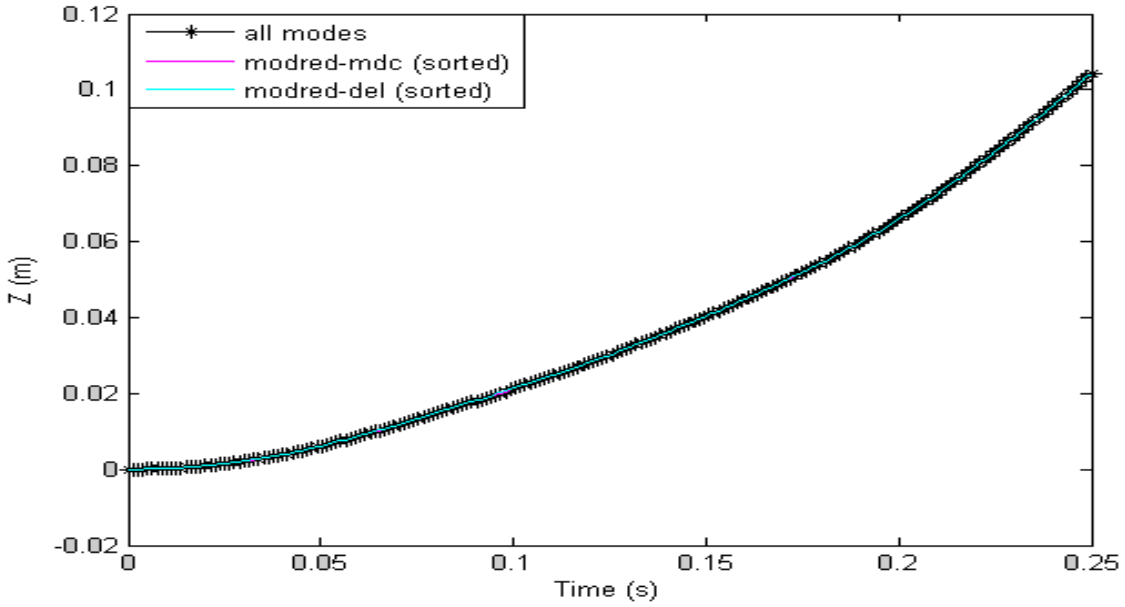

Figure 155: Heave displacement of lift bag 1 for all modes included, first 6 *sorted* modes included-'*modred-mdc'* & '*modred-del*'.

Figure 155 shows the time domain response of lift bag 1 for the full model, and two *sorted* reduced models: - '*modred-del*' and '*modred-mdc*' options. It is found that there is no visible difference in the transient response of the above models. The peak error of sorted '*modred-del*' and '*modred-mdc*' options in comparison with full model is 0.0109% and 0.00085478% respectively. This implies that both reduction method responses are valid, though sorted 'modred-mdc' option is the preferred one as it includes the low frequency effects of the eliminated modes in the reduced model.

Table 16 shows the comparative performance of various reduction methods used for modal order reduction.

Table 16: Reduction methods summary

Reduction method	Dc gain error %	Peak error %
Unsorted	+0.0796	-0.0023
Sorted	-0.3429	0.0109
Unsorted Modred-del	+0.0796	-0.0023
Unsorted Modred-mdc	-0.00087794	0.000072472
Sorted Modred-del	+0.0624	0.0109
Sorted Modred-mdc	-0.0064	0.00085478

From Table 16, it is found that *unsorted* reduced models show better performance compared to *sorted* reduced models. This is due to the reason that low frequency modes are more significant compared to high frequency modes for the marine salvage problem. The overall transient response of the system is matched well by the '*mdc*' option while the '*del*' option has slight error, which might be due to the reason that '*modred-mdc'* option minimizes the low frequency errors by including the contribution of the unused modes while '*modred-del*' option does not account for the dc gains of the eliminated modes in the reduced system. Thus it is observed that

'*modred-mdc*' is the preferred method for model order reduction in which, '*unsorted modred-mdc'*option is the optimum choice for marine salvage.

Now using '*unsorted modred-mdc'* method, heave displacements of other external lift bags in frequency and time domain are estimated and compared with *full* model responses as shown in Figures 156-161. From the plots, heave displacement is found to be increase with time.

Lift bag 2 (node 5)

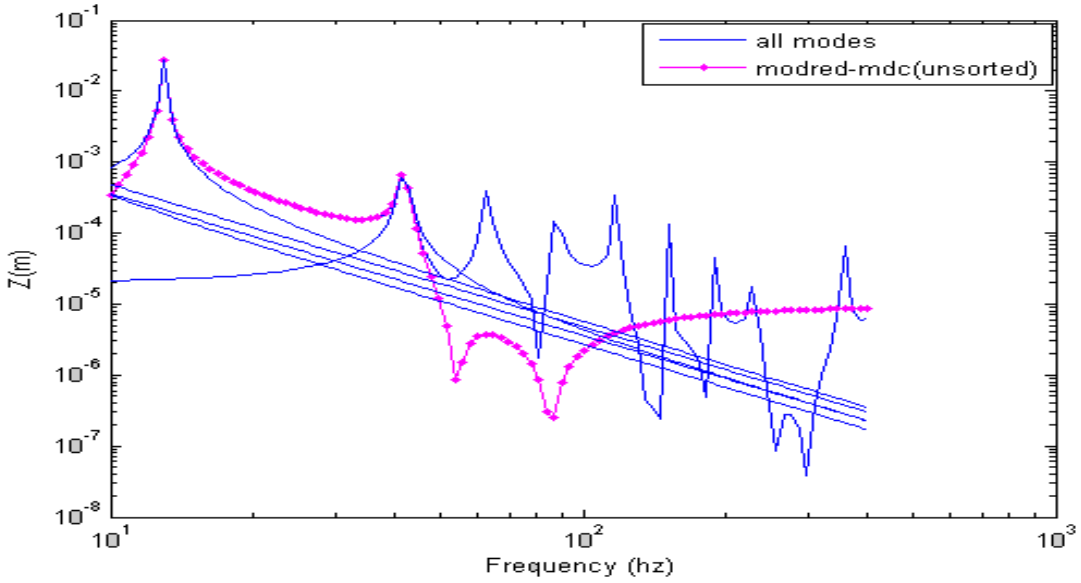

Figure 156: Heave displacement of lift bag 2 - first 6 *unsorted* modes included

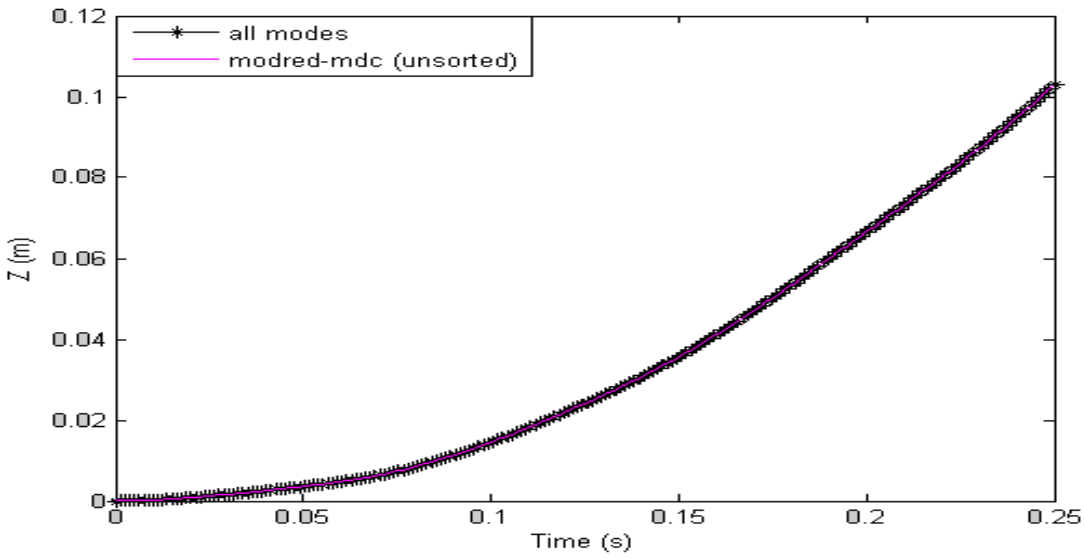

Figure 157: Heave displacement of lift bag 2 - first 6 *unsorted* modes included

Lift bag 3 (node 8)

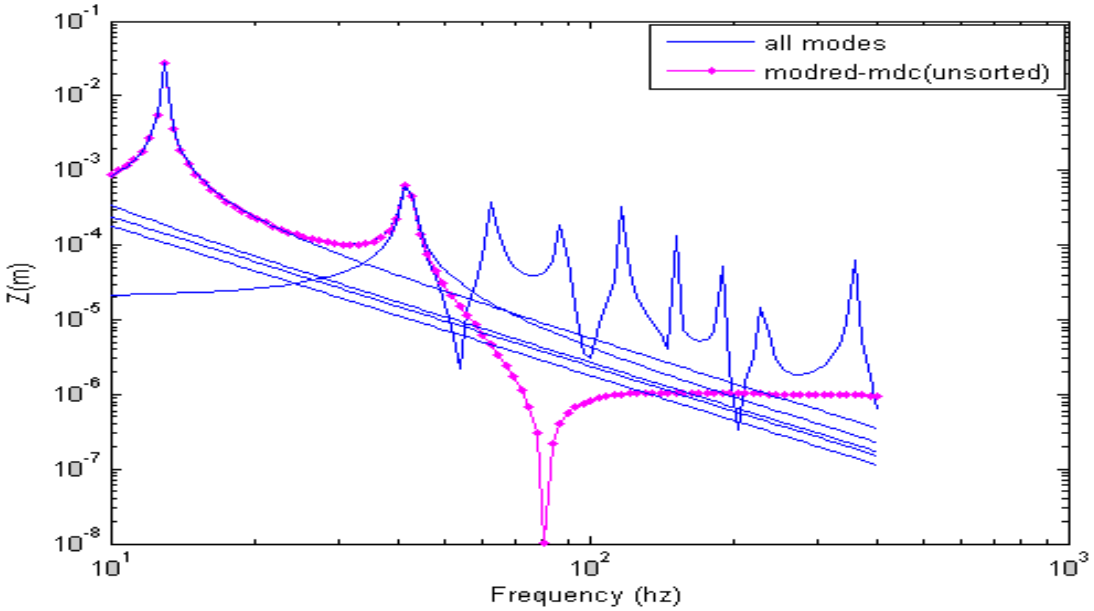

Figure 158: Heave displacement of lift bag 3 - first 6 un*sorted* modes included

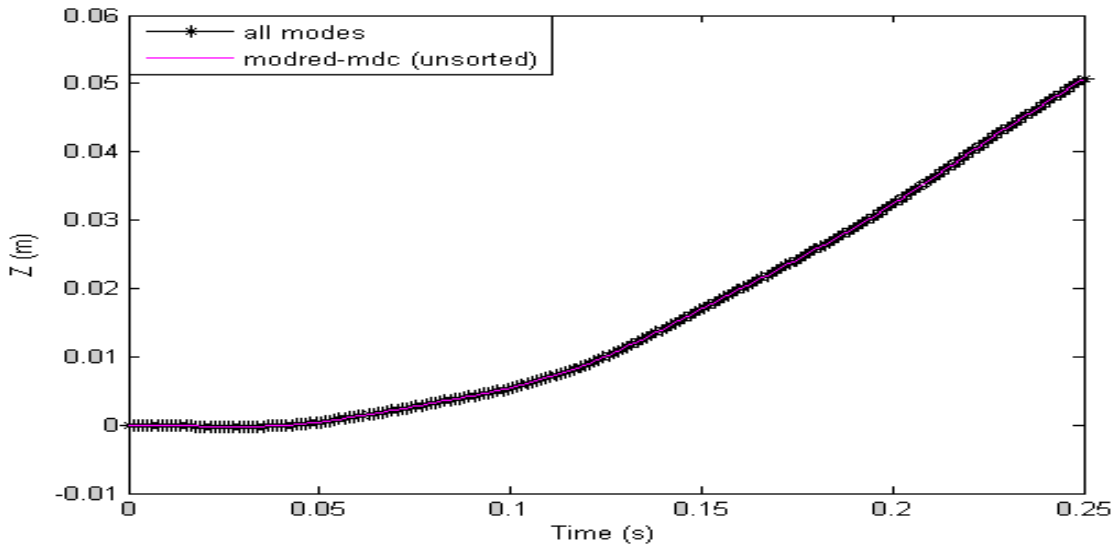

Figure 159: Heave displacement of lift bag 3 - first 6 *unsorted* modes included.

Lift bag 4 (node 11)

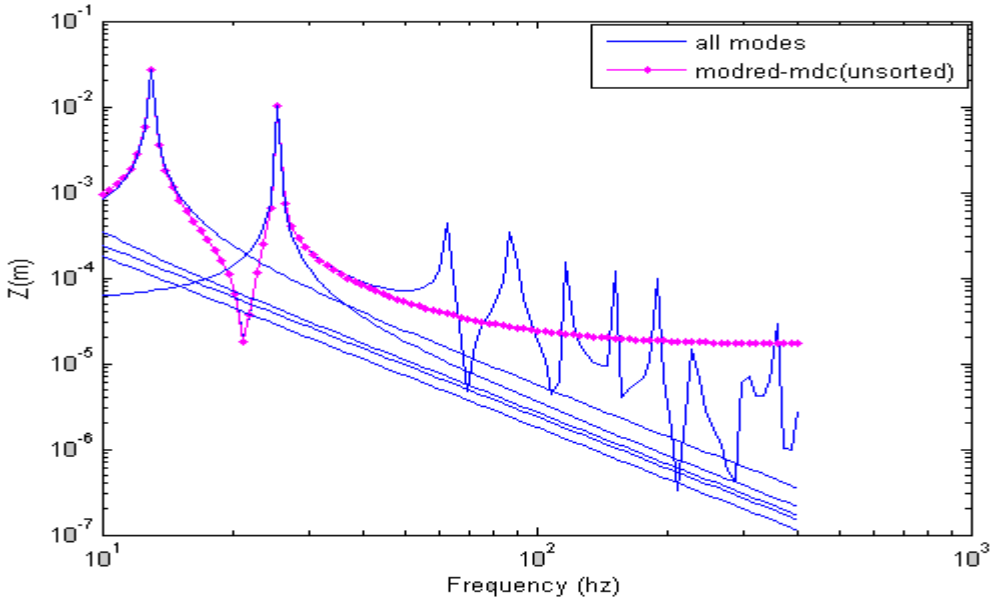

Figure 160: Heave displacement of lift bag 4 - first 6 *unsorted* modes included.

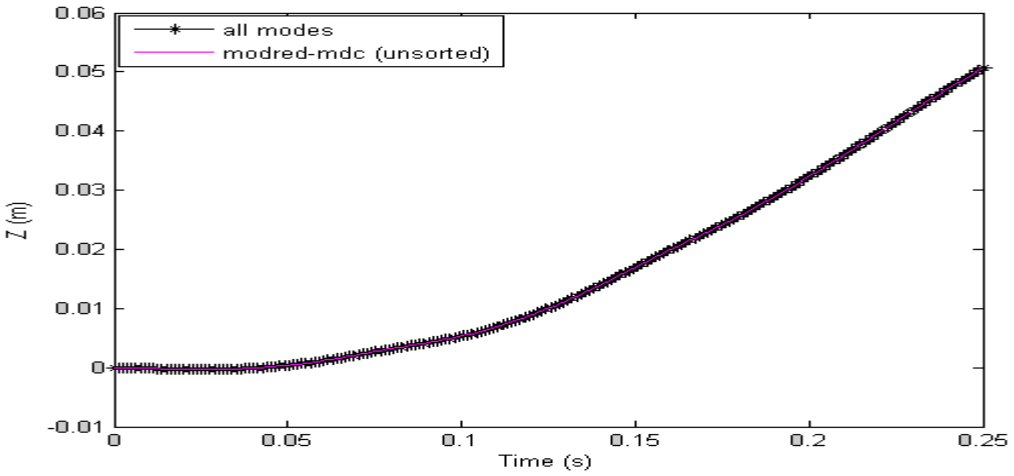

Figure 161: Heave displacement of lift bag 4 - first 6 *unsorted* modes included.

9.5.1.2.2.1.2 Heave velocity responses

The heave velocity response of the tanker obtained using '*unsorted modred-mdc*' option is plotted with respect to frequency and time as shown in Figures 162-169. The heave velocity is found to increase with time, which implies that the motion is not stable. Hence a controller should be integrated with the model to ensure hydrodynamic stability during the ascent.

<u>Lift bag 1</u> (node 2)

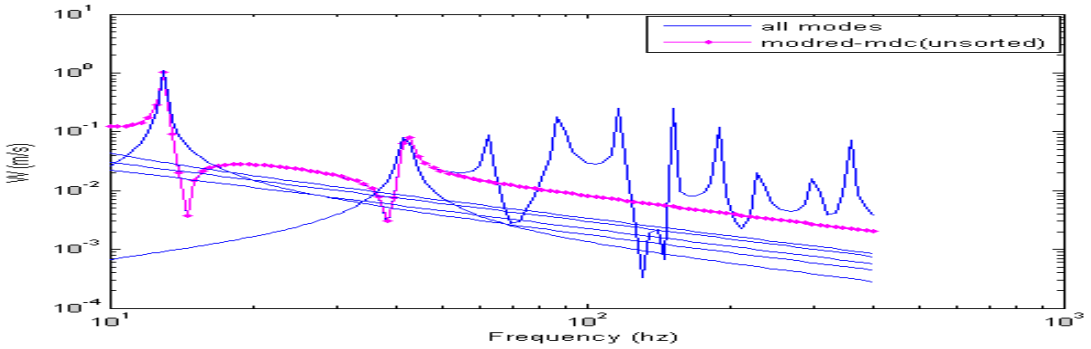

Figure 162: Heave velocity of lift bag 1- first 6 *unsorted* modes included

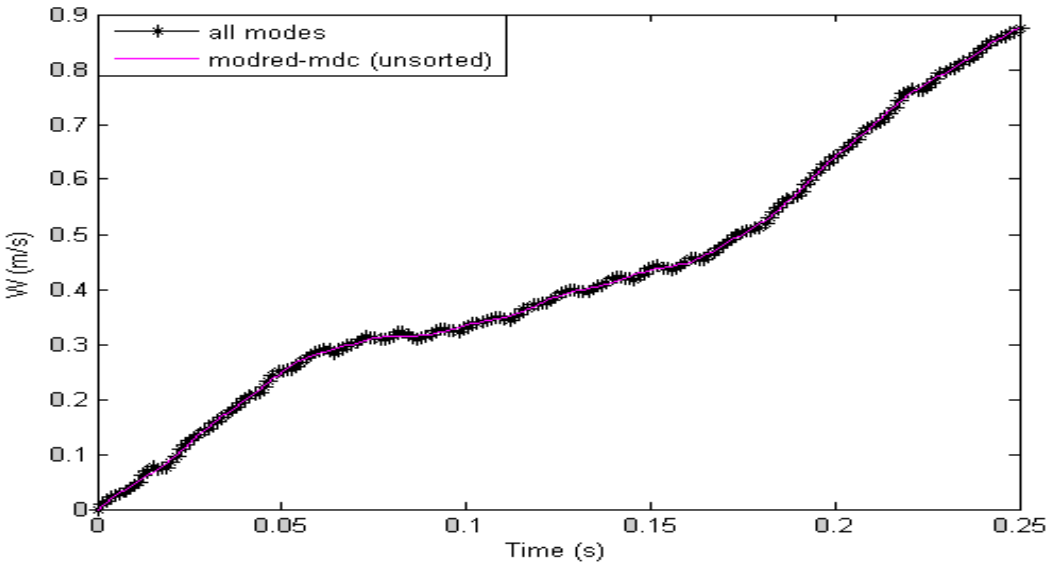

Figure 163: Heave velocity of lift bag 1- first 6 *unsorted* modes included

<u>Lift bag 2</u> (node 5)

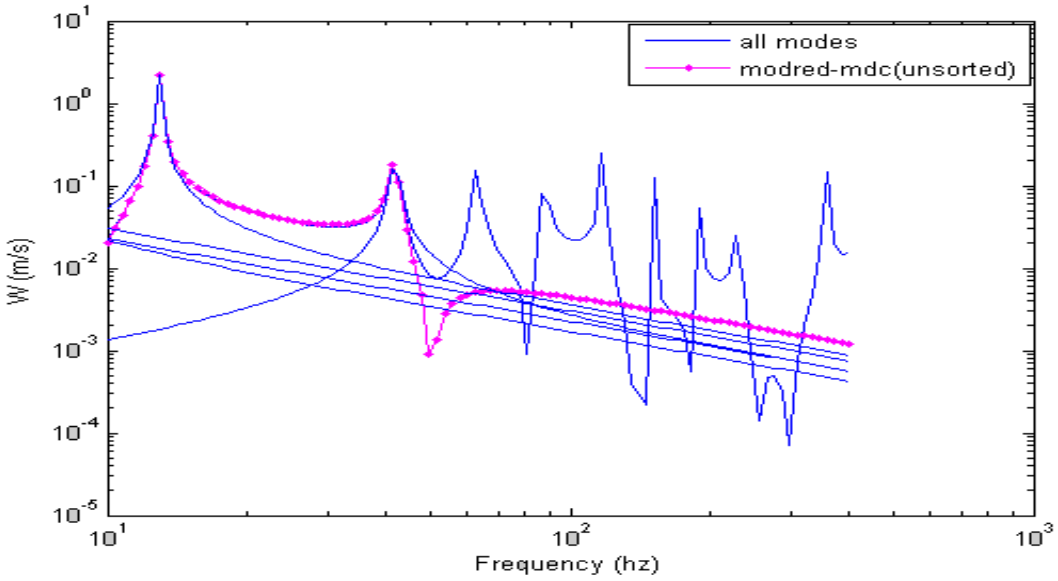

Figure 164: Heave velocity of lift bag 2- first 6 *unsorted* modes included

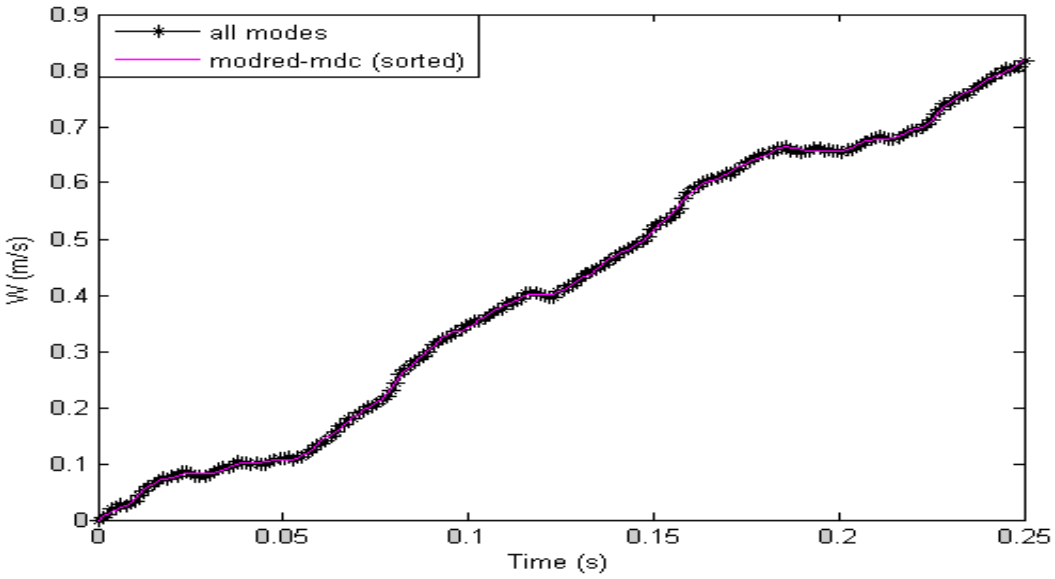

Figure 165: Heave velocity of lift bag 2- first 6 *unsorted* modes included

<u>Lift bag 3</u> (node 8)

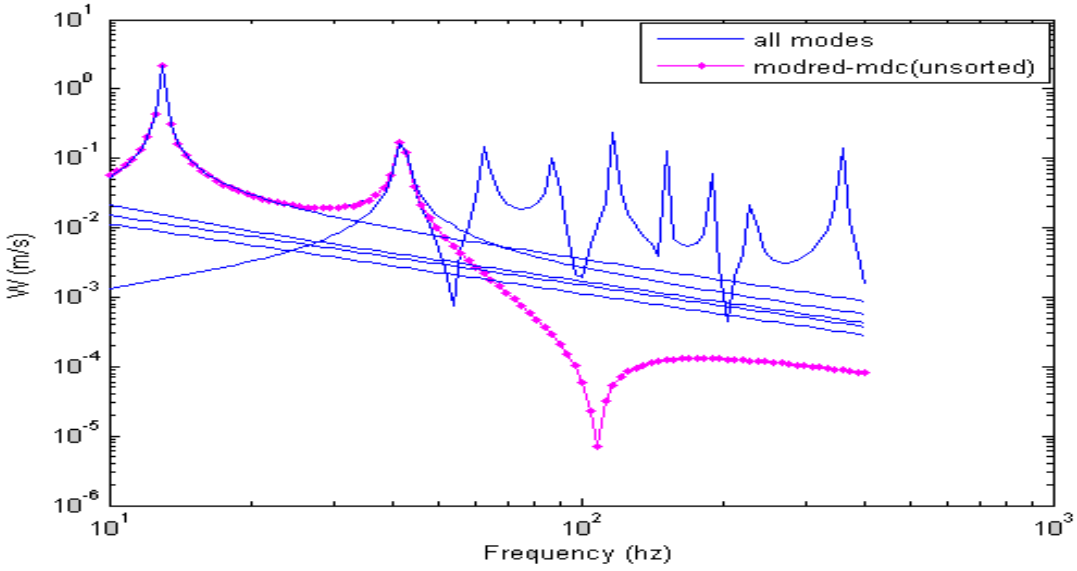

Figure 166: Heave velocity of lift bag 3- first 6 *unsorted* modes included

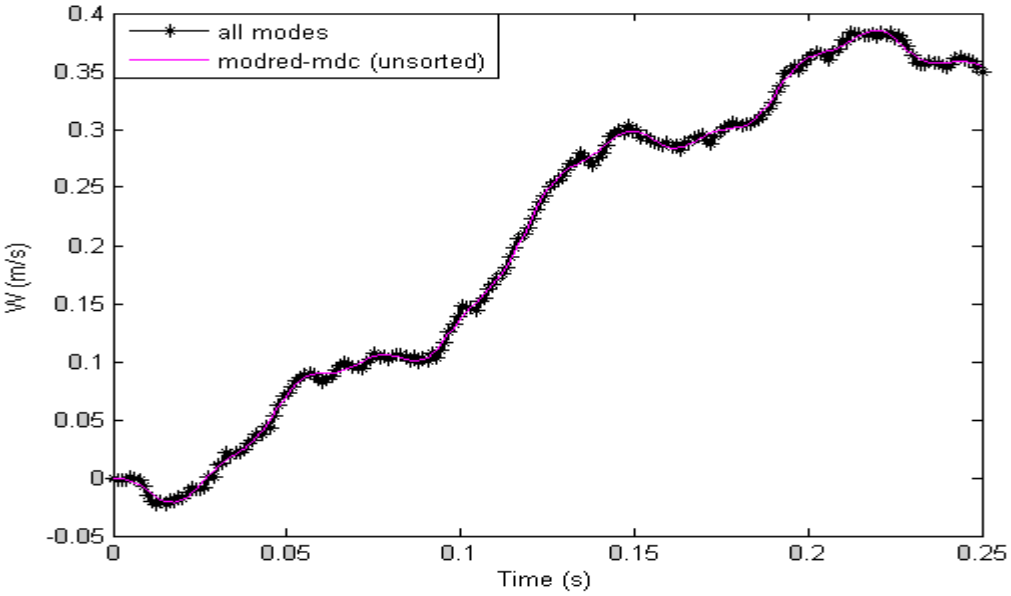

Figure 167: Heave velocity of lift bag 3- first 6 *unsorted* modes included

<u>Lift bag 4</u> (node 11)

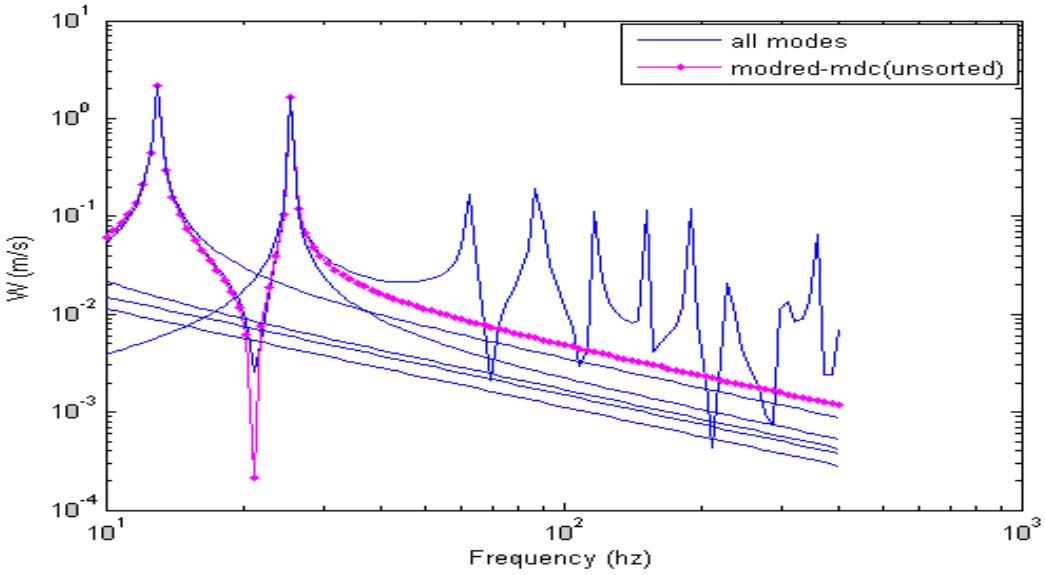

Figure 168: Heave velocity of lift bag 4- first 6 *unsorted* modes included

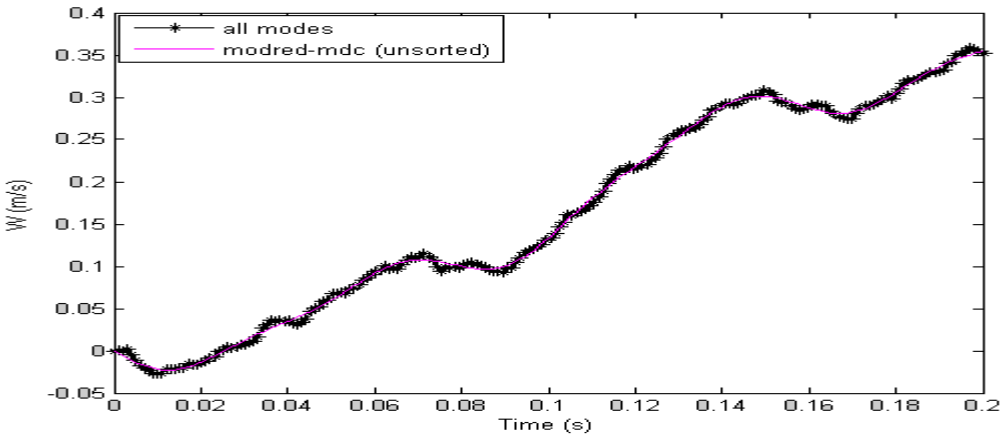

Figure 169: Heave velocity of lift bag 4- first 6 *unsorted* modes included

9.5.1.2.2.1.3 Pitch displacement

For pitch response, '*sorted modred-mdc*' method is found to be the optimum choice. The pitch displacement of the chemical tanker obtained using '*sorted modred-mdc*' is compared with the *full* model response in frequency and time domain as shown in Figures. 170 – 177. Pitch displacement of the tanker is found to be fluctuates with time, which implies the necessity of a controller to be integrated with the model.

<u>Lift bag 1</u>

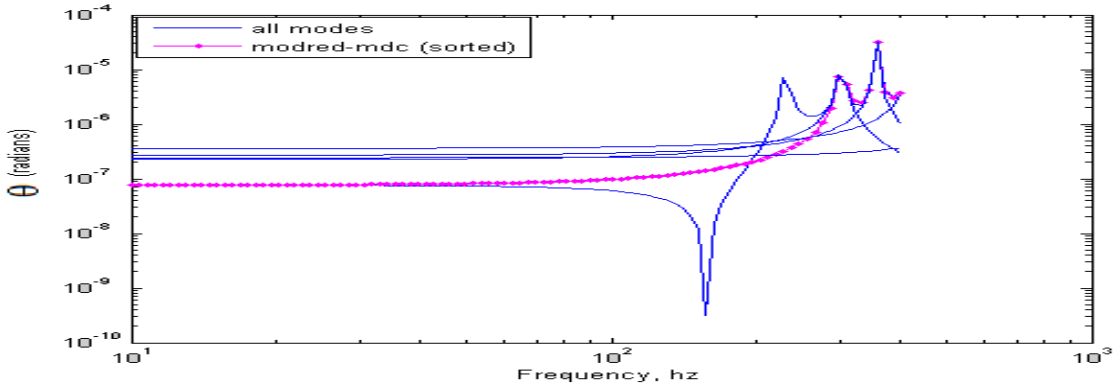

Figure 170: Pitch displacement of lift bag 1- first 6 *sorted* modes included

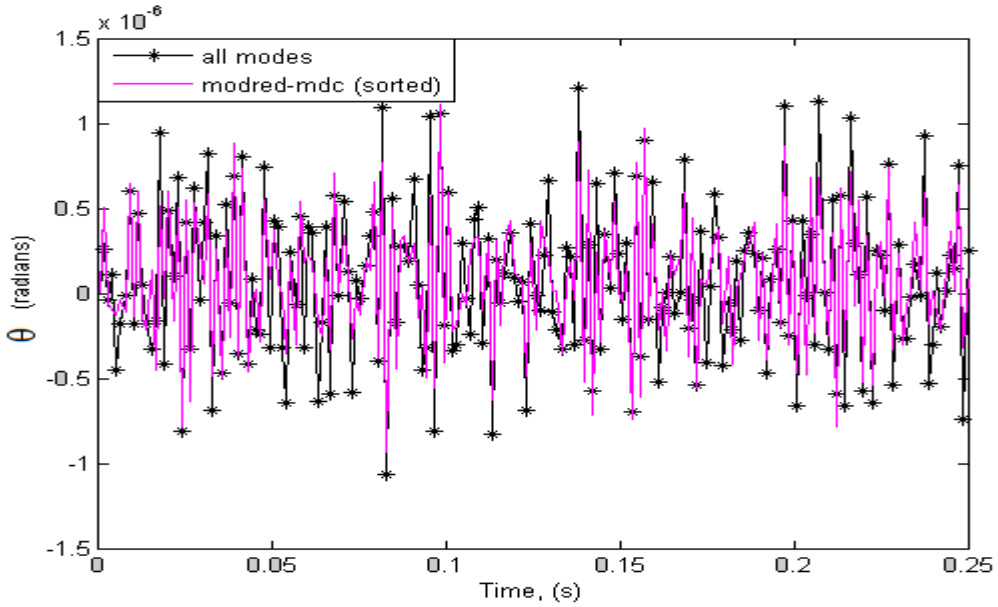

Figure 171: Pitch displacement of lift bag 1- first 6 *sorted* modes included

Lift bag 2

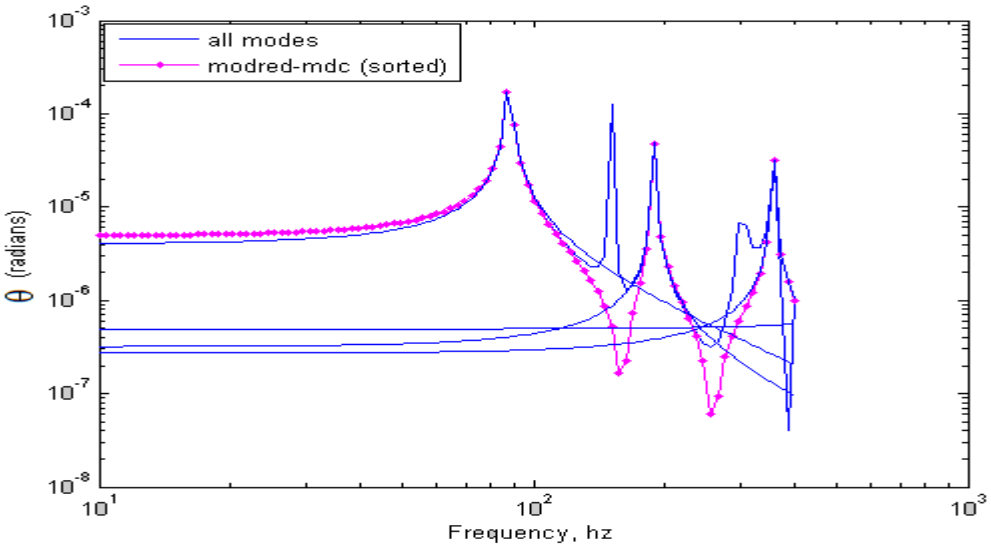

Figure 172: Pitch displacement of lift bag 2- first 6 *sorted* modes included

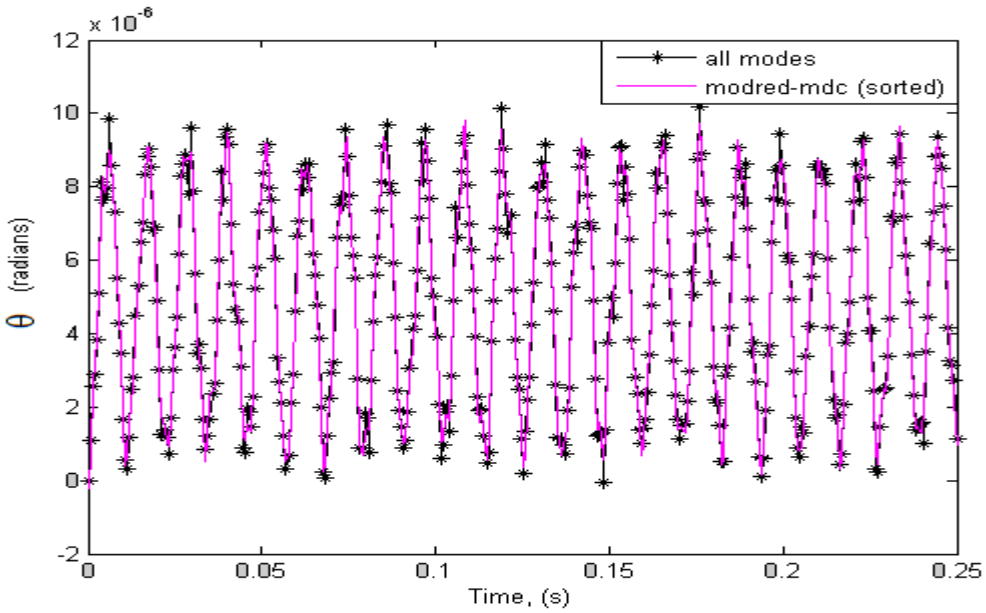

Figure 173: Pitch displacement of lift bag 2- first 6 *sorted* modes included

Lift bag 3

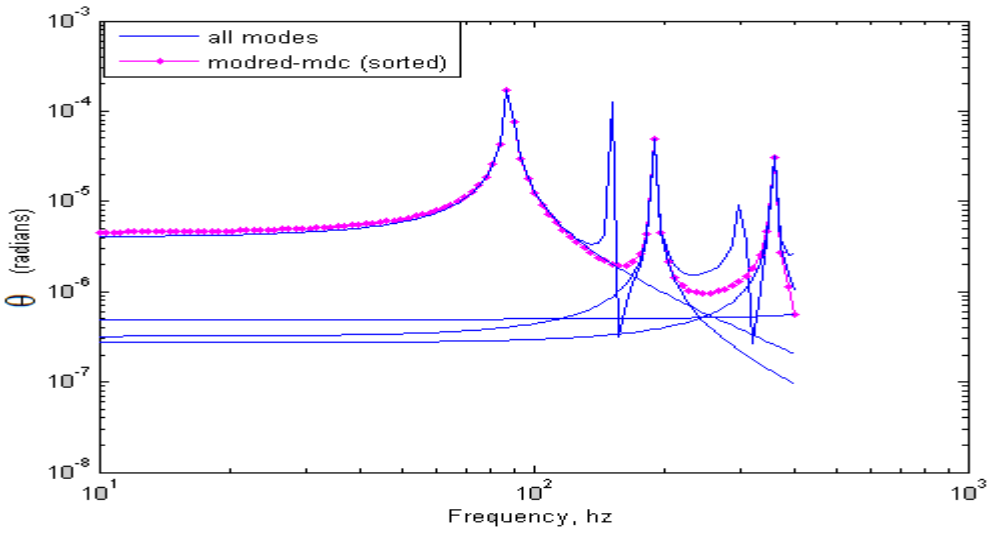

Figure 174: Pitch displacement of lift bag 3- first 6 *sorted* modes included

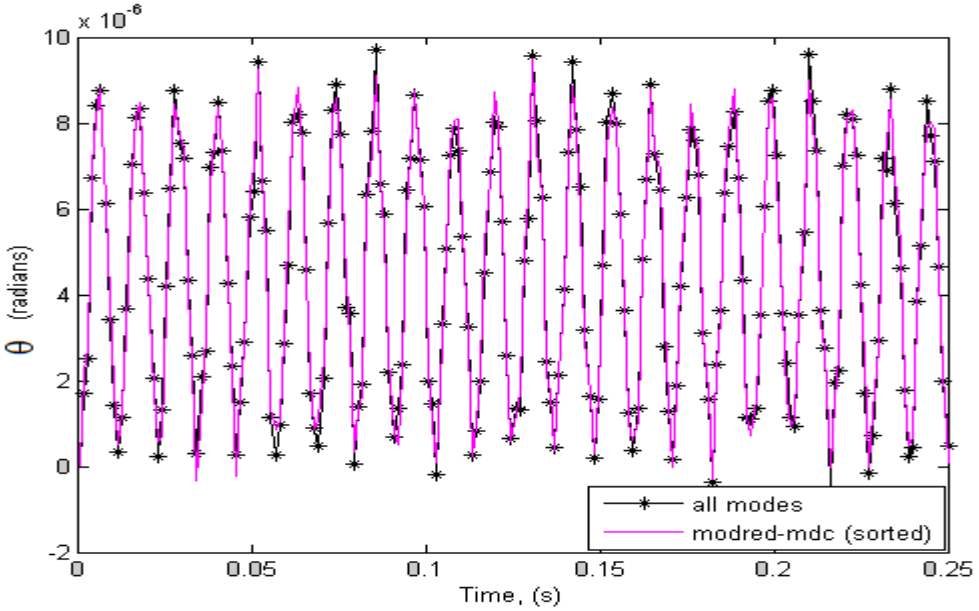

Figure 175: Pitch displacement of lift bag 3- first 6 *sorted* modes included

Lift bag 4

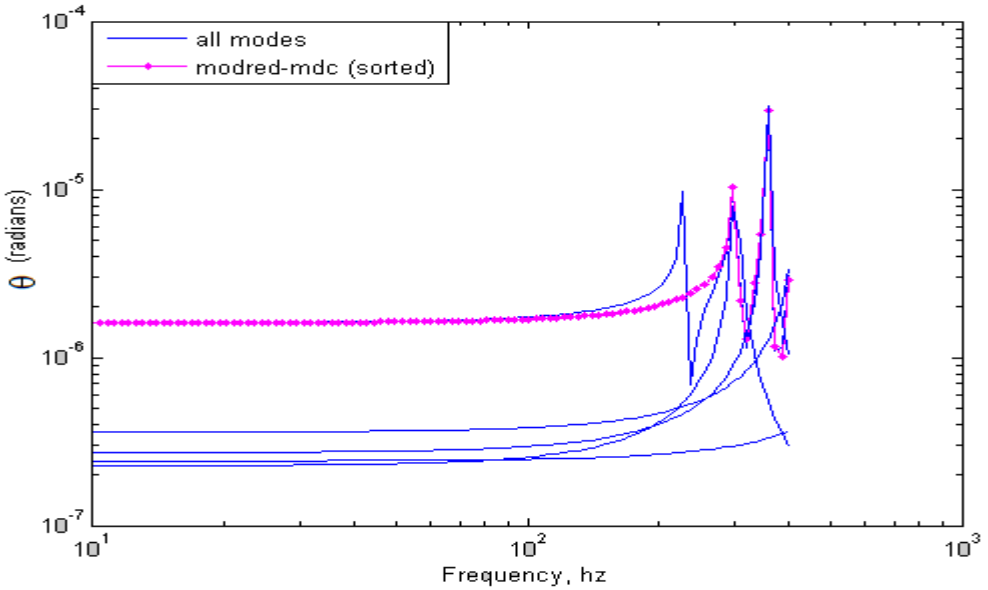

Figure 176: Pitch displacement of lift bag 4- first 6 *sorted* modes included

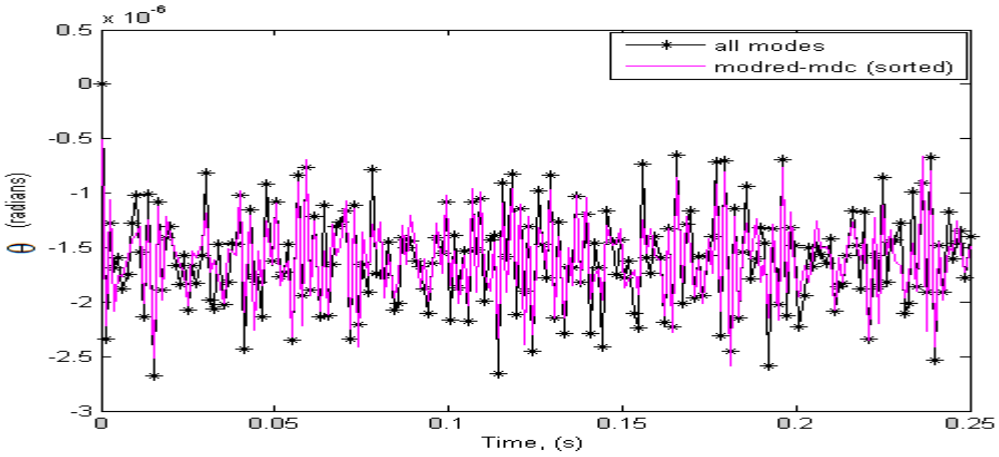

Figure 177: Pitch displacement of lift bag 4- first 6 *sorted* modes included

9.5.1.2.2.1.4 Pitch velocity

Pitch velocity variation with respect to frequency and time domain is plotted in Figures 178-185. Pitch velocity of the tanker is found to be in the order of 10^{-3}. It is noticed that pitch velocity fluctuates with time.

Lift bag 1 (node 2)

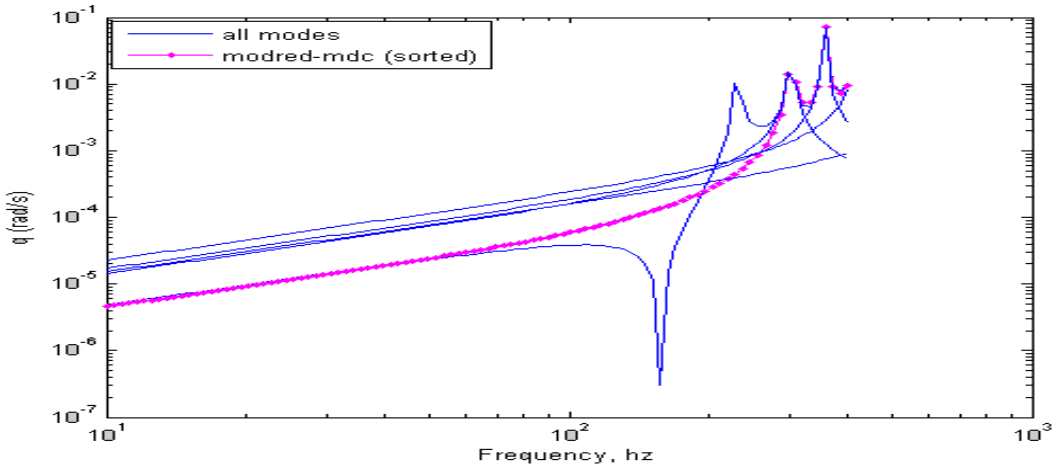

Figure 178: Pitch velocity of lift bag 1- first 6 *sorted* modes included

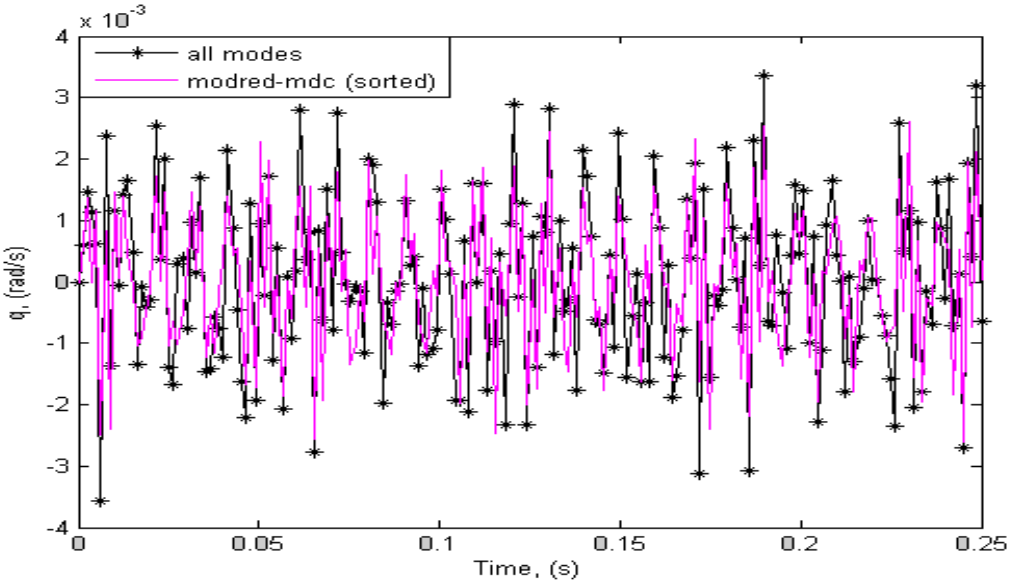

Figure 179: Pitch velocity of lift bag 1- first 6 *sorted* modes included

Lift bag 2

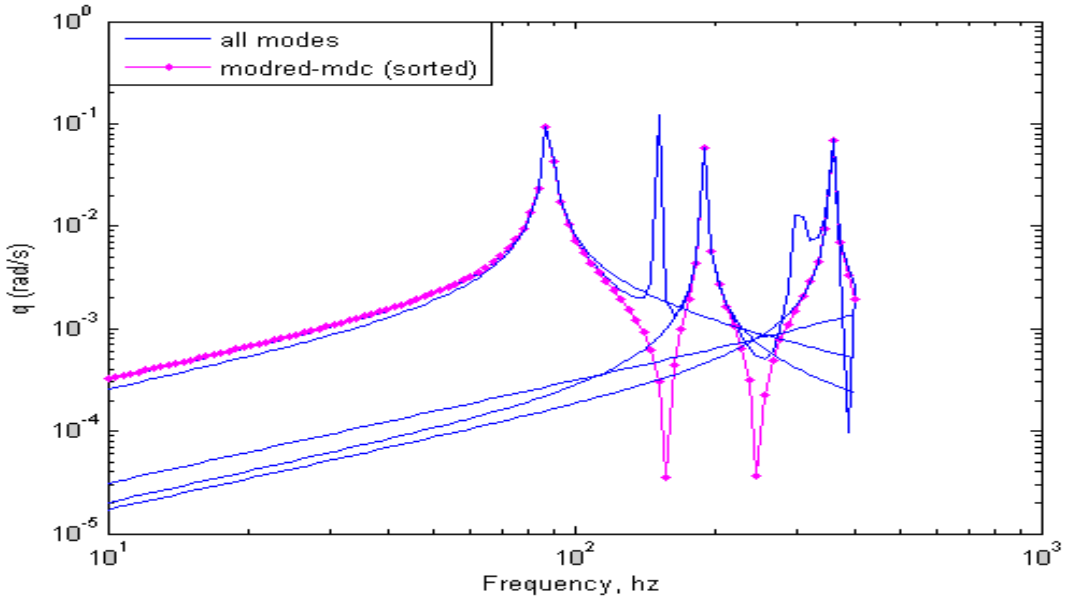

Figure 180: Pitch velocity of lift bag 2- first 6 *sorted* modes included

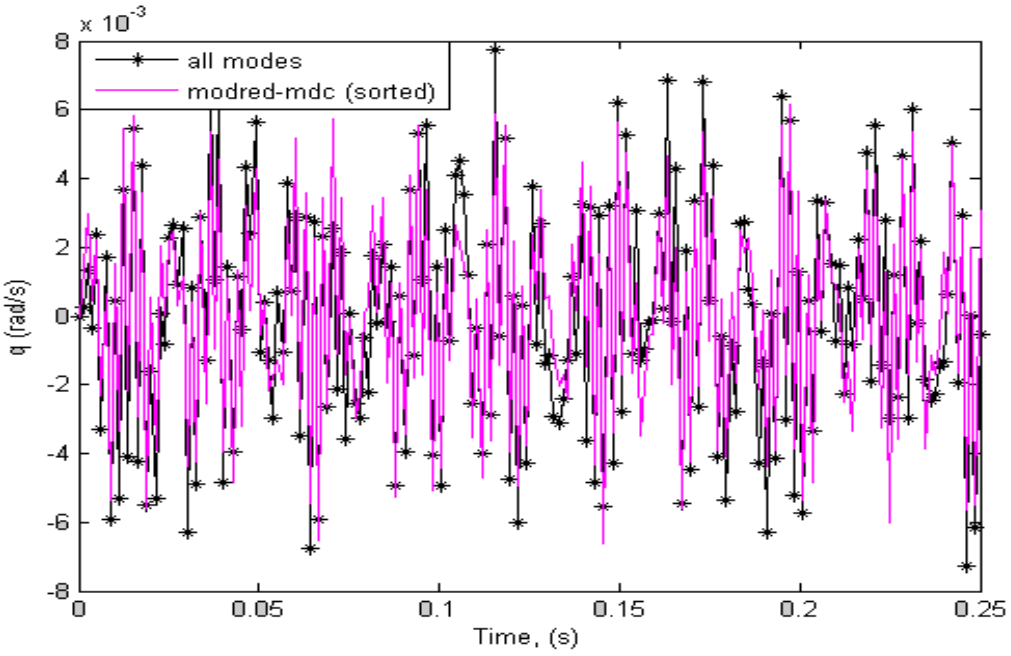

Figure 181: Pitch velocity of lift bag 2- first 6 *sorted* modes included

Lift bag 3

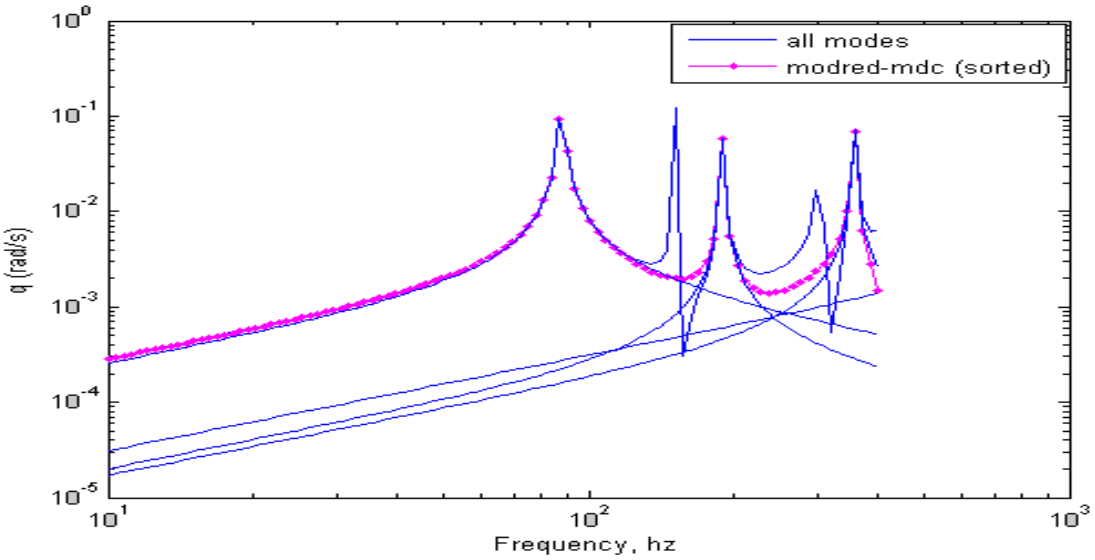

Figure 182: Pitch velocity of lift bag 3- first 6 *sorted* modes included

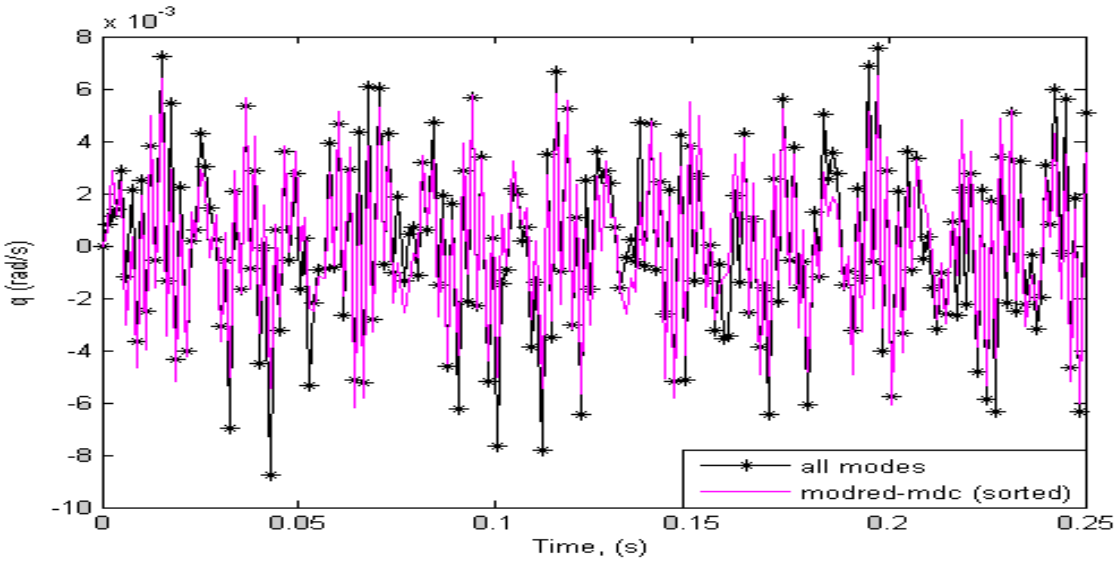

Figure 183: Pitch velocity of lift bag 3- first 6 *sorted* modes included

Lift bag 4

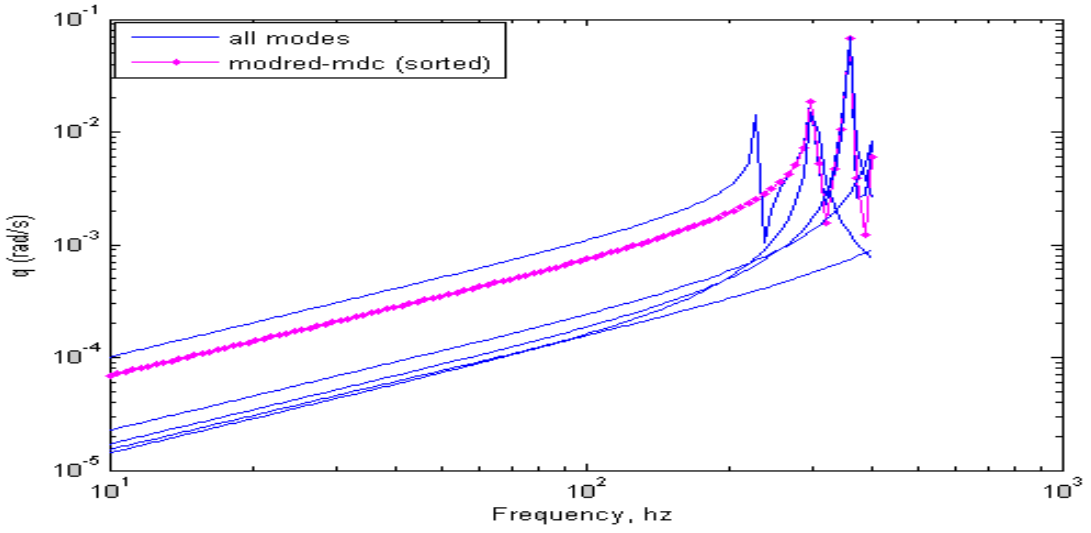

Figure 184: Pitch velocity of lift bag 4- first 6 *sorted* modes included

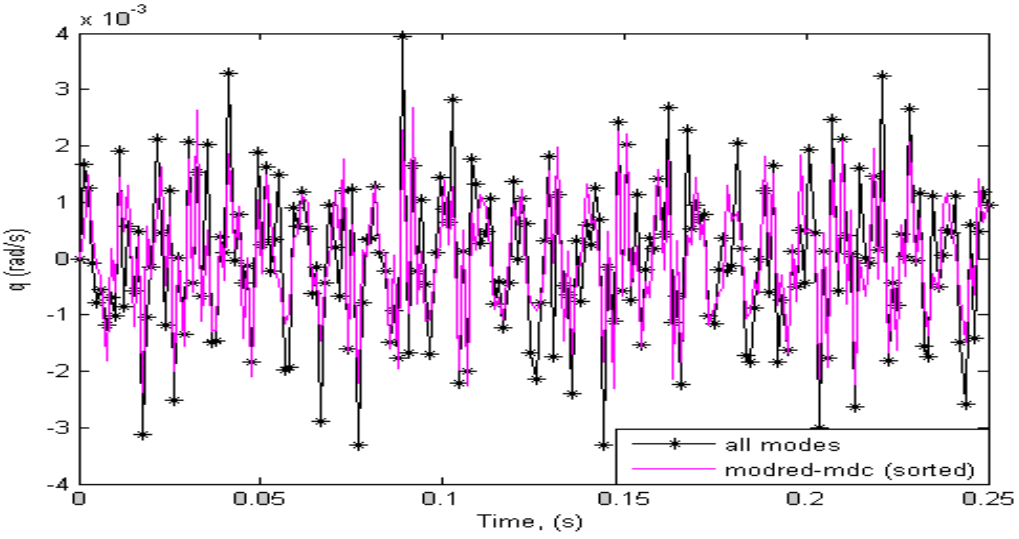

Figure 185: Pitch velocity of lift bag 4- first 6 *sorted* modes included

9.5.2 Motion Responses with Controller

From the modal analysis results, heave velocity of the tanker is found to be increasing with time. Also pitch motion is seen to be fluctuating with time. Hence in order to maintain hydrodynamic stability, it is necessary to integrate a control system with the model. By flexible body modeling approach the state space model is available for individual nodes on the beam. Thus controlled response of individual lift bags can be simulated. This is the advantage of flexible body modeling & control over rigid body modeling & control. The reduced state space model (4*4) obtained using the optimum model order reduction technique '*modred-mdc*' is used for carrying out the simulation in SIMULINK. Supervisory fuzzy logic controller is integrated to state space models corresponding to each lift bags separately to get the individual controlled responses.

From the section 4.1.1.3, the total lift force required for breakout is obtained as 3616.815 tonne and the break out time for the estimated force is found to be 400 s [35, 82]. The controlled responses obtained for a target depth of 300 m from sea bottom is plotted for the four external lift bags separately as shown in Figures 186-205.

Lift bag 1

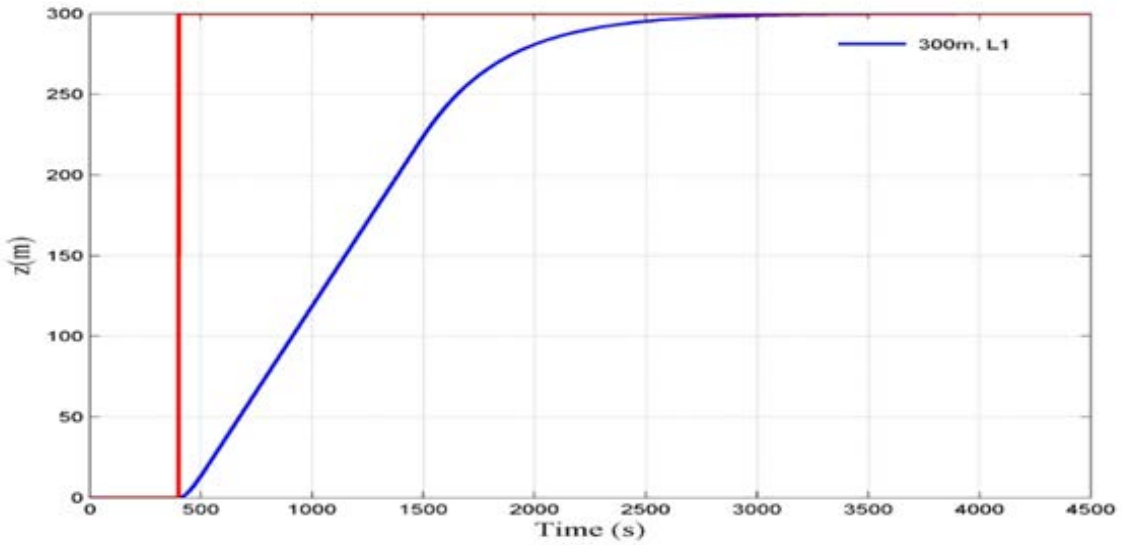

Figure 186: Variation of vertical position of lift bag 1 from sea bottom

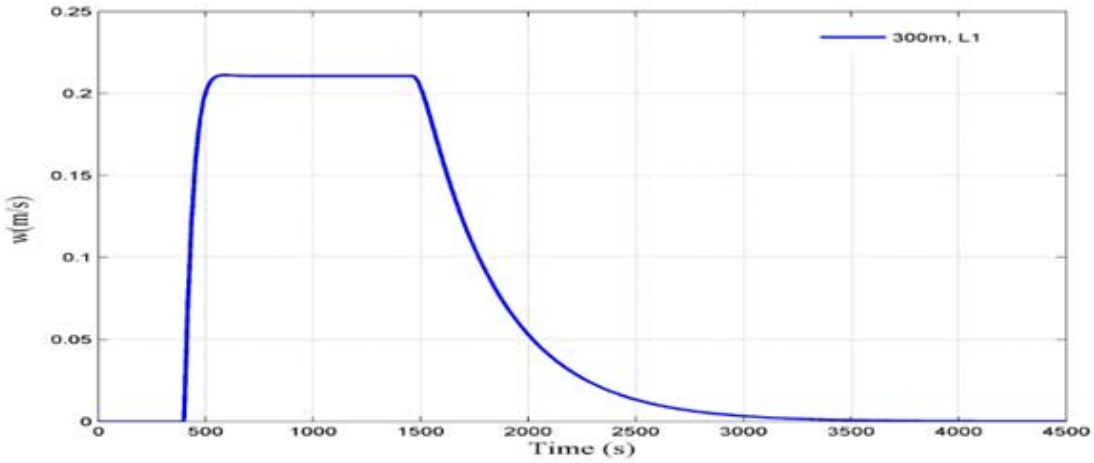

Figure 187: Variation of ascent velocity of lift bag 1

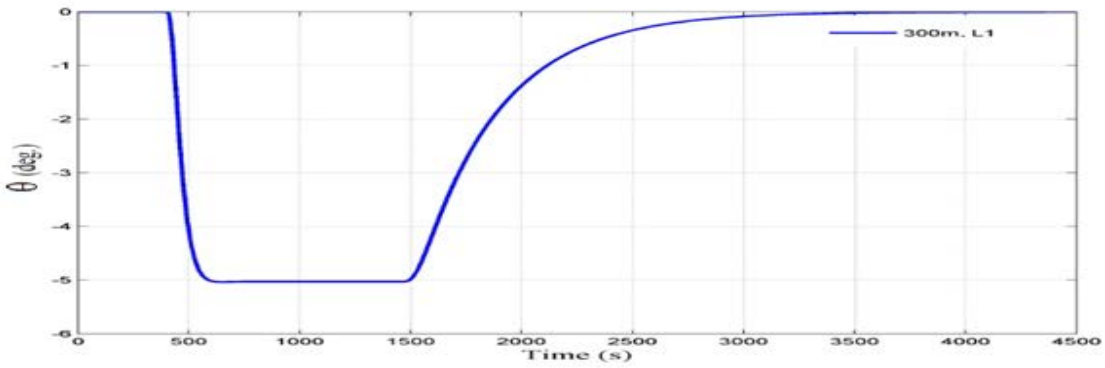

Figure 188: Variation of pitch angle of lift bag 1

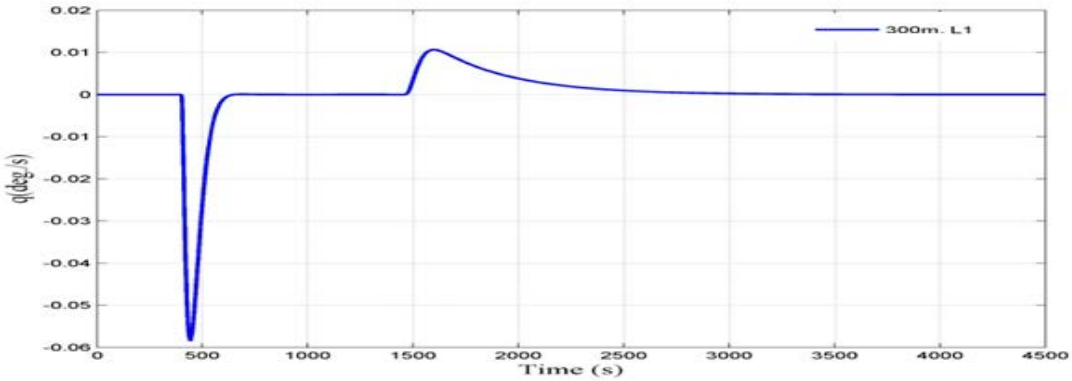

Figure 189: Variation of pitch rate of lift bag 1

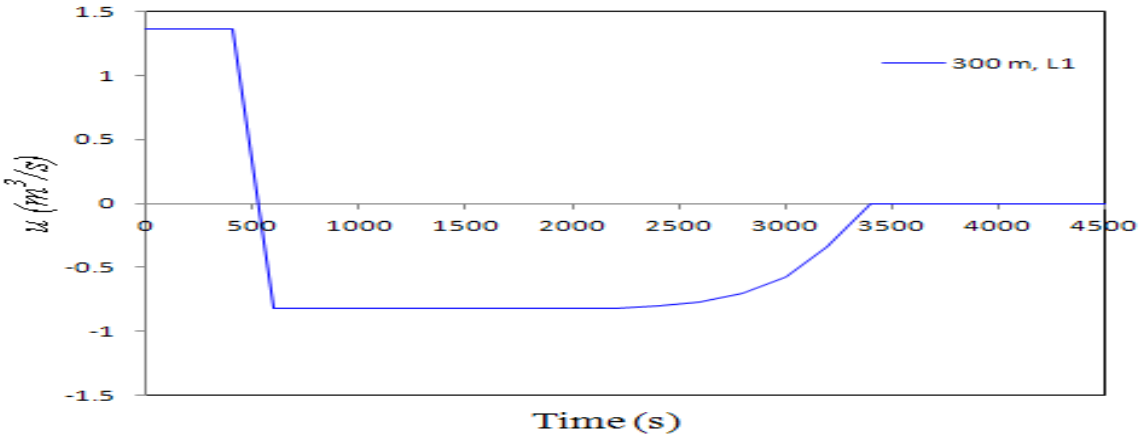

Figure 190: Net flow rate (at local pressure) in and out of lift bag 1

Lift bag 2

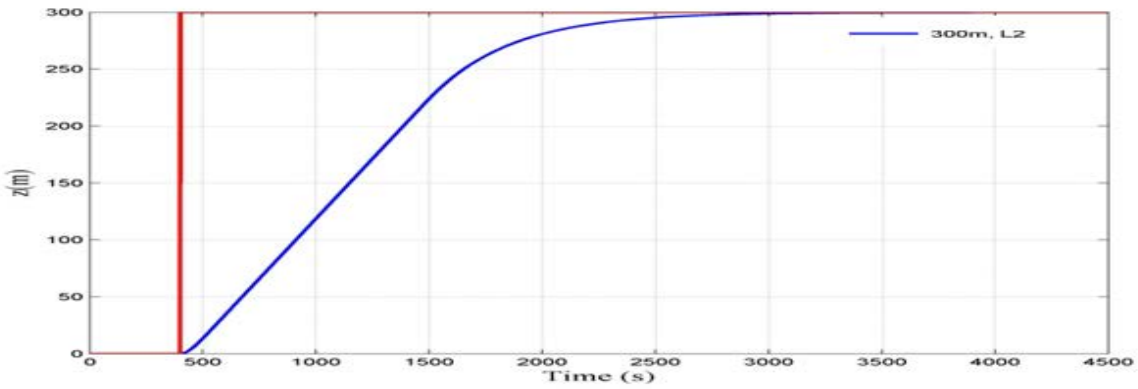

Figure 191: Variation of vertical position of lift bag 2 from sea bottom

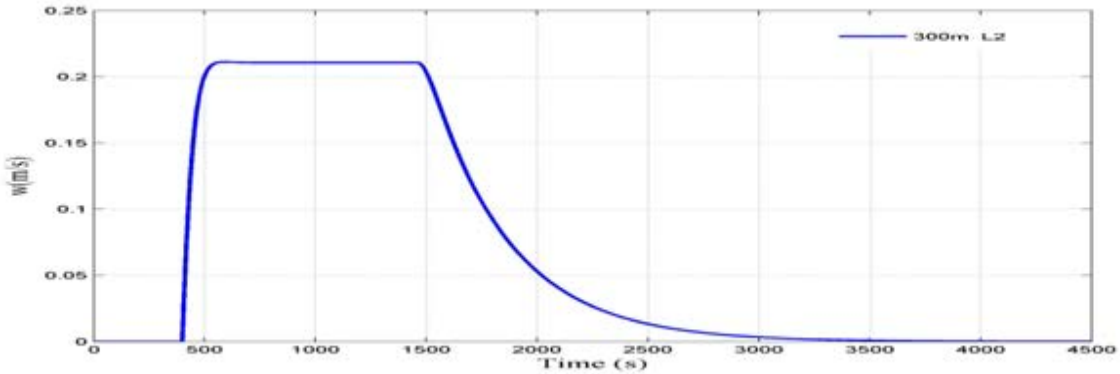

Figure 192: Variation of ascent velocity of lift bag 2

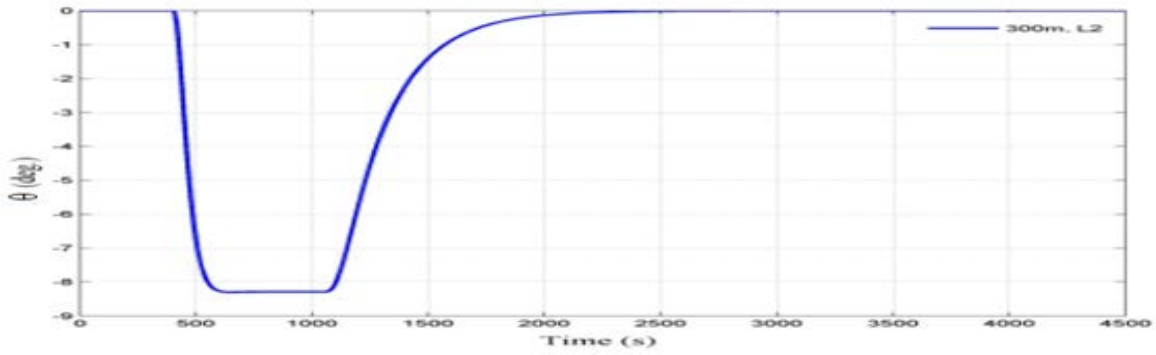

Figure 193: Variation of pitch angle of lift bag 2

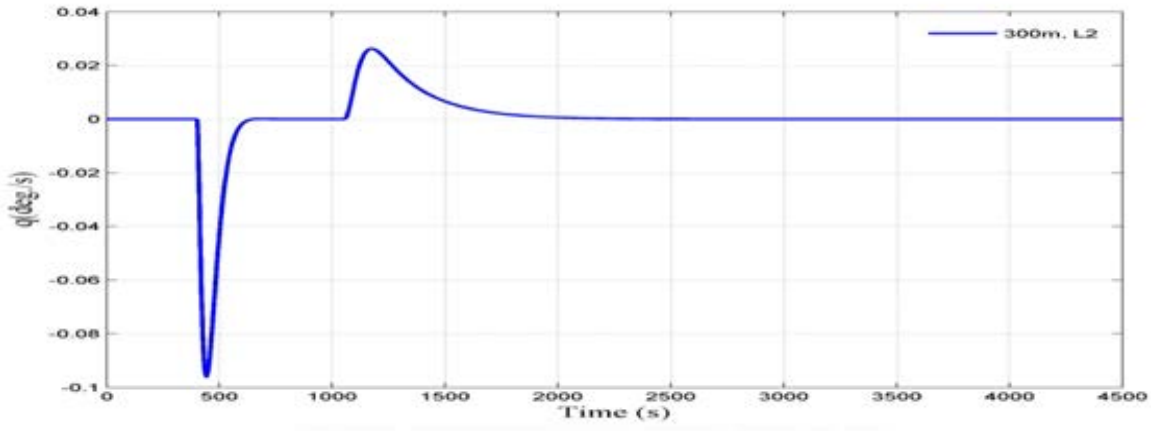

Figure 194: Variation of pitch rate of lift bag 2

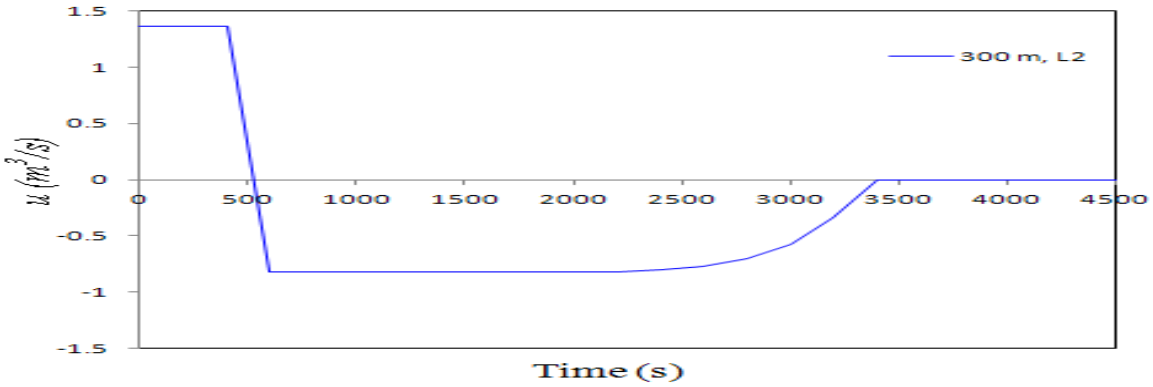

Figure 195: Net flow rate (at local pressure) in and out of lift bag 2

Lift bag 3

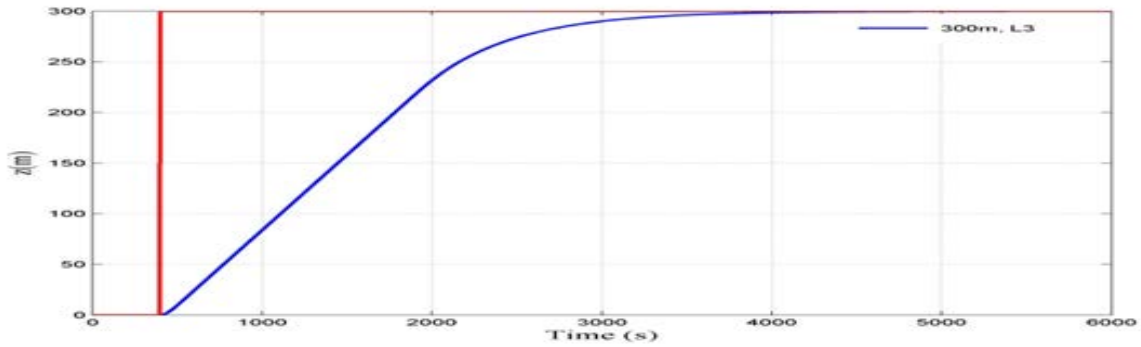

Figure 196: Variation of vertical position of lift bag 3 from sea bottom

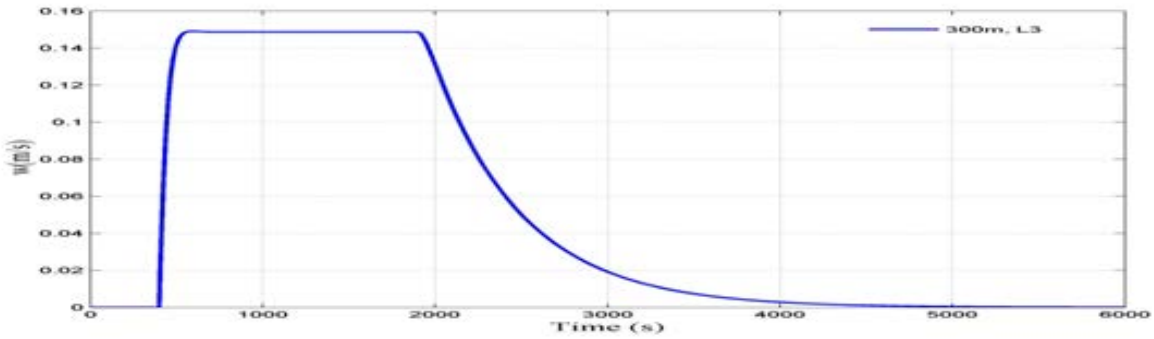

Figure 197: Variation of ascent velocity of lift bag 3

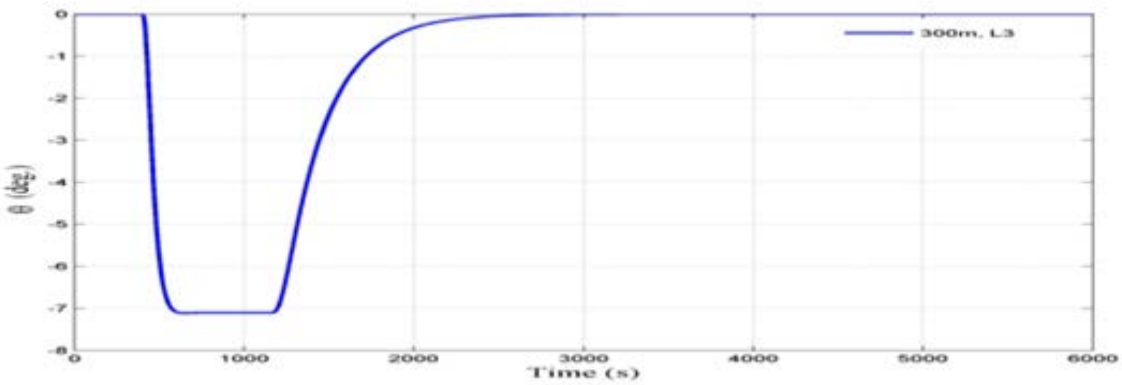

Figure 198: Variation of pitch angle of lift bag 3

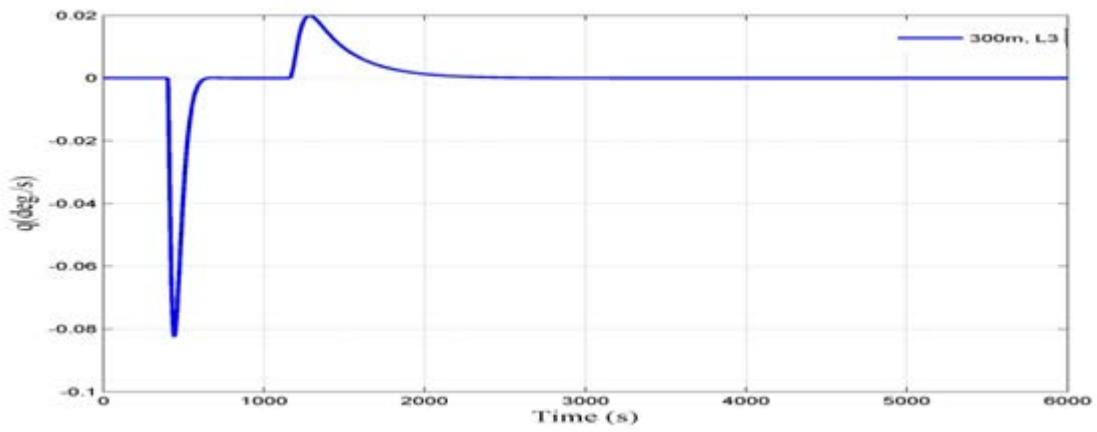

Figure 199: Variation of pitch rate of lift bag 3

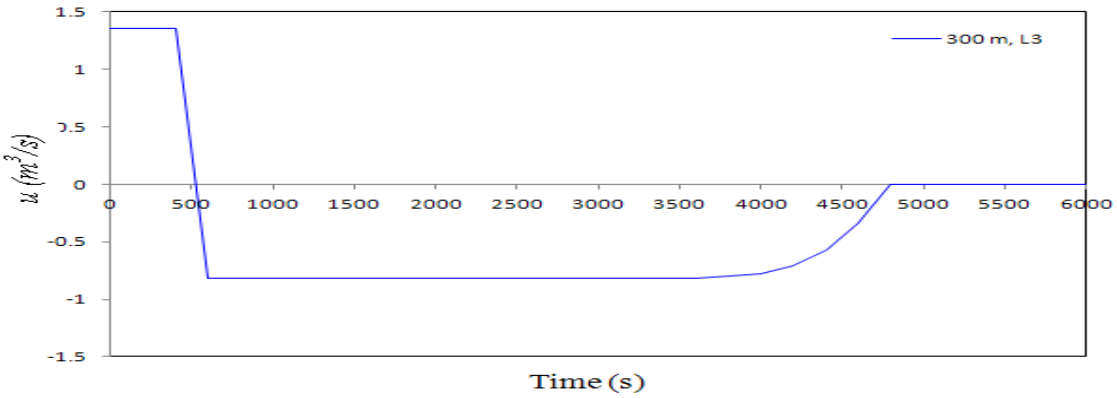

Figure 200: Net flow rate (at local pressure) in and out of lift bag 3

Lift bag 4

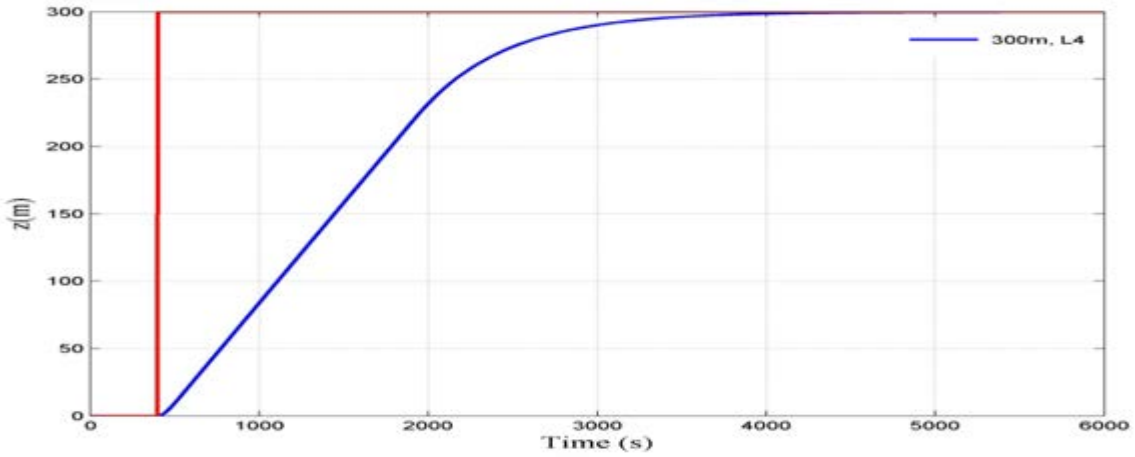

Figure 201: Variation of vertical position of lift bag 4 from sea bottom

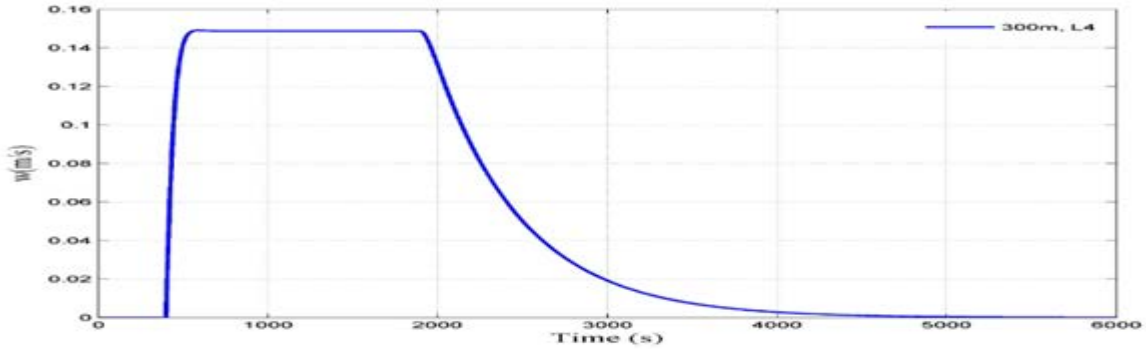

Figure 202: Variation of ascent velocity of lift bag 4

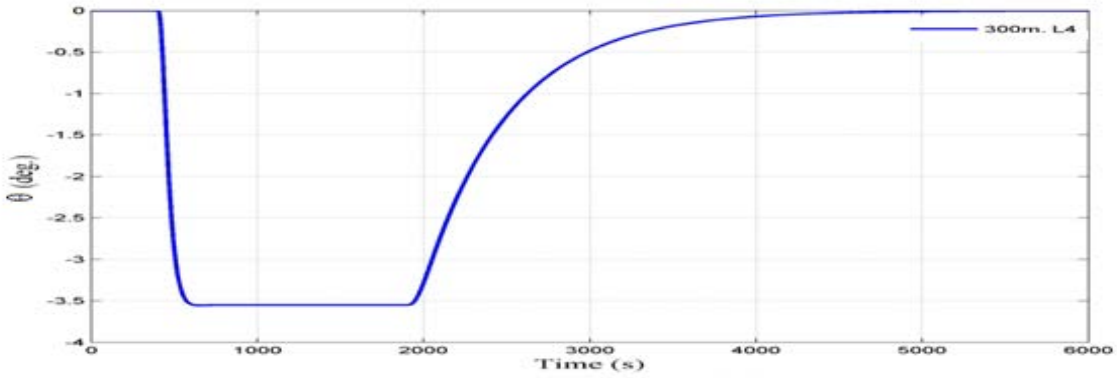

Figure 203: Variation of pitch angle of lift bag 4

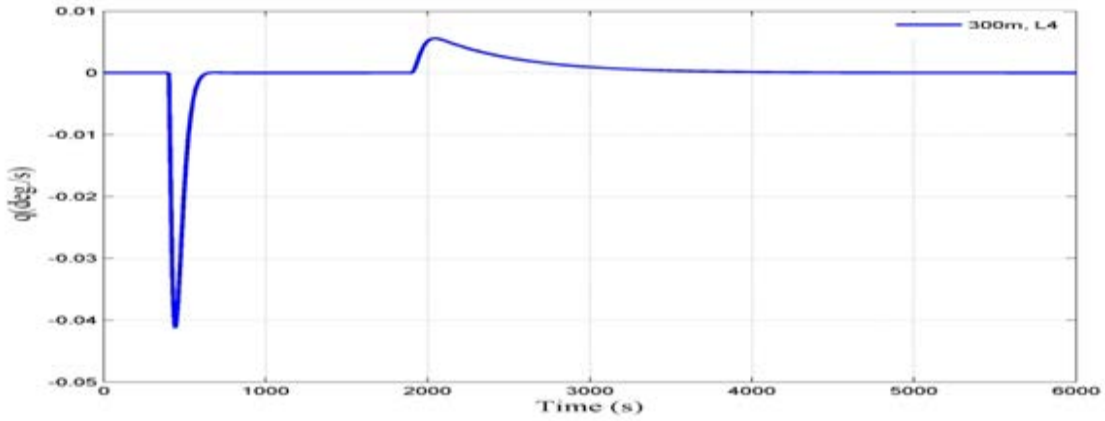

Figure 204: Variation of pitch rate of lift bag 4

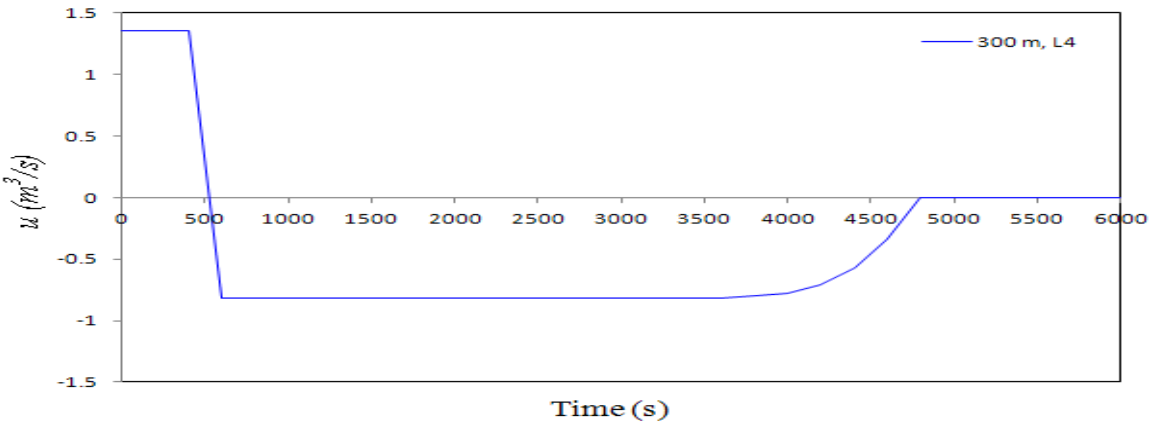

Figure 205: Net flow rate (at local pressure) in and out of lift bag 4

From the response plots (Figures 186-205), it is seen that all the four external lift bags have steady state behavior by integrating the controller in comparison with the results obtained without controller (Figures 154-185); i.e. the heave velocity of lift bags initially increases after breakout and reaches a higher stable value and then decreases to zero when the tanker reaches the target depth. Pitch response of the tanker follows the same trend as the ascent velocity curve. It is also noted that by integrating the controller, fluctuating pitch motions of lift bags avoided, hence stability ensured. From Figure 186, 191, 196 & 201, lift bag 1 and lift bag 2 reaches the target depth in 2800s, where as lift bag 3 and lift bag 4 takes 4000 s to achieve the target depth. Therefore the aft part of the tanker rises faster than bow part. This is mainly because controller is

integrated to each lift bag separately and there is no communication between the lift bags. This is one of the drawbacks of the present model. The maximum value of ascent velocity among the four lift bags is found to be 0.21 m/s < 0.6 m/s, which implies that the ascent is stable. The maximum value of pitch angle for lift bags (see Figure 193) is found to be about 8.2 degrees, which is within the required limit. Pitch rates of the lift bags become nearly equal to zero when the bags reach the target depth. Figures 190, 195, 200 & 205 shows that the control action for lift bag 1 & lift bag 2 are identical, while lift bag 3 and lift bag 4 are having the same control output. This is due to the reason that state space models of lift bag 1 and lift bag 2 are almost same, whereas lift bag 3 and lift bag 4 are having the same state space model. It is also due to the reason that there is no communication between the lift bags.

Even though the system is stable by using multiple controlled lift bags, for more uniform lifting of the vessel, it is required to build an integrated network of control system, in which there is a master controller which gives commands to all the lift bags in order to attain a uniform ascent.

9.6 Concluding Remarks

In this chapter, the real case of lifting a sunken chemical tanker using multiple controlled gas inflating bags is considered by modeling the vessel as an Euler-Bernoulli beam with free-free boundary conditions. Initially modal analysis of the chemical tanker is performed without controller to obtain the free vibration and forced vibration analysis responses and supervisory fuzzy logic controller is integrated later with the state space model of individual lift bags to obtain the controlled stable responses. The longitudinal distribution of shear force and bending moment across the vessel length is estimated and the maximum value of shear force is found to be 3.51MN, which is at node 8 (i.e. at lift bag 3) and the bending moment is 44.16 MN.m at node 5 (i.e. at lift bag 2). The modal contributions of individual modes are analyzed according to their *dc gain* value and highest dc gain is obtained for the first two rigid modes, which implies that rigid body modes are more significant compared to flexible modes for marine salvage. Finally

the effectiveness of various modal reduction techniques are investigated in both frequency and time domain to obtain the smallest state space model (4*4) that accurately represents the pertinent flexible body dynamics and '*unsorted modred-mdc*' is found to be the optimum choice for modal order reduction as it minimizes the low frequency errors by including the contribution of the unused modes in the reduced model. From the modal analysis results, the heave response of the tanker is found to be increasing with time, whereas pitch motion is seen to be fluctuating with time. Therefore, in order to maintain hydrodynamic stability, it is necessary to integrate a control system with the model. Using the flexible body modeling approach the state space model is available for individual nodes on the beam. Thus the controlled response of individual lift bags can be simulated. This is the advantage of flexible body modeling & control over rigid body modeling & control. Hence supervisory fuzzy logic controller is integrated with the 4*4 flexible state space model obtained using '*unsorted modred-mdc*' method to obtain the controlled stable responses of each external lift bags. From the response plots, it is seen that all the four external lift bags have steady state behavior. Lift bag 1 and lift bag 2 reach the target depth in 2800s, whereas lift bag 3 and lift bag 4 take 4000 s to achieve the target depth. Therefore the aft part of the tanker rises faster than bow part. This is mainly because controller is integrated to each lift bag separately and there is no communication between the lift bags. This is one of the drawbacks of the present control system. Even though the system is stable in the application of using multiple controlled lift bags, it is required to build an integrated network of controllers, in which there is a master controller which gives commands to subsidiary lift bags for attaining a more uniform ascent.

10 Conclusions

A rigid body mathematical formulation for the dynamics of raising sunken vessel using buoyant systems is derived according to the principles of underwater dynamics, thermodynamics and soil-structure interaction problems and a state space model is developed from the equation of motion in diving plane for integrating the controller in Chapter 4. In the rigid body modeling approach, additional buoyancy provided by all lift bags are considered together and the overall system behavior is analyzed. The breakout force for the proposed model is estimated based on the work of Sawicki and Mierczynski [101]. Breakout time is estimated according to Foda [35] and Mei et al [82]. The system is lineraised about the equilibrium point [49]. The effect of coupling surge motion with heave and pitch is neglected by redefining the hydrodynamic coefficients with respect to vessel's centre of gravity, instead of geometric centre [12]. Purge valve modeling is carried out according to Farrell & Wood (32).

In order to ensure hydrodynamic and structural stability during a salvage operation using buoyant systems, two control subsystems are proposed for each bag and then a supervisory controller is suggested to monitor the primary and secondary controllers. The function of the primary controller is to regulate the flow rate of filling gas inside the lift bags according to the buoyancy requirement in accordance with hydrostatic force due to weight, buoyancy and suction breakout, hydrodynamic forces and uncertainty arises due to any external disturbances. The secondary controller is proposed to regulate the purge valve opening based on suction breakout and the pressure difference between gas inside the lift bags and surrounding sea water pressure for a stable ascent. The function of the supervisory controller is to monitor or switch between primary and secondary controllers as per the depth error and depth rate for a stable ascent. The efficacies of classic controllers like PD, PID and SMC are investigated as the primary controller for regulating the flow rate of filling gas inside the lift bags in Chapter 5. A number of case studies are carried out for different target depths, with the developed linear state space model

including sensitivity analysis such as change in hydrodynamic coefficients, breakout lift force and the effect of external disturbances and uncertainty. A PD controller is found to be suitable for regulating the depth and pitch motions for smaller target depths with no overshoot and having less steady state error. But, for higher commanded depths with the same tuned coefficients, the performance of the controller is very poor, as the ascent velocity and pitch angle goes beyond the stable region. A PID controller gives satisfactory results for almost all target depths by approximating a linear deterministic model with considerable overshoot; whereas in the presence of parameter variations, non linearity and external disturbances, good results are not guaranteed. CSMC maintains hydrodynamic stability in the diving plane by satisfying the Lyapunov stability condition [49] for all commanded depths by approximating a linear state space model in comparison with PD & PID controllers even in the presence of parameter variations, external disturbances and uncertainty. The tuning effort and chattering were found to be the two major drawbacks of CSMC, which is improved by integrating it with fuzzy logic to become fuzzy sliding mode controllers as explained in Chapter 6. In FSMCs, the performance of the CSMC is improved by dynamically computing the sliding surface slope by a FLC and adaptively computing the controller gain by another FLC. FLCs are designed based on Mamdani's implification method [88]. A TIFSMC is designed first and then simplified to SIFSMC. With the development of SIFSMC, the tuning process becomes standardized and hassle free and hence the well known chattering problem associated with SMCs is avoided. It is found that both FSMCs show 30% of improvement in the tracking performance when compared to the CSMC, while maintaining its robustness. It is also noted that FSMCs are less sensitive to external disturbances and uncertainties in comparison with CSMC. The responses obtained by the SIFSMC are the same as those obtained by the TIFSMC, with the former involving a much less tuning effort and computational time. Simulation studies reveal the fact that for complicated non linear underwater operations, like marine salvage, involving uncertainty and external disturbances a closed loop control system is mandatory and an adaptive controller like SIFSMC is the optimum choice amongst the considered controllers as the primary controller for regulating the gas flow rate.

A PID controller is designed as the secondary controller for regulating the purge valve opening according to the excess buoyancy available after suction breakout and to the pressure difference between gas inside the lift bags and surrounding sea water pressure for a stable ascent in Chapter 7. A PID controller is found to be effective in maintaining the ascent velocity within the stable region. In Chapter 8, a supervisory fuzzy logic controller is designed to monitor or switch between the primary and secondary controllers as per the depth error and depth rate for a stable ascent. From the simulation studies, it is found that FLC is able to maintain hydrodynamic stability in the diving plane by suitably defining the linguistic fuzzy rules, membership functions and scaling factors, which are created based on the author's experience in conducting numerical simulation using primary and secondary controllers and also carrying out the stability analysis using trial and error method. The Gaussian membership functions are used for representing input and output variables after carrying out the stability check using various kinds of membership functions and the *centroid* method is used for defuzzification. Using a trial and error approach, the best inference mechanism to use in this case seems to be the *prod-probor* method. Because of simplicity and availability of the graphical user interface (GUI) in MATLAB the Mamdani inference engine is employed for designing the FLC. This uses *minimum* operator for a fuzzy implication and *max-min* operator for composition. The defuzzification technique used the trial and error and *Centre of Gravity approach,* which provides least integral square error.

In the rigid body modeling approach, the state space model is created by considering the total additional buoyancy provided by all lift bags together and the responses are available for the whole motion of the payload. But in actual practice, lift bags are located at different locations on the vessel and their location significantly affects the hydrodynamic and control responses.

Using the rigid body modeling approach, it is not possible to determine how the location of individual lift bags affects the hydrodynamic and control responses for a very flexible body such as a long pipe. Also in some complicated situations, it would be necessary to control individual lift bags separately to limit pipe bending, i.e. to use multiple controlled lift bags to ensure both hydrodynamic and structural stability,. For meeting these objectives, the rigid body modeling &

control approach is extended to detailed flexible beam modeling & control in Chapter 9 (however the method is still applied to the tanker).

The real case of lifting a sunken chemical tanker using adaptively controlled gas inflating bags is considered by modeling the vessel as an Euler-Bernoulli beam with free-free boundary conditions. Initially modal analysis of the chemical tanker is performed without a controller to obtain the free vibration and forced vibration analysis responses and supervisory fuzzy logic controller as explained in Chapter 8 is integrated later with the state space model of individual lift bags to obtain the controlled stable responses. Optimum location of lift bags on the vessel is determined by looking at the mode shape plots obtained from free vibration analysis of the tanker. Lift bags are normally placed on '*nodes of a mode'* where the displacement is negligible. Force modeling is carried out based on the hydrostatic, hydrodynamic, suction breakout and additional buoyancy force components as explained in Section 4.1.1.1- 4.1.1.4. The longitudinal distribution of shear force and bending moment across the vessel length is estimated and the maximum value of shear force is found to be 3.51MN, which is at node 8 (i.e. at lift bag 3) and the bending moment is 44.16 MN.m at node 5 (i.e. at lift bag 2). The modal contributions of individual modes are analyzed according to their *dc gain* value to define which ones have the greatest contribution. Highest dc gain is obviously obtained for the first two rigid modes, which implies that rigid body modes are more significant compared to flexible modes for marine salvage (although to avoid exceeding allowable hull girder moments higher modes may also be important). Finally efficacies of various modal reduction techniques are investigated in both frequency and time domain to obtain a smallest state space model (4*4) that accurately represents the pertinent flexible body dynamics. It is found that '*unsorted modred-mdc*' is the optimum choice for modal order reduction as it minimizes the low frequency errors by including the contribution of the unused modes in the reduced model. From the modal analysis results, the heave velocity of the tanker is found to be increasing with time, whereas pitch motion is seen to be fluctuating with time. Therefore, in order to maintain hydrodynamic stability, it is necessary to integrate a control system with the model. By flexible body modeling approach the state space model is available for individual nodes on the beam. Thus controlled response of individual lift bags can be simulated. This is the advantage of flexible body modeling & control over rigid body

modeling & control. Hence supervisory fuzzy logic controller is integrated with the 4*4 flexible state space model obtained using '*unsorted modred-mdc*' to obtain the controlled stable responses of each external lift bags. From the response plots, it is seen that all the four external lift bags have steady state behavior. Lift bag 1 and lift bag 2 reach the target depth in 2800s, whereas lift bag 3 and lift bag 4 take 4000 s to achieve the target depth. Therefore the aft part of the tanker rises faster than bow part. This is mainly because the controller is integrated into each lift bag separately and there is no communication between the lift bags. This is one of the drawbacks of the present control system. Even though the system is stable in the application of using multiple controlled lift bags, it will be necessary to build an integrated network of controllers, in which there is a master lift bag which gives commands to subsidiary lift bags for attaining a more uniform ascent.

11 Future Recommendations

It will be more appropriate to design a suitable breakout model to predict the exact breakout force and time for more precised results.

In the long run, it is possible to design an integrated lift system using multiple controlled lift bags to ensure a safe ascent. This system will be important for controlling the pitch rate as well as ascent rate. For that sensors need to provide at individual lift bags and there should be proper communication between a master controller and the various subsidiary lift bags by a network. Purge valves in the individual lift bags should also be controlled by another network integrated with pressure sensors connected to each lift bag.

Such a control system can be integrated with our flexible beam modeling & control approach. Using the flexible structure technique developed in this thesis the method could be used to model and control the salvage, or installation of long flexible structures such as pipes.

Publications

1 Arun Kumar.D.V, Narakorn Srinil (2011). "Salvaging of Sunken Vessels by Buoyancy Concepts", University Research Day 2010, 7th June 2011, Strathclyde University, UK.

2 Arun Kumar.D.V. (2011). "Dynamics Analysis of a Raising Sunken Vessel", UK Marine Technology Postgraduate Research Conference (UK MTPC) 2011, University of Southampton, UK.

3 Velayudhan, A K D., Srinil, N., Barltrop, N.(2011). "Sliding Mode Controller for Salvaging of Sunken Vessels", Proceedings of 15th International Conference on Computer Applications in Ship Building, Trieste, Italy.

4 Velayudhan, A K D., Srinil, N., Barltrop, N. (2012). "A New Ship Recovery Concept and Design Using Adaptively Controlled Buoyancy Systems", Proceedings of 11th International Marine Design Conference, Glasgow.

5 Velayudhan, A K D., Srinil, N., Barltrop, N. (2014). " Flexible Body Analysis of Lifting a Sunken Chemical Tanker using Multiple Controlled Gas Inflating Bags", Proceedings of 2nd International Conference on Maritime Technology, Glasgow.

References

1 Abdelhameed, M.-M.(2005). “Enhancement of sliding mode controller by fuzzy logic with applications to robotic manipulators”, *Mechatronics 15*, pp. 439-458.

2 Achawakorn, K., Jearsiripongkul, T. (2012). “Vibration Analysis of Exponential Cross-Section Beam Using Galerkin’s Method”, *International Journal of Applied Science and Technology*, Vol.2, No-6.

3 Alfro-Cid, E., McGookin, E.W., Murray-Smith, D.J., Fossen, T.I. (2005). “Genetic algorithms optimisation of decoupled Sliding Mode controllers: simulated and real results”, *Control Engineering Practice 13*, pp. 739–748.

4 Alfro-Cid, E., McGookin, E.W., Murray-Smith, D.J. (2006). “GA-optimised PID and pole placement real and simulated performance when controlling the dynamics of a supply ship”, *IEEE Proc.-Control Theory Appl.*, Vol. 153, No. 2.

5 Allen, M., Bernelli-Zazzera, F. and Scattolini, R. (2000). “Sliding mode control of a large flexible space structure”, *Control Engineering Practice 8*, pp. 861-871.

6 Antonelli, G., (2003). “Underwater Robots: Motion and Force Control of Vehicle–Manipulator Systems”. Springer, Berlin.

7 Barltrop, N.D.P. & Adams, A.J. (1991). “Dynamics of fixed marine structures”. Butterworth-Heinemann (3rd Edition).

8 Bathe, K.J. (1996). “Finite Element Procedures”, Prentice Hall, Upper saddle River, New Jersey.

9 Bakkeheim, J., Johansen, T.A., Smogeli, O.N., and. Sorensen, A.J. (2004). “Lyapunov-based Integrator Resetting with Application to Marine Thruster Control”, Department of Engineering Cybernetics, The Norwegian Institute of Technology, University of Trondheim.

10 Bazzi, B.A., Chalhoub, N.G.(2005). “Fuzzy Sliding mode Controller for a Flexible Single-link Robotic Manipulator”, *Journal of Vibration and Control 11*, pp. 295-314.

11 Bessa, W.M., Dutra, M.S., Kreuzer, E.(2008). “An adaptive fuzzy sliding mode controller for remotely operated underwater vehicles”, *Robotics and Autonomous Systems 58*, pp. 16-26.

12 Beyazay, B. (1999). “Simulation and Modelling of a soft grounding system for an AUV”, M.S.Thesis, Naval Postgraduate School, Monterey, CA.

13 Caccia, M., Veruggio, G. (2000). “Guidance and control of a reconfigurable unmanned underwater vehicle”, *Control Engineering Practice* 8, pp.21-37.

14 Casella F., A. Locatelli and N. Schiavoni. (1996). “Nonlinear Controllers for Vibration Suppression in a Large Flexible Structure”. *Control Eng. Practice*, Vol. 4, No. 6, pp.791-806.

15 Chalhoub, N.G., Kfoury, G.A. and Bazzi., B.A. (2006). “ Design of robust controllers and a non linear observer for the control of a single-link flexible robot manipulator”, *Journal of Sound and Vibration 291*, pp.437-461.

16 Chhabra, D., Chandna, P. and Bhushan, G. (2011). "Design and Analysis of Smart Structures for Active Vibration Control using Piezo-Crystals", *International Journal of Engineering and Technology*, Volume 1, No.3.

17 Choi, S. B., Cheong, C. C., and Park, D. W.(1993), "Moving switching surfaces for robust control of second-order variable structure systems", *International Journal of Control 58(1)*, pp. 229–245.

18 Choi, B.J., Kwak, S,W., Kim, B.K. (1999). "Design of a single input fuzzy logic control & its properties", *Fuzzy Sets and Systems*, 106 (3), pp.299-308.

19 Choi, S.B. and Sohn, J.W. (2006). "Chattering alleviation in vibration control of smart beam structures using piezofilm actuators: Experimental verification", *Journal of Sound and Vibration 294(3)*, pp. 640–649.

20 Choi, S.B. and Sohn, J.W. (2006). "Vibration Control of Smart Structures Using Piezofilm Actuators", *Key Engineering Materials*, Vols.306-308, pp.1205-1210.

21 Clough, R.W., Penzien, J. (1975). "Dynamics of Structures", McGraw-Hill Kogakusha Limited, New Delhi.

22 Cristi,R., Papoulias, F.A., Healey, A.J.(1990). "Adaptive Sliding Mode Control of Autonomus Under water vehicles in the diving plane", *IEEE Journal of Ocean Engineering*, Vol. 15, No.3.

23 Cybenko, G. (1989). "Approximation by superpositions of a sigmoidal function, mathematics of control", *Signals Syst.* 2. pp. 303–314.

24 Debitetto, P., (1994). “Fuzzy logic for depth control of unmanned undersea vehicles”, *In: Proceedings of the AUV Symposium*, Cambridge, MA, USA, pp. 233–241.

25 Dougherty, F. and Woolweaver, G. (1990). “At sea testing of an underwater vehicle flight control system’’, In *Proc. AUV’90*, pp**.** 51-59.

26 Drobyshevski, Y. (2004). “A note on uprighting of a ship upside – down”, *Ocean Engineering 31*, pp**.**1447-1467.

27 Eksin, I., Guzelkaya, M., Tokat, S.(2002). “Self tuning mechanism for sliding surface slope adjustment in fuzzy sliding mode controllers”, *Proceedings of the Institution of Mechanical Engineers, Part 1: Journal of Systems and Control Engineering*, pp. 216-393.

28 Eksin, I., Guzelkaya, M., Tokat, S.(2002). “Sliding surface slope adjustment in fuzzy sliding mode controllers”, *Proceedings of the 10th Mediterranean Conference on Control and Automation*, Lisbon, Portgual.

29 Eksin, I., Tokat, S., Guzelkaya, M., Soylemez, M.T. (2003). “Design of a sliding mode controller with a non linear time-varying sliding surface”, *Transactions of the Institute of Measurement and Control 25*, pp.145-162.

30 Ever Safe.(2012). “Salvage Catalog”, Retrieved on 10th July 2011, www.eversafe-marine.com.

31 Faltinsen, O.M. (1990). “Sea Loads on Ships and Offshore Structure”, Cambridge Ocean Technology Series, Cambridge University Press, Cambridge, UK.

32 Farrell, J.E. (2008). “Automated Purge Valve”, M.S.Thesis, Florida Institute of Technology, Florida.

33 Farrell, J.& Wood, S. (2009). “An Automatic Purge Valve for Marine Salvage”, *IEEE Conference*, New Jersey.

34 Fjellstad, O.E. (1994). “Control of Unmanned Underwater Vehicles in Six Degrees of Freedom: - A Quaternion Feedback Approach”, Dr.ing. Thesis, Department of Engineering Cybernetics, The Norwegian Institute of Technology, University of Trondheim.

35 Foda, M.A. (1982).“On the Extrication of large objects from the ocean bottom (the breakout phenomenon)”, *Journal of Fluid Mechanics*, Vol.117, pp. 211-231.

36 Fossen, T.I. (1994). “Guidance and Control of Ocean vehicles” , Wiley, Newyork.

37 Fossen, T.I.(2002). “Marine Control Systems – Guidance , Navigation and Control of Ships, Rigs and Underwater Vehicles”, Marine Cybernetics, Trondheim, Norway.

38 Fossen, T.I., & Johansen, T.A. (2006). “A Survey of Control Allocation Methods for Ships and Underwater Vehicles”, Department of Engineering Cybernetics, The Norwegian Institute of Technology, University of Trondheim.

39 Fossen, T.I., & Paulson, M.J. (1992). “Adaptive Feedback Linearization Applied to Steering of Ships”, Department of Engineering Cybernetics, Norwegian Institute of Technology, University of Trondheim.

40 Fossen, T.I. & Perez, T., (2009). “Kalman Filtering for Positioning and Heading Control of Ships and Offshore Rigs”, *32 IEEE Control System Magazine*.

41 Fung, R.F., Chen, K.W., Yen, J.Y. (1999). “Fuzzy sliding mode controlled slider-crank mechanism using a PM synchronous servo motor drive”, *International Journal of Mechanical Sciences 41*, pp. 337-355.

42 Fuzzy Logic Toolbox For Use with MATLAB, The Mathworks Inc., version 2, Natick, MA, 2006.

43 Galerne, A. (1988). “Development of Deep Water Technology As It Relates to Future Salvage”, *Proceedings of IEEE OCEANS’88*, A Partnership of Marine Interests, Vol.1, pp.1573-1575, Baltimore, Maryland.

44 Ge, S.S., Lee, T.H., Zhu.G. and Hong, F. (2001). “Variable Structure Control of a Distributed- Parameter Flexible Beam”, *Journal of Robotic Systems 18(1)*, pp.17-27.

45 Gores, J.N. (1972). “Marine Salvage”, David & Charles Publishing Limited, U.K.

46 Guo,Y., Woo, P.Y.(2003). “An Adaptive Fuzzy Sliding Mode Controller for Robotic Manipulators”, *IEEE Transactions on Systems, Man and Cybernetics- Part A: Systems and Humans*, vol. 33. No.2.

47 Ha, Q. P., Rye, D. C., and Whyte, H. F. D. (1999), “Fuzzy moving sliding mode control with application to robotic manipulators”, *Automatica 35(4)*, pp. 607–616.

48 Hatch M.R. (2001). “Vibration Simulation Using MATLAB and ANSYS”. Chapman & Hall/CRC, Boca Raton, Florida, ISBN 1-58488-205-0.

49 Healey, A.J. & Lienard, D. (1993). “Multivariable sliding mode control for autonomus diving and steering of unmanned underwater vehicles”., *IEEE Journal of Oceanic Engineering*, 18(3), pp. 327-339.

50 Healey , A.J., & Macro, D.B. (1992). “Slow speed fight control of autonomus under water vehicle’s experimental results with NPS AUV II”, *Proceedings of the 2nd International Offshore & Polar Engineering Conference*, pp. 523- 532.

51 Hong-jian, J., Xiao-cheng, S, Jie, Z., Juan, Li, Ming-yu, FU. (2004). “*A Semi physical Virtual Simulation System for AUV*, Mechatronic Engineering Department, Harbin Institute of Technology, Harbin, China.

52 Huang, L.C., Lin, H.P., Chung, H.Y. (2007). “Design of self tuning fuzzy sliding mode control for TORA system”, *Expert Systems with Applications 32*, pp. 201- 212.

53 Huo, S., Short, S.R., and Xue, X. (2004). “FEM Based Modal Analysis of a Damaged Free-Free Beam”. *SEM X International Congress & Exposition on Experimental Applied Mechanics*, Costa Mesa, California, USA.

54 Ishii, K., Fujii, T. Ura, T. (1995). “An on-line adaptation method in a neural network based control system for AUV’s”, *IEEE J. Ocean. Eng*. *20*, pp. 221-228.

55 Ishii, K., Fujii, T., and Ura, T. (1998). “Neural network system for online controller adaptation and its application to underwater robot”. *In Proceedings of IEEE International Conference on Robotics & Automation*, pp.756–761.

56 Ishii, K., Ura, T., (2000). “An adaptive neural-net controller system for an underwater vehicle”. *Control Engineering Practice 8*, pp. 177–184.

57 Itkis, U. (1976), “Control Systems of Variable Structure”, Wiley, New York.

58 Jantapremjit, P., Wilson, P.A. “Control and Guidance Approach using an Autonomous Underwater Vehicle”, *International Journal of Maritime Engineering.*

59 Ji-Hong Li, Pan-Mook Lee., (2005*).* “Design of an adaptive nonlinear controller for depth control of an autonomous underwater vehicle”, *Ocean Engineering 32*, 2165–2181.

60 Jomes-Rui, M.F, Sousa, J.B., Pereira, F.L. (2002). “Modelling and Control of the IES Project ROV”, Engineering Faculty of Porto University.

61 J W Automarine. (2010). “The theory of lifting bags”. Retrieved on 4th October 2010, www.jwautomarine.co.uk.

62 Karagulle, H., Malgaca, L. and Oktem, H.F. (2004). “Analysis of active vibration control in smart structures by ANSYS”. *Smart Materials and Structures 13*, pp.661–667.

63 Kashif (1999). “Intelligent Control of Diving System of an Underwater Vehicle”, M.Eng Thesis, University Teknologi Malaysia.

64 Kato, N., (1995). “Applications of fuzzy algorithm to guidance of and control of underwater vehicle”. *In: Yuh, J. (Ed.), Underwater Robotic Vehicles: Design and Control*. TSI Press, Albuquerque.

65 Keller, J.J. (2012). “Tracking control of Autonomus Underwater Vehicles”, M.S.Thesis, Naval Postgraduate School, Monterey, CA.

66 Khot et al. (2011). “Active vibration control of cantilever beam by using PID based output feedback controller”. *Journal of vibration and control -18(3),* pp.366–372.

67 Khot, S.M. & Yelve, N.P. (2011). “Modeling and response analysis of dynamic systems by using ANSYS and MATLAB”. *Journal of Vibration and Control* - 17 (6), pp. 953-958.

68 Kim, K., Choi, H-S., (2007). “Analysis on the controlled motion of a test bed AUV-SNUUV 1”, *Ocean Engineering 34*, pp.1138-1150.

69 Kodogiannis, V., (2003). “Direct adaptive control of underwater vehicles using neural networks”. *Journal of Vibration and Control 9,* pp. 605–619.

70 Kosmatopoulos et al. (1995). “High-order neural network structures for identification of dynamical systems”, *IEEE Trans. Neural Networks 6*. pp.422–431.

71 Kumar, K.R. and S. Narayanan. (2008). “The optimal location of piezoelectric actuators and sensors for vibration control of plates”, *Smart Materials and Structures*, 16(6): pp. 2680-2691.

72 Lee et al. (1999). “Discrete- Time Quasi- Sliding Mode Control of an Autonomous Underwater Vehicle”, *IEEE Journal of Ocean Engineering*, Vol.24, No.3.

73 Lee, C.C. (1990). “Fuzzy logic in control systems: fuzzy logic controller – Part 1,” *IEEE Transactions on Systems, Man & Cybernetics*, Vol.20, No. 2, pp. 404-419.

74 Lee et al. (2007). “Clonal Selection Algorithms for 6-DOF PID Control of Autonomous Underwater Vehicles”, *ICARIS 2007*, LNCS 4628, pp.182–190.

75 Lee, H., Kim, E., Kang, H. J., and Park, M. (1998), “Design of a sliding mode controller with fuzzy sliding surfaces”, *IEEE Proceedings – Control Theory and Applications 145(5)*, pp. 411–418.

76 Li, J-H., Lee, P.M. (2005). “ A neural network adaptive controller design for free-pitch angle diving behavior of an autonomous underwater vehicle”, *Robotics and Autonomous Systems 52*, pp. 132–147.

77 Lim, Y. H, Varadan, V.V., Gopinathan, S.V. and Varadan V K. (1999). “Finite element simulation of smart structures using an optimal output feedback controller for vibration and noise control”, *Smart Materials and Structures 8***,** pp. 324–337.

78 Malgaca, L. (2010). “Integration of active vibration control methods with finite element models of smart laminated composite structures”. *Elsevier Journal of Composite Structures 92*. pp. 1651–1663.

79 Manning, W. J, Plummer, A. R and Levesley, M.C. (2000). “Vibration control of a flexible beam with integrated actuators and sensors”. *Smart Materials and Structures 9*, pp. 932–939.

80 Mcgookin, E.W. (1997). “Optimisation of sliding mode controllers for marine applications: a study of methods and implementation issues”. PhD thesis, University of Glasgow.

81 Mcgookin, E.W., Murray-Smith, D.J.(2006). “Submarine manoeuvring controller’s optimisation using simulated annealing and genetic algorithms”, *Control Engineering Practice 14* , pp. 1-15.

82 Mei, C.C., Yeung, R.W. & Liu, K.F. (1985). “Lifting of a Large Object from a Porous Seabed”, *Journal of Fluid Mechanics*, Vol.152, pp. 203-215.

83 Moreira, L. Fossen, T.I., Soares, C.G. (2007). “ Path following control system for a tanker ship model”, *Ocean Engineering* 34, pp.2074-2085.

84 Nag, P.K., (2008). “Engineering Thermodynamics”, Tata McGraw-Hill Publishing Company Limited, New Delhi, India.

85 Narayanan. S, Balamurugan.V. (2003). “Finite element modelling of piezolaminated smart structures for active vibration control with distributed sensors and actuators”. *Elsevier Journal of Sound and Vibration 262*, pp. 529–562.

86 Nicholls-Lee et al. (2009). “Use of cryogenic buoyancy systems for controlled removal of heavy objects from sea bottom”, *Proceedings of the ASME 28th International Conference on Ocean ,Offshore & Arctic Engineering*.

87 Odyssey Marine Exploration. (2011). “Ship Wreck Exploration”, Retrieved on 4th November 2014, www.shipwreck.net.

88 Palm, R., Driankov, D. and Hellendoorn, H. (1997). “Model Based Fuzzy Control”, Springer-Verlag, Germany.

89 Paulsen, M, J., Egeland, O., Fossen, T.I. (1994). "An Output Feedback Controller with Wave Filter for Marine Vehicles", *Proceedings of the American Control Conference,* Baltimore, Maryland.

90 Pepijn, W.J., Colin van de Ven, F., Daniel, T., (2005). "Neural network control of underwater vehicles". *Engineering Applications of Artificial Intelligence 18,* pp.533–547.

91 Perez et al. (2006). "An Overview of the Marine System Simulator (MSS): A SIMULINK Toolbox for Marine Control Systems", *Modelling Identification and Control*, Vol.27, No.4, pp. 259-275.

92 Perez, T. & Fossen, T.I. (2007). "Kinematic Models for Maneuvering and Sea keeping of Marine Vessels, *Modeling Identification and Control*, Vol. 28, No. 1, pp. 19-30.

93 Peza-Solis, J.F., Navarro, G.S and Linares, R.C. (2009). "Modeling and Tip Position Control of a Flexible Link Robot: Experimental Results", *Computational Systems*, Vol.12. No.4, pp. 421-435.

94 Rao, S.S. (2004). "Mechanical Vibrations (4^{th} ed.)", Pearson Prentice-Hall, New Jersey.

95 Rawson, K.J. & Tupper, E, C. (2001). "Basic Ship Theory - Vol. 1", Butterworth-Heinemann publishing, Oxford.

96 Ridley, P., Fontan, J. and Corke, P. (2003). "Submarine dynamic modelling", *Proceedings of the 2003 Australasian Conference on Robotics & Automation*, pp.1-3, Brisbane.

97 Ren, J., Yang, Y. (2004). "Fuzzy Gain Scheduling Attitude Control for Hydrofoil Catamaran" , *Proceeding of the 2004 American Control Conference,* Boston,

Massachusetts.

98 Resolve.(2010). “Salvage Catalog”, Retrieved on 5th October 2010, www.resolvesalvage.com.

99 Pratap, R. “Getting Started with MATLAB”, Oxford University Press, 2003.

100 Salgado J,T., Jouvencel, B. (2003). “Using high order sliding modes for diving control of a torpedo Autonomous Underwater Vehicle”, *Oceans 2003*, San Diego, USA, pp. 934-393.

101 Sawicki, A. & Mierczynski, J. (2003). “Mechanics of breakout phenomenon”, *Computers and Geotechnics 30*, pp.231-243.

102 Singh, S.P., Pruthi, H.S., and Agarwal, V.P. (2003). “Efficient modal control strategies for active control of vibration”, *Journal of Sound Vibration*, pp. 563-575.

103 SIMULINK user manual, The Mathworks Inc., Natick, MA, 2010.

104 Slotine, J.J., Coetsee, J., (1986). “Adaptive sliding controller synthesis for non-linear systems”, *International Journal of Control* 43, pp.1631–1651.

105 Slotine, J.J., & Li,W. (1991). “Applied non - linear control”, New Jersey, USA.

106 Slotine, J.J., Shastry, S., (1983). “Tracking control of nonlinear system using sliding surfaces”, *International Journal of Control* 38 (2), pp. 465–492.

107 SMIT.(2010). “Salvage Brochure”. Retrieved on 5th October 2010, www.smit.com.

108 Soylu, S., Buckham, B., Podhorodeski, R., (2007). “Robust control of underwater

vehicles with fault-tolerant infinity-norm thruster force allocation". *In:Proceedings of the OCEANS 2007 MTS/IEEE Conference and Exhibition*,Vancouver, BC, Canada.

109 Soylu, S., Buckham, B., Podhorodeski, R.(2008). "A chattering-free sliding-mode controller for underwater vehicles with fault tolerant infinity-norm thrust allocation", *Ocean Engineering 35*, pp 1647-1659.

110 Stansbery, D.T, & Cloutier, J.R. (2000). "Position and Attitude Control of a Spacecraft using the State-Dependent Riccati Equation Technique". *Proceedings of the American Control Conference*, Chicago.

111 Subsalve.(2010). "Salvage Catalog". Retrieved on 5th October 2010, www.subsalve.com.

112 Sun et al. (2007). "Design of Vibration Controllers for Flexible Beams Using the Mechatronic Design Quotient (MDQ) Approach", *Journal of Vibration and Control*, 13 (1), pp.65-94.

113 SuSy. (2009). "Description of Work".

114 SuSy. (2010). "Ship Disaster Database and Lessons Learned".

115 SuSy.(2010). "Scenario Evaluation and System Concept Specification".

116 SuSy. (2010). "Structuring of Ship Disasters and Scenario Definition".

117 SuSy.(2010). "Analysis Report on Buoyancy Generating Media".

118 SuSy.(2010)."Requirement of the Vessel Design Selected in the Typical Scenarios".

119 SuSy. (2011). “Project Mid-term Report”.

120 Tokat, S., Eksin, I., Guzelkaya, M., (2003). “New Approaches for On-line Tuning of the Linear Sliding Surface Slope in Sliding Mode Controllers”, *Turkish Journal of Electrical Engineering*, Vol.11, No.1.

121 U.S. Navy (1969). “SALVOPS 69”, Department of Navy, Naval Ship Systems Command, NAVSHIPS 0994-012-6010, Washington, D.C.

122 U.S. Navy (1970). “SALVOPS 70”, Department of Navy, Naval Ship Systems Command, NAVSHIPS 0994-012-6020,Washington, D.C.

123 U.S. Navy (1970). “Ship Salvage Manual, Volume II- Submarine Salvage”, NAVSHIPS 0994-000-3020, Washington.

124 U.S.Navy (2004). “ Salvor’s Hand Book”, 1st January 2004.

125 U.S. Navy. (2006). “Salvage Manual Volume 1: Strandings and Harbor Clearance”, 30 September 2006.

126 Utkin, V. I. (1977), “Variable structure systems with sliding mode”, *IEEE Transactions on Automatic Control 22*, pp. 212-222.

127 Utkin,V., Guldner, J., & Shi, J. (1999). “Sliding mode control in electromechanical systems”, Taylor & Francis Ltd, London.

128 Van de Ven, P., Flanagan, C., Toal, D. (2005). “Neural network control of underwater vehicles”. *Engineering Applications of Artificial Intelligence* 18, pp. 533–547.

129 Vaudrey, K.D. (1972). “Evaluation of bottom breakout reduction methods”, Technical Note N-1227, Naval Civil Engineering Laboratory, Port Huneme, California.

130 Venugopal, K. P., Sundhakar, R., Pandya, A.S., “On-line learning control of autonomous underwater vehicles using feedforward neural networks”, *IEEE J. Ocean. Eng. 17*. pp. 308–319.

131 Vuilmet, C. “High order sliding mode control applied to a heavyweight torpedo” *Proceedings of the 2005 IEEE Conference on Control Applications*,Toronto, Canada.

132 Water Weights.(2010). “Salvage Catalog”, Retrieved on 5th October 2010, www.waterweights.com.

133 Xin, S., Zaojian, Z. (2010). “A fuzzy sliding mode controller with adaptive disturbance approximation for underwater robot”, *2nd International Asia Conference on Informatics in Control, Automation and Robotics.*

134 Xu, S.X., Koko, T.S. (2004). “Finite element analysis and design of actively controlled piezoelectric smart structures”. *Elsevier Finite Element in Analysis and Design 40 (3),* pp.241–262.

135 Yagiz, N., Hacioglu,Y. (2005). “Fuzzy Sliding Modes with Moving Surface for the Robust Control of a Planar Robot”. *Journal of Vibration and Control 11*, pp. 903-922.

136 Yagiz, N., Hacioglu,Y. (2009). “Robust Control of a Spatial Robot using Fuzzy Sliding Modes”. *Mathematical and Computer Modelling 49* , pp.114-127.

137 Yan, S. & Zhang, H. (2008). “Numerical Analysis and Control for Cantilever Flexible Beams Using PZT Patches”, *Proceedings of SPIE vol.6932. 69322T*.

138 Yang, J., Zhao, De-you, Hong, M. (2011). “An efficient method for non-stationary random vibration analysis of beams”, *Journal of Vibration and Control*, 17(13).

139 Yoerger, D.R., Cooke, J.G., Slotine, J.J.E. (1990). “The influence of thrusters dynamics on underwater vehicle behavior and their incorporation in to control system design”, *IEEE Journal of Oceanic Engineering*, vol. 15, No.3, pp. 167-179, 1990.

140 Yoerger, D.R., Slotine, J.J.E. (1985). “Robust trajectory control of underwater vehicles”, *IEEE Journal of Oceanic Engineering*, vol. 10, pp. 462-470.

141 Yorgancioglu, F., Komurcugil, H. (2008). “Single-input fuzzy-like moving sliding surface approach to the sliding mode control”, *Electrical Engineering 90*, pp. 199-207.

142 Yorgancioglu, F., Komurcugil, H. (2010). “Decoupled sliding mode controller based on time - varying sliding surfaces for fouth-order systems”, *Expert Systems with Applications 37*, pp.6764-6774.

143 Yuh, J. (1990). “A neural net controller for underwater robotic vehicles”, *IEEE J. Ocean. Eng. 15*. pp.161–166.

144 Yuh. J.(1994). “Learning Control for Underwater Robotic Vehicles”. *IEEE International Conference on Robotics and Automation*, Atlanta, GA.

145 Yuh, J. (2000). “Design and Control of Autonomous Underwater Robots: A Survey”, *Autonomous Robots 8*, pp.7–24.

146 Yuh, J. Lakshimi, R. (1993). “An intelligent control system for remotely operated vehicles”, *IEEE J. Ocean. Eng. 18*. pp. 55–62.

147 Zadeh, L. A. (1965), “Fuzzy sets”, *Information and Control 8*, pp. 338–353.

148 Zhang, J. Jiang, K., Chen, Z., and Zhao, Z., (2006). “Global Robust Fuzzy Sliding Mode Control for a Class of Non-Linear System”, *Transactions of the Institute of Measurement and Control*, pp.219-227.

149 Zhao, S., Yuh, J. (2005). “Experimental Study on Advanced Underwater Robot Control”, *IEEE Transactions on Robotics*, Vol. 21, No. 4.

150 Ziegler & Nichols. (1942). “Optimal Settings for Automatic Controllers”, *Trans. ASME 64(11)*, pp. 759–768.

Appendix A

Estimation of Additional Buoyancy Required for Inflating

Consider the problem of lifting a sunken vessel (e.g. **Pontoon model**) having weight 9.32 tons lying at sea bottom, which is at 100m from sea surface.

Given parameters:

Weight of the vessel (mass in air), W = 9.32 tonnes = 9320 kgf = 91429.20 N

Assume the vessel is made up of steel having a density of 7850 kg/m^3,

i.e. $\rho_{steel} = 7850$ kg/m^3.

But weight = volume * g*density

Therefore, volume of the steel = W/ρ_{steel} = 91429.20 /7850*9.81 = 1.187 m^3

The buoyancy force provided by seawater is,

$B = \rho g \nabla$ = 1025 * 9.81*1.187 = 11935.58 N

Therefore, in water object weight = 91429.20 -11935.58 = 79493.62 N

Total lift force (suction break out force) required to extract an object from sea bottom is the summation of in water object weight and ground reaction.

Total lift force is assumed as 1.3 times the wet weight of the vessel

= 1.3 * 79493.62 = 103341.70 N

Suppose air is used as the gas in lift bags,

Then the buoyancy provided by the inflating system is,

$= V^* (\rho_{water} - \rho_{air})^* g$

But due to compressibility, the density of air changes with respect to surrounding sea water pressure.

The absolute pressure at sea bottom,

$P_{abs}=\rho gh+P_{atm}=1025*9.81*100+101325=1106850\ N/m^2$

Therefore, density of air at sea bottom,

$\rho_{air}=P_{abs}/R*T=1106850/286.9*290=13.30\ kg/m^3$

Therefore, the minimum volume of air required for inflating,

$V = (103341.70/ (1025-13.30)*9.81 =$ **10.41** m^3

APPENDIX B

Analytical Solution of Euler- Bernoulli Beam with Free- Free Boundary Conditions

For the transverse free vibration of a beam having constant moment of inertia (*I*) and modulus of elasticity (*E*), the Euler - Bernoulli beam equation can be rewritten from Eq.(76) as,

$$EI\frac{\partial^4 z}{\partial x^4}+\rho A\frac{\partial^2 z}{\partial t^2}=0 \tag{152}$$

Where the displacement *z* is a function of both space and time.

i.e.

$$z=f(x,t) \tag{153}$$

In order to solve Eq. (152), let the displacement can be approximated as [2, 94],

$$z(x,t)=Z(x)\sin\omega_n t \tag{154}$$

Where *Z(x)* is a function of *x* alone and ω_n is the natural frequency of vibration or mode order. Therefore,

$$\frac{\partial^4 z}{\partial x^4}=\frac{\mathrm{d}^4 Z}{\mathrm{d}x^4}\sin\omega_n t \quad \text{and} \quad \frac{\partial z}{\partial t}=\omega_n Z\cos\omega_n t \tag{155-156}$$

Therefore,

$$\frac{\partial^2 z}{\partial t^2}=-\omega_n{}^2 Z\sin\omega_n t \tag{157}$$

Substituting Eq. (155) & (157) in Eq. (152) leads to:

$$EI\frac{\mathrm{d}^4 Z}{\mathrm{d}x^4}\sin\omega_n t - \rho A\omega_n^2 Z\sin\omega_n t = 0 \tag{158}$$

$$\left[\frac{\mathrm{d}^4 Z}{\mathrm{d}x^4} - \frac{\rho A\omega_n^2}{EI}Z\right]\sin\omega_n t = 0 \tag{159}$$

i.e.

$$\left[\frac{\mathrm{d}^4 Z}{\mathrm{d}x^4} - k^4 Z\right] = 0 \tag{160}$$

In which,

$$k^4 = \frac{\rho A\omega_n^2}{EI} \tag{161}$$

Let

$$Z = Z_0 e^{\lambda x} \tag{162}$$

Therefore,

$$\frac{\partial Z}{\partial x} = \lambda Z_0 \mathrm{e}^{\lambda x},\ \frac{\partial^2 Z}{\partial x^2} = \lambda^2 Z_0 \mathrm{e}^{\lambda x},\ \frac{\partial^3 Z}{\partial x^3} = \lambda^3 Z_0 \mathrm{e}^{\lambda x}\ \&\ \frac{\partial^4 Z}{\partial x^4} = \lambda^4 Z_0 \mathrm{e}^{\lambda x} \tag{163}$$

Therefore, Eq. (160) becomes:

$$\lambda^4 Z_0 e^{\lambda x} - k^4 Z_0 e^{\lambda x} = 0 \tag{164}$$

$$Z_0 e^{\lambda x}\left[\lambda^4 - k^4\right] = 0 \tag{165}$$

i.e.

$$\lambda^4 - k^4 = 0 \tag{166}$$

Which is the characteristic equation and its solutions can be obtained as follows:

$$(\lambda^2 - k^2)(\lambda^2 + k^2) = 0 \tag{167}$$

$$\lambda^2 = k^2 \;\&\; \lambda^2 = -k^2 \tag{168}$$

Therefore,

$$\lambda = k, -k, ik, -ik \tag{169}$$

Substituting the values of λ in Eq. (162) leads to:

$$Z = c_1 e^{kx} + c_2 e^{-kx} + c_3 e^{ikx} + c_4 e^{-ikx} \tag{170}$$

Where c_1, c_2, c_3 & c_4 are arbitrary constants.

But,

$$e^{\pm kx} = \cosh kx \pm \sinh kx, \quad e^{\pm ikx} = \cos kx \pm i \sin kx \tag{171}$$

Therefore, Eq. (170) becomes:

$$Z = c_1(\cosh kx + \sinh kx) + c_2(\cosh kx - \sinh kx) + c_3(\cos kx + i \sin kx) + c_4(\cos kx - i \sin kx) \tag{172}$$

i.e.

$$Z = \sin kx[i(c_3 - c_4)] + \cos kx[c_3 + c_4] + \sinh kx[c_1 - c_2] + \cos h\, kx[c_1 + c_2] \tag{173}$$

Therefore,

$$Z = A \sin kx + B \cos kx + C \sinh kx + D \cos h\, kx \tag{174}$$

Which is the general solution of beam vibration. Where A=i (c_3-c_4), B= (c_3+c_4), C= (c_1-c_2), D= (c_1+c_2). The values of A, B, C & D can be obtained by applying the boundary conditions as shown in Eq. (79) & (80).

From Eq. (174),

$$\frac{\partial Z}{\partial x} = k(A\cos kx - B\sin kx + C\cosh kx + D\sinh kx) \tag{175}$$

$$\frac{\partial^2 Z}{\partial x^2} = k^2(-A\sin kx - B\cos kx + C\sinh kx + D\cosh kx) \tag{176}$$

$$\frac{\partial^3 Z}{\partial x^3} = k^3(-A\cos kx + B\sin kx + C\cosh kx + D\sinh kx) \tag{177}$$

Now the Eqs. (79) & (80) becomes,

$$\left.\frac{d^2 z}{dx^2}\right|_{x=0} = k^2(-B + D) = 0 \Rightarrow B = D \tag{178}$$

$$\left.\frac{d^3 z}{dx^3}\right|_{x=0} = k^3(-A + C) = 0 \Rightarrow A = C \tag{179}$$

$$\left.\frac{d^2 z}{dx^2}\right|_{x=l} = k^2(-A\sin kl - B\cos kl + C\sinh kl + D\cosh kl) = 0 \tag{180}$$

$$\left.\frac{d^3 z}{dx^3}\right|_{x=l} = k^3(-A\cos kl + B\sin kl + C\cosh kl + D\sinh kl) = 0 \tag{181}$$

Replacing A=C and B=D in Eq. (180) & (181), we get,

$$(-C\sin kl - D\cos kl + C\sinh kl + D\cosh kl) = 0 \tag{182}$$

$$(-C\cos kl + D\sin kl + C\cosh kl + D\sinh kl) = 0 \tag{183}$$

After rearranging,

$$C(\sinh kl - \sin kl) + D(\cosh kl - \cos kl) = 0 \quad (184)$$

$$C(\cosh kl - \cos kl) + D(\sinh kl + \sin kl) = 0 \quad (185)$$

Eqs. (184) & (185) can be written in matrix form as:

$$\begin{bmatrix} (\sinh kl - \sin kl) & (\cosh kl - \cos kl) \\ (\cosh kl - \cos kl) & (\sinh kl + \sin kl) \end{bmatrix} \begin{bmatrix} C \\ D \end{bmatrix} = 0 \quad (186)$$

i.e.

$$\begin{vmatrix} (\sinh kl - \sin kl) & (\cosh kl - \cos kl) \\ (\cosh kl - \cos kl) & (\sinh kl + \sin kl) \end{vmatrix} = 0 \quad (187)$$

$$\sinh^2 kl - \sin^2 kl - (\cosh^2 kl + \cos^2 kl - 2\cosh kl \cos kl) = 0 \quad (188)$$

I.e.

$$\sinh^2 kl - \cosh^2 kl - \sin^2 kl - \cos^2 kl + 2\cosh kl \cos kl = 0 \quad (189)$$

But,

$$\sinh^2 kl - \cosh^2 kl = -1, \quad \sin^2 kl + \cos^2 kl = 1 \quad (190)$$

Therefore, Eq. (189) becomes,

$$-2 + 2\cosh kl \cos kl = 0 \quad (191)$$

Therefore,

$$\cosh kl \cos kl = 1 \tag{192}$$

This equation is satisfied by a number of *kl* values, each corresponding to a normal mode of vibration.

Graphical solution of the equation *coshklcoskl* =1 provides the following values as shown in Table 17 [21, 94].

Table 17 Graphical solution of *coshklcoskl*=1

$(kl)_1$	$(kl)_2$	$(kl)_3$	$(kl)_4$	$(kl)_5$	$(kl)_6$
0	4.73	7.853	10.996	14.137	17.279

Evaluation of Natural Frequencies

From Eq. (161),

$$k^4 = \frac{\rho A \omega_n^2}{EI} \Rightarrow \omega_n^2 = \frac{k^4 EI}{\rho A} \Rightarrow \omega_n = \mathrm{k}^2 \sqrt{\frac{EI}{\rho A}} = \mathrm{k}^2 \frac{l^2}{l^2} \sqrt{\frac{EI}{\rho A}} = \frac{(kl)^2}{l^2} \sqrt{\frac{EI}{\rho A}} \tag{193}$$

Therefore,

$$f_n = \frac{1}{2\pi} \left[\frac{(kl)_n}{l} \right]^2 \sqrt{\frac{EI}{\rho A}} \tag{194}$$

Where n = 2, 3, 4,……

Therefore, by substituting in the above equation the various $(kl)_n$ values, the respective natural frequencies for any mode of vibration can be found. The value $(kl)_1$ =0 is disregarded as it does not give rise to an oscillatory motion.

Evaluation of Mode Shapes

From Eqs. (174), (178) & (179),

$$Z = A\sin kx + B\cos kx + C\sinh kx + D\cos h\, kx = C(\sin kx + \sinh kx) + D(\cos kx + \cos h\, kx) \quad (195)$$

But from Eq. (184),

$$C(\sinh kl - \sin kl) + D(\cosh kl - \cos kl) = 0 \Rightarrow C = -D\frac{(\cosh kl - \cos kl)}{(\sinh kl - \sin kl)} \quad (196)$$

Substituting Eq. (196) in Eq. (195), we get,

$$Z = -D\frac{(\cosh kl - \cos kl)}{(\sinh kl - \sin kl)}(\sin kx + \sinh kx) + D(\cos kx + \cos h\, kx) \quad (197)$$

i.e.

$$Z = D\left[(\cosh kx + \cos kx) - \frac{(\cosh kl - \cos kl)}{(\sinh kl - \sin kl)}(\sinh kx + \sin kx)\right] \quad (198)$$

$$Z_n\left\{\frac{x}{l}\right\} = D\left[\left(\cosh(kl)_n\left\{\frac{x}{l}\right\} + \cos(kl)_n\left\{\frac{x}{l}\right\}\right) - \left(\frac{\cosh(kl)_n - \cos(kl)_n}{\sinh(kl)_n - \sin(kl)_n}\right)\left(\sinh(kl)_n\left\{\frac{x}{l}\right\} + \sin(kl)_n\left\{\frac{x}{l}\right\}\right)\right] \quad (199)$$

By selecting the $(kl)_n$ values from Table 17, a number of profiles is derived representing the respective modes of vibration. In order to plot the vibration profiles, the value of Z is calculated at number of positions (x/l) along the length of the beam and the resulting profile is then normalized.